CHARACTERISATION OF CD4$^+$ STEM CELLS OF THE SKIN AND THEIR ROLE IN SKIN HOMEOSTASIS AND TUMOURIGENESIS

Dissertation
for the award of the degree
"*Doctor rerum naturalium*"
of the Georg-August-Universität Göttingen
within the doctoral programme *Genes and Development*
of the Georg-August University School of Science (GAUSS)

Submitted by
Nadine Brandes
from Bremen, Germany

Göttingen 2021

Thesis advisory committee

PD Dr. Anja Uhmann
University Medical Center Göttingen
Institute of Human Genetics

Prof. Dr. Rüdiger Behr
German Primate Center
Research platform: Degenerative diseases

Prof. Dr. Sigrid Hoyer-Fender
Georg-August-Universität Göttingen
Department of Developmental Biology

Members of the examination board

Referee: PD Dr. Anja Uhmann
University Medical Center Göttingen
Institute of Human Genetics

Co-referee: Prof. Dr. Michael Schön
University Medical Center Göttingen
Department of Dermatology, Venereology and Allergology

Other members of the examination board

Prof. Dr. Rüdiger Behr
German Primate Center
Research platform: Degenerative diseases

Prof. Dr. Sigrid Hoyer-Fender
Georg-August-Universität Göttingen
Department of Developmental Biology

Prof. Dr. Peter Burfeind
University Medical Center Göttingen
Institute of Human Genetics

Dr. Nico Posnien
Georg-August-Universität Göttingen
Department of Developmental Biology

Day of the oral examination: 11.05.2021

Declaration of independent work

I hereby confirm that I have written the attached thesis on my own and that I did not use any resources than those specified. This work has not been previously submitted, either in the same or in a similar form to any other examination committee.

Place, Date	Signature

Parts of this work have been published:

Brandes N, Mitkovska SH, Botermann DS, Maurer W, Müllen A, Scheile H, Zabel S, Frommhold A, Heß I, Hahn H, Uhmann A. *Spreading of Isolated Ptch Mutant Basal Cell Carcinoma Precursors Is Physiologically Suppressed and Counteracts Tumour Formation in Mice*. Int J Mol Sci. 2020 Dec 5;21(23):9295. doi: 10.3390/ijms21239295.

I. Table of contents

II. List of figures

III. List of tables

IV. List of figures from the appendix

V. List of abbreviations

3D	Three dimensional
α-SMA	Alpha smooth muscle actin
ADRB2	β2 adrenoreceptor
BCC	Basal cell carcinoma
Blimp	B-lymphocyte-induced nuclear maturation protein
BM	Bone marrow
Bp	Base pairs
BrdU	Bromodeoxyuridine
Ca^{2+}	Calcium
cAMP	Cyclic adenosine monophosphate
Ccn	Cyclin
CCR5	CC motive chemokine receptor type 5
CD	Cluster of differentiation
Cdc	Cell division cycle
cDNA	Complementary DNA
CFE	Colony-forming efficiency
CFU	Colony-forming unit
CFU-F	Colony-forming unit fibroblast(s)
Cp	Companion
CXCR4	CXC motive chemokine receptor type 4
DAPI	4'6,-diamidin-2-phenylindol
dH_2O	Distilled water
ddH_2O	Double-distilled water
DMBA	7,12-dimethylbenz[a]anthracene
DMEM	Dulbecco`s modified eagle medium
DMSO	Dimethylsulfoxide
DNA	Deoxyribonucleic acid
dNTPs	Deoxyribonucleotide triphosphates
DP	Dermal papilla
DS	Dermal sheath
E	Embryonic day
ECM	Extracellular matrix
EDAC	Epithelial defence against cancer
EDTA	Ethylenediaminetetraacetic acid
EGF	Epidermal growth factor
EGFP	Enhanced green fluorescence protein
ER	Estrogen receptor
Erk	Extracellular signal-regulated kinases
ESC	Embryonic stem cell(s)
EtOH	Ethanol
FACS	Fluorescence activated cell sorting

FCS	Foetal calf serum
FGF	Fibroblast growth factor
FSC	Forward scatter
gDNA	Genomic DNA
Gli	Glioma-associated oncogene
H&E	Haematoxylin and eosin
HBSS	Hank's balanced salt solution
hDF	Human dermal fibroblast(s)
HF	Hair follicle(s)
HH	Hedgehog
HIV	Human immunodeficiency virus
HS	Hair shaft
HSC	Haematopoietic stem cell(s)
i.p.	Intraperitoneally
ICC	Immunocytochemistry
IFE	Interfollicular epidermis
iHF	Isolated hair follicle(s)
IL	Interleukin
IRS	Inner root sheath
JC	Junctional zone
K	Keratin(s)
Kb	Kilobase
KO	Knockout
LAT	Linker of activated T cells
Lck	Lymphocyte specific protein tyrosine kinase
Lgr	Leucine-rich repeat-containing G-protein coupled receptor
Lin^{neg}	Lineage negative
Lor	Loricin
LPC	Lower proximal cup
LRC	Label-retaining cell(s)
Lrig	Leucine rich repeats and immunoglobulin like domains
MEF	Mouse embryonic fibroblasts
MHC	Major histocompatibility complex
MKI67	Marker of proliferation Ki-67
MSC	Mesenchymal stromal/stem cell(s)
Oct-3/4	Octamer-binding transcription factor 4
ORS	Outer root sheath
PBS	Phosphate-buffered saline
PCA	Principal component analysis
PCR	Polymerase chain reaction
PDGF	Platelet derived growth factor
PDGFRα	Platelet derived growth factor receptor alpha
pen/strep	Penicillin and Streptomycin

PFA	Paraformaldehyde
PLCγ1	Phospholipase Cγ1
PTCH	Patched
R26	Rosa26
RNA	Ribonucleic acid
RT	Room temperature
SC	Stem cell(s)
Sca-1	Stem cell antigen-1
SCC	Squamous cell carcinoma
scRNA-Seq	Single-cell RNA sequencing
SDS	Sodiumdodecylsulfate
SG	Sebaceous gland(s)
sHG	Secondary hair germ
SHP-2	Src homology region 2 domain-containing phosphatase-2
SMO	Smoothened
Sos	Son of sevenless
Sox	Sex-determining region Y-Box
SSC	Side scatter
TBS	Tris-buffered saline
TBS-T	TBS-Triton X-100
TCR	T cell receptor
tdT	tdTomato
TF	Transcription factor(s)
TGF	Transforming growth factor
TNF	Tumour necrosis factor
TP	Tumour protein
TPA	12-O-tetradecanoylphorbol-13-acetate
TRIS	Tris(hydroxymethyl)aminomethane
Trp	Transformation-related protein
uHF	Upper hair follicle
UV	Ultraviolet
VEGF	Vascular endothelial growth factor
WIH-A	Wound induced hair anagen re-entry/growth
WNT	Wingless-related integration site

Commonly used abbreviations and units of measurement are not listed.

Summary

The skin represents the largest organ of the mammalian body and acts as the primary barrier against environmental stressors. Cellular maintenance and regeneration of the skin is orchestrated by a variety of skin stem cell (SC) populations. Due to their regenerative potential and plasticity, skin SC are an important research focus in regenerative medicine. However, they are also a subject of cancer research since mutations in skin SC can lead to skin tumour formation. The most common neoplasia of the human skin is the basal cell carcinoma (BCC), which most often develops due to Hedgehog (HH) signalling activating mutations in basal cells of the interfollicular epidermis (IFE) and/or from hair follicle (HF) SC. In sporadic BCC, a loss of heterozygosity of the negative HH signalling regulator *PATCHED* (*PTCH*) is most commonly observed. Recently our group described the existence of $CD4^+$ non-haematopoietic skin-resident cells, which can give rise to HH signalling-activated BCC upon homozygous *Ptch* mutation and chemical carcinogenesis. However, the cellular identity and localisation of the $CD4^+$ non-haematopoietic, skin-resident precursors were unclear. Since the knowledge about their occurrence and potential may have critical impact on the understanding of skin cancer development, the main goal of this thesis was to identify and characterise $CD4^+$ non-haematopoietic, skin-resident cells and their descendants. For this purpose, three main strategies were pursued: First, stromal cells, which can give rise to various skin cell types and which can express *Cd4/CD4* transcripts, were analysed as possible $CD4^+$ non-haematopoietic ancestors of skin-resident BCC precursors. The respective *in vivo* and *in vitro* lineage-tracing analyses revealed that a small population of murine stromal cells of the bone marrow and skin express CD4. However, $CD4^+$ stromal cells could neither be proven nor excluded as the origin of BCC due to missing methods of investigation. Second, epidermal SC were evaluated as the origin of $CD4^+$ non-haematopoietic, skin-resident cells. Using *in vivo* and *in vitro* lineage tracing, comparative and single cell transcriptome sequencing and flow cytometric analyses, rare SC-like epidermal cells of the IFE and/or the infundibulum were uncovered as $CD4^+$ non-haematopoietic cells and thus can be considered likely candidates for BCC precursor cells. Moreover, the specific characterisation of $CD4^+$ epidermal cells revealed that their progeny grows permanently and increasingly with age and upon wound healing in adult mice in all IFE layers and as multipotent HF SC of the telogen HF as well as in all compartments of the anagen HF. Thirdly, and highly relevant, the occurrence and characteristics of the previously uncovered $CD4^+$ non-haematopoietic population of human skin was investigated. Flow cytometric and *in vitro* culture analyses showed that these cells similar to their murine counterparts possess a SC-like character and most likely grow in the IFE and/or the infundibulum of human skin.

1 Introduction

1.1 The architecture of mammalian skin

The skin represents the largest organ of the mammalian body and acts as the primary barrier against environmental stressors, such as dehydration, wounding and microbial infection. The skin is composed of the interfollicular epidermis (IFE) with its interspersed pilosebaceous units and the underlying dermis and hypodermis (Figure 1).

1.1.1 The interfollicular epidermis

The IFE functions as a waterproof barrier via a multi-layered sheet of keratinocytes, which produce fibrous structural keratin proteins. These keratins form intermediate filaments by their assembly to bundles that resists cells against mechanical stress. Additionally, keratins interact with desmosomes and hemidesmosomes to achieve cell-cell adhesion and basal cell-underlying connective tissue connection [1, 2].

The innermost layer of the IFE, the basal layer (*stratum basale*), is attached to the basement membrane and is composed of a single row of columnar keratinocytes (marker proteins: Keratin [K] 5^+, $K14^+$, integrin α-6/cluster of differentiation [CD] 49^+) interrupted by epidermal stem cells (SC), melanocytes, Langerhans cells (also found in the more differentiated epidermal layers) and Merkel cells [3] (Figure 1). The keratinocytes of the basal layer produce, secrete and assemble the extracellular matrix (ECM) that constitutes the underlying basement membrane [4] (Figure 1), whereas epidermal SC of the basal layer ensure the constant renewal of the epidermis. Melanocytes make up ~8% of the epidermal cells and produce melanin that pigments skin and hair for ultraviolet (UV) light protection. Langerhans cells are tissue-resident dendritic cells that ensure immune defence and Merkel cells are mechanoreceptors essential for touch sensation (Figure 1). Proliferative active keratinocytes of the basal layer differentiate upwards and give rise to keratinocytes of the intermediate suprabasal spinous layer (*stratum spinosum*; marker proteins: $K1^+$, $K10^+$) in which the process of terminal differentiation is already initiated although the keratinocytes are still transcriptionally active. The intermediate granular layer (*stratum granulosum*) consists of flattened keratinocytes (marker proteins: $K10^+$, $Loricin^+$ [Lor], $Filaggrin^+$), which degrade their organelles. Finally, the outermost cornified layer (*stratum corneum*) contains dead, flat keratinocytes mainly consisting of fibrous structural proteins [3] (Figure 1).

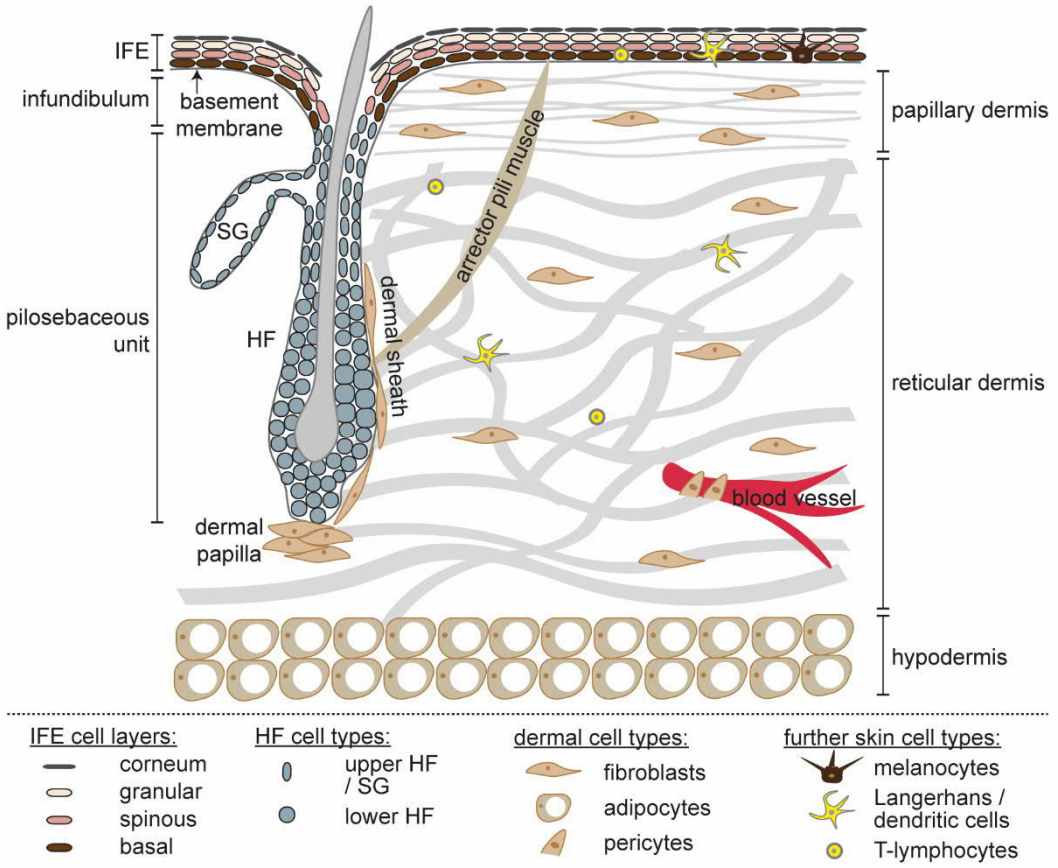

Figure 1. Schematic representation of mammalian skin with its containing cellular epidermal and dermal sublayers and populations.

The interfollicular epidermis (IFE) is interspersed with the pilosebaceous unit that comprises a hair follicle (HF), its associated sebaceous gland (SG) and the arrector pili muscle. The basement membrane separates the upper epidermal part from the lower dermal and hypodermal parts. The dermis consists of the papillary dermis, the reticular dermis, the dermal sheath and the dermal papilla. Collagen fibres of the dermis are shown in grey.

In humans two major skin types can be distinguished: the thick, hairless skin of the palms, soles and palmar surface of the digits with high numbers of *stratum corneum* layers and a *stratum lucidum* between the *stratum granulosum* and *stratum corneum*, and the thin, hairy skin of the rest of the body [3]. Human IFE forms a characteristic pattern of dermal projections up into the epidermis (dermal papillae) and alternating deep epidermal ridges (rete ridges), which extend downwards [4, 5]. The invaginations of the rete ridges increase the surface area of the epidermal-dermal junctions, a means of increasing the mechanical strength of the skin [6] and of the capillary-epidermal interface to improve the nutrient supply in the epidermis [7].

In contrast to human skin, the hairy dorsal skin of mice is much thinner (Table 1). However, due to the fact that murine tail skin contains more epidermal cell layers and fewer hair follicles (HF) than dorsal murine skin [8], it closely resembles human skin und thus can be used as a model for human body skin (Table 1). The IFE of murine tail skin is subdivided into HF-near IFE (interscale IFE) and interspersed IFE (scale IFE). While both interscale and dorsal IFE of mice undergo orthokeratotic differentiation, which is characterised by the presence of a granular layer, loss of nuclei in the cornified layers and expression of filaggrin, K10 and K2 [9],

the scale IFE differentiates in a parakeratotic manner with a lack of the granular layer, the presence of nuclei in the cornified layers and expression of K31 [9]. The orthokeratotic differentiation is histologically similar to that of normal human epidermis, whereas parakeratosis is seen in epidermal diseases of increased cell turnover (e.g. psoriasis).

Table 1. Characteristics of human and murine epidermis.

Characteristic	Human skin	Murine tail skin	Murine dorsal skin
Hair coat	Hairless	Hairless (HF arranged in triplets)	Hairy
Nucleated cell layers [8]	5.5	6.5	4
Cornified cell layers [8]	10	32	6
Structure of the IFE	Rete ridges [4, 5]	Scale and interscale [9]	-

1.1.2 The pilosebaceous unit

The IFE of human and murine skin is interspersed by pilosebaceous units each composed of a HF, sebaceous gland(s) (SG) and an arrector pili muscle responsible for piloerection. Sweat glands are not associated with the pilosebaceous units [10]. The connection between the IFE and HF is termed the infundibulum and has been described to be a subpopulation of IFE cells in an IFE-like structure, although infundibulum cells express low levels of HF marker genes [11]. The HF itself consists of eight different epithelial layers with different protein marker expression patterns. Starting from the periphery, these layers are the outer root sheath (ORS) (marker protein: $K5^+$), the companion (Cp) layer (marker proteins: $K6^+$, $K75^+$), the inner root sheath (IRS) that consists of the Henle's layer (marker protein: AE15[1]/$TCHH^+$), Huxley's layer (marker proteins: AE15/$TCHH^+$, GATA-3^+), IRS cuticle (marker proteins: AE15/$TCHH^+$, GATA-3^+) and the hair shaft (HS), which comprises the hair cuticle (marker protein: AE13[2]/$K40^+$), cortex (marker protein: AE13/$K40^+$) and medulla (marker proteins: AE15/$TCHH^+$, $K6^+$) [12]. The HS is composed of terminally differentiated, dead keratinocytes and supports physical protection, thermal insulation, camouflage, dispersion of sweat and sebum, sensory and tactile functions and social interactions [13]. The HS pigmentation, which acts as protection against UV irradiation and provides camouflage, is formed by the melanin-producing HF melanocytes [14]. Based on the developmental time point, the microanatomy and structure, four different hair types can be classified in the murine skin: guard, awl, auchene and zigzag hair [13]. Guard hairs, the largest and least abundant hairs (1-3%) [15, 16], are straight, have two rows of medulla cells and are usually associated with a pair of SG [17]. Awl and auchene

[1] AE15 antibodies detect trichohyalin (TCHH)
[2] AE13 antibodies detect K40

hairs are shorter but thicker than guard hairs and have two or more rows of medulla cells [16]. Auchene hairs differ from awl hairs only in having a single bend about midway along the hair and are thus rarely considered as a distinct type of hair [17, 18]. Awl hairs make up around 30% of the hair coat, whereas auchene hairs form only a minor fraction with a frequency of about 0.1% [15]. The most abundant hairs of the murine fur are zigzag hairs (65-70%) or undercoat hairs. These are the thinnest and shortest hairs and have only one row of medulla cells but several constrictions along the HS, forming three to four bends alternately pointing in opposite directions [15, 16]. Hair is densely innervated by sensory nerve fibres and the described hair types (guard, awl/auchene and zigzag) were shown to activate different nerve fibres, which might represent functional differences [19, 20].

In humans, the very fine, non-pigmented, downy lanugo hair covers the body of the foetus during development [3]. Prior to birth, terminal hairs for the eyebrows, eyelashes and scalp and vellus hairs for the rest of the body replace the lanugo hair [3]. Vellus hairs are short (< 2 cm), thin (diameter: < 30 mm), extend just 1 mm into the dermis and are often unpigmented, whereas terminal hairs are long (> 2 cm), thick (diameter: > 60 mm), extend more than 3 mm into the dermis and are pigmented [21]. At puberty, terminal hairs replace vellus hairs (in the armpits and pubic regions; for boys also in the face, limbs and chests), resulting in a distribution of 95 or 35% terminal hairs and 5 or 65% vellus hairs in adult males or females, respectively [3].

1.1.3 The dermis

The mammalian dermis contains several immune cell types (e.g. dendritic cells, T-lymphocytes) but is mainly composed of fibroblasts (marker proteins: platelet derived growth factor receptor alpha$^+$ [PDGFRα], PDGFRβ^+, CD90$^+$). The dermis is classified into the upper papillary dermal layer, the intermediate reticular dermal layer, the HF-associated dermal papilla (DP) and dermal sheath (DS) and the lowermost hypodermis (Figure 1). The papillary layer is close to the basement membrane and contains a high cell density and thin collagen fibres, whereas the reticular dermis that connects the papillary layer with the dermal white adipose tissue of the hypodermis is characterised by thick collagen fibres, a lower cell density [10] and the production of fibrillary ECM [22] (Figure 1). The fibroblasts of the DP at the base of each HF are densely packed and interact with neighbouring epithelial cells during HF formation and regeneration [10], whereas DS fibroblasts surround the HF from the bulge region downwards to the DP (reviewed in [23]). Both the DP and DS are separated from the epithelial HF cells by the interjacent basement membrane (reviewed in [23]) (Figure 1). However, DS fibroblasts are able to regenerate a new DP after its loss and hence are thought to serve as a cellular reservoir of DP cells (reviewed in [23]). Finally, the lowermost hypodermis consists of

adipocytes, fibroblasts and macrophages and contains loose connective tissue, elastin, blood vessels and nerves.

1.2 Development, homeostasis and repair of mammalian skin

1.2.1 The development of mammalian skin

During the development of mammalian skin the epidermis derives from the ectoderm, whereas the dermis arises from the mesoderm [3]. Shortly after gastrulation (in humans: ~4th week after fertilisation [3]; in mice: at embryonic day [E] 9.5 [24]), the epidermal component of the embryonic skin is composed of a single layer of unspecified progenitor cells (marker proteins in humans and mice: K5^{+}, K14^{+}) in which cell divisions mostly occur laterally. Starting from the 7th gestational week in humans and from E12.5-15.5 in mice, most epidermal cell divisions are oriented perpendicularly to the basement membrane leading to stratification of the epidermis [3, 25]. At the 11th week of human embryogenesis, the characteristic epidermal rete ridges form, fibroblasts migrate and start to produce ECM, generate dermal protrusions and develop dermal papillae [3]. In mice, the structure of the dermis becomes distinguishable at E18.5, after fibroblast progenitors have developed either to differentiated fibroblasts of the papillary dermis, the DP and the arrector pili, or to fibroblasts of the reticular dermis and the adipose tissue of the hypodermis [22].

The formation of HF depends on the interplay of epidermal placode cells (thickened ectodermal tissue) and underlying dermal cells via wingless-related integration site (WNT), Hedgehog (HH), notch and bone morphogenetic protein signalling. Upon surrounding of the placode cells by dermal cells, a hair germ or bud is formed. The hair bud then proliferates and invaginates into the dermis to form the hair peg, which surrounds the DP to form a functional HF. Besides, also SG develop from their respective precursors [26]. The development of murine hair occurs between E14.5 to E18.5 (guard: E14.5; awl, auchene: E16.5; zigzag: E18.5) [27]. In humans, HF develop from the 12th week after fertilisation and lanugo hairs are produced at the 5th month of embryonic development [3].

During development, skin SC receive cues from their environment, which instruct them to commit to a certain differentiation programme and generate either stratified epidermis or placode cells resulting in HF and SG. Skin SC that cluster together and form hair buds already express HF SC marker genes (e.g. *sex-determining region Y-Box* [*Sox*] *9*, *leucine-rich repeat-containing G-protein coupled receptor* [*Lgr*] *6*, *leucine rich repeats and immunoglobulin like domains* [*Lrig*] *1*, [28-31]), which are also detectable in mature HF SC niches (see chapter 1.2.5). After birth, the skin - more than any other organ - is strongly exposed to several different environmental influences (e.g. radiation, injuries). Thus, the epidermis, which is the essential protection barrier of the body against environmental stressors, is constantly renewed,

guaranteed by epidermal SC. So far, diverse epidermal SC populations have been unravelled that maintain the skin barrier and contribute to healing after injuries (see chapter 1.2.5.1). However, the mechanism of IFE homeostasis is still far from clear, although two general concepts have been proposed.

1.2.2 Concepts of stem cell mediated homeostasis of the interfollicular epidermis

The homeostasis of the IFE is closely linked to the maintenance of the epidermal SC pool, which is regulated by various signalling molecules (e.g. Notch, mitogen-activated protein kinase and the transcriptional regulator transformation-related protein [Trp] 63/tumour protein [Tp] 63 [32]). As observed in all SC, epidermal SC also differ from their progeny by their ability to self-renew and to generate differentiated cell types directly or through terminal divisions. Furthermore, a long living, slowly cycling cell state (quiescence) is proposed as an additional SC characteristic. However, a balance between proliferation and differentiation of SC is essential for tissue homeostasis [33]. In general, two SC self-renewal strategies are conceivable to maintain tissue homeostasis: asymmetric cell division (hierarchical model) and population asymmetry (stochastic model) [34] (Figure 2). A SC undergoing asymmetric cell division gives rise to two daughter cells of unequal fates: one daughter SC that stays in the SC niche and one committed daughter cell (transit-amplifying cell, TAC) that rapidly proliferates and finally differentiates (into a keratinocyte) (Figure 2). In contrast, within the population asymmetry model a SC can undergo asymmetric cell division to one daughter SC and one differentiated cell (keratinocyte) or symmetric cell division to two SC or two differentiated cells (keratinocytes) (Figure 2). In the population asymmetry model a proliferation/differentiation balance is achieved at the level of the whole SC population, since some SC get lost through differentiation, whereas others self-renew. In this model, the loss of a single SC and their stochastical replacement by a neighbour SC is termed neutral competition (stochastic model) [35].

Keratinocytes of the basal layer are highly proliferative and tend to migrate to the skin surface, where they differentiate and lose their transcriptional activity until finally becoming dead, flattened keratinocytes without cell nuclei forming the *stratum corneum* [31]. The differentiation of a basal cell and its migration to the skin surface, where it may be sloughed, takes about 8 to 9 days in murine dorsal skin and 4 weeks in adult primate skin [36, 37]. To date, the identity of IFE SC, including their characteristic features and marker expression compared with other cells of the basal layer, is still far from clear (see chapter 1.2.5). Until 2007, the hierarchical model was thought to resemble the behaviour of basal cells during epidermal homeostasis. However, Clayton and colleagues then convincingly demonstrated that only one type of progenitor cell, which undergoes symmetric and asymmetric cell divisions, is responsible for

epidermal homeostasis in mice and thus the concept of population asymmetry seems to more precisely describe the behaviour of basal cells in this process [38]. Moreover, they showed that the continual loss of clones is compensated by an expansion in the size of the neighbouring clones [38].

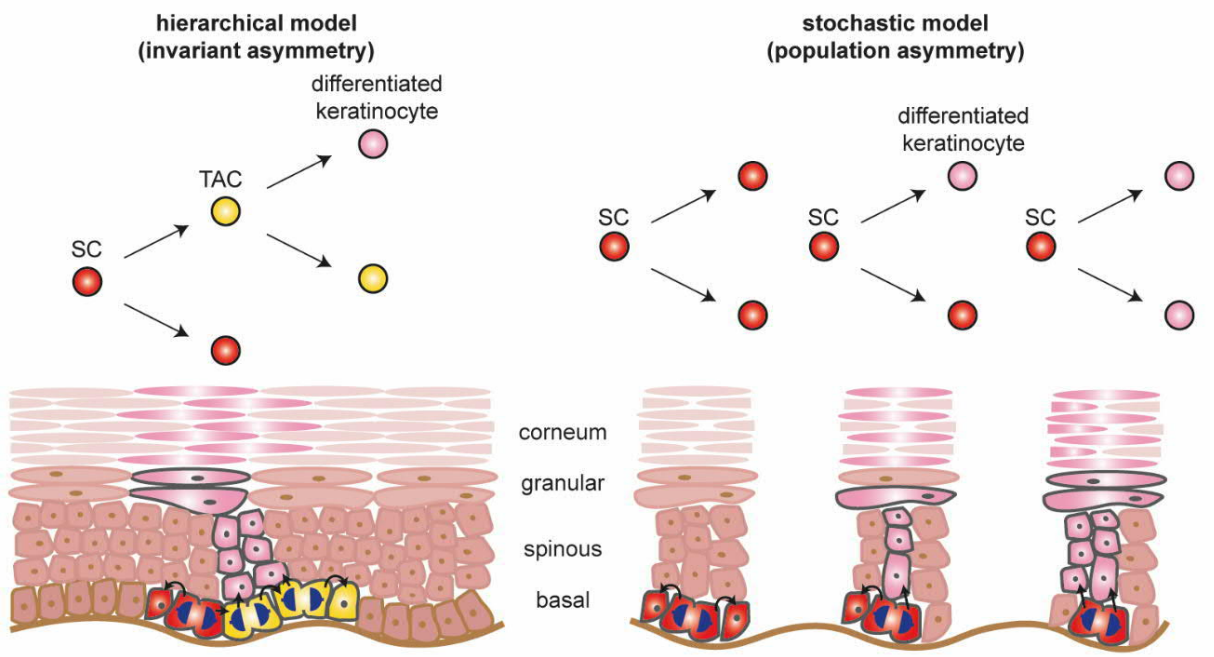

Figure 2. The hierarchical and the stochastic model of epidermal homeostasis.

The invariant asymmetry or the hierarchical model (left) suggests that a self-renewing stem cell (SC) (red) gives rise to transit amplifying cells (TAC) (yellow), which then divide into a further TAC and a differentiated keratinocyte (pink). In the population asymmetry or the stochastic model (right), cell divisions of SC result in one of three possible outcomes: two daughter SC, one daughter SC and one differentiated daughter keratinocyte, or two differentiated daughter keratinocytes, respectively. In the stochastic model, these divisions occur in a stochastic (random) manner. Reviewed in [39].

1.2.3 The hair cycle — assembly and disassembly of hair follicles

In contrast to the continual renewal of the IFE, which requires the constant activity of basal cells, the SC of the HF (see chapter 1.2.5) are activated in a cyclical manner as the HF passes continuously through cycles of growth (anagen), regression (catagen) and resting (telogen) of its lower two-thirds (Figure 3). The ‘permanent’ upper part comprises the bulge region and the upper HF (uHF). The uHF includes the isthmus, junctional zone (JC) and the SG. The ‘cycling’ lower part contains either a long stretch of suprabulbar HF epithelium (lower HF) and the bulb region in the anagen or the secondary hair germ (sHG) in the telogen phase [13] (Figure 3). At the onset of anagen HF SC of the bulge region are activated and start to proliferate (‘bulge-activation hypothesis’, [40]). After cell division, offspring of bulge SC migrate to the base of the HF (bulb region), where they are proliferatively active as so-called matrix cells. These matrix cells are able to differentiate into seven layers of the HF: the Cp layer, the IRS (Henle’s layer, Huxley’s layer, IRS cuticle) and the HS (medulla, cortex, hair cuticle) [41, 42].

During anagen progression, HF with its associated DP extend downwards into the dermis and hypodermis and reach its maximal length in late anagen (Figure 3). Noteworthy, the anagen phase is commonly divided into six subphases, termed I to VI [41]. During the early anagen (I-II), the HF is only distinguishable from telogen HF by an extended sHG, whereas in anagen III the hair bulb that engulfs the DP is formed. In anagen III to VI, matrix cells form the IRS and HS and in anagen VI the HS tip emerges through the epidermis. Anagen progression is also associated with characteristic changes in skin pigmentation and thickness noticeable by black skin colour and thickened skin in mice [41]. During catagen, matrix cells and lower ORS and IRS cells become apoptotic; hence, the HF shrinks by its lower two-thirds (Figure 3). In contrast, bulge HF SC escape apoptosis. Usually, the old HS (club hair) remains even after a new HS is formed [41, 42]. Next, HF cells become quiescent during telogen, therefore telogen HF are characterised by their minimal length. Moreover, murine telogen skin becomes thin and less pigmented than anagen skin, resulting in a pink skin colour [41]. The telogen phase can be divided into a refractory phase with quiescent, unresponsive HF SC of the bulge region and a competent phase in which bulge SC become sensitive to anagen-inducing factors [43]. Remarkably, during late telogen, sHG SC are activated and proliferate several days before bulge cells and are the major contributors to the first stage in HF regeneration [44, 45]. *In vitro* analyses indeed verified that sHG SC proliferate sooner, but are shorter-lived than bulge SC [44]. It is to be noted that for initiation of a new hair cycle the DP is essential since HF without DP are unable to re-enter the hair cycle [46]. Similarly to skin development [27], Sonic HH and Wnt signalling are essential for HF SC proliferation and anagen entry, whereas Notch (similar to IFE stratification) and later on bone morphogenetic proteins promote differentiation [32, 47]. Alterations in these signalling pathways have a critical impact on HF formation, for instance *sonic HH* knockout (KO) mice (with reduced HH-target activation, see chapter 1.3.3.1) show a diminished number of HF and a reduced keratinocyte proliferation rate that prevents the downward growth of epithelial cells during the hair cycle [48, 49]. The other way around, supra-physiological activation of HH signalling leads to *de novo* HF formation in adult murine unwounded skin, unravelling the important role of active HH signalling for HF formation [50].

The duration of the hair cycle phases differs between human and murine HF (Table 2). HF cycling of human skin and murine tail skin becomes asynchronous soon after birth [43, 51-53], whereas in murine dorsal skin the hair cycles are highly synchronised (during the 1st and 2nd hair cycle phase), but become increasingly asynchronous with age [41]. HF cycling of murine dorsal skin slows down in ageing mice as the duration of the telogen phase expands [41]. For experimental purposes, the depilation-induced synchronisation of HF cycling is commonly used to facilitate the analysis of certain hair cycle phases in adult mice [41]. Depilation immediately induces anagen development followed by catagen and telogen in a homogeneous

manner [41]. Nevertheless, it should be noted that a slight inflammatory effect following plucking has been reported [54].

Table 2. Duration of the different hair cycle phases of human and murine hair.

Hair type	Anagen (growth)	Catagen (regression)	Telogen (rest)
Human scalp hair [21]	3-5 years	10 days	3 months
Murine dorsal hair [41]	1-3 weeks	2 days	4-5 weeks

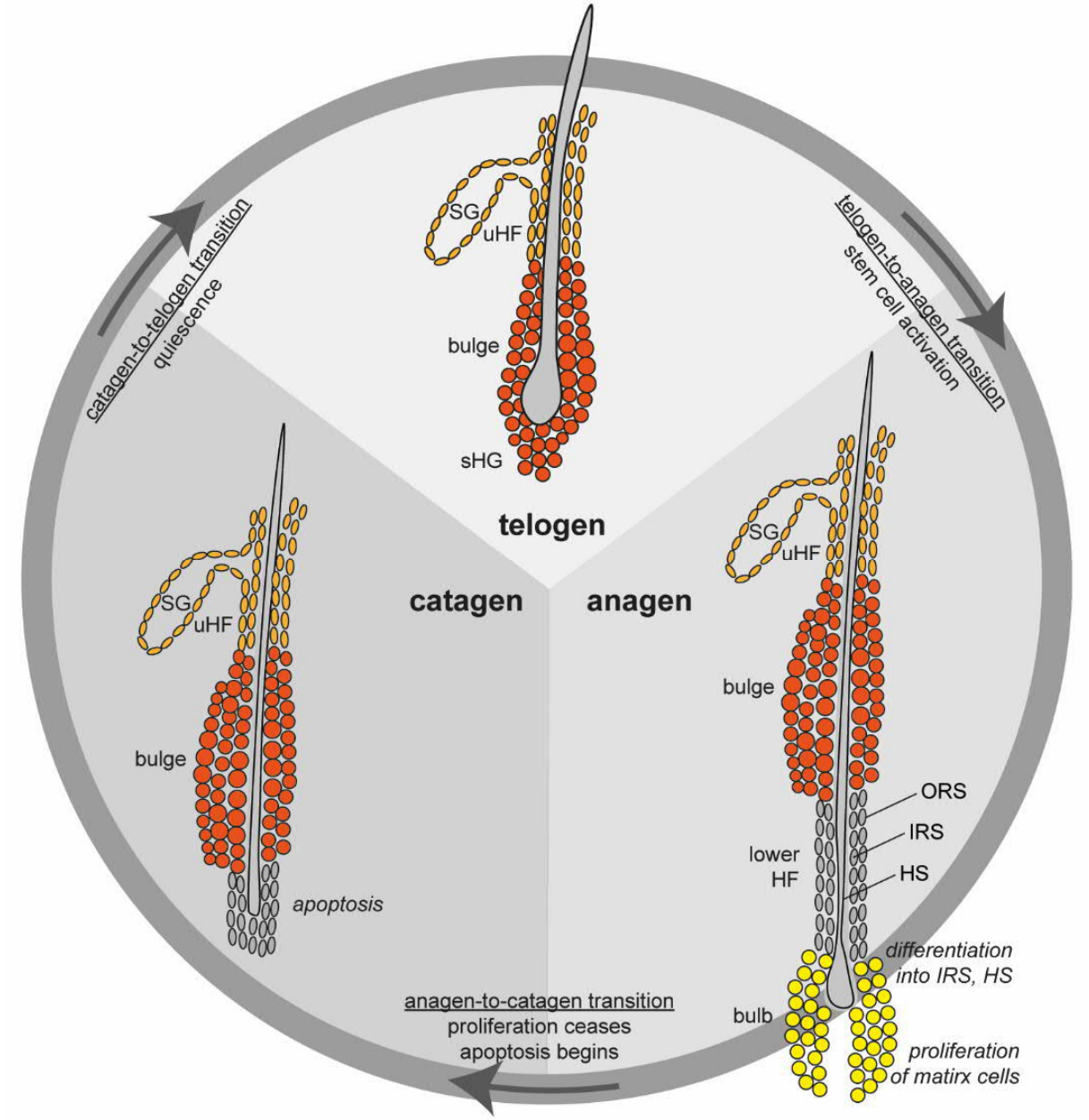

Figure 3. The hair cycle.

Hair follicles (HF) pass cycles of growth (anagen), regression (catagen) and resting (telogen). During the telogen-to-anagen transition, HF stem cells (SC) are activated. After migration, they proliferate in the bulb as matrix cells and subsequently differentiate into suprabasal cells of the inner root sheath (IRS) and hair shaft (HS). During the anagen-to-catagen transition, proliferation diminishes and the lower HF part becomes apoptotic. In the telogen phase, the HF becomes quiescent until HF SC are activated again and a new hair cycle starts. Abbreviations: ORS: outer root sheath, sHG: secondary hair germ, SG: sebaceous gland, uHF: upper HF.

1.2.4 Wound healing as restoration of the barrier function of the skin

Destruction of the skin barrier function by injury induces a complex program involving immune cells, fibroblasts and endothelial and epidermal cells to immediately regenerate the skin. The wound healing process can be subdivided into three distinct, overlapping phases: inflammation, proliferation and remodelling. Directly after tissue damage, a blood clot consisting of platelets is formed, followed by the generation of a fibrin matrix that prevents excessive blood loss [55]. Next, immune cells (e.g. neutrophils, macrophages and lymphocytes) are recruited to the wound to prevent an infection [55]. Macrophages assist in the transition from the inflammation to the proliferation stage by releasing growth factors and chemokines (e.g. platelet derived growth factor [PDGF], fibroblast growth factor [FGF], vascular endothelial growth factor [VEGF] and transforming growth factor [TGF] -α and -β) [56]. Within the subsequent proliferation phase, these factors induce migration of wound-adjacent keratinocytes to the wound edges (migratory zone), proliferation of keratinocytes behind the leading edge (proliferative zone) and matrix formation [56-58] leading to epidermal re-epithelialisation [55]. Dermal repair is achieved by TGF-β signalling, which stimulates the differentiation of fibroblasts to activated myofibroblasts (marker protein: alpha smooth muscle actin$^+$ [α-SMA]) [59, 60]. Reticular fibroblasts are involved in the initial wound healing process, whereas papillary fibroblasts are recruited only during later re-epithelialisation [22]. The last phase of wound repair, the remodelling phase, starts 2-3 weeks after injury and can last for more than a year in mammals. Redundant cells, including endothelial cells, macrophages and myofibroblasts, either undergo apoptosis or leave the wound. Finally, the re-epithelialized wound is slightly higher than the surrounding epidermis and the dermis consists of collagen and further ECM proteins at the wounded side. However, wound remodelling in humans and mice does not result in a complete regeneration since a scar tissue is formed at the healed region [60]. Noteworthy, murine skin contains a thin muscle layer (*panniculus carnosus*), which is only found in the platysma of the neck in humans and which assists in rapid wound contraction following injury and thereby enables faster wound healing compared to the process in human skin [61]. Although HF formation occurs mostly during foetal and perinatal skin development, *de novo* HF formation has also been described during wound healing in adult murine skin [13]. Nevertheless, this wound-induced HF neogenesis is only observed in large (> 1 cm in diameter) excisional wounds (removal of larger areas of skin) and resembles HF embryonic development [62]. Although wound-induced HF neogenesis has been reported in a few patient cases in humans, it is a rare phenomenon and wounds in humans do not undergo large scale, clinically obvious *de novo* hair regeneration [63, 64].

1.2.5 Stem cells of the skin: their niches and roles in homeostasis and repair

1.2.5.1 Epidermal stem cells of the skin

In mice, different epidermal SC populations have been identified and especially the plasticity of SC of the HF compartment has been investigated intensively. In the lower part of the telogen HF (bulge and sHG) CD34$^+$/K15$^+$, Lgr5$^+$ and glioma-associated oncogene (Gli) 1$^+$ SC have been identified, whereas Lgr6$^+$, Lrig1$^+$ and B-lymphocyte-induced nuclear maturation protein (Blimp) 1$^+$ SC are located in the upper part of the HF (isthmus, JC and SG) [10] (Figure 4).

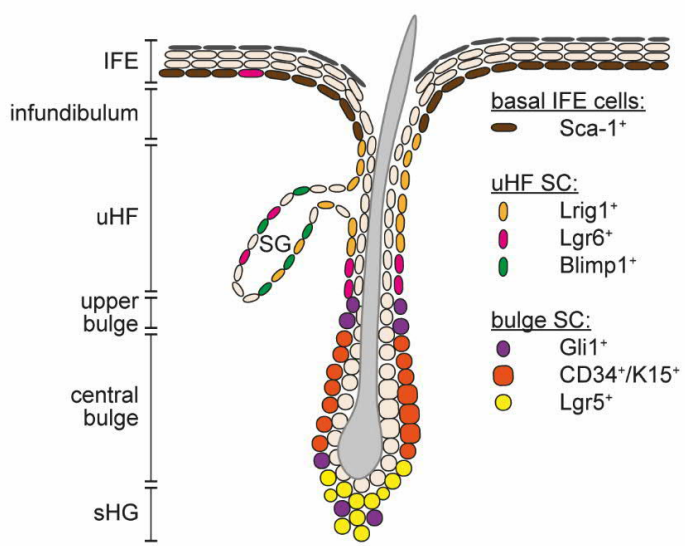

Figure 4. Schematic representation of stem cell populations including their key markers of the murine telogen hair follicle and its surrounding interfollicular epidermis.

The basal layer of the interfollicular epidermis (IFE) contains proliferative Sca-1$^+$ cells. The upper hair follicle (uHF) comprises Lrig1$^+$ stem cells (SC) in the junctional zone, Lgr6$^+$ SC in the isthmus and Blimp1$^+$ SC at the base of the sebaceous gland (SG). In the lower part of the HF, CD34$^+$/K15$^+$ bulge SC, Lgr5$^+$ lower bulge and secondary hair germ (sHG) SC and Gli1$^+$ upper and lower bulge and sHG SC can be found [10].

CD34$^+$/K15$^+$ SC of the central bulge region, Lgr5$^+$ SC of the lower bulge and sHG and Gli1$^+$ SC of the upper and lower bulge and the sHG give rise to all HF lineages (e.g. ORS, IRS, HS and matrix cells) during hair cycling demonstrating their SC identity [65-67]. Moreover, *in vitro* studies demonstrated a high colony-forming efficiency (CFE) for bulge (CD49f^{high}CD34^{high}) and sHG (Lgr5^{high}) populations [65, 68]. Furthermore, skin reconstitution assays have revealed the potential for CD34$^+$/K15$^+$ HF bulge cells to give rise to all epidermal lineages of the HF, SG and IFE after grafting [30].

In contrast to SC of the lower HF, Lrig1$^+$ JC and Lgr6$^+$ isthmus SC of the uHF maintain their own niche (JC/isthmus) but also contribute to SG maintenance [28, 69]. Besides, SG homeostasis is also sustained by Blimp1$^+$ SC at the base of the SG [70]. However, similar to SC of the bulge/sHG also SC of the uHF (Lrig1$^+$ JC and Lgr6$^+$ isthmus SC) can give rise to all epidermal lineages of the HF, SG and IFE in skin reconstitution assays [28, 30]. Tail skin of

Lrig1 KO mice exhibits epidermal hyper proliferation, indicating that *Lrig1* expression is required for balanced epidermal homeostasis [71]. Additionally, *in vitro* culture of *Lrig1*-deficient murine [30] or human [72] epidermal cells reveals a higher CFE potential and proliferation rate in comparison to that of wild type control cells. Contrarily, *Lgr6* KO mice do not show any obvious skin phenotype, neither during skin homeostasis nor upon wound healing [73].

For the evaluation of whether different HF SC populations contribute to IFE homeostasis, several cell-tracking studies in transgenic reporter mouse models have been conducted. Interestingly, $Lgr5^+$ SC of the lower bulge and the sHG and their progenies are restricted to the lower HF for up to a year after induction in *Lgr5-Enhanced green fluorescence protein (EGFP)-ires-CreER^{T2}* mice [69]. Another study using *Krt1-15-Cre* mice showed that $K15^+$ bulge SC and their progeny do not populate the IFE under normal homeostatic conditions over a 6-month period [74]. Similarly, in *Lrig1-EGFP-ires-CreER^{T2}* mice the progeny of $Lrig1^+$ SC persist in the uHF without migrating into the IFE up to a year after induction [69]. In contrast, $Lgr6^+$ SC and their offspring appear in the IFE 18 days after induction and stay for more than a year after induction in *Lgr6-EGFP-Ires-CreER^{T2}/R26R-LacZ* mice [28]. However, follow-up studies revealed the existence of a mosaic-like distribution of $Lgr6^+$ basal cells in the murine IFE [69, 73, 75] indicating that $LacZ^+$ cells of the IFE in this mouse model are more likely the offspring of $Lgr6^+$ basal cells than of $Lgr6^+$ SC of the uHF. Thus, these data suggest that neither SC of the lower HF (bulge, sHG) nor of the uHF (isthmus, JC, SG) contribute to IFE homeostasis.

In contrast to SC of the HF compartment, the identity of IFE SC in murine skin is less clear, although the basal layer is likely the IFE SC niche. It is disputed whether distinct SC populations indeed exist in the IFE, as single-cell transcriptome studies of murine epidermis did not find discrete basal layer SC populations [11, 76]. However, the basal layer contains non-quiescent, proliferating IFE cells ($CD49f^+CD34^{neg}$), which express the haematopoietic SC marker SC antigen-1 (Sca-1) [77] but possess a lower clonogenic potential compared to bulge ($CD49f^+CD34^+Sca\text{-}1^{neg}$) or uHF ($CD49f^+CD34^{neg}Sca\text{-}1^{neg}$) cells *in vitro* [78]. In skin reconstitution assays, $Sca\text{-}1^+$ ($CD49f^+CD34^{neg}$) basal IFE cells are involved in IFE epithelisation but also *de novo* HF formation can occur depending on the considered study [30, 78].

Although cells of the IFE contribute the most to tissue regeneration after injury [79], HF SC are able to leave their niche to participate in re-epithelisation and give rise to IFE cells during wound healing. Thus, the wound environment induces a downregulation of SC quiescence-associated genes and an upregulation of wound-induced stressors [80]. Subsequently, HF SC enter a transient state of ‘lineage infidelity’ characterised by a mixed HF/IFE molecular profile which switches completely after successful wound healing to an

epidermal identity [80]. For instance, after excisional wounding, bulge-derived cells migrate to the basal layer and express epidermal differentiation markers indicating a conversion into functionally differentiated keratinocytes of the IFE [74]. However, SC of the uHF contribute permanently and immediately to the wound epithelium and can form new HF (*Lgr6-EGFP-ires-CreER^{T2}/R26R-LacZ*) [28, 69], whereas SC of the bulge and/or the sHG are only involved during re-epithelisation, show a delayed contribution to wound healing and do not contribute to *de novo* HF formation (*Krt1-15-Cre*) [74, 81]. Remarkably, and similar to SC of the uHF, Gli1^{+} SC contribute permanently to early re-epithelisation [66].

While human HF also contain different SC populations which are located in the bulge region and in the sHG, human bulge/sHG cells do not express CD34 but rather express CD200, K15, K19 and/or Sox9 [82-85] (Figure 5). In resting HF CD200, K15 and K19 expression is restricted to the bulge and sHG (Figure 5), whereas in growing HF these markers are also expressed by cells of the lower ORS and bulb [83]. Although the localisation of the transcription factor (TF) Sox9 in resting HF is unclear, in growing HF Sox9 was most prominent in the ORS immediately below the human bulge [85]. However, it has been shown that CD200^{+} bulge cells grow as label-retaining cells (LRC) and possess a high CFE capacity [86]. K19^{+} bulge cells express higher levels of β1-integrin (ITGB1, CD29) than K19^{neg} ORS cells [87], indicating that CD29 serves as an additional bulge SC marker in human skin. Basal cells of the human IFE also express CD29 [88, 89]. In the foreskin, scalp and breast skin, these cells grow adjacent to the tips of the dermal papillae (Figure 5), whereas in palm and foot skin CD29^{high} cells are found at the rete ridges [87, 90]. CD29^{high} IFE cells possess higher CFE capacity compared to keratinocytes with low and intermediate CD29 expression [91]. Basal cells of the rete ridges also express the putative SC markers K15 [92] and Sox2 [93] (Figure 5). Additionally, high CD49f expression and low CD71 expression has been described for epidermal SC of the human IFE [94, 95].

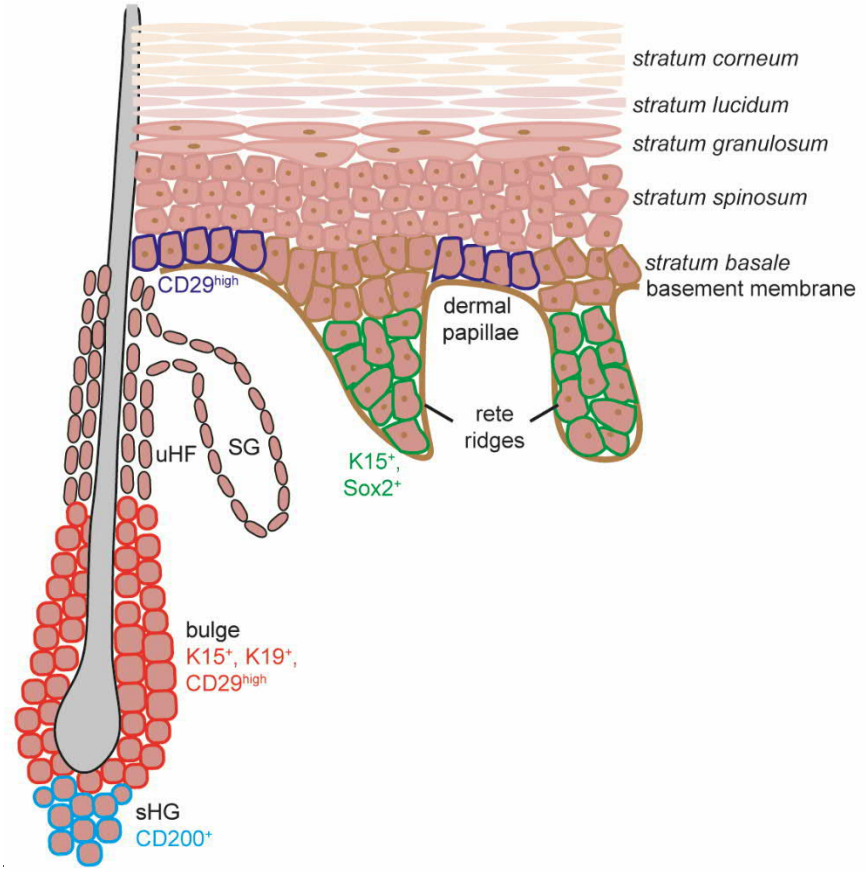

Figure 5. Schematic representation of stem cell populations including their key markers of the human telogen hair follicle and its adjacent interfollicular epidermis.

In human breast skin, the basal layer of the interfollicular epidermis contains $CD29^{high}$ stem cells (SC) at the dermal papillae, whereas $K15^{+}$, $Sox2^{+}$ SC can be found at the rete ridges. The hair follicle (HF) bulge contains $K15^{+}$, $K19^{+}$, $CD29^{high}$ SC and SC of the secondary hair germ (sHG) express CD200. Abbreviations: SG: sebaceous gland, uHF: upper hair follicle.

1.2.5.2 Mesenchymal stromal/stem cells of the skin

In addition to epidermal SC and fibroblasts, murine and human skin contains bone marrow (BM)-derived mesenchymal stromal/SC (MSC). Intriguingly, MSC have been shown to also contribute to skin maintenance especially after injury by differentiation into IFE and HF keratinocytes [96-101], SG cells [102], dermal fibroblasts, endothelial cells, pericytes [103], or myofibroblasts [104]. Although the frequency of the MSC contribution to the epidermal homoeostasis most likely remains below 0.0003% [105] or 0.14% [96], it is highly remarkable that epidermal keratinocytes can originate from $PDGFR\alpha^{+}$c-$Kit^{neg}Sca\text{-}1^{neg}$ BM-derived MSC [101]. Initially, BM-derived MSC were classified by their osteogenic differentiation potential [106], adherence to tissue culture vessels and fibroblast-like shape [107]. Moreover, they grow *in vitro* in discrete colonies initiated by single cells (colony-forming unit fibroblasts, CFU-F) [108]. To date, MSC are considered to be conceptual postnatal precursors of most, if not all, mesodermal cells [109], which have been isolated from almost all postnatal connective tissues (e.g. BM, fat tissue, dermis) [110-112] and can differentiate into mesodermal [109] and

non-mesodermal cells (e.g. epidermal cells, [96]). However, there is a considerable heterogeneity in the expression of cell surface markers in different MSC populations (depending on e.g. the tissue of origin or culture condition). Thus, the minimum criteria for the definition of MSC, which also apply for fibroblasts [113, 114], are: (1) they must be plastic-adherent under standard culture conditions; (2) ≥95% of cultured cells must be $CD105^+CD73^+CD90^+$ (human); or $CD90^+CD44^+CD29^+$ (murine), but must be negative for immune cell markers (lineage negative; Lin^{neg}); and (3) they must be able to differentiate *in vitro* into osteoblasts, adipocytes, or chondroblasts under standard conditions [115].

1.2.6 Skin ageing and skin cancer

SC of the skin are attractive targets of study for regenerative medicine, tissue repair and gene therapy due to their easy access and self-renewal capacities. For instance, transgenic epidermal SC were successfully used to regenerate the entire human epidermis to treat a seven-year-old child who suffered from a life-threatening form of the genetic disease junctional epidermolysis bullosa [116]. In this study, the authors made use of long-lived epidermal SC, which renew themselves while producing precursors that replenish terminally differentiated keratinocytes [116]. However, this impressive regenerative capacity of epidermal SC decreases with age (e.g. shown by a decreased CFE *in vitro* of keratinocytes from aged human donors [117] or aged mice [118] when compared to keratinocytes from younger individuals). Moreover, skin ageing is accompanied by a reduced number of skin SC, which is associated with thinning (atrophy), fragility, loss of elasticity, wrinkles, depigmentation, delayed wound healing and apart from that simultaneous accumulation of mutations in skin SC can lead to tumour development often observed in aged skin [3, 119, 120]. The most common age-related changes represent the loss of collagen and elastic fibres [121, 122] as well as decreased fibroblast numbers due to the reduced proliferation rate (cellular senescence) [123] in the dermis of aged skin. Beyond that, also basal cells of aged skin show cellular senescence which leads to a thinning of the epidermis and, additionally, weakening of the epidermis/dermis contact is observed due to changes of the hemidesmosomes (e.g. downregulation of collagen XVII) [124-128]. Furthermore, the total number of HF decreases with age whereas the proportion of HF remaining in the resting phase (telogen) increases [21]. Moreover, hair greying of older individuals is caused by the loss of melanocytes and melanocyte SC, which may also occur subsequent to acute stress events [129-131]. Besides, also extrinsic factors, especially solar UV radiation, play an important role during skin ageing, since UV radiation impairs the differentiation process of epidermal keratinocytes leading to a thicker epidermis [124, 132], in contrast to the thin epidermis of light-protected aged skin. Although UVA radiation penetrates the skin deeper than UVB rays, the latter is responsible for most of the tissue damaging processes, such as the production of oxygen-free radicals, which disrupt collagen

and elastic fibres [3]. Moreover, life-long exposure to solar or artificial UV radiation results in increased deoxyribonucleic acid (DNA) damage in cells of older skin leading, in combination with the weaker immune response of older skin [3], to a higher susceptibility to pathological conditions like skin cancer [133]. Tumours of the skin are classified into melanoma that derive from melanocytes, and non-melanoma skin cancer, which arise from keratinocytes [133]. The latter tumour group is subdivided into basal cell carcinoma (BCC), which develop from basal cells of the IFE and/or from HF SC and squamous cell carcinoma (SCC) that arise from squamous cells of the epidermis.

BCC represent the most common type of skin cancer [134]. They only rarely metastasize but their growth leads to tissue damage [135]. Most BCC occur sporadically, however, patients suffering from the rare heritable nevoid basal-cell carcinoma syndrome (or Gorlin syndrome) develop multiple BCC. The Gorlin syndrome is caused by a heterozygous mutation of the HH receptor and tumour suppressor gene *PATCHED* (*PTCH*) [136]. Interestingly, *PTCH* is also mutated in ~50% of all sporadic BCC [137] or even shows a loss of heterozygosity in 75% of *PTCH* mutated BCC [138] (reviewed in [139]). It is to be noted that also other signalling pathways are involved in BCC tumourigenesis, including *TP53* mutations [140] and alterations in the canonical Wnt/β-catenin pathway [141, 142] and in the epidermal growth factor (EGF) receptor signalling pathway [143]. Currently, the treatment of choice for BCC patients is surgical tumour excision. However, precise knowledge about the genetic and molecular events involved in BCC development helps to improve less invasive treatment strategies (e.g. photodynamic therapy, or application of the immune response modifier imiquimod or the HH signalling inhibitor vismodegib).

1.3 CD4 - more than an immune cell receptor

1.3.1 The CD4 receptor

The CD4 protein gained fame during the 1990's, when its role in human immunodeficiency virus (HIV) infection of T-lymphocytes was unravelled [144, 145]. Besides, it is a well-known co-receptor of the T cell receptor (TCR) on T-lymphocytes during major histocompatibility complex (MHC) class II-mediated stimulation. The recognition of MHCII-presented antigens by the CD4 protein and the TCR/CD3 complex results in T-lymphocyte activation, characterised by increased cytosolic calcium (Ca^{2+}) levels, TF activation, the enhanced production of cytokines and massive proliferation (Figure 6).

In the human genome, the *CD4* gene consists of 11 exons encoded on chromosome 12 (12p13.31), whereas the murine *Cd4* gene only contains 10 exons encoded on chromosome 6 (6 F2; 6 59.17 cM). The CD4 protein is composed of 458 (human) or 457 (mouse) amino acids (molecular weight: 51.5 kDa) and acts as a membrane-bound glycoprotein that consists

of four extracellular immunoglobulin-like domains (D1-D4), a transmembrane domain and a cytoplasmic segment [146]. The human and murine CD4 proteins are 56% homologous (extracellular immunoglobulin-like domains: 50-57% homology, transmembrane domain: 52% homology, cytoplasmic segment: 80% homology [146]). Functional binding sites are found across the extracellular part: the D1 domain binds to the MHCII [147] and to the HIV glycoprotein 120 [148], the D3 domain binds to the TCR [149] and the D4 domain binds to interleukin (IL)-16 [150] and is essential for CD4 dimerisation [151].

During antigen recognition required for T-lymphocyte activation, the TCR and the CD4 co-receptor simultaneously bind to the same antigen presenting MHCII molecule (Figure 6) (reviewed in [152] and [153]).

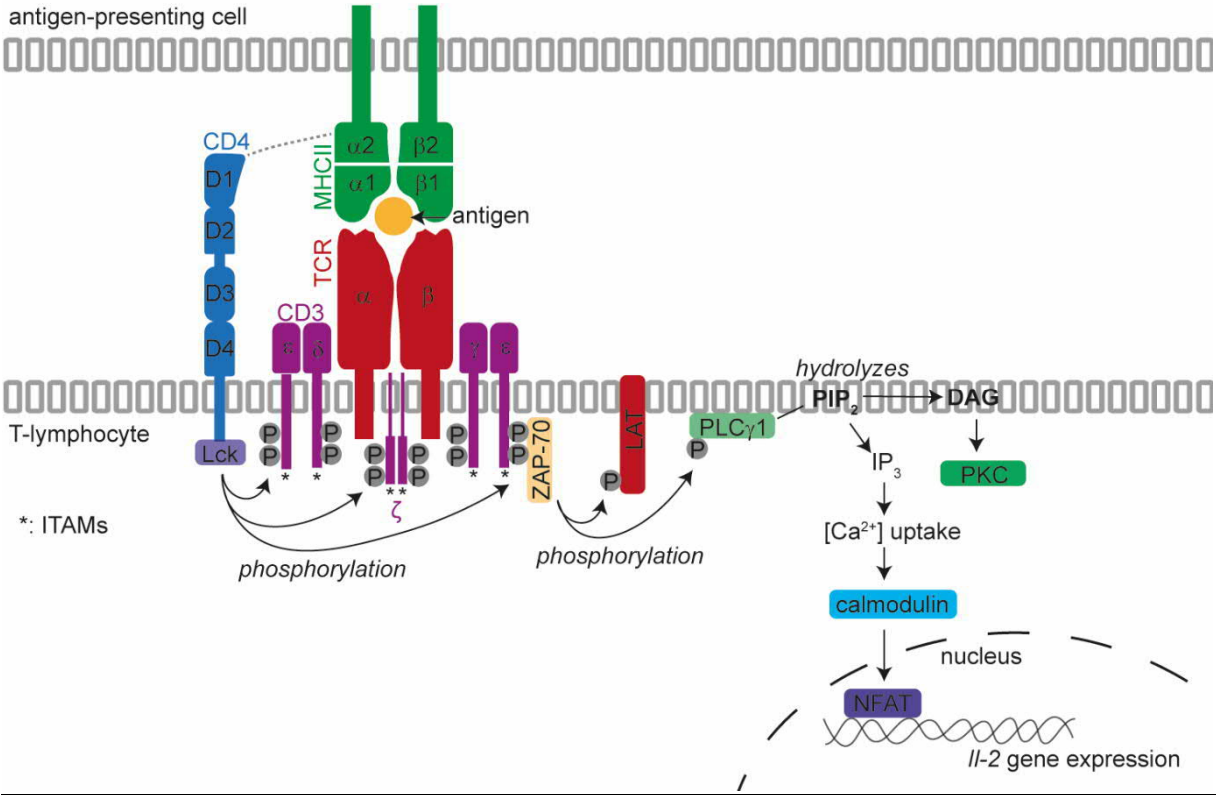

Figure 6. The CD4 co-receptor in MHCII/TCR/CD3-mediated T-lymphocyte activation.

Upon MHCII-presented antigen recognition, the CD4 co-receptor associates with the T cell receptor (TCR)/CD3-ζ complex and localises the lymphocyte-specific protein tyrosine kinase (Lck) in the proximity of the tyrosine-based activation motifs (ITAMs) of the CD3 receptor and on the ζ-dimer. After phosphorylation zeta-chain-associated protein kinase 70 (ZAP-70) binds and phosphorylates linker of activated T cells (LAT) and phospholipase Cγ1 (PLCγ1). LAT recruits additional signalling molecules, while PLCγ1 hydrolyses phosphatidylinositol biphosphate (PIP_2), which produces diacylglycerol (DAG) and 1,4,5-inositol triphosphate (IP_3). DAG activates protein kinase C (PKC), whereas IP_3 induces calcium (Ca^{2+}) increase in the cytosol. These elevated intracellular Ca^{2+} levels result in enhanced binding and thus activation of the calcium-binding protein calmodulin, which finally induce the nuclear import of nuclear factor of activated T cells (NFAT) leading to enhanced transcription of the interleukin-2 (*Il-2*) gene. Modified from [152].

The TCR then associates with the CD3 protein, a receptor with intracellular tyrosine-based activation motifs. Simultaneously, the CD4 interacting cytoplasmic lymphocyte-specific protein

tyrosine kinase (Lck) phosphorylates the intracellular tyrosine-based activation motifs of the CD3 protein. This results in the binding and activation of zeta-chain-associated protein kinase 70 and the phosphorylation of linker of activated T cells (LAT) and phospholipase Cγ1 (PLCγ1). LAT in turn recruits additional signalling molecules with Src homology 2 motifs, while PLCγ1 hydrolyses phosphatidylinositol biphosphate, which leads to the production of diacylglycerol and 1,4,5-inositol triphosphate. Diacylglycerol activates protein kinase C and 1,4,5-inositol triphosphate induces Ca^{2+} mobilisation into the cytosol, which results in enhanced binding and activation of the calcium-binding protein calmodulin. Calmodulin activates the serine/threonine phosphatase calcineurin, which induces the nuclear import of the TF nuclear factor of activated T cells and thus the nuclear factor of activated T cells-mediated transcription of *Il-2*. Finally, IL-2 promotes the proliferation and differentiation of T-lymphocytes into effector and memory T-lymphocytes.

Apart from T-lymphocytes also other haematopoietic cells including monocytes, dendritic cells and brain microglia express CD4 [154]. However, $CD4^+$ monocytes lack expression of CD3 and Lck [155, 156], indicating a TCR/CD3-independent signalling function of the CD4 receptor. Indeed, MHCII-binding to CD4 on human monocytes triggers cytokine expression, Ca^{2+} flux and differentiation into functionally mature macrophages [157, 158], and TCR-independent CD4/MHCII-engagement in T-lymphocytes induces Ca^{2+} mobilisation from intracellular stores [159]. These data demonstrate that the physiological function of the CD4 molecule is not restricted to TCR/CD3-dependent T-lymphocyte activation but may also regulate other TCR/CD3-independent processes.

1.3.2 Non-haematopoietic $CD4^+$ cells

In the context of HIV research CD4 expression was also unravelled on non-haematopoietic cells such as on BM-derived MSC and stromal cells of the lung. These and more recent analyses revealed *CD4* transcript and/or CD4 protein expression in human embryonic and foetal lung fibroblast cell lines (embryonic: L132; foetal: MRC5) [160], fibroblast cell lines from cancerous and fibrotic human lungs [161], primary isolated human BM-derived MSC, the human BM stromal cell line BL, human foreskin fibroblasts [162] and human vascular wall-derived MSC [163]. Together with the fact that lung fibroblasts of HIV-patients are also HIV-infected [164] and embryonic [165] and foetal lung fibroblasts [160] as well as human BM-derived MSC [162] are susceptible to HIV infection, although no surface CD4 protein was detectable, it was suggested that small numbers of surface CD4 protein are sufficient for HIV entry. On the other hand, numerous non-haematopoietic cell lines, which do not express CD4, are susceptible to HIV infections, albeit high numbers of virus particles are needed for an actual infection [166]. However, the results of studies which have utilized monoclonal anti-CD4 antibodies for the purpose of inhibiting CD4-based HIV entry were different. HIV infection of

embryonic [165] and foetal lung fibroblasts [160] was inhibited, whereas glioma [167, 168] and hepatoma [169] cells were still infectible in the presence of anti-CD4 antibodies.

Similar to humans, matrix fibroblasts of the murine lung and, additionally, alveolar epithelial cells of the murine lung express *Cd4* transcripts during embryonic development [170, 171]. Interestingly, *Cd4* expression occurred at distinct developmental time points: at E12.5, E18.5 as well as 1 and 7 hours postnatally and in 7-day-old mice, whereas no *Cd4* expression was detected in E16.5, E19.5, 6, 10, 16, 30 and 40 hours postnatally or in 8-week-old mice [170, 171]. Moreover, a single cell transcriptome analysis of approx. 2 x 10^6 cells derived from 61 embryos staged between E9.5 and E13.5, demonstrated *Cd4* expression in various non-haematopoietic cells, including stromal cells and epithelial cells (Appendix A, Appendix B) [172]. Furthermore, several lineage-tracing analyses using the *CD4Cre* driver mouse line revealed that various cell types descend from cells with *CD4Cre* activity, including alveolar macrophages as well as bronchial and alveolar epithelial cells of the lung [173], smooth muscle cells of myocardial blood vessels [173] and cells of growth plates, wrists and the BM [174, 175]. However, in alveolar epithelial cells and alveolar macrophages, no Cre protein was detectable, indicating that Cre expression may be either transient or occurred in their ancestors [171]. Moreover, *CD4Cre*-mediated mutations of the Ras signalling pathway have been shown to result in tumour development (Table 3). The *CD4Cre*-mediated deletion of the gene encoding for the tyrosine phosphatase SHP-2 (Src homology region 2 domain-containing phosphatase-2), leads to the development of cartilage tumours in adult *SHP-2$^{fl/fl}$ CD4Cre* mice [174] (Table 3). A contribution of T-lymphocytes to this phenotype was excluded since *SHP-2$^{fl/fl}$ CD4Cre* mice on a RAG null background lacking mature T-lymphocytes also developed these tumours [174]. Similarly, the homozygous depletion of *extracellular signal-regulated kinases* (*Erk*) *2* and *Son of sevenless* (*Sos*) *1* in *CD4Cre*-expressing cells of *Erk1*-deficient mice (*Erk1$^{-/-}$ Erk2$^{fl/fl}$ CD4Cre*) and *Sos2*-deficient mice (*Sos1$^{fl/fl}$Sos2$^{-/-}$ CD4Cre*), respectively, results in bone deformities and nodules, which also develop on a RAG null background [175-177] (Table 3). Furthermore, *CD4Cre*-mediated overactivation of Ras signalling *(KRas^{LSL2G12D} CD4Cre*) induces the formation of lung carcinoma and is lethal in young mice (< 4 weeks) [171] (Table 3).

Altogether, CD4 expression was also unravelled on non-haematopoietic cells (e.g. human BM-derived MSC [162], human/murine lung fibroblasts [160, 161, 170, 171] and murine lung epithelial cells [170, 171]) and cell-tracking studies in transgenic reporter mouse models have identified the progeny of cells with *CD4Cre* activity as various cell types populating the lung, heart and bones [173-175]. However, the function of the CD4 receptor on these non-haematopoietic cells has not been unravelled so far.

Table 3. List of observed phenotypes of different genetic mouse lines exhibiting aberrant Ras signalling in cells with *CD4Cre* activity and their offspring.

Abbreviations: AEC: alveolar epithelial cells, AMF: alveolar macrophages, BEC: bronchial epithelial cells.

Mouse strain	Phenotype	References
SHP-2$^{fl/fl}$ CD4-Cre	Observed in mice with an age of > 5 months: - Cartilage tumours - Decreased mobility - On *Rag1$^{-/-}$* background: development of cartilage tumours	[174]
Sos1$^{fl/fl}$Sos2$^{-/-}$ CD4-Cre	Observed in mice with an age of > 5 months: - Nodules on multiple joints (especially carpal joints) - Eventually development of hind limb paralysis and lameness - Proliferation of dysplastic chondrocytes - Nodules are encased by rich collagen fibrous networks - On *Rag2$^{-/-}$* background: development of carpal nodules - Effects on T-lymphocytes: Defects in T-lymphocyte migration	[176, 177]
Erk1$^{-/-}$Erk2$^{fl/fl}$ CD4-Cre	Observed in mice with an age of 10 to 20 weeks: - Bone deformities, composed of chondrocytes - On *Rag1$^{-/-}$* background: faster development of bone deformities - Effects on T-lymphocytes: Reduced number of T-lymphocytes in the spleen and lymph nodes and activated T-lymphocytes	[175]
KRas^{LSL2G12D} CD4-Cre	Observed in mice with an age of < 1 months: - AMF accumulation - Enlarged and dense lungs, due to AEC and BEC hyperplasia - Multiple adenomas - Lethality of the mice because of respiratory compromise - Effects on T-lymphocytes: Hyper activated T-lymphocytes (in the spleen)	[171]

1.3.3 Hedgehog signalling activation in CD4$^+$ cells

1.3.3.1 The hedgehog signalling pathway

The HH signalling pathway is known for its important role during the embryonic development. However, it also possesses regulatory functions in adult tissues, thus HH signalling mediates interactions between epithelial and mesenchymal compartments and drives the proliferation of precursor cells, e.g. in the adult skin (reviewed in [178]). In the absence of HH ligands (in mammals: Sonic HH, Indian HH or Desert HH) the transmembrane receptor PTCH inhibits the function of its interaction partner Smoothened (SMO) and thereby of the whole HH signalling cascade (reviewed in [178]). Binding of HH ligands to PTCH relieves the suppression of SMO, which in turn inhibits the binding of suppressor of fused to GLI TF (reviewed in [178]). This finally initiates the processing of GLI TF to transcriptional activators that accumulate in the nucleus and control the transcription of HH target genes including *Gli1*, the HH pathway antagonists *HH interacting protein* and *Ptch*, the cell cycle regulators *cyclin* (*CCN*) *D2* (G1/S-specific cyclin-D2) and *CCNE1* (G1/S-specific cyclin-E1) as well as growth factors, like *FGF4* (reviewed in [179]). The pathological activation of the HH signalling cascade especially

in precursors of adult tissues can result in tumour development, like BCC (reviewed in [139]), sarcomas [180], digestive tract tumours [181] or lung cancer [182].

1.3.3.2 Pathological activation of hedgehog signalling in haematopoietic and non-haematopoietic CD4$^+$ cells

The HH receptor PTCH plays a significant role in suppression of the HH signalling pathway since it inhibits the SMO protein and thus activation of the entire pathway. In this context, it is not surprising, that a homozygous *Ptch* KO in mice is embryonic lethal due to the resulting constitutive activation of the HH signalling cascade. However, heterozygous *Ptch* KO mice display a similar phenotype as Gorlin syndrome patients, including developmental defects of the skeleton, increased susceptibility for the development of medulloblastoma and of BCC following UV radiation [183-185]. However, for studying HH signalling overactivation in adult tissues an inducible, conditional gene depletion strategy (e.g. based on the Cre/*loxP* technique) is superior over a conventional gene KO. Indeed, the induction of a ubiquitously homozygous *Ptch* depletion in adult mice (*Ptch$^{fl/fl}$ R26CreER^{T2}*) results in hyper proliferative lesions in a plethora of tissues and in a blockade of lymphoid development at the level of the common lymphoid progenitor in the BM [186]. As a result, the generation of peripheral T- and B-lymphocytes is completely abrogated in these mice [186]. However, an additional role of HH signalling in immature, naïve or mature T-lymphocytes is highly likely since T-lymphocytes of the thymus and periphery express components of the HH signalling pathway [187-189] and it has been proposed that active HH signalling is essential for the proliferation and lymphokine production of active CD4$^+$ T-lymphocytes [190]. In order to analyse the function of HH signalling in naïve and mature T-lymphocytes in more detail the *Ptch$^{fl/fl}$ CD4Cre$^{+/-}$* mouse model was generated (for details of the *CD4Cre* deleter mouse strain see chapter 3.10.2.2). In these mice *Ptch* is homozygously deleted in all T-lymphocytes that derive from immature CD4$^+$CD8$^+$ thymocytes (CD4$^+$ and CD8$^+$ T-lymphocytes and natural killer T cells) [191, 192]. Since *Cd4*/CD4 expression is also described for monocytes, dendritic cells, brain microglia [154], B-lymphocytes, macrophages and granulocytes [146], *Ptch* depletion supposedly also occurs in these haematopoietic cells. Furthermore, non-haematopoietic cell types that descend from cells with *CD4Cre* activity were identified comprising bronchial and alveolar epithelial cells of the lung [173], smooth muscle cells of myocardial blood vessels [173] and cells of growth plates, wrists and the BM [174, 175] and thus, probably also in these cells *Ptch* is homozygously deleted. However, *Ptch$^{fl/fl}$ CD4Cre$^{+/-}$* mice are healthy, have no increased susceptibility for infections or spontaneous tumour development and show inconspicuous T-lymphocyte development and function [191, 192]. A potential impaired function of *Ptch*-depleted T-lymphocytes during tumour defence was analysed by applying the two stage DMBA (7,12-dimethylbenz[a]anthracene) and TPA (12-O-tetradecanoylphorbol-13-acetate)

chemical carcinogenesis protocol to the dorsal skin of *Ptch*$^{fl/fl}$ *CD4Cre*$^{+/-}$ mice [193]. This approach revealed, that the frequencies of the typical DMBA/TPA-induced papilloma did not differ between *Ptch*$^{fl/fl}$ *CD4Cre*$^{+/-}$ and control mice. However, the DMBA/TPA-treatment induces the development of BCC in *Ptch*$^{fl/fl}$ *CD4Cre*$^{+/-}$ mice (Figure 7), which never occured in skin of DMBA/TPA-treated wild type *Ptch* mice [193, 194]. Remarkably, DMBA/TPA-induced BCC of the *Ptch*$^{fl/fl}$ *CD4Cre*$^{+/-}$ mice do not harbour the *Hras* G61L mutation [193] which is found in over 90% of DMBA/TPA-induced papilloma and carcinoma [195, 196]. Instead, the *Ptch*$^{fl/fl}$ *CD4Cre*$^{+/-}$ BCC show high expression of *Gli1* mRNA proving the overactivation of HH signalling in these tumours [193]. Interestingly, epidermal wound-healing processes which are known to induce tumour-promoting effects by recruiting mutant tumour-initiating SC from the HF to the wound [197, 198], did not cause BCC formation in *Ptch*$^{fl/fl}$ *CD4Cre*$^{+/-}$ mice [193]. Thus the tumour-initiating agent DMBA and/or the tumour-promoting agent TPA seem to be required for BCC formation in *Ptch*$^{fl/fl}$ *CD4Cre*$^{+/-}$ mice, although these BCC show different molecular characteristics than the DMBA/TPA-induced papilloma and carcinoma [193].

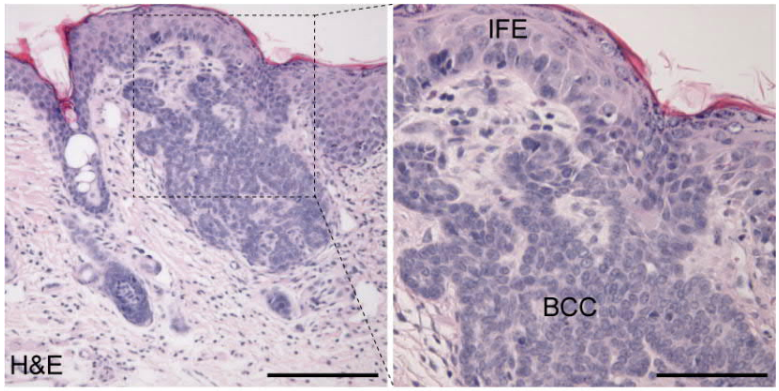

Figure 7. Basal cell carcinoma of 7,12-dimethylbenz[a]anthracene/12-O-tetradecanoylphorbol-13-acetate-treated *Ptch*$^{fl/fl}$ *CD4Cre*$^{+/-}$ skin.

Representative haematoxylin and eosin (H&E) staining of basal cell carcinoma (BCC) from 42-week-old 7,12-dimethylbenz[a]anthracene/12-O-tetradecanoylphorbol-13-acetate-treated *Ptch*$^{fl/fl}$ *CD4Cre*$^{+/-}$ skin that grows associated to the interfollicular epidermis (IFE) [199]. Scale bars: 200 µm (left), 100 µm (right).

Moreover, wild type *Ptch* mice transplanted with *Ptch*$^{fl/fl}$ *CD4Cre*$^{+/-}$ BM do not develop BCC whereas *Ptch*$^{fl/fl}$ *CD4Cre*$^{+/-}$ mice engrafted with BM from wild type mice still show BCC formation after DMBA/TPA treatment [193]. These results indicate that BCC in *Ptch*$^{fl/fl}$ *CD4Cre*$^{+/-}$ mice do not arise from a haematopoietic origin, but rather from CD4-expressing cells of the skin or at least of a non-haematopoietic origin [193]. This conclusion is substantiated by the fact, that BCC of DMBA/TPA treated *Ptch*$^{fl/fl}$ *CD4Cre*$^{+/-}$ mice show active HH signalling similar to sporadic BCC (reviewed in [139]) and BCC from Gorlin syndrome patients [136]. In fact, flow cytometric analyses verified the existence of CD4^{+} cells in the murine skin that express the keratinocyte marker CD49f, as well as the SC markers CD34 and Sca-1 [193].

1.3.3.3 Mouse models for analysing the cellular origin of *Patched*-induced basal cell carcinoma

Several lines of evidence hint towards the conclusion that DMBA/TPA-induced BCC in *Ptch*$^{fl/fl}$ *CD4Cre*$^{+/-}$ mice develop from a non-haematopoietic origin that proposedly can be isolated from the murine skin and that express CD4, CD49f, CD34 and Sca-1 [193]. BCC develop from keratinocytes of the basal IFE and/or from the HF. In the murine skin several independent SC populations maintain the IFE and HF (see chapter 1.2.5) but most of them possess tumourigenic potential when *Ptch* is homozygously depleted. Thus, outer bulge (*Gli1CreER*^{T2} deleter), inner bulge (*Hes1CreER*^{T2} deleter) and sHG cells (*Lgr5Cre* deleter) develop to BCC-like lesions that are connected to the bulge upon homozygous *Ptch* deletion [197, 200]. In uHF cells (*Lrig1CreER*^{T2} deleter) a homozygous *Ptch* depletion leads to the formation of uHF- and infundibulum-associated BCC-like lesions [200]. This shows that each of these HF SC populations (sHG, bulge, uHF) possess tumourigenic potential with respect to spontaneous BCC formation upon homozygous *Ptch* mutation. Remarkably, *Ptch* deletion in cells of the Cp layer (*Krt6a-Cre* deleter) does not *per se* induce BCC formation although ORS hyperplasia is observed with increasing mouse age. However, BCC-like lesions that arise from the IFE and ORS cells of the HF develop in this mouse model upon retinoic acid treatment which induces K6 expression in the basal layer of the IFE (and ORS) and thus induces *Ptch* deficiency in ~40% of basal IFE cells [201]. In line with the observation that also basal cells of the IFE possess BCC-forming capacities, a homozygous *Ptch* mutation in K14^{+} basal IFE cells (*K14CreER*^{T2} deleter [202]) or in K5^{+} ORS and basal IFE cells (*K5Cre* deleter [197]; *K5CreER*^{T} deleter [203]) induces spontaneous development of BCC-like lesions that originate from both IFE and HF structures. Taken together, these data demonstrate that homozygous *Ptch* depletion in a certain SC population of the HF or the IFE results in spontaneous BCC formation. This leads to the assumption that also the CD4-expressing BCC precursors in *Ptch*$^{fl/fl}$ *CD4Cre* skin might be keratinocytes (of the HF or the IFE). However, this conclusion questioned why homozygous *Ptch* depletion in CD4^{+} cells (*CD4Cre* deleter) does not *per se* induce BCC formation but only upon DMBA/TPA treatment. Therefore, in untreated *Ptch*$^{fl/fl}$ *CD4Cre* skin, the BCC-precursors either possess a lower tumourigenic potential than HF SC and basal cells of the IFE or only represent a small number of cells that remain below a critical tumour-inducing cell number regardless of their tumourigenic potential. Since BM-derived MSC give rise to a small number of epidermal keratinocytes (see chapter 1.2.5.2), they may represent CD4^{+} progenitor cells of *Ptch*$^{fl/fl}$ *CD4Cre* BCC.

2 Aim of the thesis

The skin as the outermost barrier protects against a plethora of exogenous factors and is a complex multicellular system that consists of a large variety of distinct cell populations. As skin cells need to be replaced continuously, cellular maintenance and regeneration of the skin is orchestrated by a variety of SC populations. The high regenerative capacity of skin SC, but also its reduced number related to skin ageing or the accumulation of mutations known to be responsible for tumour development, makes skin SC an important research focus. The most common neoplasia of the human skin are BCC, which mainly form due to HH signalling activating mutations. Thereby, especially the HH receptor and tumour suppressor PTCH is associated with the development of BCC. To date, it is known that biallelic *Ptch* mutations in SC of the HF as well as in basal cells of the IFE results in BCC development. However, also BM-derived MSC might present putative BCC progenitors due to their epidermal differentiation capacity. Recently our group described the existence of a skin-resident cell population, which can give rise to BCC and that expresses CD49f, CD34 and Sca-1 as well as the CD4 protein, which typically is found on immune cells (e.g. T-lymphocytes, monocytes). However, these BCC do not develop from a haematopoietic origin and similarly to human BCC show active HH signalling. Thus, the BCC-originating cell type can be described as a non-haematopoietic $CD4^+$ SC with either an epidermal keratinocyte or a BM-derived MSC identity. Since the knowledge about a potential tumour progenitor with SC-like characteristics have critical impact on the understanding of skin cancer development, the main goal of this thesis was to identify and detailly characterise the non-haematopoietic $CD4^+$ cell that can give rise to BCC. Therefore, labelling approaches (lineage tracing) should be conducted that enabled the (temporal) labelling and tracking of $CD4^+$ and their offspring cells during embryonic development, homeostasis, wound healing and ageing processes. Afterwards the verification of the findings from these approaches should be verified by CD4 protein detection. Additionally, potential differences and similarities of non-haematopoietic $CD4^+$ cells to known epidermal BCC progenitor populations should be investigated. Finally, the gained results should be transferred to the human organism by analysing whether a corresponding non-haematopoietic $CD4^+$ population also exists in human skin and which characteristics it exhibits.

3 Material

3.1 Software

Table 4. List of used software.

Software	Developer
4D	4D Deutschland GmbH, Eching, Germany
Adobe Photoshop CS5	Adobe Systems Incorporated, San Jose, USA
Adobe Illustrator 2020	Adobe Systems Incorporated, San Jose, USA
AlphaView Q SA 3.2.2	Cell Bioscience, Santa Clara, CA, USA
Cellranger (version 3.1.0)	10x Genomics, Pleasanton, CA, USA
CellSens Dimension	Olympus Optical Co., Ltd., Tokyo, Japan
BaseCaller	Illumina, San Diego, CA, USA
bcl2fastq2 v2.20.0.422 (conversion software)	Illumina, San Diego, CA, USA
BD FACSDiva™ Software	BD Biosciences, San Jose, CA, USA
DESeq2 (version 1.18.1)	[204]
Endnote X5	Thomson ISI ResearchSoft, Carlsbad, CA, USA
FastQC (version 0.11.5)	Babraham Institute, Babraham, Cambridgeshire, UK
FeatureCounts (version 1.5.0-p1)	[205]
FlowJo 7.6.5	Tree Star Inc, Oregon, USA
FluoView FV 1000	Olympus Optical Co., Ltd., Tokyo, Japan
GraphPad Prism 6	GraphPad Software, Inc., La Jolla, CA, USA
GDS 3.39	Intas Science Imaging Instruments GmbH, Göttingen, Germany
ImageJ	[206]
Leica Application Suite	Leica Microsystems GmbH, Wetzler, Germany
Loupe Browser	10x Genomics, Pleasanton, CA, USA
Microsoft Office	Microsoft Co., Redmond, WA, USA
MS-Editor	Microsoft Co., Redmond, WA, USA
NanoDrop 800 V2.3	Thermo Fisher Scientific Inc., Waltham, MA, USA
Tick@Lab	a-tune Software AG, Darmstadt, Germany
R/Bioconductor	Bioconductor Core Team (https://www.bioconductor.org/)
RStudio	RStudio, Inc., USA
STAR aligner (version 2.7.1a)	[207]

3.2 Technical equipment

Table 5. List of used technical equipment.

Technical equipment	Supplier
Agarose gel electrophoresis chamber	Peqlab Biotechnology GmbH, Erlangen, Germany
Autoclave (9216E)	Fedegari Autoclavi SpA, Albuzzano, Italy
Autoclave (Systec DX-150)	Systec GmbH & Co. KG, Linden, Germany
BD-LSR-II flow cytometer	BD Biosciences, San Jose, CA, USA
BD FACS ARIA II	BD Biosciences, San Jose, CA, USA

Technical equipment	Supplier
Centrifuge (5427 R)	Eppendorf AG, Hamburg, Germany
Centrifuges (Biofuge pico, fresco, primo, Multifuge 3LR)	Heraeus Holding GmbH, Hanau, Germany
CO_2-Incubator (6000, BBD, 6220)	Thermo Fisher Scientific Inc., Waltham, MA, USA
CO_2-Incubator (CB220-230V-G)	Binder GmbH, Tuttlingen, Germany
Confocal laser scanning microscope (FV3000)	Olympus Optical Co., Ltd., Tokyo, Japan
Cooling plate (EG1150 C)	Leica Microsystems GmbH, Wetzlar, Germany
Cryostat (CM 1900-1-1)	Leica Microsystems GmbH, Wetzlar, Germany
Digital monochrome thermal video printer (P91D)	Mitsubishi Electric Co., Tokyo, Japan
Fluorescent dissecting microscope (Leica M205FA)	Leica Microsystems GmbH, Wetzlar, Germany
Fragment Analyzer	Agilent Technologies, Santa Clara, CA, USA
Freezer (-20°C)	Siemens AG, München, Germany
Freezer (-80°C)	Sanyo Electric Co., Ltd., Osaka, Japan
Freezing container (Mr. Frosty™)	Thermo Fisher Scientific Inc., Waltham, MA, USA
Fridge (4°C)	Robert Bosch GmbH, Stuttgart, Germany
Heating block shaker (ThermoMixer©)	Eppendorf AG, Hamburg, Germany
High-precision scales (Sartorius Basic plus 2100)	Sartorius AG, Göttingen, Germany
HiSeq 4000	Illumina, San Diego, CA, USA
Ice machine	Ziegra Eismaschinen GmbH, Isernhagen, Germany
Incubator	Thermo Fisher Scientific Inc., Waltham, MA, USA
Inverted fluorescence microscope (Axiovert 25)	Carl Zeiss GmbH, Jena, Germany
Inverted research microscope (IX71)	Olympus Optical Co., Ltd., Tokyo, Japan
Isoflurane fumigation system	Drägerwerk AG, Lübeck, Germany
Liquid nitrogen tank	L'air liquid S.A., Paris, France
Magnetic stirrer (MR3000/3001)	Heidolph Instruments GmbH & Co. KG, Schwabach, Germany
Microscope (Olympus BX 60)	Olympus Optical Co., Ltd., Tokyo, Japan
Microtome (HN 40)	Leica Microsystems GmbH, Wetzlar, Germany
Microwave oven (Dimension 4)	Panasonic Corporation, Kadoma, Japan
Neubauer counting chamber	Brand GmbH & Co KG, Wertheim, Germany
NovaSep 6000	Illumina, San Diego, CA, USA
Paraffin dispenser (PAG12)	Medite Medizintechnik GmbH, Burgdorf, Germany
Paraffin tissue floating bath	Medax GmbH & Co. KG, Rendburg, Germany
Polymerase chain reaction (PCR) Thermocycler (Labcycler Basic, Labcycler Gradient)	SensoQuest GmbH, Göttingen, Germany
PCR Thermocycler (Mastercycler®)	Eppendorf AG, Hamburg, Germany
pH-meter (inoLab, pH Level 1) and electrode (SenTix 91)	WTW, Weilheim, Germany
Pipettes	Eppendorf AG, Hamburg, Germany
Platform shaker (Unimax1010)	Heidolph Instruments GmbH & Co. KG, Schwabach, Germany
Power supply for agarose gel electrophoresis	Peqlab Biotechnology GmbH, Erlangen, Germany
Precision weighing balance (ALC-210.4)	Sartorius AG, Göttingen, Germany
Spectrophotometer (NanoDrop 8000)	Thermo Fisher Scientific Inc., Waltham, MA, USA

Technical equipment	Supplier
Stereo microscope (Zeiss Stemi 2000)	Carl Zeiss GmbH, Jena, Germany
Stereo microscope (SZX12, Highlight 3100)	Olympus Optical Co., Ltd., Tokyo, Japan
Sterile workbench (Euroflow EF/A 5)	Clean Air Techniek, Woerden, Netherlands
Table centrifuge (Micro Centrifuge SD)	Carl Roth GmbH & Co. KG, Karlsruhe, Germany
Tissue embedding and dehydrating machine (TP 1020)	Leica Microsystems GmbH, Wetzlar, Germany
UV - Transilluminator	INTAS Science Imaging Instruments GmbH, Göttingen, Germany
Vacuum pump (EcoVac)	Schuett-biotec GmbH, Göttingen, Germany
Vortex mixer (Vortex-Genie2®)	Scientific Industries Inc, Bohemia, NY, USA
Water purification system (Arium® 611 VF)	Sartorius AG, Göttingen, Germany

3.3 Consumables

Table 6. List of used consumables.

Consumable	Supplier
12-well cell culture plate	Greiner Bio-One GmbH, Frickenhausen, Germany
24-well cell culture plate	Corning Incorporated, New York City, NY, USA
6-well cell culture plate	Sarstedt AG & Co., Nürnberg, Germany
µ-Slide 4-well ibiTreat plates	ibidi GmbH, Planegg-Martinsried, Germany
µ-Slide 8-well ibiTreat plates	ibidi GmbH, Planegg-Martinsried, Germany
Cell strainer (100 µm, 70 µm, 50 µm, 40 µm)	BD Biosciences Pharmingen, San Diego, USA
Centrifuge tubes (15 ml, 50 ml)	Greiner Bio-One International GmbH, Kremsmünster, Austria
Combitips advanced® (0.2 ml, 0.5 ml, 2.5 ml, 5 ml, 10 ml)	Eppendorf AG, Hamburg, Germany
Cover slips (24 mm x 60 mm; 24 mm x 40 mm)	Menzel GmbH & Co.KG, Braunschweig, Germany
Cover slips (22 mm x 22 mm)	Menzel GmbH & Co.KG, Braunschweig, Germany
Coverslips (round, Ø 12 mm) for cell culture	Th. Geyer GmbH & Co. KG, Renningen, Germany
CryoPure tubes	Sarstedt AG & Co., Nürnberg, Germany
Delicate task wipes	Kimberly-Clark Europe Ltd., Surrey, UK
Disposable needles (Sterican Ø 0.45 x 12 mm; 26 G x ½)	B.Braun AG, Melsungen, Germany
Disposable syringes (BD DiscarditTM II 1, 2, 10, 20, 50 ml)	BD Biosciences, San Jose, CA, USA
Embedding cassette	Kabe Labortechnik GmbH, Nümbrecht, Germany
Filter tips (Biosphere® 20 µl, 100 µl, 200 µl, 1000 µl)	Sarstedt AG & Co., Nürnberg, Germany
Forceps (Dumont #5)	Manufactures D'Outils Dumont SA
Glass petri dishes (Ø10 cm, Ø15 cm)	TH. Geyer GmbH & Co. KG, Renningen, Germany
Glassware	Schott AG, Mainz, Germany
Longhair electric shaver	Aesculap AG & Co. KG, Tuttlingen, Germany
Microscope glass slides	Thermo Fisher Scientific Inc., Waltham, MA, USA
Microtome blades (A35; C35)	Pfm Medical AG, Cologne, Germany
Parafilm® laboratory film	Bemis Company, Inc., Neenah, WI, USA

Consumable	Supplier
Pasteur pipettes	TH. Geyer GmbH & Co. KG, Renningen, Germany
PCR tear-a-way plates & cap strips	4titude® Ltd., Surrey, UK
Petri dishes	Ochs GmbH, Bovenden/Lenglern, Germany
Pipette tips (20 µl, 200 µl, 1000 µl)	Sarstedt AG & Co., Nürnberg, Germany
Preparation tools	Carl Roth GmbH & Co. KG, Karlsruhe, Germany
Reaction tubes (1.5 ml, 2 ml)	Sarstedt AG & Co., Nürnberg, Germany
Safeseal microtubes (1.5 ml, 2 ml)	Sarstedt AG & Co., Nürnberg, Germany
Scalpel (24)	Aesculap AG & Co.KG, Tuttlingen, Germany
Serological pipettes (2 ml, 5 ml, 10 ml, 25 ml)	Sarstedt AG & Co., Nürnberg, Germany
Small shovel	Workshop of the UMG Göttingen, Germany
Softa-Man® hand disinfectant	B.Braun AG, Melsungen, Germany
Superfrost glass slides	Thermo Fisher Scientific Inc., Waltham, MA, USA
Surgical blades	Aesculap AG, Tuttlingen, Germany
Weighing paper	Macherey-Nagel GmbH & Co. KG, Düren, Germany

3.4 Reagents and chemicals

Chemicals and reagents not listed were purchased from Sigma Aldrich Inc., St. Louis, MO, USA or from Carl Roth GmbH & Co. KG Karlsruhe, Germany.

Table 7. List of used reagents and chemicals.

Reagent or chemical	Supplier
Agarose	Bio-Budget Technologies GmbH, Krefeld, Germany
Amphotericin B	Biochrom, Berlin, Germany
Ampuwa H_2O	Fresenius Kabi Deutschland GmbH, Germany
Buprenorphin, Tamgesic®	Bayer Vital GmbH, Leverkusen, Germany
Chelex® 100 Resin	Bio-Rad Laboratories, Inc., Hercules, USA
Cresol red, sodium salt	Aldrich Chemical Company Inc., Milwaukee, WI, USA
Cryoblock embedding medium	Medite Medizintechnik GmbH, Burgdorf, Germany
DAPI (4'6,-Diamidin-2-Phenylindol)	Life Technologies Corp., OR, USA
Deoxyribonucleotide triphosphates (dNTPs)	Roche Diagnostics GmbH, Mannheim
Dimethylsulfoxide (DMSO)	Thermo Fisher Scientific Inc., Waltham, MA, USA
Dithiothreitol	Thermo Fisher Scientific Inc., Waltham, MA, USA
Eosin Y	Merck KGaA, Darmstadt, Germany
Ethanol (EtOH, 99%), unvergällt	J.T. Baker B.V., Deventer, Netherlands
EtOH (99%), vergällt	CVH Chemie-Vertreib GmbH & Co. Hannover KG, Hannover, Germany
Ethidiumbromide (0,07%)	Inna-TRAIN-Diagnostics, Kronberg, Germany
GeneRuler DNA ladder (50 base pairs [bp], 100 bp plus, 1 kilobase [kb])	Thermo Fisher Scientific Inc., Waltham, MA, USA
Glycergel mounting medium	Dako North America Inc., Carpinteria, CA, USA
GlycoBlue™ Coprecipitant	Thermo Fisher Scientific Inc., Waltham, MA, USA

Reagent or chemical	Supplier
Haematoxylin crystalline, Mayer's	Merck KGaA, Darmstadt, Germany
Hair removal cream Veet	RB Healthcare, UK
Immersion oil for microscopy (Immersion™ 518 N)	Carl Zeiss GmbH, Jena, Germany
Isofluran (Forene®)	Abbott Laboratories Inc, Santa Clara, CA, USA
Loading dye solution for DNA (6 x)	Thermo Fisher Scientific Inc., Waltham, MA, USA
Meloxicam, Metacam®	Boehringer Ingelheim Vetmedica GmbH, Ingelheim/Rhein, Germany
Pertex mounting medium	Medite Medizintechnik GmbH, Burgdorf, Germany
RNase free H_2O	Invitrogen, Carlsbad, CA, USA
Sodium chloride	AppliChem GmbH, Darmstadt, Germany
Sodiumdodecylsulfate (SDS)	AppliChem GmbH, Darmstadt, Germany
Tris(hydroxymethyl)aminomethane (TRIS) base	AppliChem GmbH, Darmstadt, Germany
TRIzol® Reagent	Life Technologies Co. Camarillo, CA, USA
Tropix® I-BLOCK™	Applied Biosystems, Waltham, MA, USA
Xylene	J.T. Baker B.V., Deventer, Netherlands

3.5 Buffers and solutions

The following buffers and solutions were prepared with double-distilled water (ddH_2O), unless otherwise specified.

Table 8. List of used buffers and solutions with their respective composition.

Buffer or solution	Composition	pH
0.2% I-BLOCK	0.2% (w/v) I-Block 0.1% (v/v) Tween 20 Dissolved in phosphate-buffered saline (PBS)	
0.25% Acetic acid	0.25% (v/v) Acetic acid	
Citric acid buffer	10 mM Sodium Citrate	6.0
Cresol	0.1% (w/v) Cresol red Dissolved in saturated sucrose-solution	
dNTPs	10 mM dATP 10 mM dCTP 10 mM dGTP 10 mM dTTP	
Ethylenediaminetetraacetic acid (EDTA)-solution (10%) for decalcification	10% (v/v) EDTA	7.4
EDTA-solution (5 mM)	5 mM EDTA Dissolved in PBS	8.0
Eosin solution	80% (v/v) EtOH 1% (w/v) Eosin y (water soluble)	

Buffer or solution	Composition	pH
Haematoxylin solution, Mayer's	300 mM Trichloro acetaldehyde hydrate 100 mM Potassium aluminum sulfate 50 mM Citric acid 35 mM Haematoxylin 75 nM Sodium iodate	
Mowiol Mounting Medium	4.3 mM Mowiol 4-88 3016.24 mM Glycerol 18502.811 mM H_2O 133 mM Tris (pH 8.5) 34.05 mM 1,4-diazabicyclo[2.2.2]octane	
Paraformaldehyde (PFA) 4%	4% (w/v) PFA Dissolved in PBS	
PB	0.5% (w/v) Milk powder 0.25% (w/v) Gelatin from porcine 0.5% (v/v) Triton X-100 Dissolved in TBS	
PBS, 10x	1.4 M NaCl 65 mM Na_2HPO_4 27 mM KCl 15 mM KH_2PO_4	7.4
PBS-Tween 20	0.1% (v/v) Tween-20 Dissolved in PBS	
Proteinase K	50 mM Tris/HCl 5 mM EDTA 10 mg/ml Proteinase K	8.0
SDS loading buffer (6x)	375 mM Tris (pH 6.8) 12% (w/v) SDS 60% (v/v) Glycerol 0.6 M Dithiothreitol 0.01% (w/v) Bromophenol blue	
Sodium-acid PBS	0.2% (v/v) Sodium acid Dissolved in PBS	
Sodium chloride (0.9%)	0.9% (w/v) Sodium chloride	
Sodium Chloride-Tris-EDTA buffer	100 mM NaCl 50 mM Tris/HCl 1 mM EDTA 1% (w/v) SDS	
Tris-boric-acid-EDTA solution, 10x	890 mM Tris/HCl (pH 8.0) 730 mM Boric acid 12.5 mM EDTA	8.0
Tris-buffered saline (TBS), 10x	150 mM NaCl 10 mM Tris/HCl (pH 8.0)	7.4
TBS-Triton X-100 (TBS-T 0.1%)	0.1% (v/v) Triton X-100 Dissolved in TBS	
TBS-Triton X-100 (TBS-T 0.5%)	0.5% (v/v) Triton X-100 Dissolved in TBS	

3.6 Media

Table 9. List of used media, supplements, antibiotics and antimycotics and coating material.

Medium, supplement, antibiotics/antimycotics or coating material	Supplier
Medium	
154-CF Medium	Invitrogen, Carlsbad, CA, USA
Dulbecco`s Modified Eagle Medium (DMEM) supplemented with 4.5 g/L Glucose, L-Glutamine	Invitrogen, Carlsbad, CA, USA
Defined Keratinocyte-SFM Basal Medium	Thermo Fisher Scientific Inc., Waltham, MA, USA
Ham`s F-12 Medium	Invitrogen, Carlsbad, CA, USA
Hank's Balanced Salt Solution (HBSS) Medium	Invitrogen, Carlsbad, CA, USA
MesenCult™ Basal Medium (Mouse)	Stemcell Technologies, Vancouver, Canada
Synth-a-Freeze Cryopreservation Medium	Thermo Fisher Scientific Inc., Waltham, MA, USA
Supplements	
Adenine	Carl Roth GmbH & Co. KG, Karlsruhe, Germany
Cholera toxin	Sigma-Aldrich Inc., St. Louis, USA
Defined Keratinocyte-SFM growth supplements	Thermo Fisher Scientific Inc., Waltham, MA, USA
Epidermal growth factor (EGF), human	R&D Systems Inc., Minneapolis, USA
Foetal calf serum (FCS)	Invitrogen, Carlsbad, CA, USA
Hydrocortisone	Sigma-Aldrich Inc., St. Louis, USA
Insulin (bovine pancreas)	Sigma-Aldrich Inc., St. Louis, USA
Isoproterenol hydrochloride	Sigma-Aldrich Inc., St. Louis, USA
L-Glutamine	Invitrogen, Carlsbad, CA, USA
MesenCult™ 10X Supplement (Mouse)	Stemcell Technologies, Vancouver, Canada
MesenPure™	Stemcell Technologies, Vancouver, Canada
Antibiotics/Antimycotics	
Amphotericin B	Sigma-Aldrich Inc., St. Louis, USA
Penicillin (10,000 U/ml) and Streptomycin (10 mg/ml) (pen/strep)	PAN Biotech GmbH, Aidenbach, Germany
Coating material	
Bovine Collagen Solution Type I	Sigma-Aldrich Inc., St. Louis, USA
Human Collagen Type IV	Merck KGaA, Darmstadt, Germany

3.6.1 Preparation of heat-inactivated, chelexed foetal calf serum

For preparing heat-inactivated, chelexed FCS, the FCS was heat-inactivated at 56 °C for 30 minutes. Next, 10 g Chelex 100 resin per heat-inactivated 50 ml FCS were swelled in 40-50 ml distilled water (dH_2O) and titrated to pH 7.4. Afterwards, the Chelex 100 resin was filtered through a Whatman filter, scraped from the filter and mixed with 50 ml heat-inactivated FCS. Then, the mixture was stirred at RT for 3 hours or at 4 °C overnight. Afterwards, chelexed FCS was filtered first through a Whatman filter and secondly sterile filtered through a 0.2 µm bottle filter. For long-term storage aliquots were stored at -20 °C.

Table 10. Composition of self-prepared or modified media.

Medium	Composition	References
154 CF solution	1% (w/v) BSA in 154CF Medium	
hkera medium	DMEM : Ham's F-12 (3:1) 5% (v/v) FCS (chelex-treated) 1% (v/v) pen/strep 5 µg/ml Insulin 0.4 µg/ml Hydrocortisone 1 µM Isoproterenol 1.8*10-4 M Adenine (After 3 to 4 days: addition of 0.01 µg/ml EGF)	Adapted from Ponec *et al.* and Gibbs *et al.* [208, 209]
HBSS solution	1% (v/v) pen/strep 0.1% (v/v) Amphotericin B in HBSS medium	
MesenCult complete medium	MesenCult™ Basal Medium (Mouse) 10% (v/v) MesenCult™ 10X Supplement (Mouse) 0.1% (v/v) MesenPure™	
feeder-free culture medium	Defined Keratinocyte-SFM Basal Medium 0.2% (v/v) Defined Keratinocyte-SFM growth supplements	
mKera medium	DMEM (Ca^{2+} free) : Ham's F-12 (3:1) 15% (v/v) FCS (chelex-treated) 1% (v/v) pen/strep 0.1% (v/v) Amphotericin B 0.4 µg/ml Hydrocortisone 1 µM Isoproterenol 4 mM L-glutamine 1 mM Sodium pyruvate 0.3 mM $CaCl_2$	[210]
mESC medium	DMEM 0.1 mM Non-essential amino acids 1 mM Sodium pyruvate 1 µM β-mercaptoethanole 2 mM L-glutamine 1 mM pen/strep 20% (v/v) FCS 1,000 U/ml Leukemia inhibitory factor	Kindly provided by Dr. Jessica Nolte-Kaitschick, Institute of Human Genetics, Göttingen, Germany

3.7 Kits

Table 11. List of used kits.

Kits	Supplier
BigDye™ Terminator v3.1 Cycle Sequencing Kit	Thermo Fisher Scientific Inc., Waltham, MA, USA
Dead Cell Removal Kit (#130-090-101)	Miltenyi Biotec B.V. & Co. KG, Bergisch Gladbach, Germany
EasySep™ Mouse Haematopoietic Progenitor Cell Isolation Kit	Stemcell Technologies, Vancouver, Canada
TruSeq® RNA Sample Preparation v2	Illumina, San Diego, CA, USA

3.8 Enzymes

Table 12. List of used enzymes.

Enzyme	Supplier
Collagenase type I	Worthington Biochemical Corporation, New Jersey, USA
Collagenase type IV	Gibco, Invitrogen GmbH, Karlsruhe, Germany
Dispase	Corning Inc., New York, NY, USA
Polymerase buffer	Molzym GmbH Co.KG, Bremen, Germany
Proteinase K	Carl Roth GmbH & Co. KG, Karlsruhe, Germany
Taq-Polymerase	Molzym GmbH & Co. KG, Bremen, Germany
Thermolysin	Sigma-Aldrich Inc., St. Louis, MO, USA
Trypsin (0.25%)	Gibco, Invitrogen GmbH, Karlsruhe
0.05% trypsin/0.02% EDTA	PAN Biotech GmbH, Aidenbach, Germany or Gibco, Invitrogen GmbH, Karlsruhe, Germany

3.9 Antibodies

3.9.1 Immunofluorescence and immunocytochemistry

Table 13. Summary of used primary and secondary antibodies used for (double) immunofluorescence and immunocytochemistry.

Secondary antibodies were obtained from Jackson ImmunoResearch if not otherwise stated and diluted 1:200. Abbreviations: Cryo: cryotome section; ICC: immunocytochemistry, IF: immunofluorescence, iHF: isolated hair follicle.

Figure	Primary antibodies (Dilution, Clone, Manufacturer)	Secondary antibodies (Catalogue#)	Application
Figure 13			
B, B’	Rat anti mouse CD4 (1:50, RM4-5, BD Biosciences)	Donkey anti rat alexa488 (#712-545-150)	IF on Cryo
D, D’	Goat anti mouse PDGFRα (1:20, AF1062, R&D Systems)	Bovine anti goat alexa488 (#805-545-150)	IF on Cryo
H, H’	Rabbit anti mouse/human Sox9 (1:2500, AB5535, Millipore)	Donkey anti rabbit alexa488 (#711-545-152)	IF on Cryo

Figure	Primary antibodies (Dilution, Clone, Manufacturer)	Secondary antibodies (Catalogue#)	Application
Figure 15			
B	Rabbit anti mouse/human K5 (1:1000, Poly19055, BioLegend)	Donkey anti rabbit alexa488 (# 711-545-152)	IF on Cryo
C-E, C', E'	Goat anti mouse PDGFRα (1:20, AF1062, R&D Systems)	Bovine anti goat alexa488 (#805-545-150)	IF on Cryo
Figure 17			
C, F	Rat anti mouse F4-80 (1:100, CI:A3-1, Serotec)	Donkey anti rat alexa488 (#712-545-150)	ICC
D, G	Mouse anti mouse/human Ki-67 (1:50, B56, BD Pharmingen)	Goat anti mouse alexa488 (Invitrogen, #A11029)	ICC
E, H	Rabbit anti mouse α-SMA (1:100, Abcam, ab5694)	Donkey anti rabbit alexa488 (# 711-545-152)	ICC
Figure 21			
A-C"	Mouse anti mouse/human Oct-3/4 (1:50, C-10, Santa Cruz) Rat anti mouse CD4 (1:50, RM4-5, BD Bioscience)	Goat anti mouse alexa488 (Invitrogen, #A11029) Donkey anti rat cy3 (#712-165-150)	ICC
Figure 22			
A-B'	Rabbit anti mouse/human CD45 (1:150, Ab10558, Abcam) Goat anti RFP (1:200, MBS448122, MyBioSource)	Donkey anti rabbit cy3 (1:400, #711-165-152) Bovine anti goat alexa488 (#805-545-150)	IF on Paraffin (Table 20, Citric acid 1)
Figure 23			
A-A'	Rabbit anti mouse α-SMA (1:100, Abcam, ab5694) Rat anti mouse CD4 (1:50, RM4-5, BD Bioscience)	Donkey anti rabbit cy3 (1:400, #711-165-152) Donkey anti rat alexa488 (#712-545-150)	IF on Cryo
B-B'	Goat anti mouse PDGFRα (1:20, AF1062, R&D Systems) Rat anti mouse CD4 (1:50, RM4-5, BD Bioscience)	Donkey anti goat cy3 (#705-165-147) Donkey anti rat alexa488 (#712-545-150)	IF on Cryo
C-C'	Rabbit anti mouse α-SMA (1:100, Abcam, ab5694)	Donkey anti rabbit alexa488 (#711-545-152)	IF on iHF
D-D'	Goat anti mouse PDGFRα (1:20, AF1062, R&D Systems)	Bovine anti goat alexa488 (#805-545-150)	IF on Cryo
Figure 30			
B, B'	Rabbit anti mouse/human K5 (1:1000, Poly19055, BioLegend)	Donkey anti rabbit alexa488 (#711-545-152)	IF on Cryo
C, C'	Rat anti mouse Sca-1 (1:100, E13 161-7, Abcam) Rabbit anti RFP (1:500, Rockland #600-401-379S)	Donkey anti rat alexa488 (#712-545-150) Goat anti rabbit cy3 (#111-165-003)	IF on Paraffin (Table 20, Citric acid 2)

Figure	Primary antibodies (Dilution, Clone, Manufacturer)	Secondary antibodies (Catalogue#)	Application
Figure 30			
D, D'	Mouse anti mouse/human Trp63 (1:100, D-9, Santa Cruz) Rabbit anti RFP (1:500, Rockland #600-401-379S)	Goat anti mouse alexa488 (Invitrogen, #A11029) Goat anti rabbit cy3 (#111-165-003)	IF on Paraffin (Table 20, Citric acid 1)
E, E'	Rabbit anti mouse K10 (1:500, Covance, #PRB-159P Rabbit anti RFP (1:500, Rockland #600-401-379S)	Goat anti mouse alexa488 (Invitrogen, #A11029) Goat anti rabbit cy3 (#111-165-003)	IF on Paraffin (Table 20, Citric acid 1)
F, F'	Rabbit anti mouse/human K5 (1:1000, Poly19055, BioLegend)	Donkey anti rabbit alexa488 (#711-545-152)	IF on Cryo
H, H'	Rabbit anti mouse/human K5 (1:1000, Poly19055, BioLegend)	Donkey anti rabbit alexa488 (#711-545-152)	IF on Cryo
I, I'	Rabbit anti mouse K10 (1:500, Covance, #PRB-159P	Donkey anti rabbit alexa488 (#711-545-152)	IF on Cryo
J, J'	Rabbit anti human Lor (1:500, Abcam, #ab176322)	Donkey anti rabbit alexa488 (#711-545-152)	IF on Cryo
K	Rabbit anti mouse K10 (1:500, Covance, #PRB-159P	Donkey anti rabbit alexa488 (#711-545-152)	IF on epidermal sheet
Figure 31			
C, C'	Rabbit anti mouse/human K5 (1:1000, Poly19055, BioLegend)	Donkey anti rabbit alexa488 (#711-545-152)	IF on Cryo
D, D'	Rat anti mouse CD34 (1:1000, MEC14.7, Serotec) Rabbit anti RFP (1:500, Rockland #600-401-379S)	Donkey anti rat alexa488 (#712-545-150) Goat anti rabbit cy3 (#111-165-003)	IF on Paraffin (Table 20, Boric acid 2)
E, E'	Rat anti mouse CD34 (1:1000, MEC14.7, Serotec) Rabbit anti RFP (1:500, Rockland #600-401-379S)	Donkey anti rat alexa488 (#712-545-150) Goat anti rabbit cy3 (#111-165-003)	IF on Paraffin (Table 20, Boric acid 2)
Figure 32			
B, B'	Rabbit anti mouse/human Sox9 (1:2500, AB5535, Millipore)	Donkey anti rabbit alexa488 (#711-545-152)	IF on iHF
C, C'	Rabbit anti mouse/human K5 (1:1000, Poly19055, BioLegend)	Donkey anti rabbit alexa488 (#711-545-152)	IF on iHF
D, D'	Mouse anti mouse/human TCHH (1:50, AE15, ThermoFisherScientific) Rabbit anti RFP (1:500, Rockland #600-401-379S)	Goat anti mouse alexa488 (Invitrogen, #A11029) Goat anti rabbit cy3 (#111-165-003)	IF on Paraffin (Table 20, Boric acid 1)
E, E'	Mouse anti mouse/human Gata-3 (1:50, HG3-31, Santa Cruz) Rabbit anti RFP (1:500, Rockland #600-401-379S)	Goat anti mouse alexa488 (Invitrogen, #A11029) Goat anti rabbit cy3 (#111-165-003)	IF on Paraffin (Table 20, Citric acid 1)

Figure	Primary antibodies (Dilution, Clone, Manufacturer)	Secondary antibodies (Catalogue#)	Application
Figure 32			
F, F'	Mouse anti mouse/human AE13 (1:1000, AE13, ThermoFisherScientific) Rabbit anti RFP (1:500, Rockland #600-401-379S)	Goat anti mouse alexa488 (Invitrogen, #A11029) Goat anti rabbit cy3 (#111-165-003)	IF on Paraffin (Table 20, Citric acid 1)
G, G'	Mouse anti mouse/human Ki-67 (1:50, B56, BD Pharmingen) Rabbit anti RFP (1:500, Rockland #600-401-379S)	Goat anti mouse alexa488 (Invitrogen, #A11029) Goat anti rabbit cy3 (#111-165-003)	IF on Paraffin (Table 20, Citric acid 1)
Figure 36			
A, A'	Guinea pig anti mouse/human K75 (1:100, GP-K6HF, Progen) Rabbit anti mouse/human K5 (1:1000, Poly19055, BioLegend)	Donkey anti guinea pig alexa488 (#706-545-148) Donkey anti rabbit cy3 (1:400, #711-165-152)	IF on iHF
B, B', D, D'	Guinea pig anti mouse/human K75 (1:100, GP-K6HF, Progen)	Donkey anti guinea pig alexa488 (#706-545-148)	IF on iHF
C, C'	Rabbit anti mouse/human K5 (1:1000, Poly19055, BioLegend)	Donkey anti rabbit alexa488 (#711-545-152)	IF on iHF
Figure 38			
B-E''	Goat anti RFP (1:200, MBS448122, MyBioSource) Rabbit anti mouse/human K5 (1:1000, Poly19055, BioLegend)	Donkey anti rabbit cy3 (1:400, #711-165-152) Donkey anti goat FITC (#705-095-147)	IF on Paraffin (Table 20, Citric acid 1)
Figure 44			
A	Rat anti mouse CD4 (1:50, RM4-5, BD Bioscience)	Donkey anti rat alexa488 (#712-545-150)	ICC
B	Rabbit anti mouse/human K5 (1:1000, Poly19055, BioLegend) Rat anti mouse CD4 (1:50, RM4-5, BD Bioscience)	Donkey anti rabbit cy3 (1:400, #711-165-152) Donkey anti rat alexa488 (#712-545-150)	ICC
Figure 45			
C-D'	Rabbit anti mouse/human K5 (1:1000, Poly19055, BioLegend) Mouse anti human K15 (1:100, LHK15, ThermoFisherScientific)	Donkey anti rabbit cy3 (1:400, #711-165-152) Goat anti mouse alexa488 (Invitrogen, #A11029)	IF on Paraffin (Table 20, Citric acid 1)
E-F'	Rabbit anti mouse K17 (1:1000, provided by P. Coulombe, Baltimore, USA) Mouse anti mouse/human TCHH (1:50, AE15, ThermoFisherScientific)	Donkey anti rabbit cy3 (1:400, #711-165-152) Goat anti mouse alexa488 (Invitrogen, #A11029)	IF on Paraffin (Table 20, Citric acid 1)

Figure	Primary antibodies (Dilution, Clone, Manufacturer)	Secondary antibodies (Catalogue#)	Application
Figure 47			
A-D	Rabbit anti mouse/human K5 (1:1000, Poly19055, BioLegend) Mouse anti mouse/human Ki-67 (1:50, B56, BD Pharmingen)	Donkey anti rabbit cy3 (1:400, #711-165-152) Goat anti mouse alexa488 (Invitrogen, #A11029)	IF on Paraffin (Table 20, Citric acid 1)
Figure 48			
C-C'	Rabbit anti mouse/human K5 (1:1000, Poly19055, BioLegend)	Donkey anti rabbit alexa488 (#711-545-152)	ICC
Figure 50			
A	Rabbit anti mouse/human Sox9 (1:2500, AB5535, Millipore)	Donkey anti rabbit alexa488 (#711-545-152)	ICC
B	Rat anti mouse CD34 (1:1000, MEC14.7, Serotec)	Donkey anti rat alexa488 (#712-545-150)	ICC
C	Rat anti mouse Sca-1 (1:100, E13 161-7, Abcam)	Donkey anti rat alexa488 (#712-545-150)	ICC
D	Rat anti mouse Sca-1 (1:100, E13 161-7, Abcam) Rabbit anti mouse K17 (1:400, provided by P. Coulombe, Baltimore, USA)	Donkey anti rat alexa488 (#712-545-150) Donkey anti rabbit cy3 (1:400, #711-165-152)	ICC
Figure 51			
-	Rabbit anti mouse/human Sox9 (1:2500, AB5535, Millipore)	Donkey anti rabbit alexa488 (#711-545-152)	ICC
Figure 55			
E-F'	Mouse anti mouse/human Trp63 (1:100, D-9, Santa Cruz)	Goat anti mouse alexa488 (Invitrogen, #A11029)	ICC

3.9.2 Flow cytometry

Table 14. Summary of used antibodies used for flow cytometry and fluorescence activated cell sorting.
All antibodies were obtained from BD Biosciences Pharmingen, USA and diluted 1:50.
Antibody (Clone)
APC-conjugated
Rat anti mouse CD44-APC (IM7)
BV421-conjugated
Hamster anti rat/mouse CD29-BV421 (Ha2/5)
FITC-conjugated
Rat anti mouse CD34-FITC (RAM34)
Rat anti mouse CD4-FITC (RM4-5)

Antibody (Clone)
PE-conjugated
Mouse anti human CD29-PE (MAR4)
Rat anti mouse PDGFRα/CD140A-PE (APA5)
Rat anti mouse CD34-PE (RAM34)
PerCP-Cy5.5-conjugated
Mouse anti mouse CD45.2-PerCP-Cy5.5 (104)
Rat anti mouse/human CD49f-PerCP-Cy5.5 (GoH3)
PE-Cy7-conjugated
Rat anti mouse CD11b-PE-Cy7 (M1/70)
Rat anti mouse CD16/CD32-PE-Cy7 (2.4G2)
Hamster anti mouse CD3ε-PE-Cy7 (145-2C11)
Mouse anti human CD4-PE-Cy7 (SK3)
Rat anti mouse CD8α-PE-Cy7 (53-6.7)
Rat anti mouse CD90-PE-Cy7 (53-2.1)
Rat anti mouse Sca1-PE-Cy7 (D7)
Hamster anti mouse TCRβ-PE-Cy7 (H57-597)

3.10 Biological material

3.10.1 Eukaryotic cell lines

Table 15. List of used eukaryotic cell lines.

Cell line	General information	Depositor
mES RI	Murine embryonic stem cell (ESC) line	Kindly provided by Dr. Jessica Nolte-Kaitschick, Institute of Human Genetics, Göttingen, Germany
NIH/3T3	Murine adult fibroblast cell line	ATCC, Manassas, VA, USA

3.10.2 Genetically modified mouse lines

The mouse lines listed in Table 16 were maintained as inbred stains on a C57BL/6N genetic background.

Table 16. List of used genetically modified mouse strains.

Mouse strain	International nomenclature	Characteristics	Genetic background	Reference/ Supplier
C57BL/6N	C57BL/6N	Wild type inbred strain	C57BL/6N	Charles River Laboratories Inc., Wilmington, NC, USA
CD4Cre	*Tg(Cd4-cre)1Cwi/BfluJ*	*Cre* recombinase under control of the *Cd4* promoter/enhancer/ silencer	C57BL/6N	[211]
CD4CreER^{T2}	*Tg(Cd4-cre/ERT2)11Gnri*	Tamoxifen inducible *Cre* recombinase under control the of *Cd4* promoter/enhancer/ silencer	C57BL/6N	[212]
CD4 KO	*B6.129S2-Cd4^{tm1Mak}/J*	*Cd4* gene deletion due to disruption of exon 5 of the *Cd4* gene	C57BL/6	[213]
R26-tdTomato	*Gt(ROSA)26Sor$^{tm9(CAGtdtomato)Hze}$*	Conditional expression of *tdTomato*	C57BL/6N	[214]

3.10.2.1 The *Cre-loxP* system

In order to identify and track cell populations *in vivo* (lineage tracing), commonly the *Cre-loxP* system for the conditional expression of reporter proteins is used. For this technique the cell-specific expression of a Cre-recombinase protein is necessary (e.g. under control of the *Cd4*-promoter/enhancer/silencer). This 38 kDa integrase was originally isolated from the bacteriophage P1 and mediates the site-specific recombination between two 34 bp *loxP* DNA recognition sequences [215, 216] resulting in a rearrangement (e.g. inversion or deletion depending on the orientation of the *loxP* sites) of the *loxP* sites-flanked ('floxed') DNA. Expression of the *Cre* recombinase gene under the control of tissue- or cell-specific promoters, then allows the conditional mutagenesis of floxed genes in transgenic mice (reviewed in [217]). The induced genetic alterations are then inherited by the ancestor cell that expressed the Cre recombinase to their progeny cells. In case of lineage-tracing approaches, the Cre recombinase deletes a floxed *STOP* cassette upstream of a reporter gene and thus activates its expression (reviewed in [217]). In this work, *R26-tdTomato* conditional reporter mice that contain a floxed *STOP* cassette upstream of the *tdTomato* (*tdT*) gene encoding for a red

fluorescence protein under the control of the ubiquitously expressed, endogenous *Rosa26* (*R26*) locus, have been used.

For a more restricted temporal or spatial control of Cre recombinase activity commonly CreER recombinases are used which represent *Cre* recombinases fused to the human estrogen receptor (ER) (reviewed in [217]) leading to a restrain of the recombinase in the cytoplasm in the absence of ER-binding ligands (e.g. estrogen or the anti-estrogen tamoxifen). However, in the presence of ER-binding ligands, CreER recombinases enter the nucleus and recombine floxed sequences/genes. As high levels of tamoxifen were required to achieve CreER activity, which often are toxic to the cell, a second generation, the $CreER^{T2}$ recombinase was developed [218]. This protein contains a mutated ER-binding site that is not activated by endogenous estrogens but by low levels of tamoxifen leading to a reduced 'leakiness' (entering of the nucleus in the absence of tamoxifen resulting in CreER background activity) of the $CreER^{T2}$ in comparison to the CreER recombinase.

3.10.2.2 The *CD4Cre* deleter mouse strain

To trace or mutate *Cd4*-expressing cells, the *CD4Cre* mouse model was used in this work. In these mice, the expression of a Cre recombinase is driven by the transgenic minimal enhancer, promoter and silencer elements of the murine *Cd4* gene [211, 219]. The enhancer, located 13 kb upstream of the transcription initiation site, is T-lymphocyte specific and together with the CD4 promoter, the enhancer directs reporter gene transcription in both $CD4^+$ and $CD8^+$ T-lymphocytes [219]. If the silencer is present, there is selective extinction of reporter gene expression in the $CD8^+$ T-lymphocytes [219]. The silencer is a 428 bp fragment located 2 kb 3' of the transcription initiation site, within the first intron of the *Cd4* gene [219]. In transgenic mice, the silencer remains fully functional, although if it is placed in reverse orientation or outside of the coding region of the *Cd4* gene, at a distance from the promoter [219]. The insertion site of the *CD4Cre* transgene has been mapped to mouse chromosome 3 and consists of concentrated copies (mean: 15-16 tandems) of the '*Cd4* minimal enhancer (chr6:124900400-124900739), almost the entire sequence of the *Cd4* promoter region till base pair 32 of exon 2 (chr6:124879661-124888625), the *Cre* gene and a 2.1 kb fragment of the *human growth factor* (*hGH*) gene, followed by a part of the *pGEM- 13Zf(+)* vector sequence (26–3179 bp)' [220]. The sequence that has been deleted upon insertion of the transgene does not contain any known gene [220]. Besides, $CD4Cre^{+/-}$, $CD4Cre^{-/-}$ and wild type mice contain similar cell numbers and subset frequencies of $CD4^+$, $CD8^+$ and $CD4^+CD8^+$ T-lymphocytes in the thymus, excluding an influence of the Cre recombinase on T-lymphocyte survival and differentiation. Only in $CD4Cre^{-/-}$ mice a reduced number of splenocytes were observed [220].

3.10.2.3 The tamoxifen-inducible *CD4CreER^{T2}* deleter mouse strain

In order to analyse a more restricted temporal or spatial expression of the *Cd4* gene the *CD4CreER^{T2}* mouse model was used [212]. In *CD4CreER^{T2}* transgenic mice, the *CreER^{T2}* fusion sequence was cloned downstream of the *Cd4*-promoter/enhancer/silencer that has been already used for the generation of *CD4Cre* mice (see above). *CD4CreER^{T2}* mice do not show any aberrant phenotype and lineage-tracing studies using these mice revealed an efficient tracking of $CD4^+$ T-lymphocytes *in vitro* and *in vivo* after tamoxifen treatment [212].

3.10.2.4 *CD4Cre R26-tdT* and the *CD4CreER^{T2} R26-tdT* lineage tracing mice

The lineage tracing reporter mouse strain *CD4Cre R26-tdT* was generated by breeding the *CD4Cre* deleter mouse strain to *R26-tdT* reporter mice (see above). Thus, in *CD4Cre R26-tdT* mice an active CD4 promoter leads to the expression of a constitutively active Cre recombinase that deletes the floxed *STOP* cassette at the *R26-tdT* locus resulting in the expression of the red fluorescent tdT protein. Since in *CD4Cre R26-tdT* mice the Cre recombinase-mediated genomic alteration is inherited to the progeny, not only cells with CD4 promoter activity but also their offspring cells can be tracked by their tdT expression (Figure 8 top).

The *CD4CreER^{T2} R26-tdT* mouse model was generated by breeding the *CD4CreER^{T2}* deleter mouse strain to *R26-tdT* reporter mice (see above). *CD4CreER^{T2} R26-tdT* mice express, in contrast to *CD4Cre R26-tdT,* a tamoxifen-inducible $CreER^{T2}$ recombinase under the control of the *Cd4*-promoter/enhancer/silencer. Thus, a deletion of the floxed *STOP* sequence of the *R26-tdT* locus and the following tdT expression occurs only in cells with an active CD4 promoter at the time of tamoxifen application, leading to tdT expression in those cells and in their offspring cells (Figure 8 bottom).

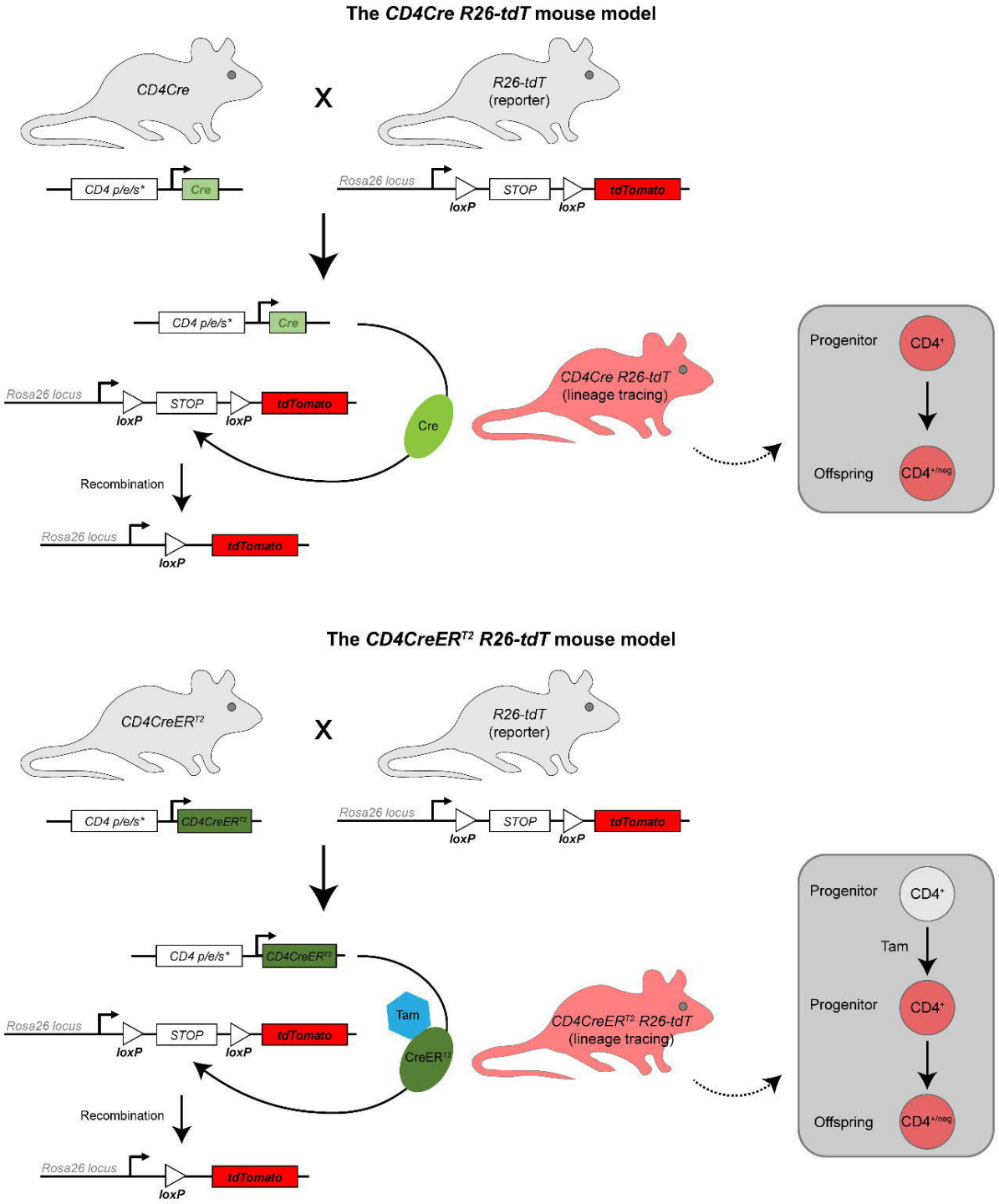

Figure 8. *In vivo* lineage tracing of CD4-expressing cells using *CD4Cre R26-tdT* and *CD4CreER^{T2} R26-tdT* mice.

Schematic representation of the genomic loci and recombination events of the lineage tracing mouse models *CD4Cre R26-tdT* (top) and *CD4CreER^{T2} R26-tdT* (bottom). Cre/CreER^{T2} recombinases are expressed under control of the *Cd4*-promoter/enhancer/silencer (p/e/s). In cells with CD4 promoter activity, the constitutively active Cre recombinase (top) or the conditional active CreER^{T2} recombinase in presence of tamoxifen (bottom) deletes the *loxP* sites-flanked *STOP* cassette of the *R26-tdT* locus leading to a *tdTomato* gene expression and thus to a labelling of *Cd4*-expressing cells and their offspring.

3.10.2.5 *CD4* knockout mice

In *CD4* KO mice the endogenous *Cd4* gene is homozygously disrupted by the insertion of a neomycin resistance cassette into exon 5 of the *Cd4* gene leading to lack of expression of the CD4 protein on thymocytes and lymph node cells [213]. However, *CD4* KO mice are healthy, fertile, show no alterations in the size of the lymphoid organs, normal numbers of T-lymphocytes and B-lymphocytes in lymph nodes as well as normal myeloid differentiation of BM cells [213]. Although the haematopoiesis of *CD4* KO mice is apparently not altered, these mice show a poor response against antigens but a relatively normal cytotoxic T-lymphocyte response against viruses in the absence of $CD4^+$ helper cells [213].

3.10.2.6 Summary of the used genetically modified mice

The sample types, if applicable the hair cycle phase, the mouse strain, age and sex for the experiments conducted in this thesis are listed in Table 17.

Table 17. Summary of skin sample type, hair cycle phase, mouse strain and mouse age and sex depicted in the Figure 13 - Figure 51.

Figure	Sample type	Hair cycle phase	Mouse strain (or cell line)	Mouse age, sex
Figure 13				
A-I'	Whole mounts, Cryotome sections	/	*CD4Cre*	18 weeks old, male
			CD4Cre R26-tdT	55 weeks old, female
J-L'	Whole mounts, Cryotome sections	/	*CD4Cre R26-tdT*	88 weeks old, male
Figure 14				
A-I'	Whole mounts, Cryotome sections	/	*CD4Cre*	18 weeks old, male
			CD4Cre R26-tdT	55 weeks old, female
J-J'	Whole mounts, Cryotome sections	/	*CD4Cre R26-tdT*	11 weeks old, female
Figure 15				
A-E'	Whole mounts, Cryotome sections	/	*R26-tdT* (n=3) *CD4Cre R26-tdT* (n=4)	E 18.5
Figure 16				
A-E	Flow cytometry	/	*CD4Cre R26-tdT*	6 weeks old, male 23 weeks old, male (n=2)
Figure 17				
A-B	*In vitro* cell culture	/	*CD4Cre R26-tdT*	23 weeks old, male
C-H	*In vitro* cell culture	/	*CD4Cre R26-tdT*	8 weeks old, male
Figure 18				
A	*In vitro* cell culture	Telogen	*CD4Cre R26-tdT*	28 weeks old, female
B, F, G, H	*In vitro* cell culture	Telogen	*CD4Cre R26-tdT*	24 weeks old, two females (material pooled)

Figure	Sample type	Hair cycle phase	Mouse strain (or cell line)	Mouse age, sex
Figure 18				
C	Flow cytometry	Middle anagen	C57Bl/6N	5 weeks old, female
		/	NIH3T3 cells	/
D	Flow cytometry	Anagen VI	C57Bl/6N	5 weeks old, female
E	Flow cytometry	Anagen VI	C57Bl/6N	5 weeks old, female
Figure 19				
A-B	Flow cytometry	/	*CD4CreER^{T2} R26-tdT*	6 weeks old, male
C	Whole mounts	/	*CD4CreER^{T2} R26-tdT*	17 weeks old, two males
Figure 20				
A, C-D	*In vitro* cell culture	/	*CD4CreER^{T2} R26-tdT*	12 weeks old, female
B, E-F	*In vitro* cell culture	Telogen	*CD4CreER^{T2} R26-tdT*	10 weeks old, three females (material pooled)
Figure 21				
A, A'	*In vitro* cell culture	/	Mouse ESC (mES RI), Passage 25	/
B-C''	*In vitro* cell culture	/	C57Bl/6N	5 weeks old, female
D	*In vitro* cell culture	/	*CD4Cre R26-tdT*	6 weeks old, male
Figure 22				
A-B'	Paraffin section	/	*CD4CreER^{T2} R26-tdT*	6 weeks old, male
Figure 23				
A	Cryotome section	Anagen VI	C57Bl/6N	5 weeks old, female
B	Cryotome section	Anagen VI	C57Bl/6N	5 weeks old, female
C	iHF	Anagen VI	*CD4Cre R26-tdT*	42 weeks old, female
D	Cryotome section	Telogen/Early anagen	*CD4Cre R26-tdT*	19 weeks old, male
Figure 24				
A	Flow cytometry	Telogen	*CD4Cre R26-tdT*	21 weeks old, female
C	Flow cytometry	Telogen	*CD4Cre R26-tdT*	23 weeks old, male
D	Flow cytometry	Telogen	*CD4Cre R26-tdT*	21 weeks old, female
E	Flow cytometry	Telogen	*CD4Cre R26-tdT*	28 weeks old, female
F	Flow cytometry	Telogen	*CD4Cre R26-tdT*	22 weeks old, female
G	Flow cytometry	Telogen	*CD4Cre R26-tdT*	21 weeks old, female
Figure 25				
B-G	Flow cytometry	Telogen	*CD4Cre R26-tdT*	56 weeks old, male

Figure	Sample type	Hair cycle phase	Mouse strain (or cell line)	Mouse age, sex
Figure 26 and Figure 27 and Figure 28				
A-E, A-D	RNA-sequencing	Telogen	*CD4Cre R26-tdT*	1st biological replicate: 29 weeks old, material from two males was pooled 2nd biological replicate: 32 weeks old, material from two males was pooled 3rd biological replicate: 32 weeks old, material from two males was pooled
Figure 29				
A	Epidermal sheet	Telogen	*CD4Cre R26-tdT*	21 weeks old, female
B	Cryotome section	Telogen	*CD4Cre R26-tdT*	59 weeks old, male
C	Whole mount	Anagen VI	*CD4Cre R26-tdT*	25 weeks old, female
D-G	iHF	Anagen VI	*CD4Cre R26-tdT*	43 weeks old, female
Figure 30				
B, B’	Cryotome section	Telogen	*CD4Cre R26-tdT*	22 weeks old, female
C, C’	Paraffin section	Telogen	*CD4Cre R26-tdT*	24 weeks old, male
D, D’	Paraffin section	Telogen	*CD4Cre R26-tdT*	59 weeks old, male
E, E’	Paraffin section	Telogen	*CD4Cre R26-tdT*	24 weeks old, male
F, F’	Cryotome section	Telogen	*CD4Cre R26-tdT*	22 weeks old, female
H, H’	Tail skin cryotome section	/	*CD4Cre R26-tdT*	55 weeks old, male
I, I’	Tail skin cryotome section	/	*CD4Cre R26-tdT*	55 weeks old, male
J, J’	Tail skin cryotome section	/	*CD4Cre R26-tdT*	55 weeks old, male
K	Tail skin epidermal sheet	/	*CD4Cre R26-tdT*	19 weeks old, male
Figure 31				
B, B’	Cryotome section	Telogen	*CD4Cre R26-tdT*	59 weeks old, male
C, C’	Cryotome section	Telogen	*CD4Cre R26-tdT*	22 weeks old, female
D, D’	Paraffin section	Telogen	*CD4Cre R26-tdT*	24 weeks old, male
E, E’	Paraffin section	Telogen	*CD4Cre R26-tdT*	24 weeks old, male

Figure	Sample type	Hair cycle phase	Mouse strain (or cell line)	Mouse age, sex
Figure 32				
B, B'	Isolated HF	Anagen VI (13- days after depilation)	*CD4Cre R26-tdT*	13 weeks old, male
C, C'	Isolated HF	Anagen VI (13- days after depilation)	*CD4Cre R26-tdT*	13 weeks old, male
D, D'	Paraffin section	Anagen VI (13- days after depilation)	*CD4Cre R26-tdT*	13 weeks old, female
E, E'	Paraffin section	Anagen VI (13- days after depilation)	*CD4Cre R26-tdT*	13 weeks old, female
F, F'	Paraffin section	Anagen VI (13- days after depilation)	*CD4Cre R26-tdT*	13 weeks old, female
G, G'	Paraffin section	Anagen II (4 days after depilation)	*CD4Cre R26-tdT*	9 weeks old, female
Figure 34 and Figure 35				
B-G'; B-C'	iHF	Anagen VI	*CD4Cre R26-tdT*	43 weeks old, female
Figure 36				
A-B', D, D'	iHF	Anagen VI	*CD4Cre R26-tdT*	28 weeks old, female
C, C'	iHF	Anagen VI	*CD4Cre R26-tdT*	47 weeks old, female
Figure 37				
B-B''	Whole mount	Anagen (VI)	*CD4Cre R26-tdT*	11 weeks old, male
C-C''	Whole mount of wounded area	Anagen VI	*CD4Cre R26-tdT*	11 weeks old, 18 days after wounding (n=2), females
Figure 38				
B-E''	Paraffin section of wounded area	Telogen	*CD4Cre R26-tdT*	14 weeks old, 35 days after wounding, female
Figure 39				
B1-B4	Dorsal skin whole mounts	Anagen VI	*CD4Cre R26-tdT*	11 weeks old, male 16 weeks old, female 25 weeks old, female 55 weeks old, female
C1-C4	Dorsal skin epidermal sheets	Telogen	*CD4Cre R26-tdT*	11 weeks old, female 21 weeks old, female 27 weeks old, female 55 weeks old, female

Figure	Sample type	Hair cycle phase	Mouse strain (or cell line)	Mouse age, sex
Figure 39				
D1-D4	Tail skin epidermal sheets	/	*CD4Cre R26-tdT*	7 weeks old, female 18 weeks old, male 22 weeks old, male 55 weeks old, female
E1-E2	Tail skin epidermal sheets	/	*CD4Cre R26-tdT*	7 weeks old, female 11 weeks old, male 18 weeks old, male 22 weeks old, male 55 weeks old, female
E3	Tail skin cryotome section	/	*CD4Cre R26-tdT*	22 weeks old, female
E4	Tail skin cryotome section	/	*CD4Cre R26-tdT*	88 weeks old, male
Figure 40				
B	Flow cytometry	Telogen	*CD4Cre R26-tdT*	5 weeks old, male and female (n=2) 9 weeks old, females (n=3) 21/22 weeks old, females (n=3) 55/59 weeks old, males (n=3)
C	Flow cytometry	Telogen	*CD4Cre R26-tdT*	55 weeks old, males (n=3)
Figure 41				
A	Flow cytometry	/	C57Bl/6N	31 weeks old, female
B	Flow cytometry	/	*CD4* KO	31 weeks old, male
C	Flow cytometry	/	C57Bl/6N *CD4* KO	31 weeks old, females (n=2) 31 weeks old, males (n=2)
Figure 42				
B	Flow cytometry	Anagen VI	C57Bl/6N	5 weeks old, male
C, H-K	Flow cytometry	Anagen VI	*CD4* KO	5 weeks old, males (n=3)
			C57Bl/6N	5 weeks old, one male and two females (n=3)
			C57Bl/6N	14 weeks old, females (n=3)
		Telogen	C57Bl/6N	3 weeks old, females (n=3)
			C57Bl/6N	11 weeks old, females (n=3)
			C57Bl/6N	18 weeks old, females (n=2)
			C57Bl/6N	30 weeks old, females (n=3)
			CD4 KO	31 weeks old, males (n=2)
			C57Bl/6N	56 weeks old, females (n=2)

Figure	Sample type	Hair cycle phase	Mouse strain (or cell line)	Mouse age, sex
Figure 42				
D-G	Flow cytometry	Anagen VI	C57Bl/6N	5 weeks old, male
			CD4 KO	5 weeks old, male
Figure 43				
	Flow cytometry	Anagen VI	C57Bl/6N	5 weeks old, male
Figure 44				
A	Cytospins	Anagen VI	C57Bl/6N	5 weeks old, one male and one female (material pooled) 5 weeks old, three females (material pooled)
B	Cytospins	Anagen VI	C57Bl/6N	5 weeks old, three females (material pooled)
			CD4 KO	5 weeks old, three males (material pooled)
Figure 45				
A, C, C', E, E'	Paraffin sections	Anagen VI	C57Bl/6N	5 weeks old, male
B, D, D', F, F'	Paraffin sections	Anagen VI after scraping off	C57Bl/6N	5 weeks old, male
Figure 46				
A-C	scRNA-Seq	Anagen VI	C57Bl/6N	5 weeks old, two males (material pooled)
Figure 47				
A-D	Paraffin sections	Anagen VI	C57Bl/6N	5 weeks old, male
Figure 48				
A-C'	*In vitro* cell culture	Telogen	*CD4Cre R26-tdT*	19 weeks old, male
Figure 49				
A-C	*In vitro* cell culture	Telogen	*CD4Cre R26-tdT*	26 weeks old, two males (material pooled)
Figure 50				
A-D	*In vitro* cell culture	Telogen	C57Bl/6N	18 weeks old, two males (material pooled)
Figure 51				
-	*In vitro* cell culture	Telogen	*CD4Cre R26-tdT*	47 weeks old, two females and one male (material pooled)

3.10.3 Patient samples

Human skin samples from healthy women were obtained from breast reduction surgeries from the Clinic for Plastic, Aesthetic and Reconstructive Surgery, Operative Breast Centre of the Evangelical Hospital Göttingen-Weende, Germany (head: Claudia Choi-Jacobshagen). Analyses of human skin samples from breast reduction surgery have been approved by the Ethics Committee of the University Medical Center Göttingen and were done in compliance

with ethical and legal regulations (file number: 6/10/19). All patients signed a written consent. Histology samples were taken from all patients.

Table 18. Summary of experiment type, patient number and patient age depicted in the Figure 52 - Figure 56.

Figure	Experiment type	Patient number	Age at the day of surgery
Figure 52			
A	Flow cytometry	25	56 years old
B	Flow cytometry	23, 26	22-24 years old
		22, 25, 28	56-58 years old
Figure 53			
-	*In vitro* culture of epidermal cells for medium establishment	19	50 years old
Figure 54			
-	*In vitro* culture of FACS-isolated cells for feeder-free culture establishment	25	56 years old
Figure 55			
-	*In vitro* culture of FACS-isolated cells and Trp63 staining	25	56 years old
Figure 56			
Top	*In vitro* culture of FACS-isolated cells and clonal growth assay	26	22 years old
Bottom		22	56 years old

4 Methods

4.1 Animal experiments

All experiments using animals were performed in compliance with all German legal and ethical requirements and have been approved by the Lower Saxony State Office for Consumer Protection and Food Safety (file number: 33.9-42502-04-15/1926 and 33.8-42502-04-20/3535). Housing and breeding of animals were performed within the animal facility at the Institute of Human Genetics or at the European Neuroscience Institute, University Medical Center Göttingen, Germany. In general, mice were housed at a 12 hours light-dark cycle at 20 ± 2 °C and a relative humidity of 55 ± 10%. The mice were housed individually or in groups in individually ventilated Makrolon type 2 cages located in air-flow racks. Health checks were performed daily by animal caretakers. Mice received tap water and food pellets *ad libitum*. Mice were weaned at the age of 3 weeks and were numbered by ear clipping. Tail tip or ear punch biopsies were taken and were used for genotyping of the respective mice (see chapter 4.7.1 and 4.7.2). The *CD4* KO mice were housed and bred within the animal facility at the European Neuroscience Institute, University Medical Center Göttingen, Germany, in individually ventilated GM500 cages in air-flow racks (SEALSAFE PLUS Maus GM500 DGM). *CD4* KO immunocompromised mice only received autoclaved water and food. All used mouse lines are listed in Table 16.

4.1.1 Tamoxifen application

To induce recombination of the floxed *tdT* locus in *CD4CreER^{T2} R26-tdT* mice 1 mg of tamoxifen in 100 µl solvent was injected i.p. for three to five consecutive days resulting in a total dose of 3 mg or 5 mg tamoxifen per mouse, respectively. Tamoxifen was prepared by mixing 200 mg tamoxifen with 20 ml sunflower seed oil and 800 µl pure EtOH. The solutions were stored at -20 °C in 1 ml syringes.

4.1.2 Depilation of murine dorsal skin

To synchronise the hair cycle of murine dorsal skin, depilation with a beeswax-colophonium mixture was executed. For this purpose, beeswax and colophonium were mixed in a 1:1 ratio and melted in a boiling water bath for about 20 minutes to form a homogeneous, creamy and turbid emulsion. Meanwhile, the mouse was anesthetized by inhalation anesthesia (Isofluran, Forene®), laid on a heated pad and the eyes were wetted with a 0.9% sodium chloride solution. A paper template was placed on the back of the mouse to mark the area to be depilated (approx. 3 x 1.5 cm). The paper template was covered with two layers of gauze bandages and

800 µl of the melted beeswax-colophonium mixture was pipetted on top. After approximately 8 minutes, the beeswax-colophonium mixture was cold enough so that the hair was carefully pulled off the skin together with the paper template, the cooled beeswax-colophonium mixture and the gauze bandages. The procedure took about 15 minutes per mouse.

4.1.3 Wounding of murine dorsal skin

Mice were medicated with the systemic analgetic Buprenorphin, Tamgesic® (0.1 mg/kg), which was applied i.p. and Meloxicam, Metacam® (0.1 mg/kg) that was given orally. Approximately 30-45 minutes later, an inhalation anesthesia (Isofluran, Forene®) was conducted, the mice were laid on a heated pad and the eyes were wetted with a 0.9% sodium chloride solution. Then, the dorsal skin was shaved with a longhair electric shaver and disinfected using 70% EtOH. Incisional wounds with a length of 0.5 cm were cut into the left and right side from the spinal column of the dorsal skin. The procedure took less than 10 minutes per mouse.

4.2 Tissue isolation from mice

All mice were euthanized by cervical dislocation under deep CO_2 narcosis.

4.2.1 Isolation of organ and embryo whole mounts

For organ whole mount preparations thymus, heart, lung, gut, skeletal muscle, bone, brain and pituitary gland from adult mice or whole embryo preparations from embryos at E18.5 were collected, washed in 1x PBS and fixed in 4% paraformaldehyde (PFA) solution for 2-24 hours, depending on the size of the respective organ. Bones were decalcified (see chapter 4.2.2). Before embedding organ whole mount preparations in either paraffin or cryoblock embedding medium, the organs were analysed for their tdT expression using a fluorescent dissecting microscope (Leica M205FA) equipped with a digital DFC camera (Leica DFC 450C) and the software Leica Application Suite.

4.2.2 Decalcification of murine bones

For decalcification of bones from murine fore and hind legs, the fat and muscle tissue were completely removed. Then, the bones were fixed in 4% PFA solution for 3-5 days and afterwards decalcified in ethylenediaminetetraacetic acid (EDTA)-solution (10%, pH 7.4) for ~3 weeks. The decalcification was tested by cutting the bone with a razor blade. Finally, the decalcified bones were embedded in paraffin or in cryoblock embedding medium.

4.2.3 Isolation of dorsal and tail skin

For isolation of dorsal skin samples, the back skin of the mice was shaved with a longhair electric shaver. Then, the dorsal skin was removed by using forceps and a scissor and subsequently was cut into pieces (0.5 x 0.5 cm^2). The obtained skin pieces were either used for isolation of keratinocytes or fibroblasts or were fixed in 4% PFA solution overnight and used for whole mount preparation, isolation of isolated HF (iHF), epidermal sheets or were embedded in paraffin or cryoblock embedding medium for histological analyses (Table 19). For the preparation of skin whole mounts and iHF from dorsal skin, only late anagen skin was used, as HF reach their maximum length in the late anagen phase [41] and are clearly visible from the dermal side after removal of the *subcutis*. In other hair cycle phases (e.g. telogen, early anagen, catagen), HF are too small for isolation of iHF or their visualisation in whole mount preparations. On the contrary, epidermal sheets from dorsal skin were prepared only from telogen skin, since telogen HF do not reach the dermis [41] and thus the efficient separation of epidermal and dermal tissue is possible. Paraffin and frozen tissue samples were taken from different hair cycle phases. The recognition of the hair cycle phase was achieved by taking into account the stage-dependent skin changes during hair cycle progression as skin thickness and pigmentation changes [41]. During the telogen phase, the skin is pink and thinnest, while during anagen progression, it becomes darker (due to an increased melanin production) and thicker until it is black and thickest in the late anagen phase (anagen VI) [41] (Figure 9 A). During the catagen phase the skin becomes thinner and lighter again [41].
For isolation of tail skin, the tail was slit lengthways with a scalpel. Then, the skin was peeled from the tail and cut into pieces (0.5 x 0.5 cm^2). The tail skin whole mount preparations were either used for the isolation of epidermal sheets or directly fixed in 4% PFA solution overnight and embedded in paraffin or cryoblock embedding medium (Table 19). The hair cycle phases of tail skin are asynchronous, thus for preparation of epidermal sheets or embedding for histological examination no particular hair phase can be taken in account (Table 19).

Table 19. Summary of skin sample types taken from different indicated hair cycle phases.
For the isolation method, chapters are given in the last column. Abbreviation: iHF: isolated hair follicle.

Sample type	Hair cycle phase	Chapter
Keratinocyte isolation	All phases	4.4.1.1
Fibroblast isolation	Independently	4.4.2.2
Whole mount preparations of dorsal skin	Late anagen	4.2.4
iHF of dorsal skin	Late anagen	4.2.5
Epidermal sheets of dorsal skin	Telogen	4.2.6
Epidermal sheets of tail skin	Asynchronous	4.2.6
Paraffin samples of dorsal/tail skin	All phases/Asynchronous	4.3.1
Cryotome samples of dorsal/tail skin	All phases/Asynchronous	4.3.4

Representative images of the different sample types analysed by transmitted-light bright field microscopy are shown in Figure 9.

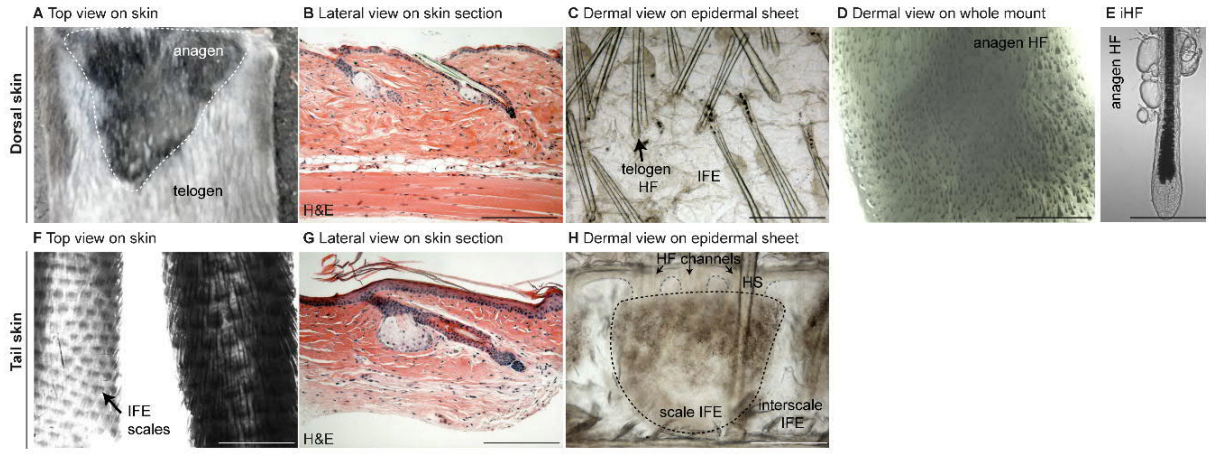

Figure 9. Overview of different murine dorsal and tail skin tissue isolates.

(A-E) Representative images of the dorsal view **(A)**, an H&E-stained lateral paraffin section **(B)**, dermal view on an epidermal sheet preparation (telogen) **(C)** or a whole mount preparation (late anagen) **(D)** and lateral view on an iHF (late anagen) **(E)** of murine dorsal skin. **(F-H)** Representative images of the dorsal view **(F)**, an H&E-stained lateral paraffin section **(G)** and dorsal view of an epidermal sheet **(H)** of murine tail skin. Scale bars: Magnifications: 2.5 mm in **F**; 1 mm in **D**; 200 µm in **B, C, G, H**; 100 µm in **E**. Abbreviations: IFE: interfollicular epidermis, iHF: isolated hair follicle, H&E: Haematoxylin and eosin, HF: hair follicle(s).

4.2.4 Isolation of murine whole mount preparations from dorsal skin

For whole mount preparations of isolated and fixed anagen dorsal skin, the *subcutis* was removed using two forceps - by holding the skin with one and peel off the *subcutis* with the other forceps. Afterwards, anagen HF were easily visible. The whole mount preparations were stored in either 1x PBS (for 1-2 weeks), or in 1x PBS containing 0.2% sodium azide for long-term storage (up to 2 months) at 4 °C. For analysis of the tdT expression the whole mount preparations were examined using a fluorescent dissecting microscope (Leica M205FA) equipped with a digital DFC camera (Leica DFC 450C) and the software Leica Application Suite.

4.2.5 Isolation of murine isolated hair follicles from dorsal skin

For the preparation of iHF according to Sequeira *et al.* [221], whole mount preparations from dorsal skin were transferred upside down in a petri dish (Ø10 cm) filled with 1x PBS. Then, iHF were extracted by grabbing and pulling out the respective HF with one and holding the epidermis with another forceps under usage of a stereo microscope (Zeiss Stemi 2000). iHF were stored in either 1x PBS (for 1-2 weeks), or in 1x PBS containing 0.2% sodium azide for long-term storage (up to 2 months) at 4 °C.

4.2.6 Isolation of epidermal sheets from murine dorsal or tail skin

The isolation of murine epidermal sheets from dorsal or tail skin was performed according to the protocol described by Braun *et al.* [222]. The establishment of the optimal trypsin incubation time of 27 hours for dorsal skin to achieve the dissociation of the epidermal and dermal tissue was performed previously [223]. For fixation, staining and storage of epidermal sheets, 12-well plates with 2 ml liquid per well were used and transfer of the sheets was performed with a small skimmer to avoid disintegration of the thin epidermal sheets.

For the isolation of epidermal sheets of murine dorsal telogen epidermis, the skin was shaved with a longhair electric shaver. Afterwards, the remaining hair was removed using hair removal cream for 5 minutes. The skin was removed by using forceps and a scissor and subsequently cut into pieces (0.5 x 0.5 cm^2). Then, the skin pieces were incubated in trypsin (0.25%) at 4 °C for 27 hours. On the next day, the epidermis was peeled off the dermis and fixed in 4% PFA solution for 2 hours.

In order to prepare epidermal sheets from murine tail skin, the tail was slit lengthways with a scalpel. Next, the skin was peeled off the tail and cut into pieces (0.5 x 0.5 cm^2). Subsequently, the skin pieces were incubated in EDTA-solution (5 mM) at 37 °C for 4 hours. Afterwards, epidermal sheets were peeled off the dermis and fixed in 4% PFA solution for 2 hours.

Epidermal sheets were stored in either 1x PBS (for 1-2 weeks), or 1x PBS containing 0.2% sodium azide for long-term storage (up to 2 months) at 4 °C.

4.3 Immunohistochemistry

Immunofluorescence stainings were documented on a confocal laser scanning microscope equipped with the software Fluoview FV100 (Olympus Corporation, Japan). Immunohistochemical stainings were documented on an Olympus BX 60 microscope equipped with the software CellSens Dimension (Olympus Corporation, Japan).

4.3.1 Paraffin embedding and sectioning

Tissue samples were fixed in 4% PFA solution, then transferred into 1x PBS and stored at 4 °C until embedding. The paraffin embedding was performed by Anke Frommhold and in cooperation with the Institute of Neuropathology, University Medical Center Göttingen, Germany. The paraffin-embedded tissues were cut into 4-5 µm sections on a microtome and mounted onto superfrost glass slides or microscope glass slides. The slides were dried at 37 °C overnight.

4.3.2 Haematoxylin and eosin staining

For haematoxylin and eosin (H&E) staining, paraffin sections were dewaxed by treatment with xylene twice for 10 minutes. Then, the sections were rehydrated by a descending alcohol series (99% → 96% → 80% → 70% EtOH) with final immersion into dH_2O. Next, the sections were incubated in haematoxylin solution for 20 minutes at room temperature (RT). Afterwards, the slides were washed under warm running tap water until excessive haematoxylin was completely dissolved from the slides. Then, the slides were stained with 1% eosin solution for 20 seconds and shortly washed in dH_2O. Directly after washing, the samples were dehydrated with an ascending alcohol series (70% → 80% → 96% → 99% EtOH) and dipped twice in fresh xylene. Finally, the sections were mounted with Pertex mounting medium.

4.3.3 Immunofluorescence staining of paraffin sections

Paraffin sections were dewaxed by treatment with xylene for 20 minutes. Subsequently, the slides were rehydrated in a descending alcohol series (99% → 96% → 70% EtOH) with final immersion into dH_2O. Next, slides were washed and permeabilised in 1x TBS-T 0.1% washing buffer. Antigen retrieval was performed as summarized in Table 20.

Table 20. Summary of used antigen retrieval methods.

Antigen retrieval	Treatment	pH
Citric acid 1	Microwave cooking at 600 Watt for 1x 4 minutes and 4x 3 minutes	6.0
Citric acid 2	Incubation at 55 °C in preheated citric acid for 30 minutes	6.0
Boric acid 1	Incubation at 58 °C in preheated 0.2 M boric acid for **10 minutes**	5.1
Boric acid 2	Incubation at 58 °C in preheated 0.2 M boric acid for **20 minutes**	5.1

Afterwards, the sections were washed in 1x TBS-T 0.1% washing buffer and the tissue was circled with a hydrophobic barrier marker. Non-specific antibody-binding was blocked by incubating the sections in 0.2% I-BLOCK blocking buffer for 20 minutes at RT. Primary antibodies were diluted in 1x TBS buffer according to Table 13 and applied on the tissue samples. Incubation was performed overnight at 4 °C in a wet chamber. On the next day, tissue samples were washed three times with 1x TBS-T 0.1% washing buffer and subsequently, the secondary antibody solution applied. For this purpose, secondary antibodies were diluted in 1x TBS buffer according to Table 13. The incubation was performed for 60 minutes at RT in a wet chamber. Afterwards, the tissue samples were washed again three times with 1x TBS-T 0.1% washing buffer. Finally, the samples were mounted with DAPI mounting medium and dried for at least 2 hours.

4.3.4 Embedding and sectioning of frozen tissue

Tissue samples were fixed in 4% PFA solution, then transferred into 1x PBS and stored at 4 °C until embedding. To prevent ice crystal formation due to freezing of water within the tissues that ruptures cell membranes, creates holes within the cells and produces loose ECM, the cryoprotectant sucrose was applied to the samples. Therefore, the tissues were treated with 5% sucrose in 1x PBS at 4 °C for 1 hour and then with 20% sucrose in 1x PBS at 4 °C overnight. Afterwards, the tissue samples were embedded using cryoblock embedding medium on dry ice and stored until sectioning at -80 °C. Sectioning was performed on a cryostat at -25 °C and the 6 µm sections were mounted onto superfrost glass slides. The slides were dried at RT for 2 hours and either stored at -20 °C or directly used for immunofluorescence stainings.

4.3.5 Immunofluorescence staining of cryotome sections

Dried cryotome sections were washed and permeabilised in 1x TBS-T 0.1% washing buffer and a barrier marker was used to circle the tissue with a hydrophobic barrier. Non-specific antibody-binding was blocked by incubating in 0.2% I-BLOCK blocking buffer for 20 minutes at RT. Primary antibodies were diluted in 1x TBS buffer according to Table 13 and applied on the tissue samples. Incubation was performed overnight at 4 °C in a wet chamber. On the next day, the samples were washed with 1x TBS-T 0.1% washing buffer and subsequently, the secondary antibodies that were diluted in TBS buffer according to Table 13 and applied. The incubation was performed for 60 minutes at RT in a wet chamber. Afterwards, the tissue samples were washed again with TBS-T 0.1% washing buffer. Finally, the samples were mounted with DAPI mounting medium and dried for at least 2 hours. For long-term storage the stainings were frozen at -20 °C.

4.3.6 Immunofluorescence staining of epidermal sheets and isolated hair follicles

For each epidermal sheet, one well of a 12-well plate and for each iHF one well of µ-Slide 8-well ibiTreat plate was used as otherwise sheets or iHF stuck together during antibody staining.

For immunofluorescence staining, epidermal sheets or iHF from murine dorsal skin were washed in 1x TBS-T 0.1% washing buffer for 5 minutes at RT and blocked by incubating in 0.2% I-BLOCK blocking buffer for 30 minutes at RT. Primary antibodies were diluted in 1x TBS-T 0.1% washing buffer according to Table 13 and applied on the samples. Incubation was performed overnight at 4 °C. On the next day, the samples were washed with 1x PBS-Tween

20 for 4 hours at RT with shaking. Secondary antibodies were diluted in 1x TBS-T 0.1% washing buffer according to Table 13. The incubation with the secondary antibodies was performed overnight at 4 °C. Afterwards, the samples were washed with 1x PBS-Tween 20 for 4 hours at RT. All washing and incubation steps were performed under continuous motion. Finally, the samples were mounted with DAPI mounting medium between two cover slides and dried for at least 2 hours.

Epidermal sheets from murine tail skin were stained according to Jensen *et al*. [90]. First, the sheets were permeabilised and blocked in PB buffer for 30 minutes at RT. Primary antibodies were diluted in PB buffer according to Table 13 and applied on the samples. Incubation was performed overnight at RT. On the next day, the samples were washed with 1x PBS-Tween 20 for 4 hours at RT. Secondary antibodies were diluted in PB buffer according to Table 13. The incubation with the secondary antibodies was performed overnight at RT. Afterwards, the samples were washed with 1x PBS-Tween 20 for 4 hours at RT. All washing and incubation steps were performed under continuous motion. Finally, the samples were mounted with DAPI mounting medium between two cover slides and dried for at least 2 hours.

To measure single tdT-marked clones, the number and size of tdT^+ single clones were determined using ImageJ. For this, greyscale images of the tdT fluorescence channel were first thresholded (using >Image>Adjust>Threshold) and then the particles analysed (using >Analyze>Analyze Particles).

For long-term storage the stainings were frozen at -20 °C.

4.3.7 Immunocytochemistry

In order to stain *in vitro* cultured cells (immunocytochemistry, ICC), the cells cultured on cover slips in 24-well plates were fixed in 4% PFA solution for 10 minutes and stored until staining in 1x PBS at 4 °C. For antibody staining the cells were washed and permeabilised with 1x TBS-T 0.1% washing buffer or in 1x TBS-T 0.5% (the latter one was used for permeabilisation of the cell nuclei membrane) for 30 minutes at RT. Non-specific antibody-binding was blocked by incubating in 0.2% I-BLOCK blocking buffer for 20 minutes at RT. Primary antibodies were diluted in 1x TBS buffer according to Table 13 and applied on the cover slips. Incubation was performed overnight at 4 °C. On the next day, the samples were washed with 1x TBS-T 0.1% washing buffer and subsequently, the secondary antibodies that were diluted in 1x TBS buffer according to Table 13 were applied. The incubation was performed for 60 minutes at RT. Afterwards, the cover slips were washed again with 1x TBS-T 0.1% washing buffer and finally mounted with DAPI mounting medium on superfrost slides and dried for at least 2 hours. For long-term storage the stainings were frozen at -20 °C.

4.3.8 Summary of the different antibody staining protocols

Table 21 summarizes the different staining protocols for paraffin and cryotome sections, epidermal sheets from dorsal and tail skin, iHF from dorsal skin and *in vitro* cultured cells with the individual steps.

Table 21. Summary of the different immunofluorescence antibody staining protocols.

Step	Paraffin sections	Cryotome sections	Epidermal sheet from dorsal skin	iHF from dorsal skin	Epidermal sheet from tail skin	ICC
Dewaxing and rehydration	Xylene for 20 minutes at RT; descending alcohol series	/				
Permeabilisation	1x TBS-T 0.1% washing buffer for 5 minutes at RT	1x TBS-T 0.1% washing buffer at RT (gently)	1x TBS-T 0.1% washing buffer for 5 minutes at RT		/	1x TBS-T 0.1% or 1x TBS-T 0.5% washing buffer for 30 minutes at RT
Antigen retrieval	See Table 20	/				
Blocking	0.2% I-BLOCK blocking buffer for 20 minutes at RT		0.2% I-BLOCK blocking buffer for 30 minutes at RT		PB buffer for 30 minutes at RT	0.2% I-BLOCK blocking buffer for 20 minutes at RT
Primary antibody incubation	Solved in 1x TBS, overnight, 4 °C		Solved in 1x TBS-T 0.1%, overnight, 4 °C, shaking		Solved in PB buffer, overnight, RT, shaking	Solved in 1x TBS, overnight, 4 °C
Washing step	1x TBS-T 0.1% washing buffer three times	1x TBS-T 0.1% washing buffer (gently)	1x PBS-Tween 20 for 4 hours at RT with shaking			1x TBS-T 0.1% washing buffer
Secondary antibody incubation	Solved in 1x TBS, 1 hour, RT		Solved in 1x TBS-T 0.1%, overnight, 4 °C, shaking		Solved in PB buffer, overnight, RT, shaking	Solved in 1x TBS, 1 hour, RT
Washing step	1x TBS-T 0.1% washing buffer three times	1x TBS-T 0.1% washing buffer (gently)	1x PBS-Tween 20 for 4 hours at RT with shaking			1x TBS-T 0.1% washing buffer
Mounting	DAPI mounting		DAPI mounting between two cover slides			DAPI mounting

4.3.9 Hoechst staining

For Hoechst staining of nuclei, fixed skin whole mount preparations were incubated for 10 minutes at RT in the dark in a Hoechst solution (Hoechst 33258 [10mg/ml] 1:1000 diluted in Ampuwa H_2O). After washing in 1x PBS the skin was mounted on a µ-Slide 4-well ibiTreat plate using Mowiol mounting medium.

4.4 Cell isolation

4.4.1 Keratinocyte isolation

The CD4 surface protein is highly sensitive towards dissociation with trypsin. Thus, a 5 minutes treatment of haematopoietic cell lines with a 0.25% trypsin solution results in a 50% reduction of detectable CD4 surface proteins [224]. To avoid the trypsin-mediated CD4 removal from the cell surface, primary keratinocytes were isolated using a thermoylsin-based dissociation, which is commonly used to detach epidermal cells from the skin [225, 226].

4.4.1.1 Isolation of epidermal keratinocytes from dorsal skin of adult mice

In order to isolate keratinocytes from murine dorsal skin, skin pieces (see chapter 4.2.3) were washed in HBSS solution (HBSS containing 1% penicillin and streptomycin [pen/strep] and 0.1% Amphotericin B, Table 10) and then placed the epidermal side downwards into thermolysin-HBSS solution-filled wells of a 6-well plate (per mouse: 100 µg thermolysin solved in 3 ml HBSS solution). After incubation at 37 °C for 2 hours, the epidermal cells were scraped off the skin into a Ø10 cm petri dish filled with 10 ml HBSS solution by using a scalpel. Subsequently, 10 ml 154 CF medium (154 CF containing 1% BSA, Table 10) was added to the epidermal isolates and the mixture was stirred at ~200 rpm for 20 minutes at RT. Next, the cell suspension was filtered through a 70 µm cell strainer and harvested into a 50 ml centrifuge tube. The cell plate was rinsed with 10 ml 154 CF medium in order to collect the remaining cells, which were then also filtered through the 70 µm cell strainer and harvested into the same 50 ml centrifuge tube. A second filtration step was performed using a 40 µm cell strainer and the isolates were collected in a new 50 ml centrifuge tube. From the next step, all further steps were performed on ice. After centrifugation of the isolates at 200 x g for 7 minutes at 4 °C, the supernatant was aspirated. The pellet was resuspended in 154 CF medium and the cells were counted in a Neubauer counting chamber (see chapter 4.6.2). Afterwards, the cells were either stained for flow cytometric measurements or for fluorescence activated cell sorting (FACS) (see chapter 4.5) and/or used for *in vitro* culture (see chapter 4.6.3.1).

4.4.1.2 Isolation of epidermal keratinocytes from human breast skin

Normal human skin samples were obtained from breast reduction surgeries (see chapter 3.10.3). At first, fresh skin samples were transferred into a cold HBSS-filled Ø10 cm petri dish and either shortly stored at 4 °C or directly cut into strips with a size of 0.5 cm x 1.5 cm. Subsequently, the skin strips were transferred with the epidermis facing upwards into a fresh Ø15 cm petri dish filled with dispase-HBSS solution (HBSS medium containing 10% [v/v] dispase) and incubated for 12 to 16 hours at 4 °C. Dispase is a protease that cleaves fibronectin, collagen IV and to a lesser extent also collagen I, therefore the connection between the epidermis and dermis becomes loose and the upper epidermal part can be removed. The following day, the epidermis was removed from the dermis using forceps and stored in a Ø10 cm petri dish filled with HBSS medium. The isolated epidermis was then cut with a scalpel into approx. 1 mm^2 small pieces and transferred into a 50 ml centrifuge tube with 0.25 mg/ml thermolysin solved in 20 ml preheated HBSS medium. The mixture was incubated for 40 minutes at 37 °C with carefully mixing every 5 minutes. Afterwards, the cell suspension was transferred to a new Ø10 cm petri dish filled with 20 ml hkera medium (Table 10) and incubated for 20 minutes at RT while it was stirred at 100 - 200 rpm. Afterwards the cell suspension was filtered twice through a 70 µm cell strainer and centrifuged at 200 x g for 5 minutes at 4 °C. The supernatant was discarded and the pellet was resuspended in 5 ml hkera medium. The cell number of the isolates was determined using a Neubauer counting chamber (see chapter 4.6.2). Afterwards, the cells were either stained for flow cytometric analysis, FACS (see chapter 4.5) and/or used for *in vitro* culture (see chapter 4.6.3.2) or cryopreserved (see chapter 4.6.1) in FCS and 5% DMSO.

4.4.2 Fibroblast isolation

4.4.2.1 Isolation of mouse embryonic fibroblasts

For the isolation of mouse embryonic fibroblasts (MEF), C57BL/6N wild type embryos on E 12.5 to 13.5 were collected and placed in a Ø10 cm petri dish filled with prewarmed (37 °C) 1x PBS. Then, head, limbs and tail and all organs of the embryos were removed. The remaining embryonic tissue was placed in a new Ø10 cm petri dish, cut into small pieces and digested in a sterile glass bottle containing sterile glass beads, a magnetic stirrer and a 0.05% trypsin/0.02% EDTA solution at 37 °C for 5 minutes under continuous stirring at 300 rpm. To neutralize trypsin, DMEM containing 10% FCS and 1% pen/strep was added to the cell suspension. Finally, the cells were seeded in culture flasks or petri dishes and cultured in DMEM with 10% FCS and 1% pen/strep. MEF were then mitotic inactivated (see chapter 4.6.5) and cryopreserved (see chapter 4.6.1) in DMEM containing 10% FCS and 10% DMSO (v/v).

4.4.2.2 Isolation of dermal fibroblast from adult mice

For the isolation of dermal fibroblasts from dorsal skin of adult mice a protocol according to Walmsley *et al.* [227] was conducted. Therefore, dorsal skin pieces (see chaper 4.2.3) were washed in 1x HBSS solution and subcutaneous fat was removed under a stereo microscope (Zeiss Stemi 2000). Next, the skin pieces were minced using razor blades and dissecting scissors until the tissue pieces had a diameter of 2-3 mm. Then, the tissue was transferred into 50 ml centrifuge tubes containing 1 mg/ml collagenase IV in 20 ml DMEM and were incubated for 60 minutes at 37 °C. Thereby the skin from up to five mice was treated in one tube. Next, the cell isolates were passed through a 10 ml syringe (without needle) for three to five times and additionally incubated for further 30 minutes at 37 °C while mixing every 5 minutes. Then, the digested tissue was pipetted up and down three to five times using a 10 ml pipette and the suspension was passed through a 100 µm cell strainer into a new 50 ml centrifuge tube. The cell strainer was washed with 20 ml DMEM containing 10% FCS. After centrifugation at 300 x g for 8 minutes at 4 °C, the supernatant was removed by also removing the upper whitish fat layer prior to the remaining supernatant to avoid adipocyte contamination. The cell pellet was resuspended in 20 ml DMEM containing 10% FCS and directly passed through a 70 µm cell strainer into a new 50 ml centrifuge tube. The cell strainer was washed with 10 ml DMEM containing 10% FCS. Finally, the cell suspension was centrifuged at 300 x g for 8 minutes at 4 °C, resuspended in DMEM containing 10% FCS and either stored on ice for subsequent staining for flow cytometric analysis (see chapter 4.5) or used for *in vitro* culture (see chapter 4.6.4.1).

4.4.2.3 Isolation of dermal fibroblasts from human breast skin

Dermal tissue obtained from isolation of keratinocytes from human skin samples (see chapter 4.4.1.2) was washed in HBSS solution, minced using a scalpel and subsequently transferred into a glass bottle containing glass beads, a magnetic stirrer and 10 ml 0.05% trypsin/0.02% EDTA solution. After an incubation for 15 minutes at 37 °C under continuous stirring, additional 50 ml HBSS solution was added and the cell suspension was filtered through a 100 µm cell strainer. Next, the cells were centrifuged at 200 x g for 5 minutes at 4 °C and finally, the human dermal fibroblasts (hDF) were seeded in a Ø10 cm petri dish filled with DMEM medium (containing 0.1% Amphotericin B, 1% pen/strep, 10% FCS) and *in vitro* cultured (see chapter 4.6.4.2).

As an alternative method to obtain *in vitro* growing hDF the fat layer of small human skin pieces (0.5 x 0.5 cm^2) was removed and the remaining skin pieces were stuck to a Ø10 cm petri dish which was afterwards filled with DMEM medium (containing 0.1% Amphotericin B, 1%

pen/strep, 10% FCS). Upon subsequent *in vitro* culture the fibroblasts grew out from the skin pieces.
Finally, hDF were mitotic inactivated (see chapter 4.6.5) and/or cryopreserved (see chapter 4.6.1) in DMEM containing 10% FCS and 10% DMSO (v/v).

4.4.2.4 Isolation of bone marrow-derived cells from adult mice

To isolate cells from murine BM, cords, muscle and fat tissue of the bones (femurs and/or tibias) were removed. Then, BM-derived cells were collected by flushing the femurs and/or tibias with a 10 ml syringe with a needle (26 gauge) and 10 ml MesenCult™ basal medium (mouse) into a Ø10 cm petri dish. However, BM-derived cells itself must not be pressed through syringe and needle, since stromal cells are very sensitive to shear forces. Afterwards, the cells were transferred into a 15 ml tube and counted using a Neubauer counting chamber (see chapter 4.6.2). Finally, BM-derived cells were used for *in vitro* culture (see chapter 4.6.4.3).

4.4.3 T-lymphocyte isolation

For the isolation of murine T-lymphocytes, the thymus of adult mice was removed and transferred to a 100 µm cell strainer placed in a Ø10 cm petri dish filled with 10 ml HBSS medium. Then, the thymus was pressed through the cell strainer into the HBSS medium by using the stamp of a 10 ml syringe. The cell suspension was transferred into a 15 ml centrifuge tube, centrifuged at 200 x g for 7 minutes at 4 °C and the supernatant discarded. After resuspension in 1x PBS, the cells were counted using a Neubauer counting chamber (see chapter 4.6.2) and antibody-stained for flow cytometric analyses (see chapter 4.5).

4.5 Flow cytometry and fluorescence activated cell sorting

For flow cytometric analyses as well as for FACS, single-cell suspensions of isolated murine or human cells were centrifuged at 200 x g for 7 minutes at 4 °C. The supernatants were discarded, each cell pellet was resuspended in 100 µl HBSS medium containing the respective antibodies for following flow cytometric analyses/FACS (Table 14) and incubated in the dark for 30 to 45 minutes on ice. Afterwards, the cells were washed with 3 ml 154 CF/1%BSA medium and centrifuged at 200 x g for 7 minutes at 4 °C. The supernatants were discarded and the cell pellets were resuspended in 500-800 µl 154 CF/1%BSA medium. Keratinocytes were filtered through a 50 µm cell strainer before the analysis. For flow cytometric analyses the BD-LSR-II flow cytometer using the BD-FACSDiva software was used. The data were analysed using the software FlowJo 7.6.5 (Tree Star Inc, Oregon, USA). For FACS the BD

FACS ARIA II was used at the Cell-Sorting Facility, University Medical Center Göttingen, Germany.

4.5.1 Fluorescence activated cell sorting of murine keratinocytes

The gating strategy for the FACS-based isolation of tdT^{+} CD49f^{+}CD34^{+}Sca-1^{neg}, tdT^{neg} CD49f^{+}CD34^{+}Sca-1^{neg}, tdT^{+} CD49f^{+}CD34^{+}Sca-1^{+} and tdT^{neg} CD49f^{+}CD34^{+}Sca-1^{+} epidermal cells from *CD4Cre R26-tdT* dorsal skin, is shown in Figure 10. Initially, living cells were gated using forward scatter (FSC) and side scatter (SSC) plots (FSC-A/SSC-A [P1], FSC-W [P2] and SSC-W [P3]). Next, CD49f-positive cells (P4) were gated to distinguish CD34^{+}Sca-1^{neg} (P5), CD34^{+}Sca-1^{+} (P6), CD34^{neg}Sca-1^{neg} and/or CD34^{neg}Sca-1^{+} cells. Finally, the CD34^{+}Sca-1^{neg} (P5) and the CD34^{+}Sca-1^{+} (P6) populations were sorted for being tdT^{+} and tdT^{neg} (P7-P10). Similarly, CD49f^{+}CD34^{+}Sca-1^{neg} (P5) and CD49f^{+}CD34^{neg}Sca-1^{+} murine epidermal cells were sorted from *CD4Cre R26-tdT* mice. Besides, this gating strategy was also used to receive CD49f^{+}CD34^{neg}Sca-1^{neg}, CD49f^{+}CD34^{neg}Sca-1^{+}, CD49f^{+}CD34^{+}Sca-1^{neg} (P5) and CD49f^{+}CD34^{+}Sca-1^{+} (P6) cells from wild type and *CD4* KO mice.

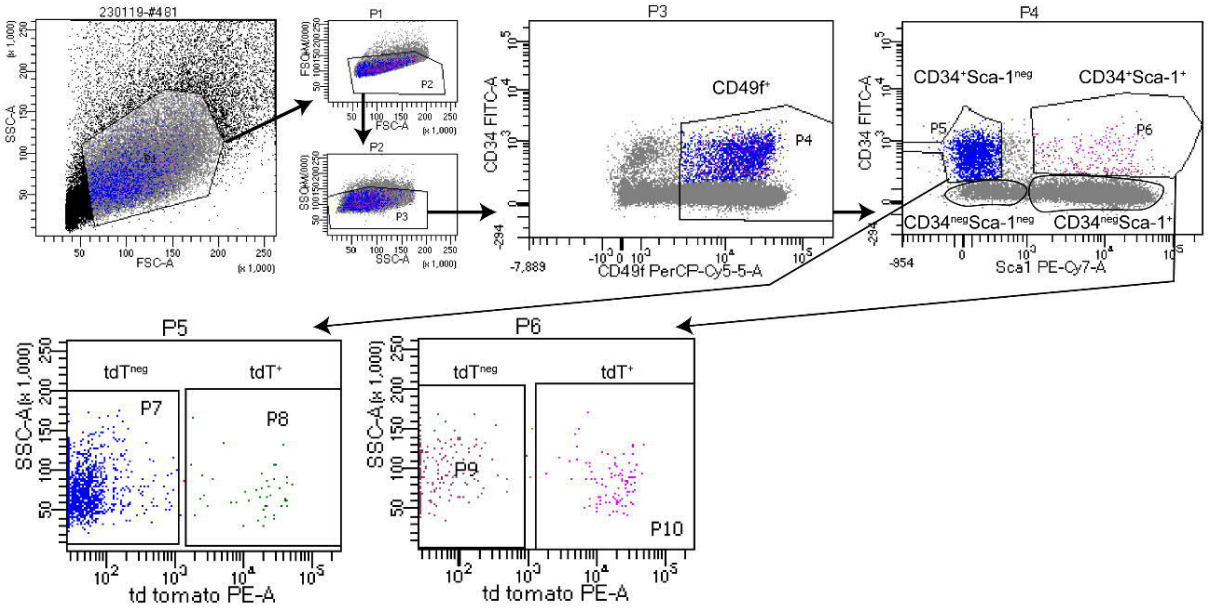

Figure 10. Gating strategy for fluorescence activated cell sorting of tdT^{+} CD49f^{+}CD34^{+}Sca-1^{neg}, tdT^{neg} CD49f^{+}CD34^{+}Sca-1^{neg}, tdT^{+} CD49f^{+}CD34^{+}Sca-1^{+} and tdT^{neg} CD49f^{+}CD34^{+}Sca-1^{+} murine epidermal cells.

Gating strategy for isolation of tdT^{+} CD49f^{+}CD34^{+}Sca-1^{neg}, tdT^{neg} CD49f^{+}CD34^{+}Sca-1^{neg}, tdT^{+} CD49f^{+}CD34^{+}Sca-1^{+} and tdT^{neg} CD49f^{+}CD34^{+}Sca-1^{+} epidermal cells from murine dorsal skin of *CD4Cre R26-tdT* mice. First, living cells were gated using FSC-A/SSC-A (P1), FSC-W (P2) and SSC-W (P3) plotting. Then, CD49f-expressing cells were chosen (P4) and were split into CD34^{+}Sca-1^{neg} (P5) and CD34^{+}Sca-1^{+} (P6) cells. Based on their tdT expression (visualised using the PE-channel) finally tdT^{+} and tdT^{neg} CD49f^{+}CD34^{+}Sca-1^{neg} (P7/P8) as well as tdT^{+} and tdT^{neg} CD49f^{+}CD34^{+}Sca-1^{+} (P9/P10) cells were sorted. Used antibodies were CD49f-PerCP-Cy5.5, Sca-1-PE-Cy7 and CD34-FITC (Table 14).

4.5.2 Fluorescence activated cell sorting of human keratinocytes

In order to obtain pure isolates of $CD4^+$ $CD49f^+CD29^+$ human epidermal SC FACS-based isolation of human antibody-stained keratinocytes was performed (Figure 11). For this purpose, first living keratinocytes were gated using FSC-A/SSC-A (P1), FSC-W (P2) and SSC-W (P3) plotting and subsequently $CD49f^+CD29^+$ cells were chosen (P4). These human epidermal SC ($CD49f^+CD29^+$) were further separated into $CD4^+$ and $CD4^{neg}$ cells.

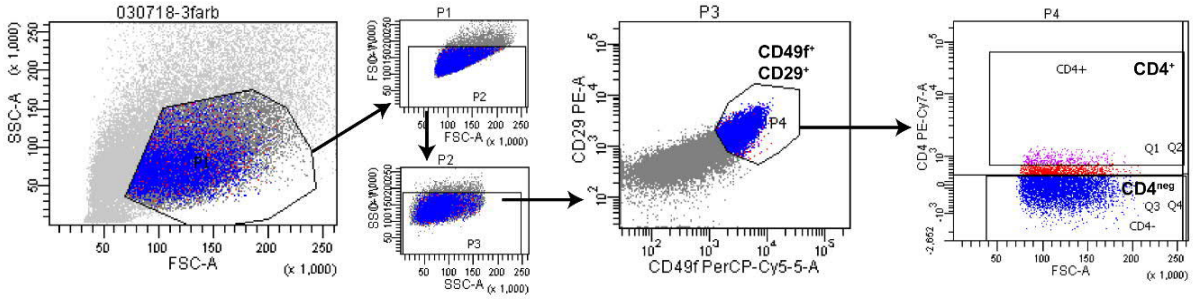

Figure 11. Gating strategy for fluorescence activated cell sorting of $CD4^+$ $CD49f^+CD29^+$ and $CD4^{neg}$ $CD49f^+CD29^+$ human epidermal cells.

(A) Gating strategy for isolation of $CD4^+$ $CD49f^+CD29^+$ and $CD4^{neg}$ $CD49f^+CD29^+$ epidermal cells from human skin. First, living cells were gated using FSC-A/SSC-A (P1), FSC-W (P2) and SSC-W (P3) plotting. Then, $CD49f^+CD29^+$ cells were chosen (P4) and were split into $CD4^+$ and $CD4^{neg}$ cells. These $CD4^+$ $CD49f^+CD29^+$ and $CD4^{neg}$ $CD49f^+CD29^+$ cells were sorted. Representative data are shown from patient #25. The same gating strategy was used and similar data were obtained with skin cells from patient #22 and 26 (data not shown). Used antibodies were CD49f-PerCP-Cy5.5, CD4-PE-Cy7 and CD29-PE (Table 14).

4.6 Cell culture methods

In vitro cell culture was performed in an atmosphere of 37 °C, 5% CO_2 with 95% humidity. The medium was changed three times a week and cultures were split when they reached > 90% confluence or when the keratinocyte colonies touched each other. Passaging of cells was performed by medium removal and incubation at 37 °C, 5% CO_2 and 95% humidity for 5-10 minutes or until all cells were detached in 0.05% trypsin/0.02% EDTA solution (5 ml per Ø10 cm petri dish), except for human primary keratinocytes that were detached with 10% dispase/HBSS solution and subsequent 0.05% trypsin/0.02% EDTA solution (see chapter 4.6.3.2). Afterwards, the cells were diluted in the respective cell culture medium, centrifuged at 200 x g for 5 minutes at 4 °C, the supernatant aspired and the cell pellet resuspended in cell culture medium before seeding. For cultivation of human primary keratinocytes on feeder cells additional mitotic inactivated MEF or hDF (see chapter 4.6.5) were seeded (~400,000 MEF or ~100,000-500,000 hDF per Ø10 cm petri dish).

4.6.1 Cell freezing

Long-time preservation of cell lines was ensured by cryoconservation of cells in liquid nitrogen. For this purpose, cells were detached with 0.05% trypsin/0.02% EDTA solution (5 ml per Ø10 cm petri dish), centrifuged at 200 x g for 5 minutes at 4 °C, the supernatant aspired and the cell pellet resuspended in the respective cell culture medium containing 10% DMSO (v/v), except for primary human keratinocytes FCS with 5% DMSO (v/v) was used. Per CryoPure tube 1 ml of the cell suspension was transferred and immediately frozen at -80 °C in a Mr. Frosty™ freezing container equipped with 99% isopropanol. After 24 hours, the cells were transferred in a liquid nitrogen tank for long-time storage.

4.6.2 Cell counting

To determine cell numbers, cells were counted with a Neubauer counting chamber. For this purpose, cells were detached with 0.05% trypsin/0.02% EDTA solution (5 ml per Ø10 cm petri dish), centrifuged at 200 x g for 5 minutes at 4 °C, the supernatant aspired and the cell pellet resuspended in 1 ml of the respective cell culture medium. Then, 10 µl from the cell suspension were transferred into a Neubauer counting chamber. All cells that laid in one big quadrant (containing 16 small quadrants) were counted and the cell number per ml was calculated with the following formula:

$$\frac{\text{Cells}}{\text{ml}} = \text{Counted cells} * 10^4$$

4.6.3 Keratinocyte *in vitro* culture

4.6.3.1 *In vitro* culture of murine keratinocytes from dorsal skin

Murine primary keratinocytes were cultured either under feeder-free conditions on collagen-coated dishes in feeder-free culture medium (Table 10) or on mitomycin C-inactivated NIH3T3 feeder cells (see chapter 4.6.5) (~60,000 NIH3T3 per well of a 24-well plate) in mKera medium (Table 10) without passaging.

For collagen I-coating, 1 ml of the solution (Bovine Collagen Solution Type I) was added per well of a 6-well plate and incubated for 30 minutes at 37 °C. Afterwards, excess fluid was removed from the coated surface and dried for at least 1 hour at RT. Next, it was rinsed with 1x PBS and the coated plates either stored covered with 1x PBS at 4 °C or medium added and used for cell cultivation.

For collagen IV-coating, 200 µl of a 10 µg/ml collagen IV solution (solved in 0.25% acetic acid) was added per well of a 24-well plate and incubated for 1 hour at RT. Afterwards, excess fluid was removed from the coated surface and washed first with 1x PBS and then with dH_2O. After

air-drying the plate, it was either covered with 1x PBS and stored at 4 °C for up to 6 months or directly used for cultivation. Approximately 100,000 or 600,000 primary murine keratinocytes per well of a 24-well plate or a 6-well plate, respectively, were seeded.

4.6.3.2 *In vitro* culture of human keratinocytes from breast skin

Human primary keratinocytes were cultured either under feeder-free conditions on collagen I-coated dishes (for coating procedure see chapter 4.6.3.1) in feeder-free culture medium (Table 10) or on mitomycin C-inactivated hDF or MEF (see chapter 4.6.5) (~400,000 MEF or ~100,000-500,000 hDF per Ø10 cm petri dish) in hkera medium (Table 10). For cultivation on feeder cells in hkera medium, 3-4 days after seeding, 0.01 µg/ml human EGF was added to the medium when the first medium exchange was performed. Subsequently, every 2-3 days the medium was changed until the colonies were big enough for expansion. For passaging, the keratinocytes were detached from the culture dish by incubating the cells in 10% dispase/HBSS solution for 3 minutes at 37 °C. Afterwards, the dispase solution was aspirated carefully and 0.05% trypsin/0.02% EDTA solution was added for 1 minute at RT. Then, the solution was pipetted up and down until the cells detached and the suspension became turbid. The detached cells were transferred into a centrifuge tube containing 5 ml hkera medium. Remaining cells and cell colonies were harvested by adding additional 0.05% trypsin/0.02% EDTA on the culture dish and pipetting up and down. After all cells were transferred into the centrifuge tube, the cells were centrifuged at 200 x g for 5 minutes at 4 °C. Since the co-cultured feeder cells detach similarly to the keratinocytes, it was not necessary to add additional fibroblasts when seeding the cells onto a similar plate size. For expansion of the culture, additional mitomycin C-inactivated hDF or MEF were seeded (~400,000 MEF or ~100,000-500,000 hDF per Ø10 cm petri dish).

4.6.4 Fibroblast *in vitro* culture

4.6.4.1 *In vitro* culture of murine dermal fibroblasts from dorsal skin

The murine dermal fibroblasts from dorsal skin were cultured in MesenCult complete medium on Ø10 cm cell culture dishes. Because fibroblasts adhere to plastic, they do not need coated surfaces.

4.6.4.2 *In vitro* culture of human dermal fibroblasts from breast skin

hDF were cultured in DMEM medium containing 10% FCS and 1% pen/strep on Ø10 cm cell culture dishes.

4.6.4.3 *In vitro* culture of murine bone marrow-derived stromal cells

Since freshly isolated Lin^{neg} BM-derived cells did not adhere or grow *in vitro*, cells isolated from the whole BM (see chapter 4.4.2.4) were seeded and expanded in MesenCult complete medium (Table 10) on Ø10 cm cell culture dishes. To then exclude immune cells from further analyses *in vitro* cultured whole BM-derived cells at passage one were subjected to Lin^{neg} selection. For this purpose, the BM-derived cells were detached using 0.05% trypsin/0.02% EDTA solution as described above and subsequently the EasySep™ Mouse Haematopoietic Progenitor Cell Isolation Kit, according to the manufacturer's protocol, used. Thereby all T-lymphocytes, B-lymphocytes, macrophages/monocytes, dendritic cells, natural killer (NK) cells, granulocytes and erythrocytes were targeted and removed from the cell suspension by antibody-based selection of the antigens CD5, CD11b, CD19, CD45R/B220, Ly6G/C(Gr-1) and TER119. BM-derived cells and BM-derived Lin^{neg} cells were either stored on ice for subsequent staining for flow cytometric analysis (see chapter 4.5) or further cultivated in MesenCult complete medium (Table 10) and used for ICC staining (see chapter 4.3.7).

4.6.5 Mitotic inactivation by mitomycin C-treatment of cells

Mitomycin C is a cytostatic drug that inhibits cell division due to its DNA-intercalation and thus inducing covalent linkage of DNA strands.
For mitotic inactivation of fibroblasts (e.g. NIH/3T3, MEF or hDF), the cells were grown until they reached a confluence of 80-90%. Then, they were washed three times with 1x PBS and treated with 2 mg mitomycin C from *Streptomyces caespitosus* in 200 ml DMEM containing 1% pen/strep and 10% FCS for 2.5 (murine fibroblasts) or 3 hours (hDF) at 37 °C. Afterwards, the mitomycin C solution was aspirated and cells were washed with 1x PBS. To detach inactivated cells from cell culture dishes, 0.05% trypsin/0.02% EDTA solution was added as described above and cryopreserved (see chapter 4.6.1). To proof successful mitotic inactivation, mitomycin C-treated cells as well as untreated cells were thawed and seeded at the same density on Ø 10 cm cell culture dishes, simultaneously. 1 day and also 1 week after seeding the cell number of both cultures was compared.

4.6.6 Rhodamine B and nile blue A staining (clonal growth assay)

To analyse the CFE of primary keratinocytes, staining with rhodamine B and nile blue A was performed [228]. Thereby, nile blue A stains basic substances blue (e.g. cell nuclei, elastic fibrils), while rhodamine B stains epithelial cells red-violet (e.g. differentiated keratinocytes, keratinized epidermal cells). For the staining, human *in vitro* cultured keratinocytes were fixed with 4% PFA for 10 minutes and washed with 1x PBS. Then, the cells were directly stained on

the culture dish by staining with 0.1 mg/ml nile blue A in dH_2O for 20 minutes at RT and subsequently with 0.1 mg/ml rhodamine B in dH_2O for 20 minutes at RT. Next, cells were washed with dH_2O and then allowed to dry. Finally, rhodamine B and nile blue A stainings were documented on a stereo microscope (SZX12) equipped with the software CellSens Dimension (Olympus Corporation, Japan) and the total number of colonies as well as the number of colonies that exceed a diameter of 0.5 mm were counted.

4.7 Molecular biology

4.7.1 Isolation of genomic deoxyribonucleic acid

Mouse tail tip or ear punch biopsies were used to isolate genomic DNA (gDNA) and to perform polymerase chain reaction (PCR)-based genotyping of transgenic mice. For gDNA isolation, each biopsy was digested in 500 µl of sodium chloride-tris-EDTA buffer containing 0.25 mg proteinase K at 55 °C overnight. On the next day, the samples were shaken thoroughly and then centrifuged at 13,000 rpm for 10 minutes at RT. 300 µl of the supernatant was transferred into 1 ml of pure denatured EtOH to precipitate the gDNA. The samples were centrifuged at 13,000 rpm for 30 minutes at 4 °C, supernatants were discarded and pellets were washed with 200 µl of 70% EtOH and centrifuged again at 13,000 rpm for 10 minutes at 4 °C. The supernatants were discarded and pellets were dried upside down at 55 °C for ~10 minutes. The isolated gDNA was dissolved in 125 µl H_2O and shaken at 1,400 rpm for 10 minutes at 42 °C.

4.7.2 Polymerase chain reaction

Genotyping of mice was performed by PCR using the gDNA isolated from mouse tail tip or ear punch biopsies. Each reaction contained 10-100 ng of gDNA template, 0.5 µM forward primer, 0.5 µM reverse primer, 0.2 µM dNTPs, 0.3 mM $MgCl_2$, 10% (v/v) Cresol, polymerase buffer, 0.1 U MolTaq polymerase and was filled with dH_2O to 10 µl. All used primers and the size of PCR products are noted in Table 22. The cycling conditions used for genotyping are listed in Table 23.

Table 22. Primers used for polymerase chain reaction-based genotyping of transgenic mice.

Mouse line	Primer name	Primer sequence (5'-3' orientation)	Amplicon size	Manufacturer/ Reference
CD4 KO Wild type (wt)	*CD4KO-wtF*	CCT CTT GGT TAA TGG GGG AT	381 bp	The Jackson Laboratory, Bar Harbor, ME, USA
	CD4KO-wtR	TTT TTC TGG TCC AGG GTC AC		

Mouse line	Primer name	Primer sequence (5'-3' orientation)	Amplicon size	Manufacturer/ Reference
CD4 KO Mutant (mut)	*CD4KO-mutF*	GTG TTG GGT CGT TTG TTC G	225 bp	The Jackson Laboratory, Bar Harbor, ME, USA
	CD4KO-wtR	TTT TTC TGG TCC AGG GTC AC		
CD4Cre	*CD4Cre-F*	GGT TAT CAA GGT CCT GAG GAA G	420 bp	Eurofins MWG Operon, Deutschland
	CD4Cre-R	CTC GTG ATC GAC CGG TAA TGC		
CD4CreER^{T2}	*CD4CreER^{T2}-F*	GCG GTC TGG CAG TAA AAA CTA TC	~100 bp	The Jackson Laboratory, Bar Harbor, ME, USA
	CD4CreER^{T2}-R	GTG AAA CAG CAT TGC TGT CAC TT		
R26-tdtomato wt	*R26-tdtomato-wtF*	AAG GGA GCT GCA GTG GAG TA	297 bp	The Jackson Laboratory, Bar Harbor, ME, USA
	R26-tdtomato-wtR	CCG AAA ATC TGT GGG AAG TC		
R26-tdtomato mut	*R26-tdtomato-mutF*	GGC ATT AAA GCA GCG TAT CC	196 bp	The Jackson Laboratory, Bar Harbor, ME, USA
	R26-tdtomato-mutR	CTG TTC CTG TAC GGC ATG G		

Table 23. Cycling conditions used for genotyping of transgenic mice.

	Temperature	Time	Cycles	Temperature	Time	Cycles
	CD4Cre			***R26-tdTomato, CD4* KO**		
First denaturation	95 °C	4 minutes		94 °C	4 minutes	
Denaturation	95 °C	25 seconds		94 °C	20 seconds	
Annealing	57 °C	45 seconds	30x	60 °C	20 seconds	33x
Elongation	72 °C	45 seconds		72 °C	45 seconds	
Final elongation	72 °C	5 minutes		72 °C	5 minutes	
Hold	15 °C	forever		10 °C	forever	
	CD4CreER^{T2}					
First denaturation	95 °C	5 minutes				
Denaturation I	95 °C	20 seconds				
Annealing I	65 °C	15 seconds	10x			
Elongation I	72 °C	10 seconds				
Denaturation II	95 °C	15 seconds				
Annealing II	60 °C	15 seconds	28x			
Elongation II	72 °C	10 seconds				
Final elongation	72 °C	2 minutes				
Hold	15 °C	forever				

4.7.3 Agarose gel electrophoresis

DNA fragments of different fragment sizes were separated by agarose gel electrophoresis. Before loading, the samples were mixed with 6x loading buffer. Depending on the size of the DNA fragments to be analysed, the 0.8-2% (w/v) agarose gels were prepared. The DNA was visualised in the agarose gel by adding a few drops of ethidium bromide (0.07%) to the still liquid gel. DNA separation was performed in a gel electrophoresis apparatus filled with 1x tris-boric-acid-EDTA solution with a constant voltage of 100 V. A DNA ladder was loaded as a marker to examine the size of the DNA fragments. The documentation was performed on a UV Transilluminator and GDS 3.39 (INTAS Science Imaging Instruments GmbH, Germany) software.

4.7.4 Ribonucleic acid isolation

The protocol for ribonucleic acid (RNA) isolation from small amounts of cells was obtained from the NGS Service Facility for Integrative Genomics, University Medical Center Göttingen, Germany. The protocol is suitable for RNA isolation out of 20 mg tissue or 5 x 10^5 cells. RNA isolation was performed on ice if not indicated otherwise. Filter tips and equipment was RNase-free and the workplace cleaned with RNaseZAP to avoid RNase contamination. Firstly, the cell pellet was resuspended in 360 µl TRIzol® Reagent for 5 minutes at RT. After addition of 72 µl chloroform, the samples were vortexed for 30 seconds and centrifuged at 12,000 x g for 15 minutes at 4 °C. Then, colourless upper aqueous phase that contains the RNA was isolated, 180 µl 70% EtOH and 1 µl of GlycoBlue™ Coprecipitant were added, followed by an overnight incubation at -20 °C. On the next day, RNA was pelleted by centrifugation at 12,000 x g for 45-55 minutes at 4 °C, washed twice with 70% EtOH, dried at 37 °C and solved in 10 µl RNase free H_2O. The RNA concentrations were measured using a NanoDrop (Table 24).

Table 24. Summary of the FACS population, biological replicate, mouse age, number of cells and ribonucleic acid concentration.

Each sample consists of the material from two sex-matched mice.

Population	Biological replicate	Mouse age	# of cells after FACS	RNA concentration [in ng/µl]
P7: tdT^{neg} $CD49f^{+}CD34^{+}Sca1^{neg}$	1st	29 weeks old	176492	0.5959
	2nd	32 weeks old	134359	0.0999
	3rd	32 weeks old	189796	0.3271
P8: tdT^{+} $CD49f^{+}CD34^{+}Sca1^{neg}$	1st	29 weeks old	6997	0.0392
	2nd	32 weeks old	954	0.002
	3rd	32 weeks old	6932	0.03

Population	Biological replicate	Mouse age	# of cells after FACS	RNA concentration [in ng/µl]
P9: tdT^{neg} $CD49f^{+}CD34^{+}Sca1^{+}$	1st	29 weeks old	16972	0.0341
	2nd	32 weeks old	20448	0.0148
	3rd	32 weeks old	15223	0.0207
P10: tdT^{+} $CD49f^{+}CD34^{+}Sca1^{+}$	1st	29 weeks old	10676	0.0287
	2nd	32 weeks old	2917	0.006
	3rd	32 weeks old	5734	0.0119

4.7.5 Whole transcriptome sequencing

RNA quality control (Fragment Analyzer, Agilent Technologies, USA), complementary DNA (cDNA) library preparation (TruSeq® RNA Sample Preparation v2; Illumina, USA) and RNA sequencing (HiSeq 4000; Illumina, USA) were performed at the NGS Service Facility for Integrative Genomics, University Medical Center Göttingen, Germany. For raw read and quality check, sequence images were transformed with Illumina software BaseCaller to BCL files, which was demultiplexed to fastq files with bcl2fastq2 v2.20.0.422. The sequencing quality was asserted using FastQC (http://www.bioinformatics.babraham.ac.uk/projects/fastqc/) (version 0.11.5). For mapping and normalisation, sequences were aligned to the reference genome M. musculus (mm10 version 96, https://www.ensembl.org/Mus_musculus/Info/Index) using the STAR aligner (version 2.7.1a) [207] allowing for two mismatches within 50 bases. Read counting was performed using featureCounts [205] (version 1.5.0-p1). Read counts were analysed in the R/Bioconductor environment (version 3.4.4, www.bioconductor.org) using the DESeq2 [204] package version 1.18.1. Candidate genes were filtered using an absolute log2 fold-change > 1 and FDR-corrected p-value < 0.05. Genes were annotated using the M. Musculus gene version 96 Gene transfer format (GTF) file. Final data visualisation was performed with RStudio (RStudio, Inc., USA) and GraphPadPrism 6 (GraphPad Software, Inc., USA).

A principal component analysis (PCA) plot is shown (Figure 12) to visualise the genetic distance between the sequenced populations (for population description see Table 24).

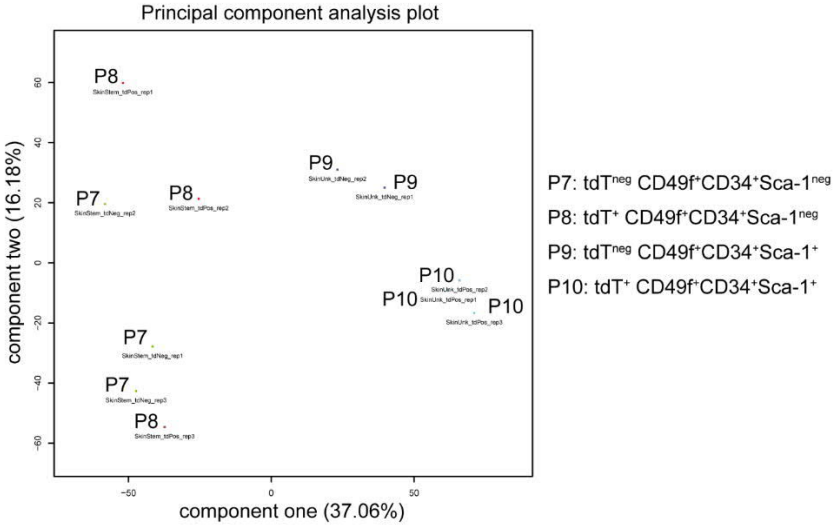

Figure 12. Principal component analysis plot to visualise genetic distance and relatedness between the populations that were analysed via whole transcriptome sequencing.

The principal component analysis verifies genetic relatedness between the sorted CD49f^{+}CD34^{+}Sca1^{neg} cells independent of tdT expression (P7: tdT^{neg} CD49f^{+}CD34^{+}Sca1^{neg}; P8: tdT^{+} CD49f^{+}CD34^{+}Sca1^{neg}). Distant to the CD49f^{+}CD34^{+}Sca1^{neg} cells are the CD49f^{+}CD34^{+}Sca1^{+} cell populations (component one on x-axis) of which the tdT^{neg} (P9) populations differ slightly compared to the tdT^{+} (P10) populations (component two on y-axis).

4.7.6 Single-cell transcriptome sequencing

Single-cell RNA sequencing (scRNA-Seq), including cDNA amplification, library preparation, sequencing and bioinformatic data analysis was performed at the Cologne Center for Genomics (CCG), Germany. For this purpose, a single-cell suspension of ~5 x10^{6} freshly isolated murine cells from dorsal skin (see chapter 4.4.1.1) was frozen at -80 °C in Synth-a-Freeze Cryopreservation Medium and shipped to the CCG on dry ice. At the CCG, the viability after thawing was determined to be ~50% living cells by trypan blue staining. Thus, the dead cell removal kit (Miltenyi Biotec B.V. & Co. KG, Bergisch Gladbach, Germany) was conducted that resulted in an enrichment of ~85% of living cells. Then, the single-cell suspension was filtered through a 40 µm cell strainer and 1x PBS supplemented with 0.04% BSA used to avoid the formation of cell clusters. Afterwards, the sequencing was performed using the BigDye™ Terminator v3.1 Cycle Sequencing Kit and the library was sequenced in Illumina NovaSeq 6000. The fastq files were demultiplexed using bcl2fastq2 from illumina and the produced fastq files were analysed with cellranger (v3.1.0) (with the following options: cellranger count --id=SID123348; --transcriptome=refdata-cellranger-mm10-3.0.0; --fastqs=PRID4437TX98/fastq123348 --sample=123348; --expect-cells=10000 --chemistry=auto --jobmode=slurm). For mapping and normalisation, sequences were aligned to the reference genome M. musculus (mm10). In total 13,397 cells were sequenced with 23,117 mean reads per cell and 2,236 median genes per cell. Final data visualisation was performed with Loupe Browser (10x Genomics, Pleasanton, CA, USA), RStudio (RStudio, Inc., USA) and GraphPadPrism 6 (GraphPad Software, Inc., USA).

5 Results

Ptch$^{fl/fl}$ *CD4Cre* mice never develop BCC spontaneously but only upon DMBA/TPA treatment. Based on this observation it was concluded that a *CD4Cre*-mediated homozygous *Ptch* depletion is not sufficient for BCC development [193]. In fact, this conclusion stands in contrast to 'classical' BCC mouse models, in which *Ptch* is simultaneously mutated in a large proportion of HF SC (e.g. *Lgr5Cre Ptch*$^{fl/fl}$ [197]) or basal IFE cells (e.g. *K14CreER*^{T2} *Ptch1*$^{fl/fl}$ *Ptch2*$^{tm1/tm1}$ [202]) and in which BCC develop spontaneously. However, these facts also question whether the BCC precursors of *Ptch*$^{fl/fl}$ *CD4Cre* skin either possess a lower tumourigenic potential than HF SC and basal IFE cells or only represent a small number of cells that remain below a critical tumour-inducing cell number regardless of their tumourigenic potential. Since the BCC-precursors of *Ptch*$^{fl/fl}$ *CD4Cre* skin might originate from either epidermal keratinocytes as 'classical' BCC-precursors (e.g. bulge, sHG, uHF or basal IFE cells) or from non-epidermal stromal cells (e.g. BM-derived MSC) that are described as epidermal and thus putative BCC progenitors, those cell types were evaluated as the putative source of *Ptch*$^{fl/fl}$ *CD4Cre* BCC.

5.1 *CD4Cre* activity and CD4 expression in murine stromal cells

Skin-residing non-epidermal cells, like cells of mesodermal origin e.g. haematopoietic or stromal cells, might be considered as BCC-precursors in *Ptch*$^{fl/fl}$ *CD4Cre* mice since in addition to CD4^{+} immune cells (e.g. T-lymphocytes, monocytes) also *Cd4/CD4* expression has been described on stromal cells (e.g. BM-derived MSC) (see chapter 1.3.2) and thus *Ptch* should be depleted in those cell types. However, a haematopoietic origin of *Ptch*$^{fl/fl}$ *CD4Cre* BCC has been already excluded [193]. Thus stromal cells such as BM-derived MSC remain as a possible source of *Ptch*$^{fl/fl}$ *CD4Cre* BCC since (a) they can be isolated from almost all postnatal connective tissues including the skin [110-112], (b) they possess the potential to differentiate into multiple skin cell types [96-100, 102] and (c) can express *Cd4/CD4* transcripts [160-164, 170, 171].

To investigate this intriguing possibility and to unravel whether non-haematopoietic descendants of cells with *CD4Cre* activity exist, first the progeny of *CD4Cre*-expressing cells was tracked in cells of the lung, heart, cartilage, BM, skeletal muscle, gut, brain and pituitary gland. Secondly, the expression of the *CD4Cre*-transgene as well as of the CD4 protein in BM-derived MSC and skin-derived dermal fibroblasts was analysed.

5.1.1 The progeny of *CD4Cre*-targeted cells repopulates embryonic skin and lung as well as various adult tissues

To track the progeny of *CD4Cre*-targeted cells the lineage tracing *CD4Cre R26-tdT* strain was generated by breeding *CD4Cre*-driver (for details regarding the mouse model see chapter 3.10.2.2) and *R26-tdT* reporter mice (for details regarding the mouse model see chapter 3.10.2.4). The resulting *CD4Cre R26-tdT* mice, in which *CD4Cre*-expressing cells and their progeny are tagged by the red fluorescence protein tdT, were then used to identify offspring cells of *CD4Cre*-expressing cells in different tissues, including those that have been previously reported [173-175]. Figure 13 and Figure 14 show representative images of whole mount and cryotome section analyses from organs of a *CD4Cre* control mouse and a 55-week-old *CD4Cre R26-tdT* mouse (exception: bone section: 88 weeks old; pituitary gland section: 11 weeks old). Besides, also the organs of 11 and 22-week-old *CD4Cre R26-tdT* mice were analysed but showed a similar tdT expression pattern (data not shown). Since the *CD4Cre*-transgene is highly expressed in thymocytes [173] first the tdT expression of *CD4Cre R26-tdT* thymi was analysed. Indeed, *CD4Cre R26-tdT* thymi show a strong tdT signal, which was not observed in control thymi from *CD4Cre*-diver mice lacking the *R26-tdT* reporter transgene (Figure 13 A, A'). The tdT expression of thymocytes on cellular level was confirmed by the analysis of anti-CD4 antibody staining of *CD4Cre R26-tdT* thymus sections (Figure 13 B, B'). Besides, also in lung, heart, ear and bone of *CD4Cre R26-tdT* mice a strong tdT expression was observed (Figure 13 C-L'). None of the control mice showed tdT signals in any of the investigated organs (Figure 13 C-L'). According to Thunemann *et al.*, in the lung of *CD4Cre R26-tdT* mice, tdT^+ bronchial epithelial cells, surrounded by $tdT^{neg}PDGFR\alpha^+$ fibroblasts, were detected (Figure 13 D, D') [173]. Beyond that, tdT^+ cells were also found in the cardiac muscle (Figure 13 F, F') [173], the elastic cartilage of the ear (Figure 13 H, H'), the bones of the hind legs and in the BM (Figure 13 J-L') [174, 175]. Due to their morphological appearance, these tdT^+ cells most likely represent cardiac muscle cells (Figure 13 F'), chondrocytes (Figure 13 H') and immune cells or stromal cells of the BM (Figure 13 K', L'), respectively.

These results recapitulate the previously reported existence of non-haematopoietic lung epithelial cells, cardiac muscle cells, chondrocytes and BM cells as descendants of *CD4Cre*-expressing cells in the lung, heart and bone of mice.

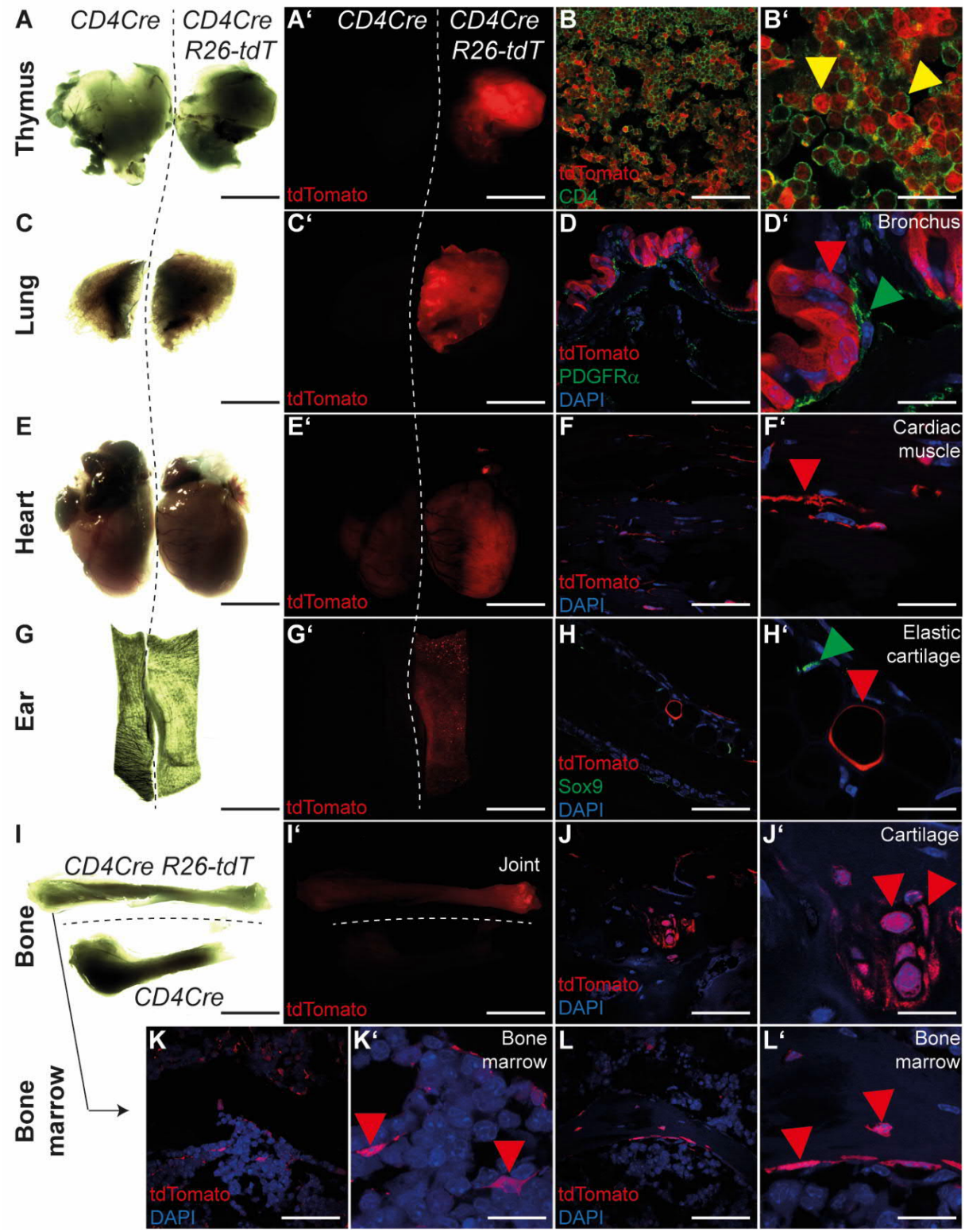

Figure 13. The progeny of *CD4Cre*-targeted cells grows in the thymus, lung, heart, cartilage and bones.

Representative images of whole mount organ preparations **(A, A', C, C', E, E', G, G', I, I')** of a 18-week-old *CD4Cre* (control) and a 55-week-old *CD4Cre R26-tdT* mouse and cryotome sections **(B, B', D, D', F, F', H, H', J, J', K, K', L, L')** of a 88-week-old (bone) or a 55-week-old (thymus, lung, heart, ear) *CD4Cre R26-tdT* mouse. Cryotome sections of the thymus, the lung and the ear were stained with the T-lymphocyte marker CD4 **(B, B')**, the pan-fibroblast marker PDGFRα **(D, D')** or the chondrocyte marker Sox9 **(H, H')**, respectively. Naïve tdT signal shown in red. Red arrowheads: tdT^+ cells, green arrowheads: cells positive for the respective protein marker expression, yellow arrowheads: double positive cells. Nuclei were visualised with DAPI (blue). Scale bars: 2.5 mm in **A, A', C, C', E, E', G, G', I,** I'; 33 µm in **B, D, F, H, J, K, L**; 10 µm in **B', D', F', H', J', K', L'**. For details regarding the mice and antibody staining, see Table 17 and Table 13, respectively.

Remarkably, the analyses of *CD4Cre R26-tdT* skeletal muscle, gut, brain and pituitary gland revealed that tdT$^+$ cells also grow in these tissues, but never in *CD4Cre* control organs (Figure 14 A-J'). On cellular level tdT$^+$ cells were identified in the skeletal muscle (Figure 14 B, B'), in the villi and in the *lamina muscularis mucosae* of the gut (Figure 14 D, D*, D'), in the cerebellum (Figure 14 F, F') as well as in the cerebrum (Figure 14 H, H') and in the pituitary gland (Figure 14 J, J').

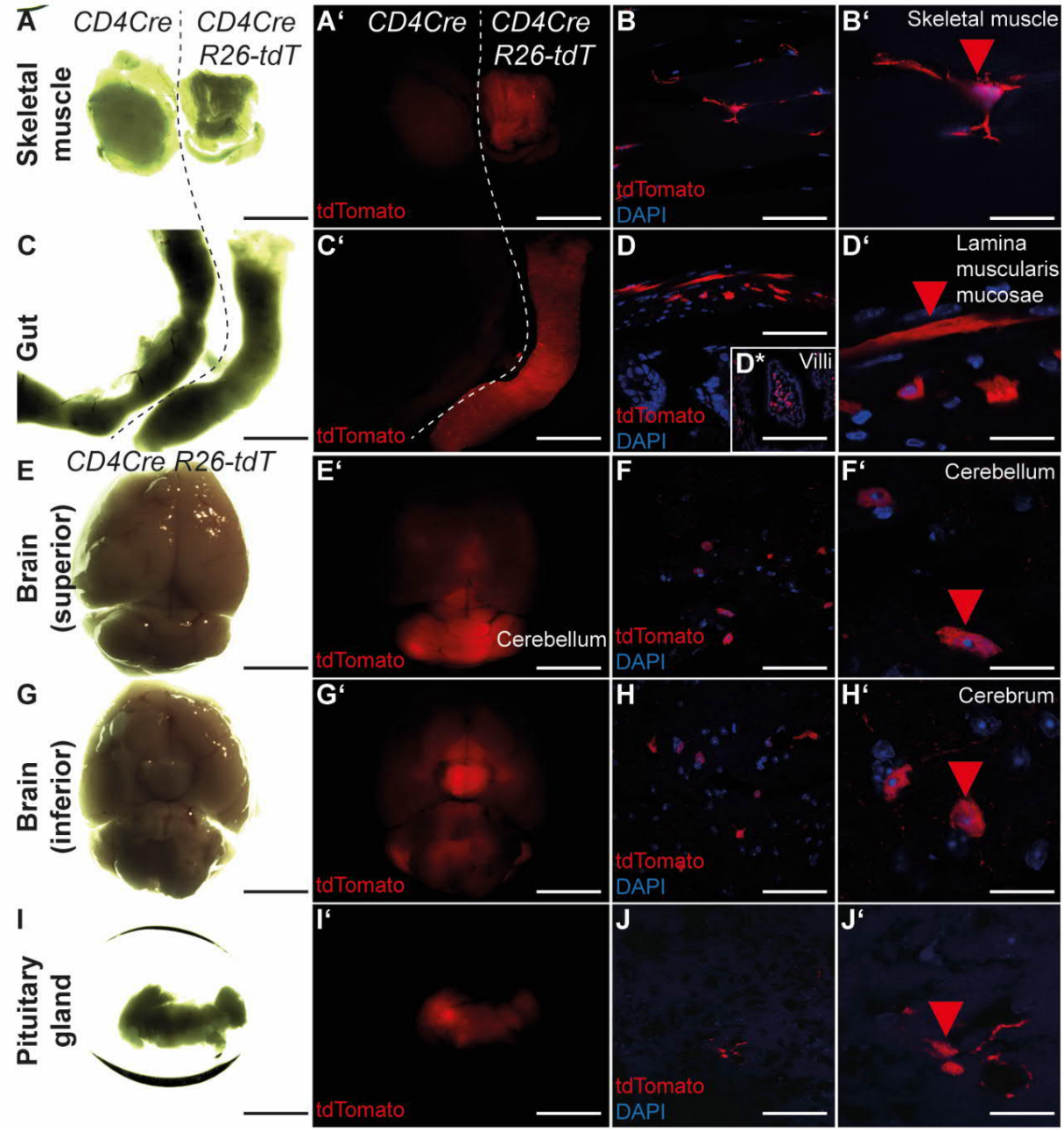

Figure 14. The progeny of *CD4Cre*-targeted cells grow in skeletal muscle, gut, brain and pituitary gland.

Representative images of whole mount organ preparations **(A, A', C, C', E, E', G, G', I, I')** of a 18-week-old *CD4Cre* (control) and a 55-week-old *CD4Cre R26-tdT* mouse and cryotome sections **(B, B', D, D', F, F', H, H', J, J')** of a 11-week-old (pituitary gland) or a 55-week-old (skeletal muscle, gut, brain) *CD4Cre R26-tdT* mouse. Naïve tdT signal shown in red. Red arrowheads: tdT$^+$ cells. Nuclei were visualised with DAPI (blue). Scale bars: 2.5 mm in **A, A', C, C', E, E', G, G', I, I'**; 72.6 µm in **D***; 33 µm in **B, D, F, H, J**; 10 µm in **B', D', F', H', J'**. For details regarding the mice see Table 17.

As stated above, differently aged *CD4Cre R26-tdT* adult mice (11, 22 or 55 weeks old) did not show differences in the tdT expression pattern of the analysed organs. Since a *Cd4* expression has also been described for alveolar epithelial cells during mouse embryonic development [170, 171], next the tdT expression pattern of *CD4Cre R26-tdT* embryos was analysed. Indeed, whole mount embryo preparations revealed that the skin of E18.5 *CD4Cre R26-tdT* embryos contains tdT^+ cells, which were never observed in the *R26-tdT* control embryos (Figure 15 A). Interestingly, only the dermis but never the epidermis of the skin contains tdT^+ cells (Figure 15 B, C), which most likely represent fibroblasts due to their elongated morphological appearance (Figure 15 C). In line with Chen *et al.* [170, 171] and similarly to the adult lung (Figure 13 C-D'), also the embryonal lung of *CD4Cre R26-tdT* mice contains tdT^+ bronchial epithelial cells that are surrounded by $tdT^{neg}PDGFR\alpha^+$ fibroblasts (Figure 15 D-E'). However, the number of tdT^+ bronchial epithelial cells of the embryonic lung is much less compared to the adult lung (compare Figure 13 D, D' and Figure 15 D-E') suggesting that *CD4Cre* expression is not restricted to the embryonic development or that the bronchial epithelial progeny of *CD4Cre*-expressing cells are strongly multiplied during murine development and/or adolescence.

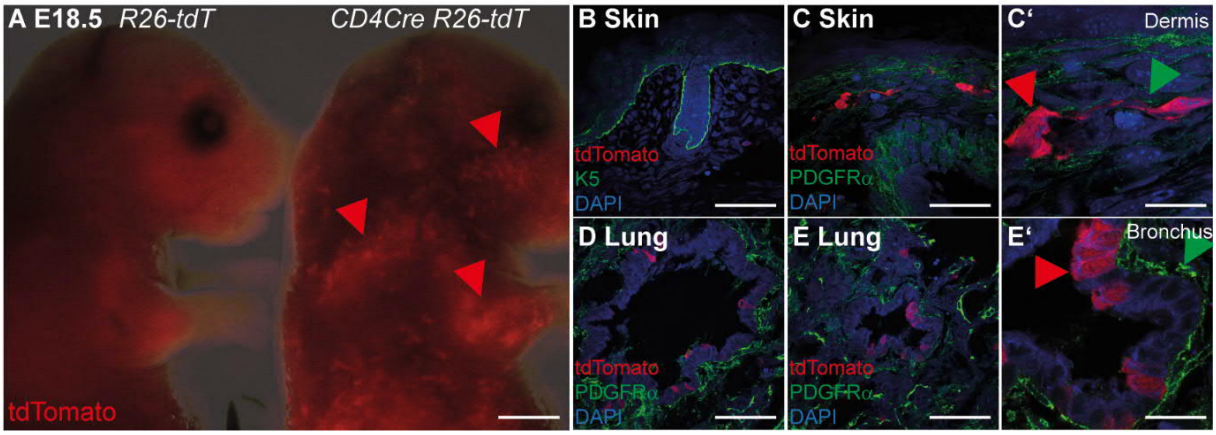

Figure 15. The progeny of *CD4Cre*-targeted cells populates embryonic skin and lung.

(A) Representative image of whole embryo preparation at embryonic day (E) 18.5 of a *R26-tdT* (control) and a *CD4Cre R26-tdT* embryo. **(B-E)** Representative images of immunofluorescent stained cryotome sections of embryonic skin **(B-C')** and lung **(D-E')** of E18.5 *CD4Cre R26-tdT* embryos with the basal layer and outer root sheath marker K5 **(B)** or the pan-fibroblast marker PDGFRα **(C-E)**. Naïve tdT signal shown in red. Red arrowheads: tdT^+ cells, green arrowheads: PDGFRα positive cells. Nuclei were visualised with DAPI (blue). Scale bars: 1.25 mm in **A**; 33 µm in **B, C, D, E**; 10 µm in **C', E'**. For details regarding the mice and antibody stainings, see Table 17 and Table 13, respectively.

Except for tdT^+ dermal fibroblasts and tdT^+ bronchial epithelial cells, no tdT^+ cells were observed in any other organ in E18.5 *CD4Cre R26-tdT* embryos. During development of the thymus, common lymphoid progenitors colonize the epithelial tissue and develop into thymocytes on E10-12 [229]. Initially, only double negative ($CD4^{neg}CD8^{neg}$) thymocytes are present until E14, whereas first $CD4^{low}$ thymocytes are detectable at E15 but account less than 2.5% and, subsequently, from E16-18 double positive ($CD4^+CD8^+$) thymocytes arise from 0.3%

to 60%, respectively [230]. However, since recombination at the *R26-tdT* locus and thus tdT expression occurs time-delayed this may explain the absence of tdT^+ cells in the thymus of E18.5 *CD4Cre R26-tdT* embryos. However, it can be assumed that the progeny of *CD4Cre*-expressing cells in adult tissues (e.g. in the cardiac muscle, in cartilage and BM of the bones) either descent from the unravelled tdT^+ embryonic cell types or more probable that the *CD4Cre*-transgene is expressed again during adolescence or adulthood in non-haematopoietic cells.

5.1.2 *CD4Cre* activity and CD4 expression in stromal cells *in vitro*

In adult mice, cells of different germinal layers descent from *CD4Cre*-expressing cells since tdT^+ cells with endodermal (lung epithelium), mesodermal (cartilage, muscle, T-lymphocytes in the thymus) and ectodermal (nervous system) origin have been detected in *CD4Cre R26-tdT* mice. This indicates that either independent precursor cells from different germinal layers or a common ancestor represent the origin of the different tdT^+ cell types in *CD4Cre R26-tdT* mice. However, since in late *CD4Cre R26-tdT* embryos only dermal fibroblasts and bronchial epithelial cells descent from *CD4Cre*-expressing cells it is very likely that the *CD4Cre*-expressing ancestor/s of tdT^+ cells can also be identified in adult *CD4Cre R26-tdT* mice (hypothetically with exception of the lung and the dermis). Possible candidate cell types, that possess the potential to give rise to mesodermal (e.g. cartilage and muscle cells) [109] and ectodermal cells [96], are stromal cells like BM-derived MSC or fibroblasts. These cells have been determined in and isolated from almost every tissue (e.g. BM, fat tissue, dermis) [110-112] and also have been shown to express *Cd4* during murine embryogenesis [170, 171] (Figure 15). Thus, *Cd4*-expressing stromal cells potentially present the putative progenitor for tdT^+ cells descending from different germinal layers in *CD4Cre R26-tdT* mice. Therefore, the existence of stromal cells that (1) derive from cells with *CD4Cre* activity, (2) show *CD4Cre* activity and/or (3) express the CD4 surface protein was analysed next. For this purpose, *in vitro* cultured BM-derived MSC and dermal fibroblasts from *CD4Cre R26-tdT* and from tamoxifen-inducible *CD4CreER^{T2} R26-tdT* reporter mice (for details regarding the mouse model see chapter 3.10.2.3 and 3.10.2.4) were investigated. Finally, anti-CD4 antibody staining to detect the surface protein were conducted.

BM-derived MSC are plastic-adherent, show a fibroblast-like morphology (spindle-shaped) and are $CD90^+CD44^+CD29^+$ but Lin^{neg} [115]. To analyse whether BM-derived MSC descent from *CD4Cre*-expressing cells, whole BM cells as well as Lin^{neg} BM cells (for details see chapter 4.4.2.4 and 4.6.4.3) from *CD4Cre R26-tdT* mice were *in vitro* cultured and subsequently analysed for tdT and the MSC marker expression via flow cytometry (Figure 16). This analysis indeed revealed that ~4% of complete BM cells (Figure 16 A) and ~2% of Lin^{neg} BM cells (Figure 16 B) express tdT. The MSC markers CD90, CD44, CD29 are simultaneously

expressed on ~30% or ~20% of complete BM cells or of Lin^{neg} BM cells, respectively (Figure 16 C-E). However, since macrophages are the major contamination in BM-derived MSC culture, the complete BM cell culture most properly contains high amounts of (tdT$^+$) CD90$^+$CD44$^+$CD29$^+$ macrophages. However, macrophage-depleted culture of Lin^{neg} BM-derived cells consist of ~6% cells that express tdT, CD90, CD44 and CD29 and thus might represent MSC that descent from *CD4Cre*-expressing cells.

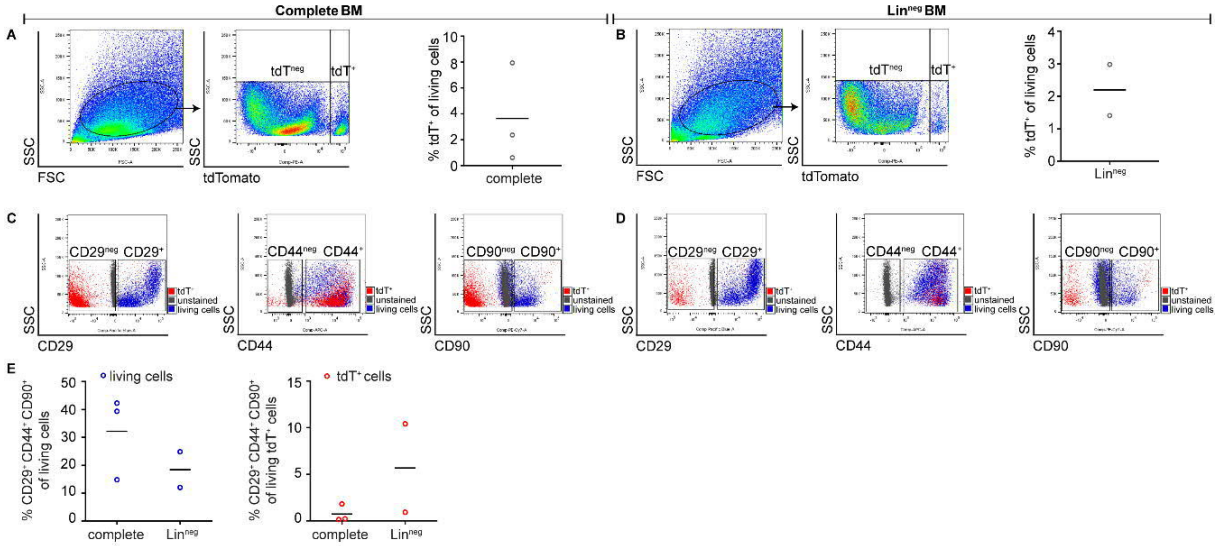

Figure 16. The progeny of *CD4Cre*-targeted cells comprises bone marrow-derived mesenchymal stromal/stem cells.

(A-E) Flow cytometric analyses of 45,000-500,000 stained cultured bone marrow (BM) cells **(A, C, E)** or lineage negative (Lin^{neg}) BM cells **(B, D, E)** in passage one isolated from BM of 6-week-old (BM) and two 23-week-old (BM, Lin^{neg} BM) *CD4Cre R26-tdT* mice and cultured in MesenCult complete medium. **(A, B)** Left panels: SSC/FSC plots for gating living cells and SSC/tdT (PE-channel) plot for visualisation of tdT expression on living cells. Right panels: Quantification of tdT$^+$ cells of BM cells **(A)** and of Lin^{neg} BM cells **(B)**. **(C, D)** SSC/CD29 (left), SSC/CD44 (middle), SSC/CD90 (right) plots with 10,500 unstained cells (grey), 8,400 or 54,400 living cells (blue) and 6,800 or 1,700 tdT$^+$ cells (red) of BM cells **(C)** and of Lin^{neg} BM cells **(D)**, respectively. **(E)** Quantification of CD29$^+$CD44$^+$CD90$^+$ cells of living cells (left) and of tdT$^+$ cells (right) among BM cells **(A, C)** and Lin^{neg} BM cells **(B, D)**. For details regarding the mice see Table 17.

Indeed, microscopical analyses of *in vitro* cultured whole BM and Lin^{neg} BM cells from a *CD4Cre R26-tdT* mouse revealed that the BM of adult mice contains non-haematopoietic cells that descent from *CD4Cre*-expressing cells and that grow with three different morphologies: a roundish (red arrows), a spindle-shaped (red arrowheads) and a flattened-shaped (red double arrowheads) morphology (Figure 17 A-B). For characterisation of the BM-derived cells subsequently immunofluorescence stainings against the macrophage marker F4-80, the marker of proliferation Ki-67 (MKI67) and the myofibroblast marker α-SMA were conducted (Figure 17 C-H).

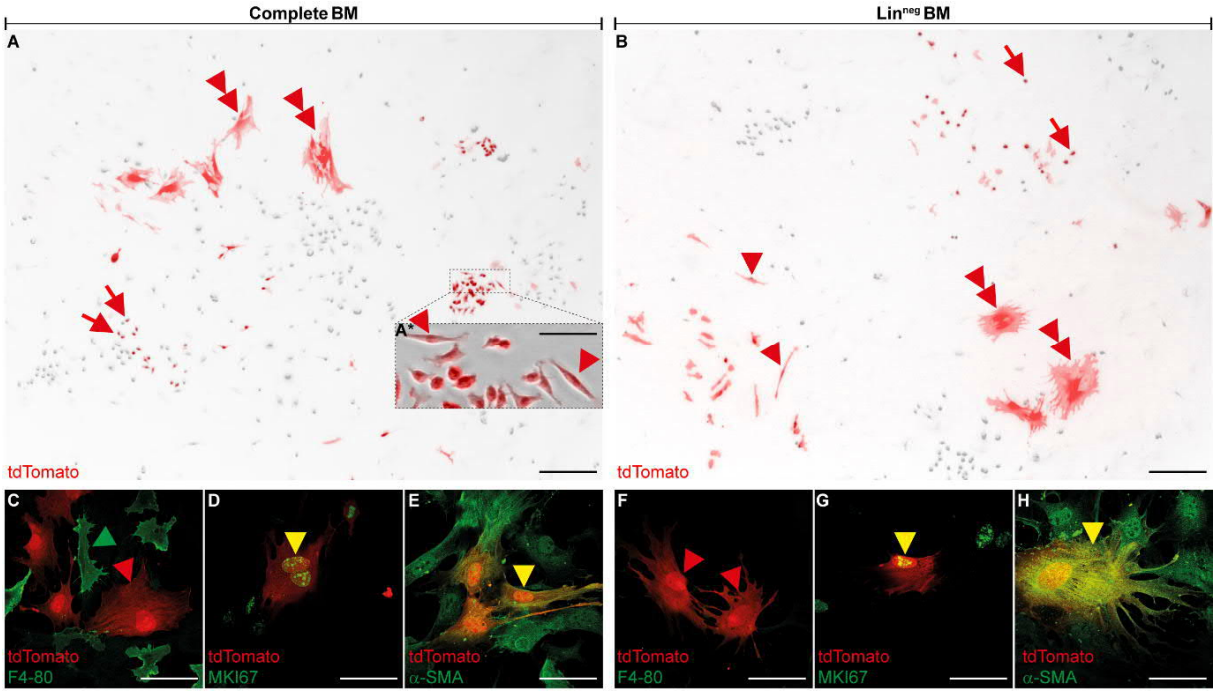

Figure 17. The progeny of *CD4Cre*-targeted cells comprises roundish, spindle-shaped and flattened α-SMA$^+$ bone marrow-derived cells.

(A-B) Representative images of cultured bone marrow (BM) cells **(A, A*)** or lineage negative (Lin^{neg}) BM cells **(B)** in passage one isolated from BM of a 23-week-old *CD4Cre R26-tdT* mouse and cultured in MesenCult complete medium. Naïve tdT signal is shown in red. Red arrowheads: tdT$^+$ spindle-shaped cells; red double arrowheads: tdT$^+$ flattened-shaped cells; red arrows: tdT$^+$ roundish cells. **(C-H)** Representative images of cultured BM cells **(C-E)** or Lin^{neg} BM cells **(F-H)** in passage one isolated from BM of a 8-week-old *CD4Cre R26-tdT* mouse, cultured in MesenCult complete medium and stained against the macrophage marker F4-80 **(C, F)**, the proliferation marker MKI67 **(D, G)** and the myofibroblast marker α-SMA **(E, H)**. Naïve tdT signal is shown in red. Red arrowheads: tdT$^+$ cells; green arrowhead: F4-80$^+$ cell; yellow arrowheads: double positive cells. Scale bars: 166 µm in **A, B**; 40 µm in **A***; 33 µm in **C-H**. For details regarding the mice and antibody stainings, see Table 17 and Table 13, respectively.

These analyses confirmed the macrophage-free culture of Lin^{neg} BM cells (Figure 17 F) in contrast to the whole BM culture in which a huge number of F4-80$^+$ macrophages were found (Figure 17 C). However, a gross number of tdT$^+$F4-80^{neg} cells were found in both the whole BM and the Lin^{neg} BM cell culture (Figure 17 C, F) demonstrating the existence of non-haematopoietic, plastic-adherent BM cells that descent from *CD4Cre*-expressing cells. Beyond that, the analysis showed that tdT$^+$ BM-derived cells actively proliferate *in vitro* due to their expression of the proliferation marker MKI67 (Figure 17 D, G). Furthermore, most of the flattened-shaped cells, but none of the spindle-shaped nor roundish tdT$^+$ cells, express the myofibroblast marker α-SMA (Figure 17 E, H). Since α-SMA is expressed by several murine BM-derived MSC lines [231] and on myofibroblasts that are an intermediate state of skin-derived fibroblasts or BM-derived MSC and smooth muscle cells during wound healing processes (reviewed in [59]) flattened-shaped (tdT$^+$) α-SMA$^+$ cells (Figure 17 H) most likely represent myofibroblasts that developed from spindle-shaped MSC in response to stress during cultivation. Based on their morphological appearance the small tdT$^+$ roundish cell type most properly represents haematopoietic SC (HSC), that do not express lineage markers

(Lin^{neg}) but can express the *CD4Cre* transgene [232]. Thus, it was assumed that the spindle-shaped tdT$^+$ F4-80^{neg} α-SMA^{neg} plastic-adherent cell type represents BM-derived MSC that descent from *Cd4*-expressing ancestor cells and represent the rare tdT$^+$ Lin^{neg} CD90$^+$CD44$^+$CD29$^+$ cell population that was found by flow cytometric analyses (Figure 16).

Similar to the culture of BM-derived cells, cultivation of *CD4Cre R26-tdT* skin-derived cells under fibroblast growth conditions (see chapter 4.6.4.1) resulted in growth of tdT$^+$ roundish (red arrows), tdT$^+$ spindle-shaped (red arrowheads) and tdT$^+$ flattened-shaped (red double arrowheads) cells (Figure 18 A, B). Based on their morphological appearance the tdT$^+$ roundish cell type might represent skin-resident immune cells such as T-lymphocytes, whereas tdT$^+$ spindle-shaped cells most properly have a fibroblast identity and tdT$^+$ flattened-shaped cells might represent myofibroblasts that developed from dermal fibroblasts in response to stress during cultivation.

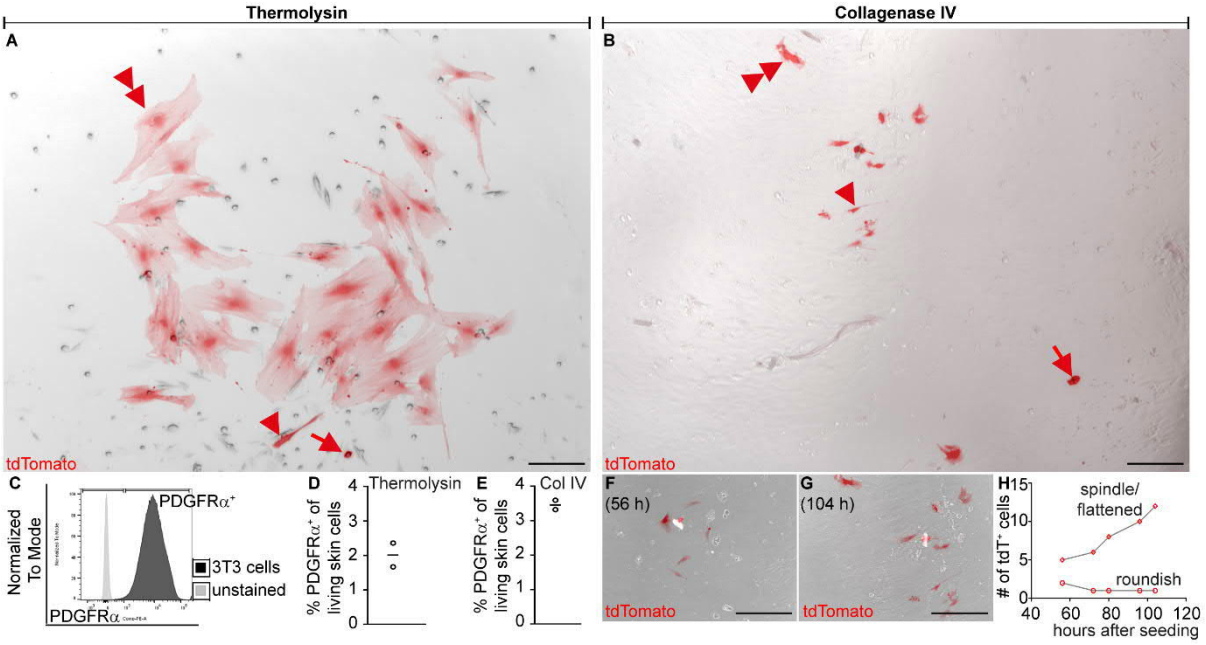

Figure 18. The progeny of *CD4Cre*-targeted cells comprises dermal fibroblasts that can be isolated via thermolysin or collagenase IV digestion of murine skin.

(A,B) Representative image of skin-derived cells isolated from the dorsal skin of a 28-week-old **(A)** or of two 24-week-old *CD4Cre R26-tdT* mice **(B)** and cultured for 7 days **(A)** or 4 days **(B)** in passage one in MesenCult complete medium. Red arrowheads: tdT$^+$ spindle-shaped cells; red double arrowheads: tdT$^+$ flattened-shaped cells; red arrow: a tdT$^+$ roundish cell. **(C-E)** Flow cytometric analyses of 300,000 stained NIH3T3 cells **(C)**, 700,000 unstained skin cells **(C)** or 2,500,000 stained skin cells from dorsal skin of wild type mice isolated with thermolysin **(D)** or collagenase IV (Col IV) **(E)**. **(C)** Histogram plot of gated living cells (not shown) for expression of the pan-fibroblast marker PDGFRα for NIH3T3 and unstained skin cells. PDGFRα$^+$ cells were gated according to the PDGFRα expression of NIH3T3 cells. **(D)** Portion of PDGFRα$^+$ cells among living skin cells after thermolysin **(D)** and Col IV **(E)** isolation. **(F-G)** Representative images of isolated skin cells (described under **[B]**) after culture for 56 **(F)** or 104 hours **(G)** and number of tdT$^+$ cells with a spindle/flattened or roundish morphology between 56 to 104 hours **(H)**. Naïve tdTomato signal is shown (red, A,B,F,G). Scale bars: 166 µm in **A, B**; 200 µm in **F, G**. For details regarding the mice see Table 17.

The isolation procedure of skin-derived fibroblasts with either thermolysin or collagenase IV did not impact the occurrence of the different shaped cell types (Figure 18 A, B) albeit the

collagenase IV treatment resulted in a slightly increased number of initially isolated PDGFRα^+ fibroblasts (~3.5%) compared to the thermolysin treatment (~2%) (Figure 18 C-E). Interestingly, 56 to 104 hours after seeding the number of tdT$^+$ roundish cells decreased (from two to one tdT$^+$ cell), whereas the number of tdT$^+$ spindle-shaped or flattened-shaped cells increased (from five to 12 tdT$^+$ cells) (Figure 18 F-H). This indicates that the tdT$^+$ spindle-shaped and/or flattened-shaped cells represent skin-derived (myo) fibroblasts that either actively proliferate or express the *CD4Cre*-transgene *in vitro*, whereas the tdT$^+$ roundish cells, which might be immune cells (e.g. T-lymphocytes), did not proliferate but rather die under the used *in vitro* culture conditions.

Taken together these results demonstrate that descendants of cells with *CD4Cre* activity grow as stromal cells *in vitro* and can be isolated from BM and skin. Nevertheless, the analysis of *CD4Cre R26-tdT* mice/cells did not allow for determination of the time point of a *CD4Cre*-mediated recombination and thus the ancestor cell type, which expresses *Cd4*/CD4. Thus, next the *CD4CreER^{T2} R26-tdT* mouse model, in which a *CreER^{T2}*-mediated recombination of the *R26-tdT* locus depends on *Cd4* expression and the simultaneous tamoxifen-application, was used. As an initial control experiment, the tdT expression of thymocytes of a *CD4CreER^{T2} R26-tdT* mouse 17 days after the first injection with tamoxifen, which was done on five consecutive days, was verified by flow cytometry (Figure 19) [233]. In contrast to tdT^{neg} *CD4CreER^{T2} R26-tdT* thymocytes, which are mainly double positive (CD4$^+$CD8$^+$), their tdT$^+$ counterparts are double positive (CD4$^+$CD8$^+$), single CD4$^+$ or single CD8$^+$ and rarely double negative (CD4^{neg}CD8^{neg}) (Figure 19 A, B). These data perfectly fit to the expected outcome after tamoxifen-mediated *CD4CreER^{T2}*-depended labelling of thymocytes. Since immature thymocytes develop from double negative, to double positive and finally to mature single CD4$^+$ or CD8$^+$ T-lymphocytes, tamoxifen-treatment of *CD4CreER^{T2} R26-tdT* mice leads to a labelling of double positive, single CD4$^+$ and single CD8$^+$ *CD4CreER^{T2} R26-tdT* thymocytes. 17 days after the first tamoxifen injection mainly the offspring of initially labelled double positive thymocytes (e.g. single CD4$^+$ and CD8$^+$ thymocytes) can be detected whereas the number of tdT$^+$ double positive thymocytes declines after stopping inducer application (Figure 19). Thus, at the time point of analysis many of the initially labelled double positive thymocytes have already been developed to tdT$^+$CD4$^+$ and tdT$^+$CD8$^+$ T-lymphocytes. Beyond flow cytometric analyses, whole organ preparations showed that the thymus of a tamoxifen-treated *CD4CreER^{T2} R26-tdT* mouse strongly expressed tdT 6 days after the first injection with tamoxifen, which was done on three consecutive days, whereas no tdT signal was detectable in the control mouse (Figure 19 C). Thus, a *CreER^{T2}*-mediated recombination in absence of tamoxifen, which would result in background activity, was excluded for the *CD4CreER^{T2} R26-tdT* mouse line. Together these data demonstrate that the *CD4CreER^{T2} R26-tdT* mouse model can be utilized for determination of the *Cd4* expression time point.

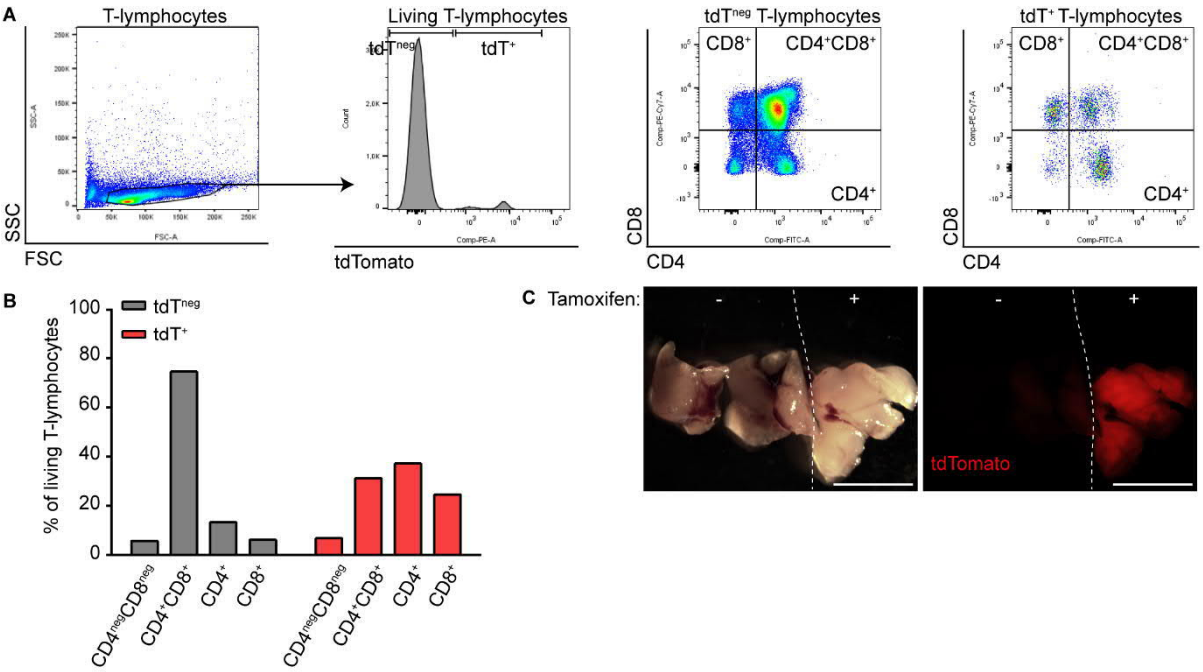

Figure 19. Tamoxifen dependent lineage tracing of CD4-expressing *CD4CreER^{T2} R26-tdT* thymocytes.

(A) Flow cytometric analyses of 100,000 thymocytes of a *CD4CreER^{T2} R26-tdT* mouse 17 days after the first tamoxifen injection. Outer left panel: SSC/FSC plots for gating living thymocytes; middle left panel: histogram for visualisation of tdT expression of living thymocytes; right panels: CD4/CD8 plot for visualisation of CD4 and CD8 expression of living tdT^{neg} (middle right) and tdT^{+} (outer right) thymocytes. **(B)** Quantification of tdT^{neg} (grey) and tdT^{+} (red) double negative (CD4^{neg}CD8^{neg}), double positive (CD4^{+}CD8^{+}) and single positive (CD4^{+} and CD8^{+}) *CD4CreER^{T2} R26-tdT* thymocytes from the analyses shown in **(A)**. **(C)** Representative images of thymus preparations of *CD4CreER^{T2} R26-tdT* mice 6 days after the first tamoxifen treatment ('+') or control ('-'). Naïve tdT signal is shown (red, C). Scale bars: 2.5 mm in **C**. For details regarding the mice see Table 17.

To evaluate whether stromal cells can express *Cd4* and an activation of the *CD4CreER^{T2}* transgene is possible under *in vitro* culture conditions BM- and skin-derived stromal cells from *CD4CreER^{T2} R26-tdT* mice were isolated, cultured in tamoxifen-supplemented medium and analysed for tdT expression (Figure 20 A, B). Indeed, these experiments revealed that flattened-shaped Lin^{neg} BM-derived cells start to express tdT 4 days after starting tamoxifen application (red double arrowheads) (Figure 20 A, C, D). Similarly, also skin-derived cells express tdT under fibroblast growth conditions starting 8 days after initial tamoxifen treatment (Figure 20 B, E, F). However, in contrast to tdT^{+} Lin^{neg} BM-derived cells skin-derived tdT^{+} cells were roundish (red arrows) or spindle-shaped (red arrowheads) 8 days after starting tamoxifen treatment (Figure 20 E). Flattened-shaped skin-derived tdT^{+} cells (red double arrowheads) occurred 13 days after starting the tamoxifen treatment (Figure 20 F). These results strongly indicate that *in vitro* cultured BM-derived and skin-derived stromal cells not only express the *CD4Cre* and *CD4CreER^{T2}* transgenes but may also be positive for CD4 protein expression. To evaluate this conclusion next Lin^{neg} BM-derived MSC of wild type mice were analysed for CD4 expression under *in vitro* culture conditions.

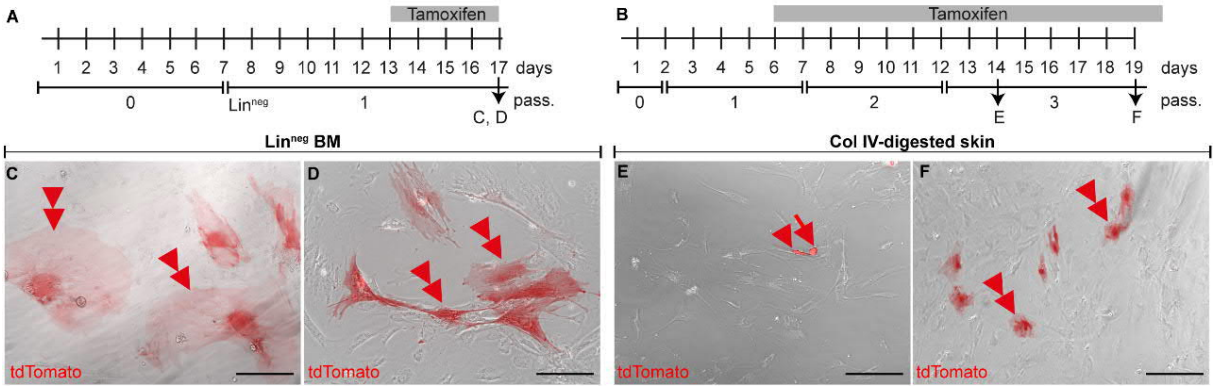

Figure 20. Tamoxifen supplementation on stromal cells of the bone marrow and the skin induces *CD4CreER^{T2}* activity *in vitro*.

(A, B) Schematic overviews of the experimental *in vitro* culture setups for bone marrow (BM)-derived **(A)** and skin-derived stromal cells **(B)**. **(C,D)** Representative images of lineage negative (Lin^{neg}) BM-derived cells isolated from BM of a 12-week-old *CD4CreER^{T2} R26-tdT* mouse 17 days in passage (pass.) one after culturing in MesenCult complete medium supplemented with tamoxifen from day 13 to 17 post seeding (10 µM solved in DMSO [v/v]). **(E,F)** Representative images of collagenase IV (Col IV) digested skin cells isolated from dorsal skin of three 10-week-old *CD4CreER^{T2} R26-tdT* mice 14 days **(E)** and 19 days **(F)** (passage 3) after culturing in MesenCult complete medium supplemented with tamoxifen from day 6 to 14 or 19 post seeding (10 µM solved in DMSO [v/v]). **(C-F)** Naïve tdT signal is shown (red). Red arrowheads: tdT$^+$ spindle-shaped cells; red double arrowheads: tdT$^+$ flattened-shaped cells; red arrow: tdT$^+$ roundish cells. Scale bars: 300 µm in **C-F**. For details regarding the mice see Table 17.

It is to be noted that the identification of BM derived MSC is challenging since, as already mentioned, currently no specific marker is known that identifies MSC. However, the classical MSC determination is achieved through proof of plastic adherence under standard culture conditions and co-expression of the markers CD90, CD44, CD29 (mostly via flow cytometry) and the absence of immune cell markers (Lin^{neg}). Noteworthy, the CD4 surface protein is highly sensitive towards dissociation with trypsin. Thus, trypsin treatment for detachment of cultured BM-derived MSC would result in a reduced CD4 surface protein detection [224] which impedes flow cytometric measurements of the cultures. However, due to the capability of BM-derived MSC to differentiate into mesodermal [109] and ectodermal cells [96], multipotency of these cells can be hypothesized. The expression of stemness markers, like the octamer-binding TF 4 (Oct4, Oct-3/4 or POU5F1) [234], which is usually used to identify pluripotent ESC [235], can be used for determination of SC-characteristics of BM-, adipose tissue-, heart- and dermis-derived human MSC [236] and Stro-1$^+$ MSC derived from the pedicle periosteum of deers [237]. Hence, a simultaneous analysis of the expression of Oct-3/4 and CD4 was conducted by immunofluorescent stainings of *in vitro* cultured murine Lin^{neg} BM-derived cells. As a control for Oct-3/4 expression the mouse ESC cell line mES RI was also analysed. As shown in Figure 21 mES RI cells strongly express Oct-3/4 but did not stain positive for CD4 (Figure 21 A, A'). In contrast, Lin^{neg} BM-derived cells grow in discrete colonies arising from one single cell (CFU-F) [108] and express Oct-3/4 and CD4 simultaneously (Figure 21 B-C''). Moreover, analysis of the colony-forming capacity of *CD4Cre R26-tdT* Lin^{neg} BM-derived cells revealed tdT expression and thus *CD4Cre* activity in the centre of a CFU (Figure 21 D).

Together these results strongly argue in favour of a CD4 expression of BM-derived MSC with a stemness character.

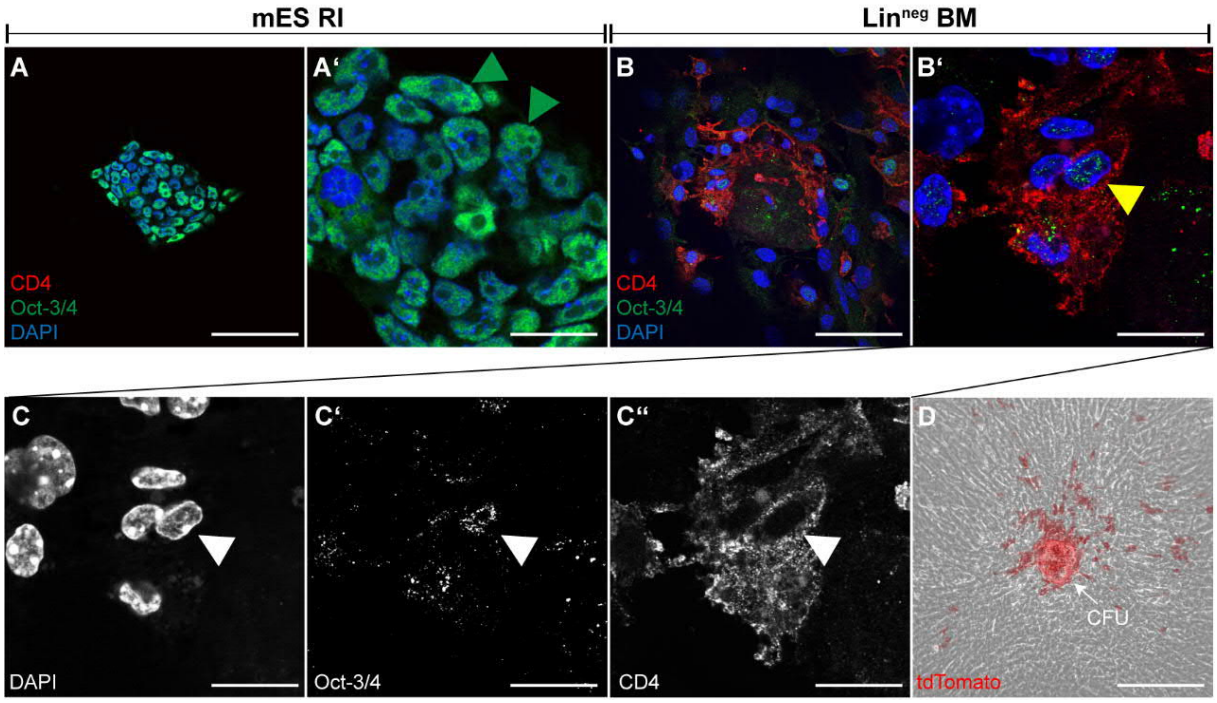

Figure 21. Bone marrow-derived lineage negative cells express Oct-3/4 and CD4.

(A-C'') Immunofluorescence staining against CD4 (red) and the pluripotency marker Oct-3/4 (green) of mouse embryonic stem cells (mES RI) cultured in passage 25 in mESC medium (A, A') and of bone marrow (BM)-derived lineage negative (Lin^{neg}) cells isolated from BM of a 5-week-old wild type mouse cultured in passage one in MesenCult complete medium (B-C''). Yellow arrowhead: CD4^{+}Oct-3/4^{+} cell. C-C'': single channels from B' shown in greyscale. White arrowheads: the same cell. **(D)** Representative image of cultured BM-derived cells isolated from a 6-week-old *CD4Cre R26-tdT* mouse cultured in passage 0 in MesenCult complete medium that grow in a colony-forming unit (CFU). Naïve tdT signal is shown (red, D). Scale bars: 200 µm in **D**; 33 µm in **A, B**; 10 µm in **A', B', C, C', C''**. For details regarding the mice and antibody staining, see Table 17 and Table 13, respectively.

5.1.3 *CD4Cre* activity and CD4 expression in stromal cells *in vivo*

The *in vitro* analyses of Lin^{neg} BM-derived MSC and skin-resident fibroblasts strongly indicated a CD4 promoter activity and proved the expression of the CD4 protein in Lin^{neg} BM-derived Oct-3/4^{+} cells. However, to also evaluate whether stromal cells of the BM and the skin express *Cd4 in vivo*, paraffin cross sections of BM and skin from the inducible *CD4CreER^{T2} R26-tdT* mouse, that were taken 17 days after the first injection with tamoxifen, which was done on five consecutive days, were investigated. For this, the sections were stained against RFP to visualise the tdT protein and against the immune cell marker CD45 (expressed by HSC and all mature immune cells, incl. T-lymphocytes, B-lymphocytes, dendritic cells, NK cells, monocytes, macrophages, granulocytes). Remarkably, these analyses demonstrated the existence of RFP^{+}CD45^{neg} non-haematopoietic cells in the BM and dermis of *CD4CreER^{T2} R26-tdT* mice (Figure 22).

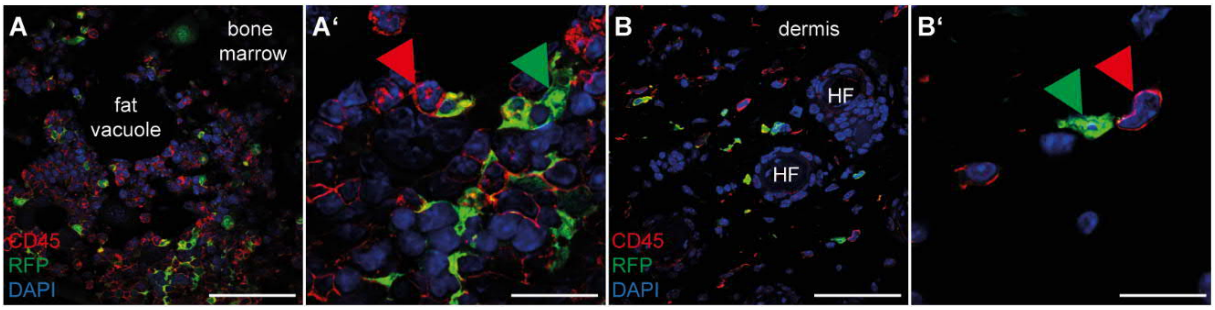

Figure 22. The progeny of *CD4CreER^{T2}*-targeted cells grows in murine bone marrow and dermis.

(A-B’) Representative images of immunofluorescent stained paraffin sections of the bone marrow of the bone of front leg **(A, A’)** and of the skin dermis with hair follicles (HF) **(B, B’)** of *CD4CreER^{T2} R26-tdT* mice 17 days after the first tamoxifen treatment. tdT expression was visualised using an anti-RFP antibody. Haematopoietic cells were stained by using an anti-CD45 antibody. Nuclei were visualised with DAPI (blue). Green arrowheads: RFP^{+} cells. Red arrowheads: CD45^{+} cells. Scale bars: 33 µm in **A, B**; 10 µm in **A’, B’**. For details regarding the mice and antibody staining, see Table 17 and Table 13, respectively.

Together with the *in vitro* culture analyses, these findings strongly suggest that RFP^{+}CD45^{neg} cells represent BM-derived MSC or dermal fibroblasts, respectively. To substantiate this conclusion, next stainings against CD4 and the DS marker α-SMA or the fibroblast marker PDGFRα were conducted. These analyses revealed that the skin of wild type mice indeed contains CD4^{+}α-SMA^{+} and CD4^{+}PDGFRα^{+} fibroblasts in the DS, which surrounds HF (Figure 23 A-B’). Beyond that, DS fibroblasts and dermal fibroblasts of the reticular dermis of *CD4Cre R26-tdT* mice stain positive for tdT and α-SMA (Figure 23 C, C’) or PDGFRα (Figure 23 D, D’), respectively. This demonstrates that the progeny of *CD4Cre*-expressing cells grows *in vivo* as fibroblasts. However, and beyond that, also tdT^{+} epidermal cells that are associated with the HF were found (Figure 23 D, red arrowhead).

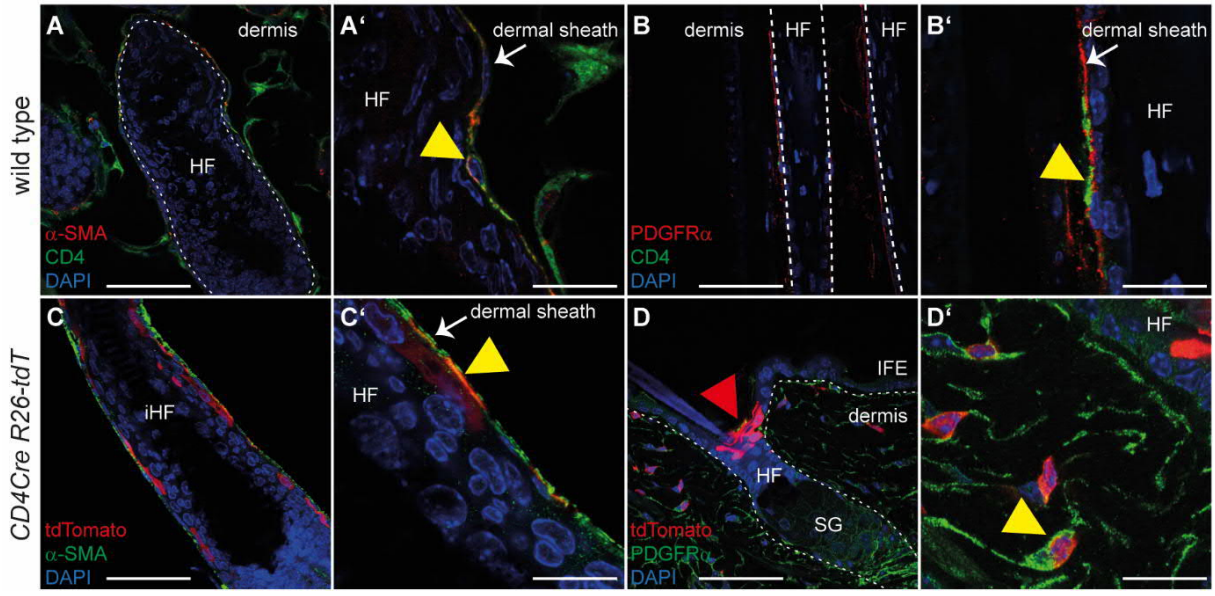

Figure 23. CD4^{+} cells and the progeny of *CD4Cre*-expressing cells grow as fibroblasts in the murine dermis.

(The legend continues on the next page.)

(A-D') Representative images of antibody stainings against CD4 **(A-B'),** the dermal sheath marker α-SMA **(A, A', C, C')** and the pan-fibroblast marker PDGFRα **(B, B', D, D')** on cryotome sections **(A-B', D, D')** or isolated hair follicles (iHF) **(C, C')** from wild type **(A-B')** or *CD4Cre R26-tdT* **(C-D')** mice. Progeny cells of *CD4Cre*-expressing cells were detected by their naïve tdTomato (red) expression (**C-D')**. Nuclei were visualised with DAPI (blue). Yellow arrowheads: double positive cells, red arrowhead: tdT^+ cells; dotted lines: epidermal-dermal junction. Scale bars: 33 µm in **A, B, C, D**; 10 µm in **A', B', C', D'**. Abbreviations: IFE: interfollicular epidermis, SG: sebaceous gland. For details regarding the mice and antibody staining, see Table 17 and Table 13, respectively.

5.1.4 Summary and conclusion

The first part of this work demonstrates the existence of $CD4^+$ non-haematopoietic stromal cells in BM and skin of adult mice. Furthermore, the results of this section indicate that the progeny of these cells either remains as stromal cells in the origin tissues (e.g. BM stroma or skin dermis) or differentiate into non-connective tissue cells (e.g. cartilage cells, epidermal cells). Moreover, the results also suggest that $CD4^+$ BM-derived MSC may represent putative BCC precursor cells. However, albeit neither a migration to the epidermis nor the (trans-) differentiation into epidermal cells has been proven so far, only the current knowledge about the high regenerative potential of BM-derived MSC justifies this assumption. Nevertheless, extensive transplantation studies including difficult experimental surgeries would be necessary to proof this conclusion because neither intravenous transplantations nor epidermal wounding seem to be sufficient for effective tracking and analysis of the involvement of BM-derived MSC to skin regeneration [101, 238]. This is the case since a) only intra-BM transplantation but not simple intravenous transplantation of MSC leads to a broad contribution of grafted MSC to the host BM [238] and b) only skin transplantation instead of skin-wounding induces the recruitment and differentiation of grafted MSC to epidermal $K5^+$ cells [101]. Since the establishment of such approaches are very time-consuming (often years) and requires specialized knowledge, the focus of this thesis was next laid on the epidermal cell population that descent from *CD4Cre*-expressing cells (Figure 23 D, red arrowhead) and thus from $CD4^+$ cells (properly stromal cells).

5.2 Non-haematopoietic, epidermal CD4-expressing cells and their progeny grow in the murine adult skin

5.2.1 Determination of non-haematopoietic, epidermal cells that descent from *CD4Cre*-targeted ancestors

The results of the first part demonstrated that the skin of adult *CD4Cre R26-tdT* mice contains tdT^+ epidermal cells in the infundibulum region of telogen HF (Figure 23). Since these cells most likely represent epidermal keratinocytes und thus might be potential BCC progenitors, next the identity, localisation, behaviour and number were investigated. For this purpose, first epidermal isolates of the dorsal skin during the resting phase (telogen) of *CD4Cre R26-tdT* mice were analysed via flow cytometry (for details regarding the isolation procedure see chapter 4.4.1.1). This hair cycle phase was chosen since tdT^+ epidermal cells were initially identified in telogen HF (Figure 23) and because analysis of the most prominent hair cycle phase - the telogen hair phase [41] - guarantees comparability between different experiments. The flow cytometric analysis revealed that three different tdT-expressing populations exist in the dorsal skin of adult *CD4Cre R26-tdT* mice that were subdivided according to their tdT expression level to tdT^{low}, tdT^+ and tdT^{high} cells (Figure 24 A).

Since CD4 expression is found in various skin-infiltrating immune cells (e.g. epidermal T-lymphocytes and Langerhans cells, dermal dendritic cells and macrophages) [11, 76] a large proportion of tdT^+ cells in the epidermal isolates might represent immune cells. Thus, *CD4Cre R26-tdT* epidermal isolates were tested for their expression of the general immune cell marker CD45, the T-lymphocyte markers CD3ε and TCRβ as well as the markers for macrophages, dendritic cells and Langerhans cells: CD11b and CD16/CD32 (Figure 24 B). These approaches revealed that the tdT^{low} population consists of different proportions of immune cells (~19.3% $CD45^+$ cells [Figure 24 C], ~2.2% $CD3\varepsilon^+$ cells [Figure 24 D], ~10.9% $TCR\beta^+$ cells [Figure 24 E], ~26.5% $CD11b^+$ cells [Figure 24 F], ~25.9% $CD16/CD32^+$ cells [Figure 24 G]) and a large proportion of $CD45^{neg}$ non-haematopoietic cells (~63.2%, Figure 24 H). The tdT^+ population consists only of a minor fraction of $CD45^{neg}$ non-haematopoietic cells (~22.5%, Figure 24 H) but of a large amount of $CD45^+$ immune cells (~77.5%, Figure 24 C) comprising ~15.1% $CD3\varepsilon^+$ cells (Figure 24 D), ~33.2% $TCR\beta^+$ cells (Figure 24 E), ~6.8% $CD11b^+$ cells (Figure 24 F) and ~13.4% $CD16/CD32^+$ cells (Figure 24 G). In contrast to the tdT^{low} and tdT^+ fractions, the tdT^{high} population consists mainly of $CD45^{neg}$ non-haematopoietic cells (~73.2%, Figure 24 H) and of only a small fraction of $CD45^+$ haematopoietic cells (~26.8%, Figure 24 H), that subdivides into ~2.8% $CD3\varepsilon^+$ cells (Figure 24 D), ~9.7% $TCR\beta^+$ cells (Figure 24 E), ~15.2% $CD11b^+$ cells (Figure 24 F) and ~17.1% $CD16/CD32^+$ cells (Figure 24 G). These results demonstrate that the skin-derived tdT^+ fraction of *CD4Cre R26-tdT* mice mainly consists of immune cells, whereas the tdT^{low} and tdT^{high} populations contain large numbers of

non-haematopoietic cells. Moreover, these data show that the dorsal skin of adult mice contains non-haematopoietic cells that descent from *CD4Cre*-targeted cells suggesting the existence of a non-haematopoietic CD4 or at least *CD4Cre*-expressing ancestor cell.

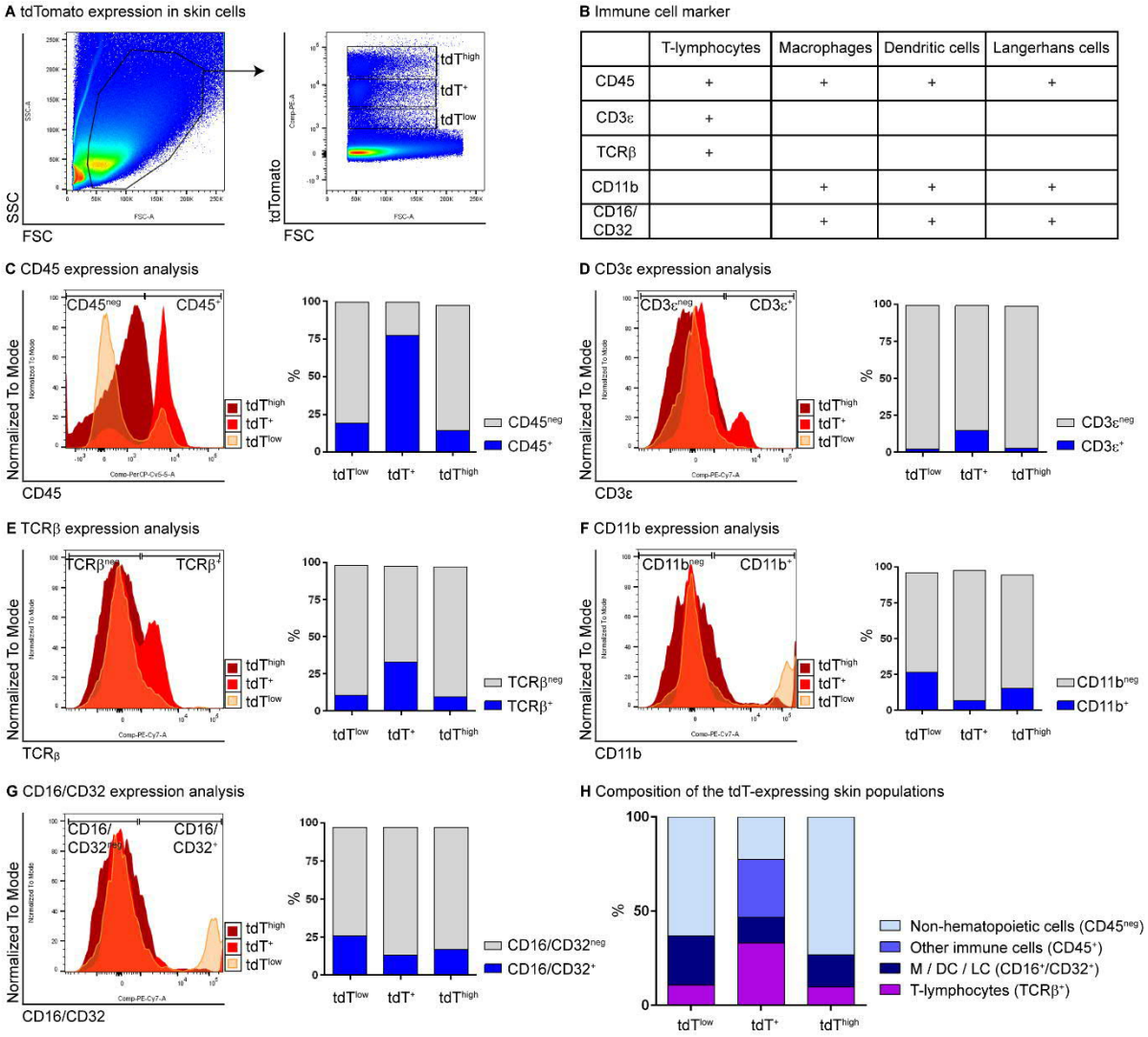

	T-lymphocytes	Macrophages	Dendritic cells	Langerhans cells
CD45	+	+	+	+
CD3ε	+			
TCRβ	+			
CD11b		+	+	+
CD16/ CD32		+	+	+

Figure 24. The dorsal skin of adult mice contains non-haematopoietic and haematopoietic progeny of *CD4Cre*-targeted cells.

(A) Flow cytometric analyses of 2,500,000 cells isolated from the dorsal skin of a 21-week-old *CD4Cre R26-tdT* mouse. Left panel: SSC/FSC plot for gating living cells. Right panel: tdT (PE-channel)/FSC plot for visualisation of tdT expression on living cells. Three different tdT-expressing populations were distinguishable; tdT^{low}: tdT low expressers; tdT^{+}: tdT intermediate expressers; tdT^{high}: tdT high expressers. **(B)** Overview of skin-resident immune cells and respective surface markers for their identification. **(C-G)** Flow cytometric analyses plot (left panel) and quantification (right panel) of CD45 **(C)**, CD3ε **(D)**, TCRβ **(E)**, CD11b **(F)** and CD16/CD32 **(G)** expression for the tdT^{low}, tdT^{+} and tdT^{high} populations. For each analysis, 2,500,000 cells isolated from the dorsal skin of 21 to 28-week-old *CD4Cre R26-tdT* mice were measured. Gating for living cells and the different tdT populations see **(A)**. **(H)** Graphical representation of the composition of the three different tdT-expressing populations based on the flow cytometric measurements shown in **C, E** and **G**. Abbreviations: M: macrophages, DC: dendritic cells, LC: Langerhans cells. For details regarding the mice see Table 17.

So far, the identity of the non-haematopoietic skin-resident tdT-expressing cells (tdT^{low}, tdT^{+} and tdT^{high}) was unknown. Thus, the *CD4Cre R26-tdT* epidermal isolates were flow

cytometrically analysed for their expression of the epidermal surface marker proteins CD49f (α6 integrin), CD34 and Sca-1 whose determination is sufficient for distinction of three main epidermal populations of telogen skin (IFE, uHF, bulge) [78]. Thus, the co-expression of CD49f, a marker of basal epidermal cells, and the HSC marker CD34 defines epidermal SC of the HF bulge region [78, 239], which represent self-renewal multipotent SC that contribute to the HF but not to the SG or the IFE under homeostatic conditions [74, 239, 240]. Accordingly, the epidermis also contains epidermal SC populations that maintain the IFE and reside most probably in the basal layer [38]. Although the localisation or marker of IFE SC are still unclear, proliferative basal layer cells are known to express Sca-1 [77]. Those expression is restricted to the basal layer of the IFE and the infundibulum region [78, 241]. CD49f expression is continuous throughout the basal layer of the IFE and HF [78, 241]. Accordingly, CD49f colocalises with Sca-1 on cells of the basal layer and of the infundibulum region [78]. As a result, three different epidermal populations are distinguishable by flow cytometric analysis of epidermal isolates: bulge cells that express CD49f and CD34 ($CD49f^{+}CD34^{+}Sca\text{-}1^{neg}$), IFE and infundibulum cells that express CD49f and Sca-1 ($CD49f^{+}CD34^{neg}Sca\text{-}1^{+}$) and cells of the uHF isthmus and JC that express CD49f but neither CD34 nor Sca-1 ($CD49f^{+}CD34^{neg}Sca\text{-}1^{neg}$) [78] (Figure 25 A).

For the flow cytometric-based analysis of *CD4Cre R26-tdT* skin isolates, the different tdT-expressing epidermal populations were identified (tdT^{neg}, tdT^{low}, tdT^{+} and tdT^{high}) (Figure 25 B), then $CD49f^{+}$ cells were gated, which were finally subdivided based on their expression of CD34 and Sca-1 into: $CD49f^{+}CD34^{+}Sca\text{-}1^{neg}$ bulge cells, $CD49f^{+}CD34^{neg}Sca\text{-}1^{+}$ cells of the IFE and infundibulum and/or $CD49f^{+}CD34^{neg}Sca\text{-}1^{neg}$ isthmus and JC cells (Figure 25 B-E) [78, 228]. In addition to these already described epidermal populations a so far undescribed $CD49f^{+}CD34^{+}Sca\text{-}1^{+}$ population was detected (Figure 25 B).

Noteworthy, the keratinocyte marker CD49f is also expressed by T-lymphocytes and macrophages, but dendritic cells and Langerhans cells are excluded due to the selection of $CD49f^{+}$ cells. T-lymphocytes express Sca-1 but not CD34 ($CD49f^{+}CD34^{neg}Sca\text{-}1^{+}$), whereas macrophages express neither Sca-1 nor CD34 ($CD49f^{+}CD34^{neg}Sca\text{-}1^{neg}$). Therefore, $CD49f^{+}CD34^{neg}Sca\text{-}1^{+}$ cells might include not only cells of the IFE and infundibulum, but also T-lymphocytes. Similarly, $CD49f^{+}CD34^{neg}Sca\text{-}1^{neg}$ cells might comprise isthmus and JC cells as well as macrophages. Nevertheless and according to Jensen *et al.* [78], the analyses revealed that tdT^{neg} $CD49f^{+}$ cells represent mainly IFE cells (~82%) and to a smaller amount JC/isthmus (~11.3%), bulge (~4.6%) and $CD34^{+}Sca\text{-}1^{+}$ (~2%) cells (Figure 25 B, F). With exception for $CD34^{+}Sca\text{-}1^{+}$ cells, this distribution reflects the previously described literature references of ~60% IFE cells, ~9.3% JC/isthmus cells and ~3.7% bulge cells in skin isolates of wild type mice [228].

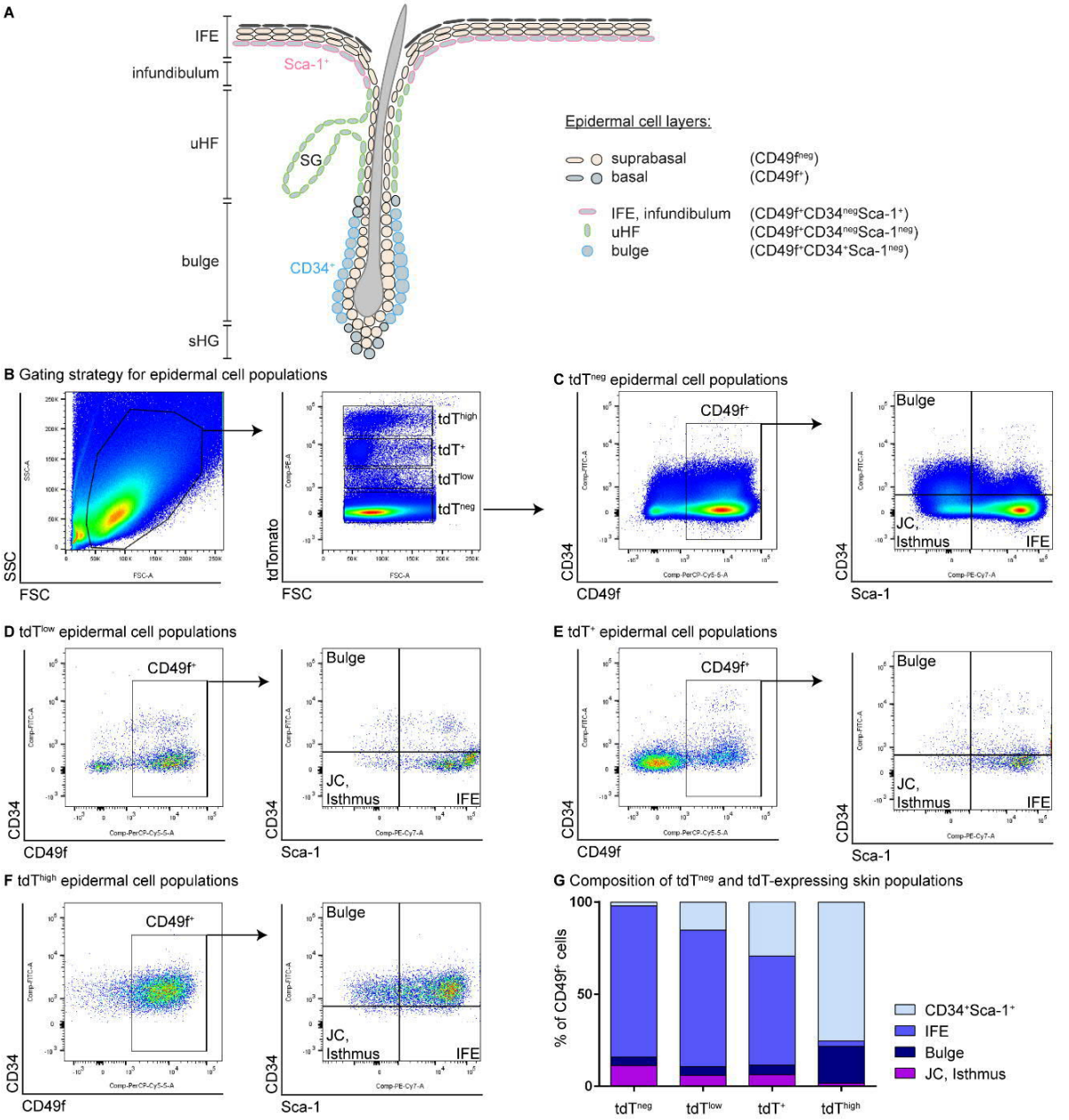

Figure 25. The non-haematopoietic progeny of *CD4Cre*-targeted cells grows as epidermal cells in the dorsal skin of adult mice.

(A) Schematic representation of a murine telogen hair follicle (HF) and its containing cellular subpopulations according to [78]. **(B-G)** Flow cytometric analyses of 2,500,000 cells isolated from the dorsal skin of a 56-week-old *CD4Cre R26-tdT* mouse. **(B)** Left panel: SSC/FSC plot for gating living cells. Middle left panel: tdT (PE-channel)/FSC plot for visualisation of tdT expression on the gated cells. Three different tdT-expressing populations were distinguishable; tdT^{low}: tdT low expressers; tdT^{+}: tdT intermediate expressers; tdT^{high}: tdT high expressers. **(C)** Left panel: CD34/CD49f plot for visualisation of CD49f expression on the gated tdT^{neg} cells. Right panel: CD34/Sca-1 plot to distinguish $CD34^{neg}Sca\text{-}1^{neg}$ (JC and isthmus), $CD34^{+}Sca\text{-}1^{neg}$ (bulge), $CD34^{neg}Sca\text{-}1^{+}$ (IFE) and $CD34^{+}Sca\text{-}1^{+}$ cells on the gated $tdT^{neg}CD49f^{+}$ cells [78]. **(D-F)** Left panel: CD34/CD49f plot for visualisation of CD49f expression on the gated tdT^{low} **(D)**, tdT^{+} **(E)** and tdT^{high} **(F)** cell populations of **B**. Right panel: CD34/Sca-1 plot to distinguish $CD34^{neg}Sca\text{-}1^{neg}$ (JC and isthmus), $CD34^{+}Sca\text{-}1^{neg}$ (bulge), $CD34^{neg}Sca\text{-}1^{+}$ (IFE) and $CD34^{+}Sca\text{-}1^{+}$ cells on the gated $CD49f^{+}tdT^{low}$ **(D)**, $CD49f^{+}tdT^{+}$ **(E)** and $CD49f^{+}tdT^{high}$ **(F)** cells. **(G)** Graphical representation of the composition of the tdT^{neg} and the three different tdT-expressing populations based on the flow cytometric measurements shown in **B-E**. Abbreviations: JC: junctional zone, IFE: interfollicular epidermis, SG: sebaceous gland, sHG: secondary hair germ, uHF: upper HF. For details regarding the mice see Table 17.

The tdT^{low} CD49f^{+} population also consists of a large number of IFE cells (~74%) and small amounts of bulge (~4.7%) and JC/isthmus (~6%) cells (Figure 25 C, F). However, the number of CD34^{+}Sca-1^{+} cells increases from ~2% in the tdT^{neg} population to ~15.3% in the tdT^{low} fraction (Figure 25 B, C, F). Similarly, tdT^{+} CD49f^{+} cells contain mainly cells of the IFE (~59%), few bulge (~5.2%) and JC/isthmus (~6.3%) cells, but even more CD34^{+}Sca-1^{+} cells (~29.3%) compared to the tdT^{neg} and tdT^{low} fractions (Figure 25 B, C, D, F). As shown previously, the skin-derived tdT^{low} and tdT^{+} fractions contain immune cells (Figure 24), so some proportion of T-lymphocytes and macrophages may be among the tdT$^{low/+}$ IFE and JC/isthmus cells, respectively. Remarkably, the tdT^{high} CD49f^{+} population almost exclusively consists of CD34^{+}Sca-1^{+} cells (~75.2%) and bulge cells (~20%) and contains very few JC/isthmus (~1.7%) and IFE (~3%) cells (Figure 25 E, F). Thus, the tdT^{high} CD49f^{+} population contains mostly (> 95%) non-haematopoietic, CD34^{+} cells. In conclusion, these data demonstrate that in adult mice the non-haematopoietic progeny of *CD4Cre*-targeted cells grows as epidermal cells of the IFE and HF (bulge, JC/isthmus) but also as CD49f^{+}CD34^{+}Sca-1^{+} cells. Since the latter population has not been characterised so far, next the identity of these cells was investigated via transcriptome-based differential gene expression analysis.

5.2.2 The epidermal progeny of *CD4Cre*-targeted cells possesses a hair follicle stem cell and infundibulum transcriptional identity

The non-haematopoietic progeny of *CD4Cre*-targeted cells grows in the epidermis as IFE, bulge and isthmus/JC cells (Figure 25). However, since the tdT^{high} population almost exclusively consists of bulge cells and of the so far undescribed CD49f^{+}CD34^{+}Sca-1^{+} cells, the identification of the cellular identity of CD49f^{+}CD34^{+}Sca-1^{+} cells was highly relevant. For this purpose, a transcriptome-based differential gene expression analysis of bulge cells (CD49f^{+}CD34^{+}Sca-1^{neg}) in comparison to CD49f^{+}CD34^{+}Sca-1^{+} cells was performed. Beyond that, it was also analysed whether tdT-expressing bulge and CD49f^{+}CD34^{+}Sca-1^{+} cells differ from their tdT^{neg} counterparts. Thus, the four populations: tdT^{neg} CD49f^{+}CD34^{+}Sca-1^{neg}, tdT^{+} CD49f^{+}CD34^{+}Sca-1^{neg}, tdT^{neg} CD49f^{+}CD34^{+}Sca-1^{+} and tdT^{+} CD49f^{+}CD34^{+}Sca-1^{+} were isolated via FACS (for gating strategy see chapter 4.5.1) and the transcriptome of each population was determined (for biological replicates etc. see chapter 4.7.4). PCA was used to visualise genetic distance and relatedness between the populations (Figure 12 in chapter 4.7.5). Unfortunately, it was not possible to analyse the sequenced data of one sample of the tdT^{neg} CD49f^{+}CD34^{+}Sca-1^{+} population. However, the PCA plot showed that the sequenced samples from the CD49f^{+}CD34^{+}Sca-1^{+} population differed from those of the bulge population (Figure 12, component one on x-axis). Thereby all replicates from the bulge population irrespectively of their tdT expression showed similar expression patterns. Nevertheless, the samples of the tdT^{+} CD49f^{+}CD34^{+}Sca-1^{+} population differed from the tdT^{neg} counterparts

(Figure 12, component two on y-axis), indicating a contamination with tdT$^+$ immune cells in the tdT$^+$ CD49f$^+$CD34$^+$Sca-1$^+$ population. However, the detailed differential gene expression analyses revealed that both tdT^{neg} as well as tdT$^+$ bulge and CD49f$^+$CD34$^+$Sca-1$^+$ cells mainly consist of non-haematopoietic epidermal cells (see below).

In general, the expression profile of the different IFE layers can be described as *K14*$^+$/*Ly6a*$^+$ basal, *Ptgs1*$^+$/*K1*$^+$ differentiated and *Lor*$^+$ keratinized epidermal cells (Figure 26 A). The different cell populations of a telogen HF are characterised by *Lgr5* expression of lower bulge and sHG cells, *Postn* expression of central outer bulge cells, *K6a* expression of inner bulge cells, *Gli1* expression of upper outer bulge cells and *K79*/*Lrig1* expression of uHF cells (Figure 26 A). Thus, based on the high expression levels of outer bulge marker genes (*Gli1*, *Postn*) (Figure 26 B) the identity of tdT^{neg} CD49f$^+$CD34$^+$Sca-1^{neg} cells as HF SC of the outer bulge region was verified. Since these cells additionally showed a high expression of the lower bulge and sHG marker gene *Lgr5*, lower bulge and sHG cells may have been also purified when basal CD34$^+$Sca-1^{neg} cells were FACS-isolated (Figure 26 B). Remarkably, the tdT^{neg} CD49f$^+$CD34$^+$Sca-1$^+$ population showed low expression of outer bulge (*Gli1*, *Postn*) and lower bulge and sHG marker (*Lgr5*) genes (Figure 26 B), but high expression of uHF (*K79*, *Lrig1*) (Figure 26 C), pan-HF (*Aqp3*, *Sostdc1*) (Figure 26 D) and IFE (*K14*, *Ly6a*, *Ptgs1*, *K1*) (Figure 26 E) marker genes. Indeed, a subpopulation of basal IFE cells, which in addition to the IFE signature also expresses 'low levels of uHF markers such as *Krt79*, the bulge marker *Postn*, and pan-HF markers like *Sostdc1*, *Aqp3*, and *Fst*' [11] has been described as basal cells of the infundibulum, the structure that connects the HF to the IFE. Thus, tdT^{neg} CD49f$^+$CD34$^+$Sca-1$^+$ cells most likely represent basal cells of the infundibulum. Moreover, both tdT^{neg} CD49f$^+$CD34$^+$Sca-1^{neg} and tdT^{neg} CD49f$^+$CD34$^+$Sca-1$^+$ cells express the inner bulge marker gene *K6a* at a comparable level (Figure 26 B). However, although *K6a* is predominantly expressed in the inner bulge, its expression can also be detected in outer bulge cells and in basal IFE and infundibulum cells [11]. Noteworthy, marker genes of the keratinized IFE (e.g. *Lor*) were not expressed (data not shown) excluding a contamination of the sorted basal cell populations with keratinized epidermal cells. However, expression of the suprabasal IFE marker genes *Ptgs1* and *K1* that are expressed highly by the tdT^{neg} CD49f$^+$CD34$^+$Sca-1$^+$ cells and weakly by the tdT^{neg} CD49f$^+$CD34$^+$Sca-1^{neg} cells (Figure 26 E) are also detectable in basal IFE and infundibulum cells and in outer bulge cells [11].

Finally and most interestingly, tdT$^+$ CD49f$^+$CD34$^+$Sca-1^{neg} and tdT$^+$ CD49f$^+$CD34$^+$Sca-1$^+$ cells do not differ from their tdT^{neg} counterparts regarding their gene expression levels of the main epidermal populations demonstrating that tdT$^+$ CD49f$^+$CD34$^+$Sca-1^{neg} cells present mainly HF SC of the outer bulge and sHG, whereas tdT$^+$ CD49f$^+$CD34$^+$Sca-1$^+$ cells most likely are basal cells of the infundibulum (Figure 26 B-E).

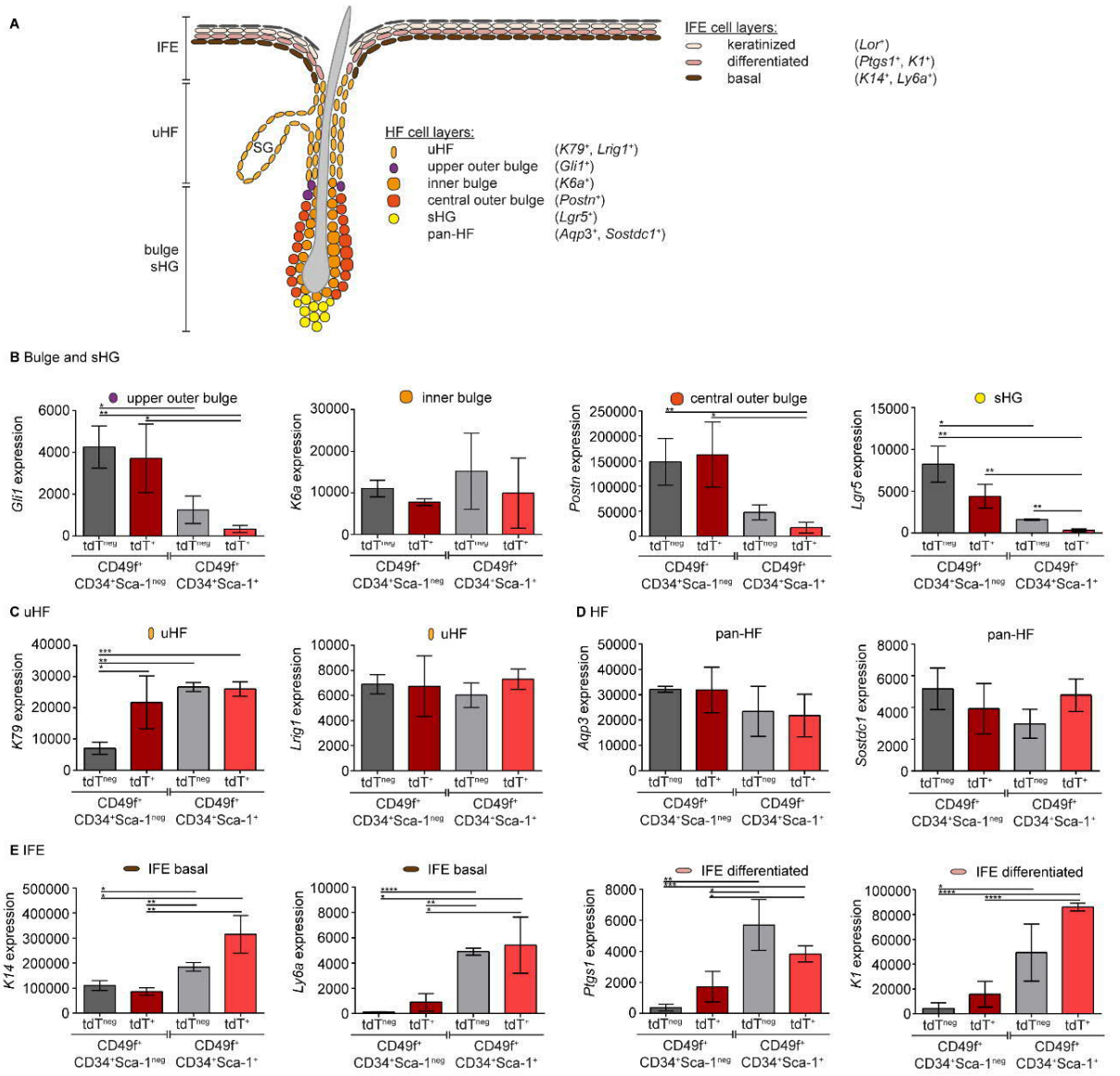

Figure 26. Transcriptome-based differential gene expression analysis of the non-haematopoietic epidermal progeny of *CD4Cre*-targeted cells reveal their hair follicle stem cell and infundibulum identity.

(A) Schematic representation of a murine telogen hair follicle (HF) and the interfollicular epidermis (IFE) and their containing cellular HF subpopulations and the sublayers of the IFE with their key markers. HF and IFE markers were chosen based on marker genes of the main epidermal cell populations of telogen epidermis that have been identified using quantitative single-cell RNA-sequencing [11]. **(B-E)** Transcriptome-based differential gene expression analysis of tdT$^+$ and tdT^{neg} CD49f$^+$CD34$^+$Sca-1^{neg} cells as well as tdT$^+$ and tdT^{neg} CD49f$^+$CD34$^+$Sca-1$^+$ cells of 29 to 32-week-old *CD4Cre R26-tdT* mice. FACS-based sorting of the cellular populations was performed as described in chapter 4.5.1. Mean ± SEM. * P < 0.05, ** P < 0.01, *** P < 0.001, **** P < 0.0001. Significance was tested by the Holm-Sidak method. Abbreviations: SG: sebaceous gland, sHG: secondary hair germ, uHF: upper HF. For details regarding the mice see Table 17.

These assumptions were further substantiated by an heatmap analysis of additional markers that are known to be expressed by the main epidermal populations of telogen dorsal skin (Figure 27). The results showed that both tdT^{neg} and tdT$^+$ CD49f$^+$CD34$^+$Sca-1^{neg} cells express high levels of bulge (e.g. *Cd34, K15*) and sHG marker genes (e.g. *K24, Sfrp1*), but low levels of IFE marker genes (e.g. *Bhlhe40, K16*) (Figure 27) verifying their identity as HF SC of the

bulge and sHG. HF SC of the bulge and of the sHG are quiescent during the resting (telogen) phase and thus express TF that govern HF SC quiescence, such as *Nfatc1* [242]*, Foxc1* [243] and *Lhx2* [244]. Indeed, the tdT^{neg} and tdT^{+} CD49f^{+}CD34^{+}Sca-1^{neg} cells also express high levels of the HF SC quiescence TF: *Nfatc1, Foxc1* and *Lhx2* (Figure 27). Moreover, the tdT^{neg} and tdT^{+} CD49f^{+}CD34^{+}Sca-1^{neg} cells showed high expression levels of the TF *Sox9* (Figure 27) that is required for formation of the HF bulge [245]. However, these cells also express SG marker genes (e.g. *Ces1d, Cidea*) (Figure 27).

Contrary to CD49f^{+}CD34^{+}Sca-1^{neg} cells of the bulge and sHG, tdT^{neg} and tdT^{+} CD49f^{+}CD34^{+}Sca-1^{+} cells showed high expression levels of IFE (e.g. *Bhlhe40, K16*), medium levels of uHF (e.g. *Klk10, Lgr6*) and low levels of SG (e.g. *Ces1d, Cidea, Prdm1* that encodes Blimp1), bulge (e.g. *Cd34, K15*) and sHG (e.g. *K24, Sfrp1*) marker genes (Figure 27). Based on this expression pattern the CD49f^{+}CD34^{+}Sca-1^{+} cells, which have not been described so far, have to be assigned to the epidermal cells of the infundibulum. Interestingly, tdT^{neg} and tdT^{+} CD49f^{+}CD34^{+}Sca-1^{+} cells show high gene expression levels of the proliferation marker *Mki67*, cell division cycle (Cdc) proteins (e.g. *Cdc20*, *Cdca8*) and Ccn proteins (e.g. *Ccnb1, Ccnb2*) (Figure 27) indicating their proliferative activity.

Thus, this analysis confirms the identity of tdT^{neg} and tdT^{+} CD49f^{+}CD34^{+}Sca-1^{neg} cells as quiescent HF SC of the bulge and of the sHG of telogen dorsal skin and reveals that tdT^{neg} and tdT^{+} CD49f^{+}CD34^{+}Sca-1^{+} cells belong to the infundibulum compartment as they express marker genes of both, the IFE and HF. Beyond that, the transcriptome profiles of the analysed tdT^{+} cell populations demonstrate that basal epidermal cells of the infundibulum and HF including SC of the HF bulge and sHG of resting HF descent from *CD4Cre*-expressing ancestor cells.

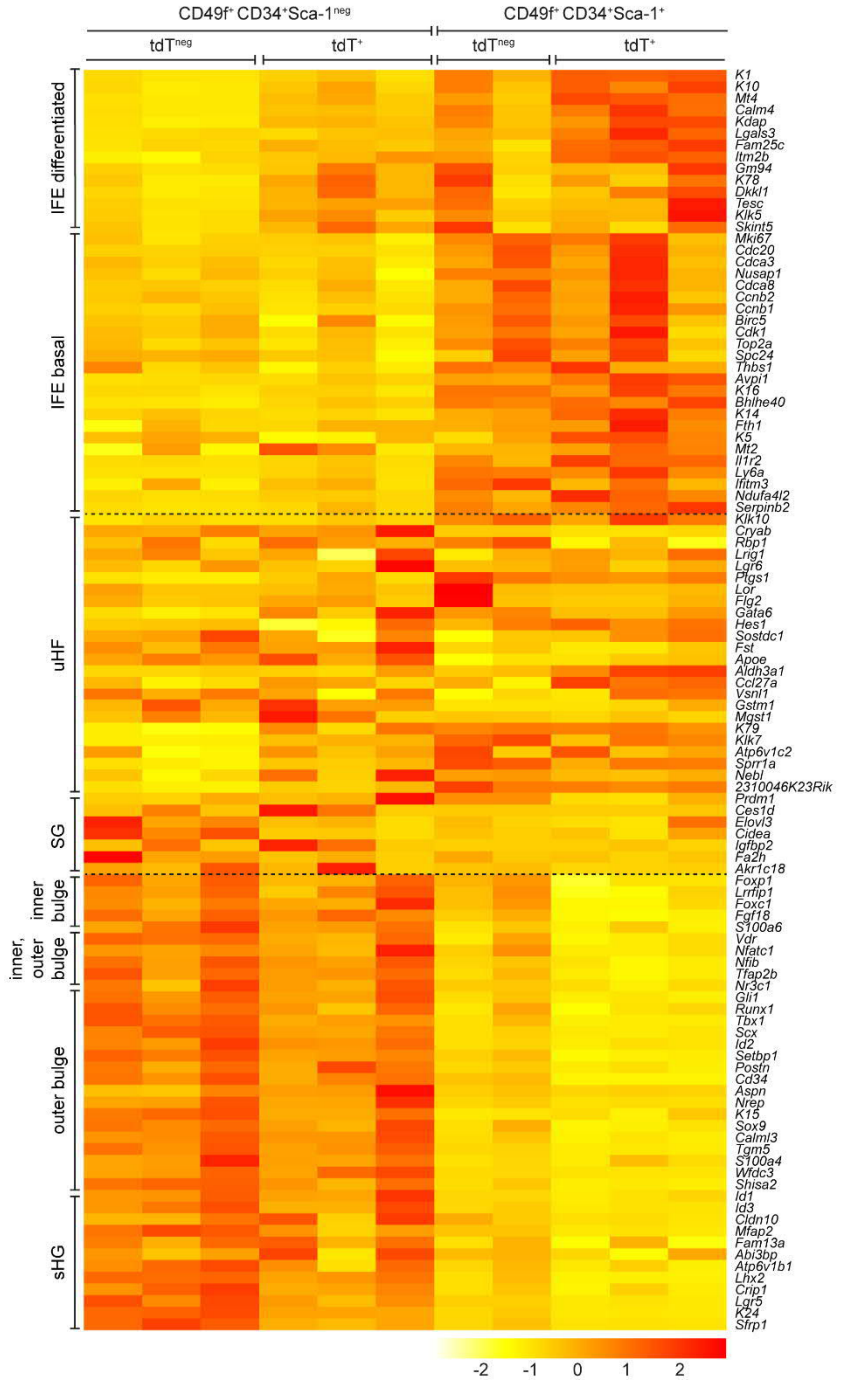

Figure 27. An heatmap analysis confirms the hair follicle stem cell and infundibulum identity of the progeny of *CD4Cre*-targeted cells isolated from murine dorsal telogen skin.

Heatmap analysis of differential gene expression of tdT^{+} and tdT^{neg} CD49f^{+}CD34^{+}Sca-1^{neg} and tdT^{+} and tdT^{neg} CD49f^{+}CD34^{+}Sca-1^{+} cells isolated from 29 to 32-week-old *CD4Cre R26-tdT* mice. FACS-based sorting of the cellular populations was performed as described in chapter 4.5.1. Hair follicle (HF) and interfollicular epidermis (IFE) markers were chosen based on marker genes of the main epidermal cell populations of telogen epidermis that have been identified using quantitative single-cell RNA-sequencing [11]. Color-coding: Red indicates high expression, whereas yellow indicates low expression of the respective gene. Abbreviations: SG: sebaceous gland, sHG: secondary hair germ, uHF: upper HF. For details regarding the mice see Table 17.

However, albeit the expression pattern of both tdT$^+$ populations do not significantly differ from their tdT^{neg} counterparts with respect to the epidermal marker genes (Figure 26 and Figure 27) the expression of genes associated with T-lymphocyte function were under the most up-regulated genes in the tdT$^+$ populations compared to tdT^{neg} cells (Figure 28). This shows that sorting of tdT$^+$ cells from skin isolates leads to a contamination with T-lymphocytes to some extent.

A Volcano plot (up-regulated genes in tdT$^+$ vs tdT^{neg} populations)

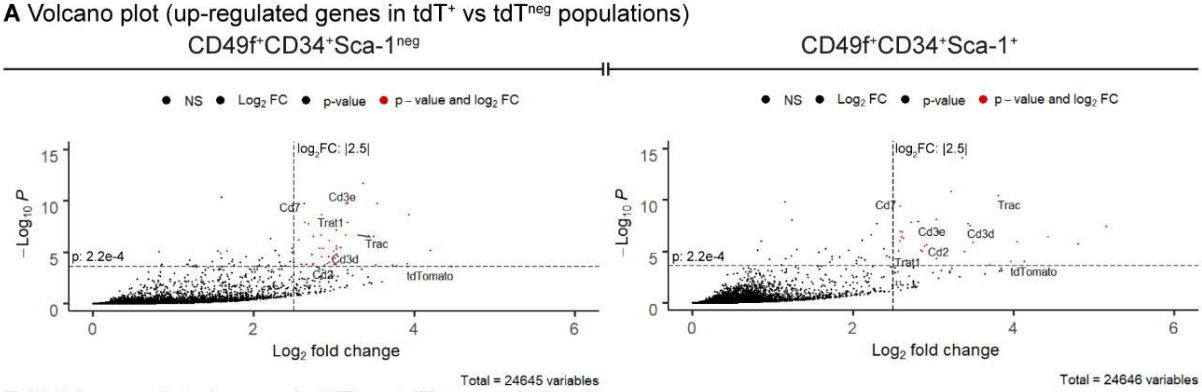

B List (up-regulated genes in tdT$^+$ vs tdT^{neg} populations)

CD49f$^+$CD34$^+$Sca-1^{neg}:

Gene	Name
Nsg2	Neuronal vesicle trafficking-associated protein 2
Nkg7	Protein NKG7
Cd2	T-cell surface antigen CD2
Cxcr6	C-X-C chemokine receptor type 6
Ctsw	Cathepsin W
Ifng	Interferon gamma
Cd96	T-cell surface protein tactile
Trac	T cell receptor alpha constant
Itgae	Integrin alpha-E;Itgae
Sit1	Signaling threshold-regulating transmembrane adapter 1
Lat	Linker for activation of T-cells family member 1
Cd7	T-cell antigen CD7
Jaml	Junctional adhesion molecule-like
Cd3d	T-cell surface glycoprotein CD3 delta chain
Cd3e	T-cell surface glycoprotein CD3 epsilon chain
Ly6g5b	Lymphocyte antigen 6 complex locus protein G5b
Cd8b1	T-cell surface glycoprotein CD8 beta chain
Trat1	T-cell receptor-associated transmembrane adapter 1
Klrd1	Natural killer cells antigen CD94
Zap70	Tyrosine-protein kinase ZAP-70
Itk	Tyrosine-protein kinase ITK/TSK
Cd6	T-cell differentiation antigen CD6
P2ry10	Putative P2Y purinoceptor 10
Ptpn5	Tyrosine-protein phosphatase non-receptor type 5
Tbx21	T-box transcription factor TBX21
B3galt5	Beta-1,3-galactosyltransferase 5
Trac	Nuclear receptor corepressor 2
Cd8a	T-cell surface glycoprotein CD8 alpha chain
Grap2	GRB2-related adaptor protein 2
Xcl1	Lymphotactin
tdTomato	*CD4Cre* activity

CD49f$^+$CD34$^+$Sca-1$^+$:

Gene	Name
Itgb7	Integrin beta-7
Trac	Nuclear receptor corepressor 2
Trdc	T cell receptor delta, constant region (Fragment)
Kir3dl1	Killer cell immunoglobulin-like receptor 3DL1
Trac	T cell receptor alpha constant
Cd2	T-cell surface antigen CD2
Rhoh	Rho-related GTP-binding protein RhoH
Rasal3	RAS protein activator like-3
Rgs1	Regulator of G-protein signaling 1
Pkib	cAMP-dependent protein kinase inhibitor beta
Il22ra2	Interleukin-22 receptor subunit alpha-2
Xcl1	Lymphotactin
Il2rg	Cytokine receptor common subunit gamma
Olfm3	Noelin-3
Jaml	Junctional adhesion molecule-like
Ms4a4b	Chandra protein
Atp8b4	Phospholipid-transporting ATPase
Cd163l1	CD163 molecule-like 1
Neurl3	E3 ubiquitin-protein ligase NEURL1B
Neurl3	E3 ubiquitin-protein ligase NEURL3
Sox17	Transcription factor SOX-17
Ikzf1	DNA-binding protein Ikaros
Itk	Tyrosine-protein kinase ITK/TSK
Cd83	CD83 antigen;Cd83
Cxcr6	C-X-C chemokine receptor type 6
Cst7	Cystatin-F
Cytip	Cytohesin-interacting protein
Cd69	Early activation antigen CD69
Itgae	Integrin alpha-E;Itgae
Ly6a	Lymphocyte antigen 6A-2/6E-1
Akna	Microtubule organization protein AKNA
Prf1	Perforin-1
Kcna3	Potassium voltage-gated channel subfamily A member 3
P2ry10	Putative P2Y purinoceptor 10
Arhgap45	Rho GTPase-activating protein 45
Slfn4	Schlafen 4
Sh2d2a	SH2 domain-containing protein 2A
CD7	T-cell antigen CD7
Trat1	T-cell receptor-associated transmembrane adapter 1
Tcrg-C1	T cell receptor gamma, constant 1 (Fragment)
Tcrg-V5	T cell receptor gamma, variable 5
Cd3d	T-cell surface glycoprotein CD3 delta chain
CD3e	T-cell surface glycoprotein CD3 epsilon chain
Naip5	Baculoviral IAP repeat-containing protein 1e
tdTomato	*CD4Cre* activity

Figure 28. Most up-regulated genes in tdT$^+$ CD49f$^+$CD34$^+$Sca-1^{neg} and tdT$^+$ CD49f$^+$CD34$^+$Sca-1$^+$ cells compared to the respective tdT^{neg} counterparts.

(A) Volcano plot of up-regulated genes in tdT$^+$ against tdT^{neg} CD49f$^+$CD34$^+$Sca-1^{neg} cells (left) and tdT$^+$ against tdT^{neg} CD49f$^+$CD34$^+$Sca-1$^+$ cells (right). Not significant changed genes are presented in black, whereas significant (p-value below 2.2*10^{-4}) up-regulated (log_2FC above 2.5) genes are shown in red. **(B)** List of up-regulated genes of tdT$^+$ CD49f$^+$CD34$^+$Sca-1^{neg} cells (left) and tdT$^+$ CD49f$^+$CD34$^+$Sca-1$^+$ cells (right) in correlation to the respective tdT^{neg} counterparts. Abbreviations: FC: fold change, log: logarithm, NS: not significant, vs: versus. For details regarding the mice see Table 17.

5.2.3 The epidermal progeny of *CD4Cre*-targeted cells grows as keratinocytes of the interfollicular epidermis and hair follicles

The flow cytometric and transcriptome analyses strongly indicated that the non-haematopoietic epidermal progeny of *CD4Cre*-targeted cells represent keratinocytes of the HF bulge, of the uHF of resting HF and of basal cells of the IFE and infundibulum. This conclusion is noteworthy because although all of these populations have high tumourigenic potential in case of a homozygous *Ptch* mutation [197, 200, 202], *Ptch*$^{fl/fl}$ *CD4Cre* mice do not spontaneously develop BCC [193]. Thus, to exclude false conclusions about the identity of the progeny of *CD4Cre*-targeted cells it was verified whether these indeed grow as keratinocytes of the HF bulge, of the uHF of resting HF and of basal layer cells of the IFE and infundibulum. For this purpose, *CD4Cre R26-tdT* skin samples were co-stained against tdT and a variety of marker proteins for identification of the respective epidermal populations. Furthermore, the *in vivo* growth behaviour of tdT epidermal cells was analysed to evaluate putative SC properties and/or transit-amplifying character of these cells.

Initial microscopic analysis of the tdT protein expression of dorsal skin preparations from adult *CD4Cre R26-tdT* mice revealed the growth of tdT$^+$ cells in the IFE, the HF-near IFE (Figure 29 A, B) as well as in anagen HF (Figure 29 B, C). Moreover, detailed investigations of the occurrence of tdT$^+$ cells in HF of the different types of hair (zigzag, awl/auchene and guard) (see chapter 1.1) showed tdT-expressing cells in the HF of zigzag, awl/auchene and guard hairs (Figure 29 D-F). Besides, the analyses revealed that the tdT$^+$ HF comprise mainly zigzag (~80%) and to a smaller amount awl/auchene (~17%) and guard (~3%) hairs (Figure 29 G) which reflects the previously described physiological distribution of the murine, dorsal hair types (~67.5% zigzag, ~30% awl/auchene and ~2% guard) [15].

To proof that tdT$^+$ cells of the *CD4Cre R26-tdT* epidermis indeed represent keratinocytes of the IFE, sections of dorsal *CD4Cre R26-tdT* skin were stained against the basal layer markers K5, Sca-1 and Trp63 (Figure 30 A). These analyses confirmed the existence of tdT$^+$K5$^+$, RFP$^+$Sca-1$^+$ and RFP$^+$Trp63$^+$ (in paraffin sections tdT was visualised by anti-RFP antibody co-staining) keratinocytes in the basal layer (Figure 30 B-D'). During skin homeostasis, basal cells of the IFE differentiate to cells of the spinous and granular layer and finally to the *stratum corneum* while migrating upwards to the skin surface (Figure 30 A). To investigate whether tdT$^+$ keratinocytes of the basal layer also can give rise to cells of the differentiated spinous and granular layer co-stainings against RFP and the IFE suprabasal cell marker K10 were performed. This approach demonstrated that the upper suprabasal layer indeed contains RFP$^+$K10$^+$ cells (Figure 30 E, E'). Moreover, also in the infundibulum that connects the IFE with the HF tdT$^+$K5$^+$ basal cells (Figure 30 F, F') as well as tdT$^+$K5^{neg} suprabasal, inner layer cells were detected (Figure 30 F, F'). This is noteworthy, because the transcriptome-based differential gene expression analysis suggested an infundibulum identity for the tdT$^+$

CD49f$^+$CD34$^+$Sca-1$^+$ cell population (see chapter 5.2.2) and indeed basal (K5$^+$) tdT$^+$ are detectable in this epidermal region.

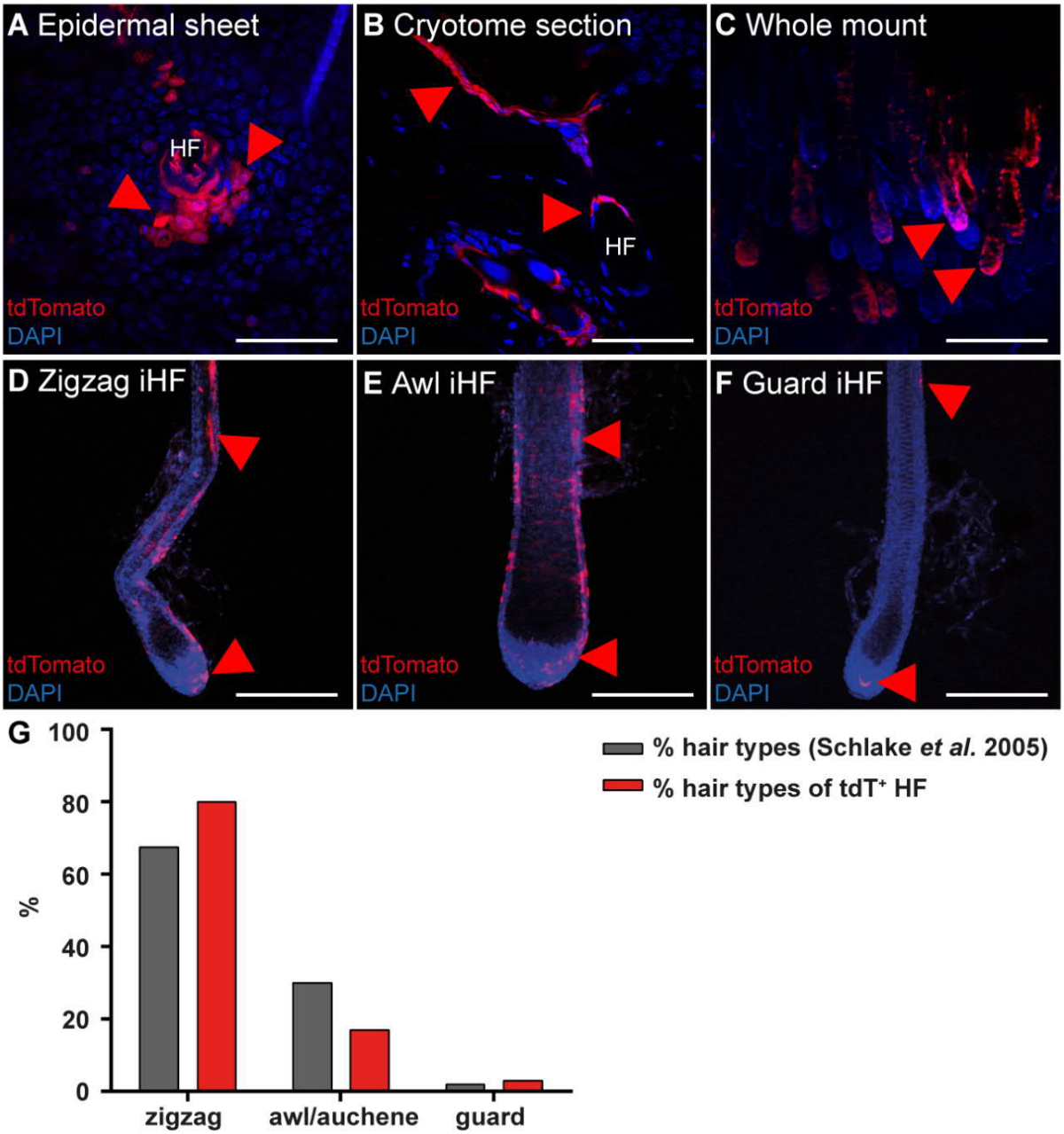

Figure 29. The progeny of *CD4Cre*-targeted cells grows in the interfollicular epidermis and hair follicles including zigzag, awl and guard hairs of murine dorsal skin.

(A-F) Representative images of an epidermal sheet **(A)**, a cryotome section **(B),** a whole mount epidermis preparation with anagen hair follicles (HF) **(C)** and isolated HF (iHF) in anagen phase **(D-F)** isolated from the dorsal skin of *CD4Cre R26-tdT* mice. Naïve tdT signal is shown (red). Nuclei were visualised with DAPI (blue). Red arrowheads: tdT$^+$ epidermal cells. **(G)** Quantification of zigzag, awl/auchene and guard hairs of wild type HF (grey) [15] and tdT$^+$ HF (red). Scale bars: Magnifications: 200 µm in **A, C**; 100 µm in **D, E, F**; 33 µm in **B**. For details regarding the mice see Table 17.

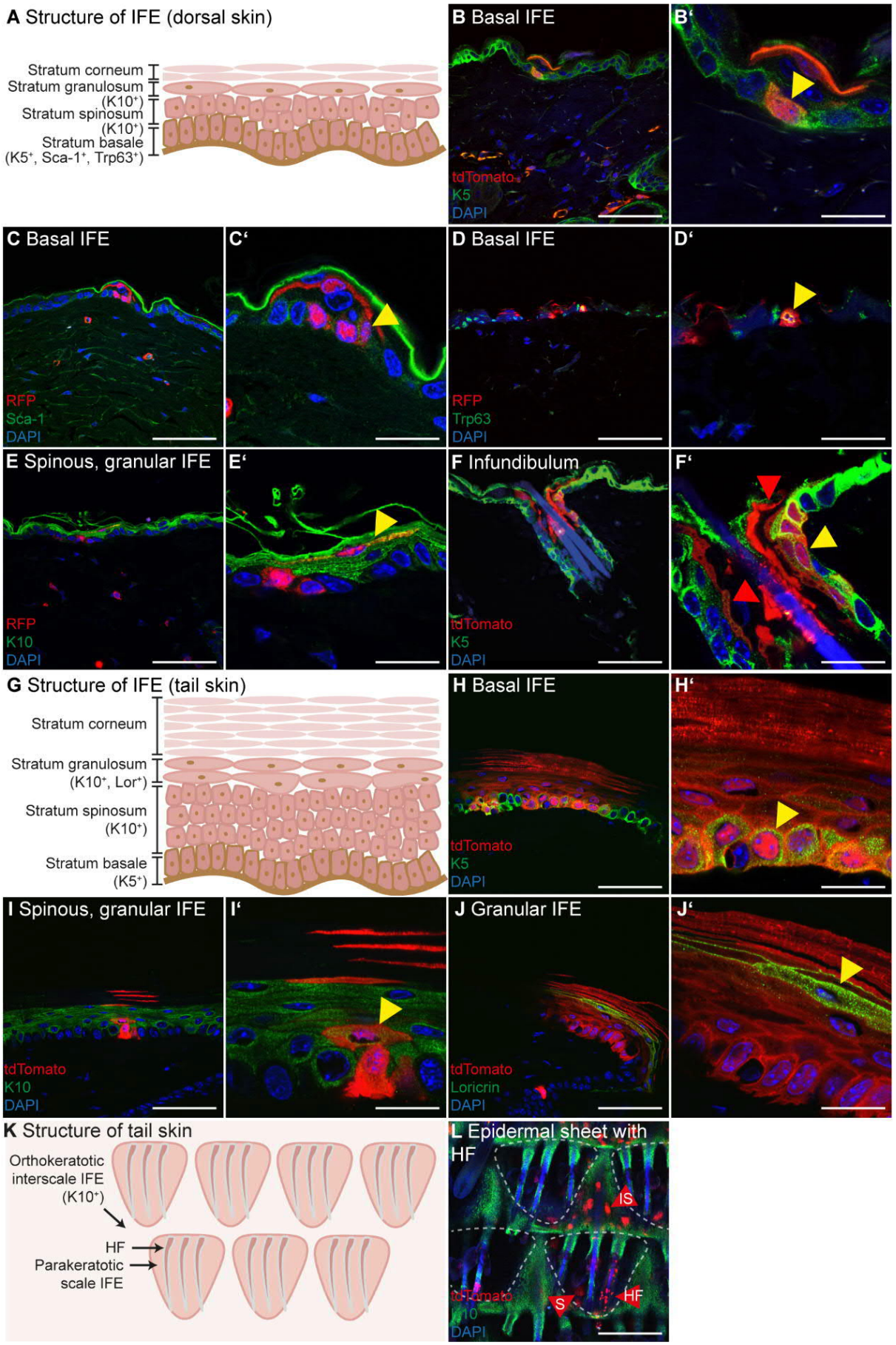

Figure 30. The progeny of *CD4Cre*-targeted cells grows in all layers of the interfollicular epidermis of murine dorsal and tail skin.

(The legend continues on the next page.)

(A, G, K) Schematic representation of the sublayers and respective key markers of the interfollicular epidermis (IFE) of murine dorsal **(A)** and tail skin **(G)** as well as of the morphological structure of murine tail skin **(K)**. **(B-F', H-J')** Representative images of antibody stainings against basal cell markers K5 **(B, B', F, F', H, H')**, Sca-1 **(C, C')** and Trp63 **(D, D')**, the spinous and granular cell marker K10 **(E, E', I, I', L)** and the granular cell marker Loricrin (Lor) **(J, J')** on cryotome **(B, B', F, F', H-J')** or paraffin sections **(C-E')** of the IFE **(B-E', H-J')** or the infundibulum **(F, F')** of dorsal skin **(B-F')** or tail skin **(H-J')** from *CD4Cre R26-tdT* mice. In cryotome sections **(B, B', F, F', H-J')** the naïve tdTomato protein was visualised (red), whereas in paraffin sections anti-RFP antibody stainings **(C-E')** were performed. **(L)** Representative image of an epidermal sheet of *CD4Cre R26-tdT* tail skin. The naïve tdT protein is visualised (red). The sheet was stained with the interscale IFE marker K10. Nuclei were visualised with DAPI (blue). Red arrowheads: tdT^+ cells, yellow arrowheads: double positive cells. Scale bars: 200 µm in **K**; 33 µm in **B, C, D, E, F, H, I, J**; 10 µm in **B', C', D', E', F', H', I', J'**. Abbreviations: HF: hair follicle, IS: interscale IFE, S: scale IFE. For details regarding the mice and antibody staining, see Table 17 and Table 13, respectively.

However, the tail skin epidermis of mice contains more epidermal cell layers and fewer HF and thus on the one hand facilitates analyses of suprabasal IFE layer but also more precisely resembles the morphology of human skin [8] (Figure 30 G). Hence, also murine tail skin was stained against K5, K10 and the granular cell marker Lor. In fact, these stainings identified tdT^+K5^+ basal cells (Figure 30 H, H'), tdT^+K10^+ spinous and granular cells (Figure 30 I, I') and tdT^+Lor^+ granular cells (Figure 30 J, J') in murine tail skin. Moreover, immunofluorescent stainings of epidermal sheet preparations also revealed that tdT^+ cells were not restricted to $K10^+$ orthokeratotic interscale IFE, but also grow in $K10^{neg}$ parakeratotic scale IFE and in HF (Figure 30 K, L).

In summary these data show, that the progeny of *CD4Cre*-targeted cells grows as basal and suprabasal cells in the IFE and infundibulum of murine dorsal and/or tail skin. Based on the localisation of tdT^+ cells as progenies of *CD4Cre*-expressing cells it is conceivable that these cells or their ancestors possess SC or TAC capacities. Indeed, label-retaining assays (e.g. with bromodeoxyuridine, BrdU), for distinction of LRC and TAC (TAC lose their label due to numerous cell divisions over time) showed that tdT^+BrdU^+ cells are trackable in the *CD4Cre R26-tdT* epidermis up to 90 days after initial DNA labelling. Thus, a LRC identity of *CD4Cre*-expressing ancestors or of their epidermal progenies has to be assumed [223, 246-248].

Besides, the flow cytometry analysis (Figure 25) and the transcriptome data (Figure 26, Figure 27) suggest that SC of the HF bulge and the uHF of resting HF also descend from *CD4Cre*-expressing cells. To proof this assumption the HF compartment (Figure 31) of *CD4Cre R26-tdT* dorsal skin was more detailed analysed. Indeed, these approaches confirmed the existence of tdT^+ cells in the uHF and HF bulge compartment of resting HF (Figure 31 B, B'). Moreover, tdT^+ cells of the uHF express the ORS marker K5 (Figure 31 C, C') and tdT^+ cells of the HF bulge region the bulge marker CD34 (Figure 31 D-E'). Indeed, the antibody-stained skin sections confirmed the identity of the progeny of *CD4Cre*-targeted cells as keratinocytes of the HF bulge and of the uHF of resting HF.

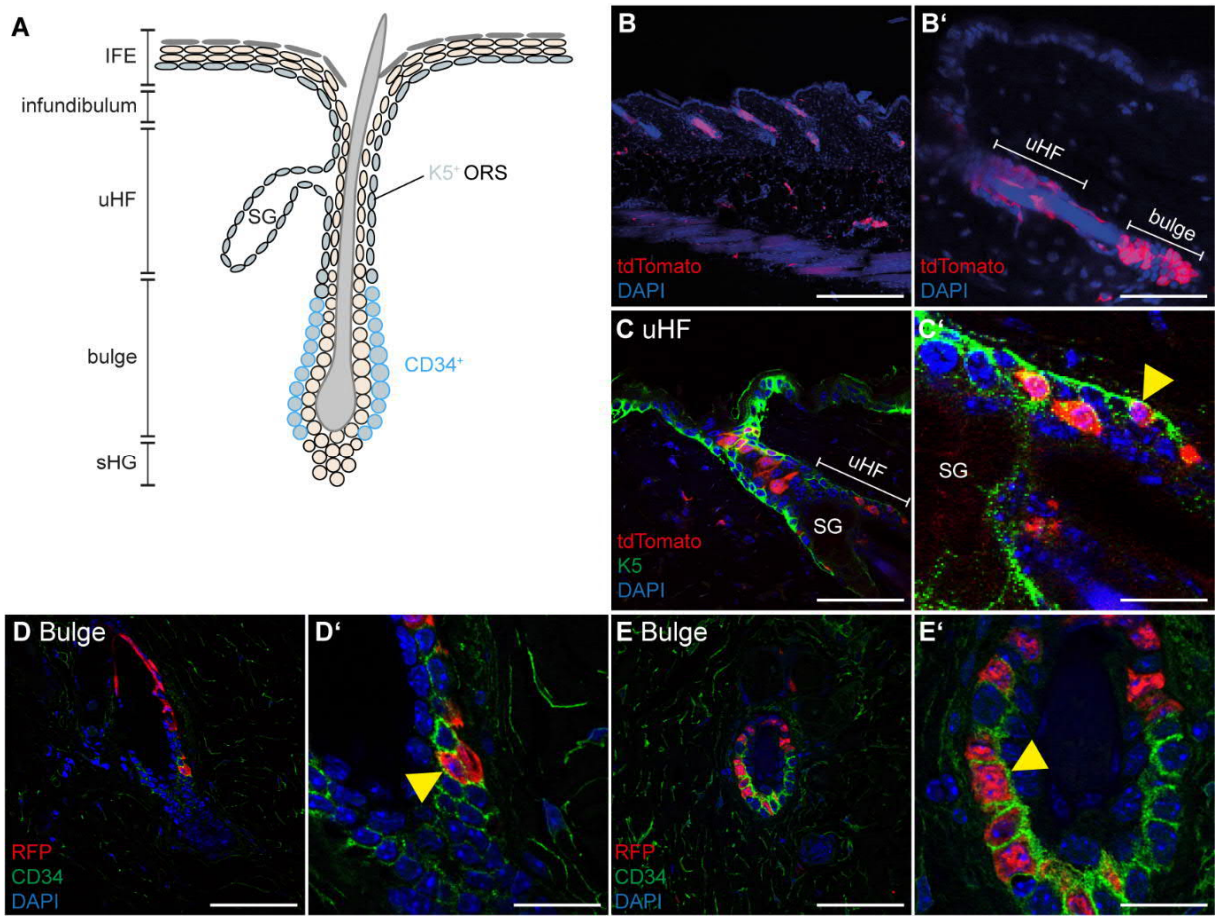

Figure 31. The progeny of *CD4Cre*-expressing cells grow as outer root sheath and bulge keratinocytes in resting hair follicles of murine dorsal skin.

(A) Schematic representation of a murine telogen hair follicle (HF) and its respective HF subpopulations, layers and key marker proteins. **(B-E')** Representative images of antibody stainings against the outer root sheath marker K5 **(C, C')** and the bulge marker CD34 **(D-E')** on cryotome sections **(B-C')** or paraffin sections **(D-E')** of telogen *CD4Cre R26-tdT* dorsal skin. Naïve tdTomato is shown in **B-C'** (red), whereas anti-RFP antibody staining was performed for visualisation of tdT expression on paraffin sections **(D-E')**. Nuclei were visualised with DAPI (blue). Yellow arrowheads: double positive cells. Scale bars: 200 µm in **B**; 33 µm in **B', C, D, E**; 10 µm in **C', D', E'**. Abbreviations: IFE: interfollicular epidermis, SG: sebaceous gland, sHG: secondary hair germ, uHF: upper HF. For details regarding the mice and antibody staining, see Table 17 and Table 13, respectively.

5.2.4 Epidermal stem cell-like cells that descent from *CD4Cre*-targeted cells populate the entire hair follicle

During transition from the resting (telogen) phase to the growing (anagen) phase of the hair cycle SC of the HF bulge and sHG become activated and start to migrate to the bulb region at the base of the HF [13]. In the bulb region, matrix cells represent the proliferative active population that give rise to seven layers of the HF: the Cp layer, the IRS (Henle's layer, Huxley's layer, IRS cuticle) and the HS (medulla, cortex, hair cuticle) [4, 13]. To investigate whether the progeny of *CD4Cre*-targeted cells in the HF bulge of resting HF act like real bulge SC during telogen-to-anagen transition and thus populate growing HF, sections and iHF of dorsal *CD4Cre R26-tdT* skin at the late anagen phase were analysed for the co-expression of tdT and marker proteins of the different anagen HF compartments (Figure 32).

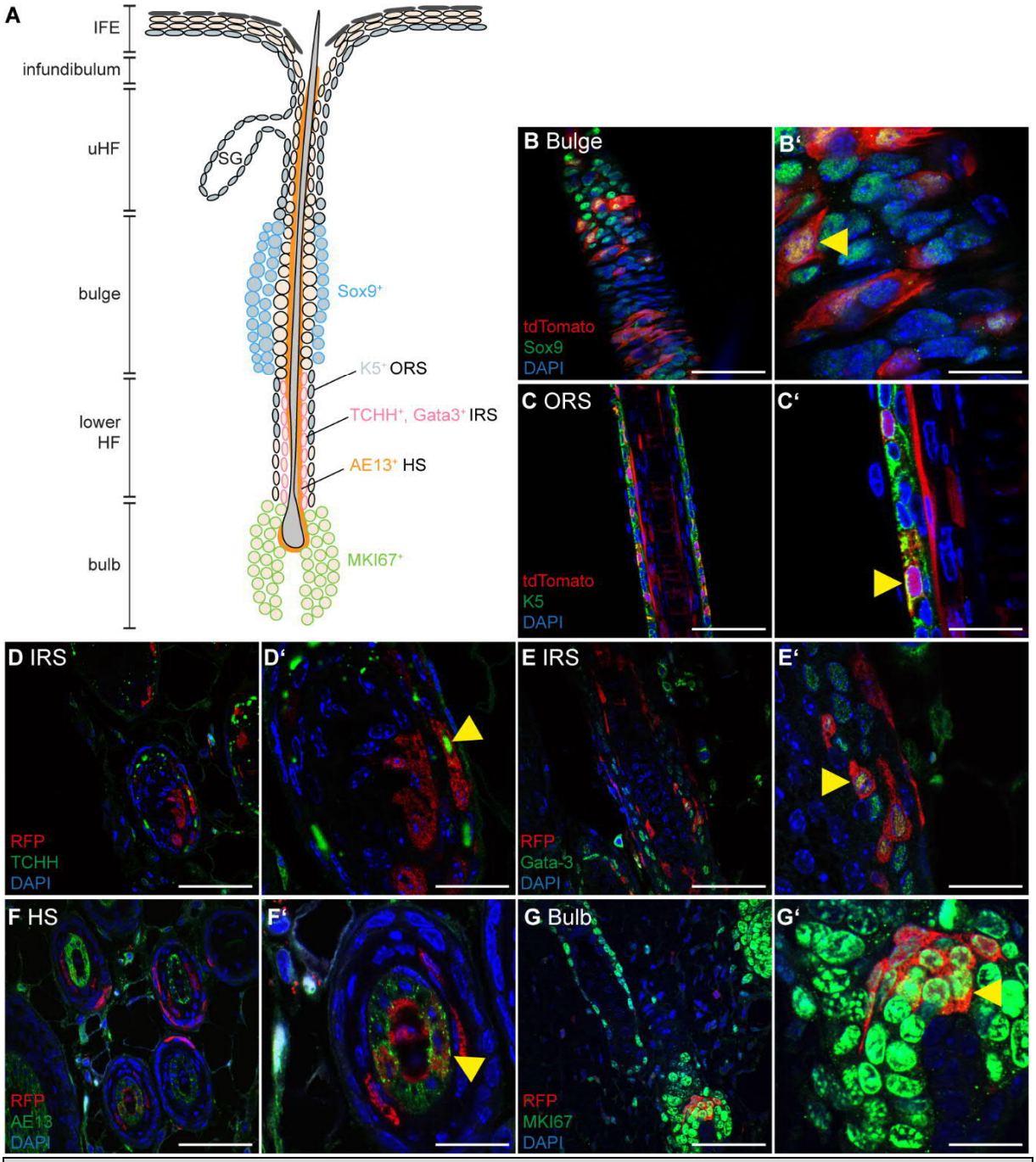

Figure 32. The progeny of *CD4Cre*-targeted cells populates all hair follicle layers in growing hair follicles of murine dorsal skin.

(A) Schematic representation of a murine anagen hair follicle (HF) and its respective HF subpopulations, layers and key marker proteins. **(B-G')** Representative images of antibody stainings against the bulge marker Sox9 **(B, B')**, the outer root sheath (ORS) marker K5 **(C, C')**, the inner root sheath (IRS) marker TCHH **(D, D')** and Gata-3 **(E, E')**, the HF marker AE13 **(F, F')** and the proliferation marker MKI67 **(G, G')** on iHF **(B-C')** or paraffin sections **(D-G')** of anagen *CD4Cre R26-tdT* dorsal skin. Naïve tdTomato is shown in **B-C'** (red), whereas anti-RFP antibody staining was performed for visualisation of tdT expression on paraffin sections **(D-G')**. Nuclei were visualised with DAPI (blue). Yellow arrowheads: double positive cells. Scale bars: 33 µm in **B, C, D, E, F, G**; 10 µm in **B', C', D', E', F', G'**. Abbreviations: HS: hair shaft, IFE: interfollicular epidermis, SG: sebaceous gland, uHF: upper HF. **(G, G')** MKI67 immunofluorescence staining was performed in advance of this work [223]. For details regarding the mice and antibody staining, see Table 17 and Table 13, respectively.

This approach indeed revealed that anagen HF contain tdT$^+$Sox9$^+$ bulge cells (Figure 32 B, B'), tdT$^+$K5$^+$ ORS cells (Figure 32 C, C'), RFP$^+$TCHH$^+$ and RFP$^+$Gata3$^+$ IRS cells (Figure 32

D-E'), RFP^+AE13^+ HS cells (Figure 32 F, F') and proliferating RFP^+MKI67^+ matrix cells in the bulb region (Figure 32 G, G'). These results demonstrated that the progeny of *CD4Cre*-targeted cells persists as HF bulge cells in resting HF, becomes activated during anagen initiation, is able to proliferate and subsequently differentiate into inner HF layers and thus contributes to HF growth.

To evaluate the localisation of the progeny of *CD4Cre*-targeted cells in the HF throughout all hair cycle phases (anagen I-VI, catagen, telogen), the telogen dorsal skin of 8 to 10-week-old *CD4Cre R26-tdT* mice was synchronised by warm wax depilation and afterwards isolated at different hair cycle phases [223, 248]. These analyses showed that tdT^+ cells were detectable during the entire hair cycle and in all compartments of the HF including the SG [223, 248]. In more detail, tdT^+ cells were localised in the infundibulum, isthmus, bulge and in the sHG during telogen phase and at the onset of anagen, while the bulb region and the ORS were repopulated at anagen III. During anagen IV, tdT^+ cells were detectable first in the IRS and during anagen V in the HS. Moreover, $MKI67^+tdT^+$ cells were detected in the bulge region during the anagen phases II-IV and during telogen phase. Furthermore, $MKI67^+$ tdT^+ cells were observed in the sHG of telogen HF and in the matrix cell compartment of anagen III-VI HF [223, 248]. In addition, proliferative active tdT^+ epidermal cells were also detected in the basal layer of the IFE, in the infundibulum and in the SG [223, 248]. Taken together these results show that the progeny of *CD4Cre*-targeted cells are able to grow in the entire HF and persist during all hair cycle phases [223, 248]. Thus, it has to be concluded that at least the progeny of *CD4Cre*-targeted cells has SC-like character with respect to homeostasis and regeneration of the HF and IFE.

Recently, it has been discovered that the outer layer of anagen HF consists of two clonally unrelated groups: the $K14^+$ basal ORS and the $K75^+$ Cp that originate from separate cell lineages and have distinct modes of growth [249] (Figure 33). The basal ORS has an anisotropic growth activity as it is absent from the proximal part of the HF but repopulates the ORS of the distal part of the HF (rORS clone) and descends from a suprabulbar zone [249]. In contrast, the Cp layer SC progenitor can be found in the germinative layer of the bulb and produce not only the Cp layer but also the IRS and HS [249]. As a result, descendant cells can be found in the germinative layer of the HF proximal end, in internal structures (Cp layer, IRS, HS) and in the outer layer of the distal part of the HF (complex clone) [249]. Furthermore, the outer layer of the HF contains a third lineage that is restricted to the HF bulb, contributes to the outermost layer of the bulb and surrounds the germinative layer (lower proximal cup, LPC) [249]. The LPC and complex clones are suggested to share a common precursor since whenever descendants are found in the LPC they also are found in the Cp and in internal structures [249].

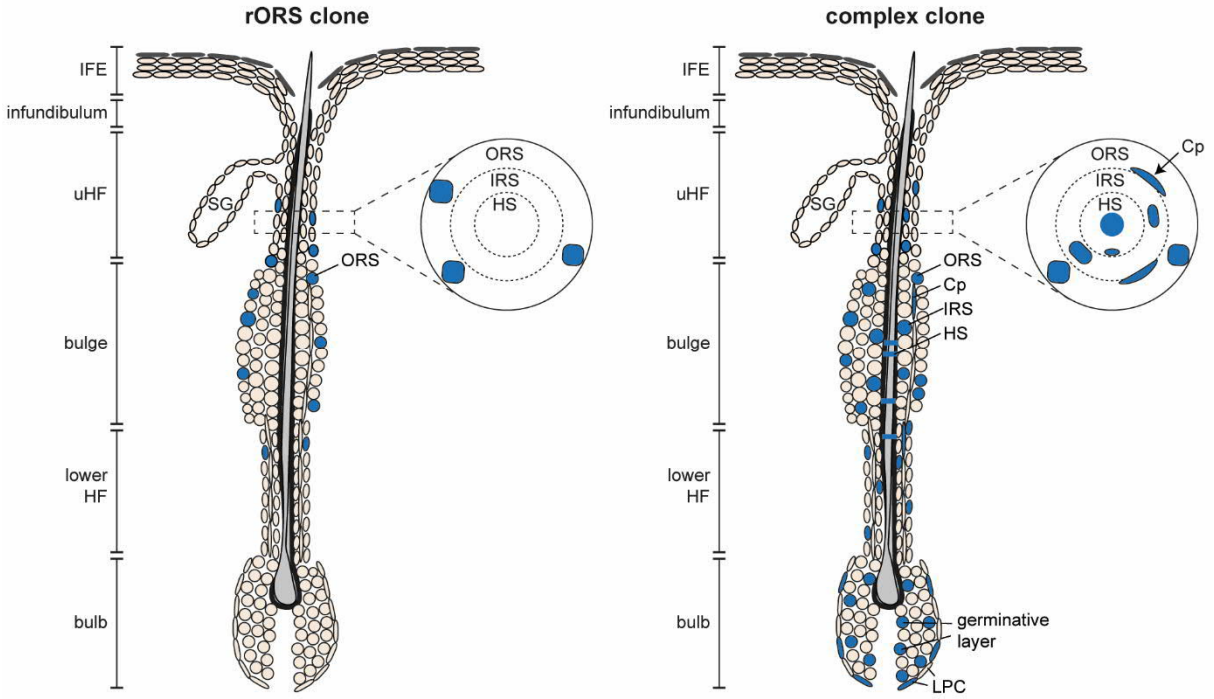

Figure 33. Proximal-distal and radial contribution of rORS and complex clones to the hair follicle layers.

Schematic representation of murine anagen hair follicles (HF) and its respective HF subpopulations and layers including the contribution of rORS (left) and complex (right) clones to the layers. rORS clones contribute to the distal part of the HF outer root sheath (ORS), whereas complex clones give rise to all HF lineages including the ORS, companion (Cp) layer, inner root sheath (IRS), hair shaft (HS) and lower proximal cup (LPC). Modified from [249].

So far, tdT^+K5^+ ORS cells were identified (Figure 32), indicating that some of the progeny cells of *CD4Cre*-targeted ancestors might grow as rORS clones with an anisotropic mode of growth in the distal part of the HF. In addition, tdT^+ cells were found in internal structures (RFP^+TCHH^+ IRS, $RFP^+Gata\text{-}3^+$ IRS and RFP^+AE13^+ HS) and in the proximal part of the anagen HF (RFP^+MKI67^+ bulb) of *CD4Cre R26-tdT* dorsal skin (Figure 32); hence, the stem/transient-amplifying mode of growth by complex clones is more likely for the progeny of *CD4Cre*-targeted cells. However, to proof this assumption the clone type of tdT^+ iHF of late anagen (VI) *CD4Cre R26-tdT* dorsal skin was determined based on the localisation of tdT^+ cells within the iHF. For this purpose, randomly 144 iHF were isolated from the dorsal skin of a 43-week-old *CD4Cre R26-tdT* mouse and analysed for endogenous tdT expression. In total, 35 iHF contained tdT^+ cells (~24%). Of those five tdT^+ iHF were excluded due to their damage during the preparation process. The remaining 30 tdT^+ iHF were used for determination of the clone type. This analysis indeed revealed that tdT^+ cells can grow as both clone types – four of 30 iHF (13%) contained tdT^+ cells exclusively in the ORS of the distal part of the HF (rORS clones) (Figure 34 A, B-D') and 22 of 30 iHF (73%) contained tdT^+ cells in the HF proximal end (bulb), in internal structures (IRS, HS) and in the outer layer of the distal part of the HF (complex clones) (Figure 34 A, E-G'). Whenever tdT^+ cells were found in the different internal and outer layers (complex clones) it was not possible to further distinguish whether the tdT^+ cells also grow as $K14^+$ ORS cells (rORS clones) (Figure 34 F, F').

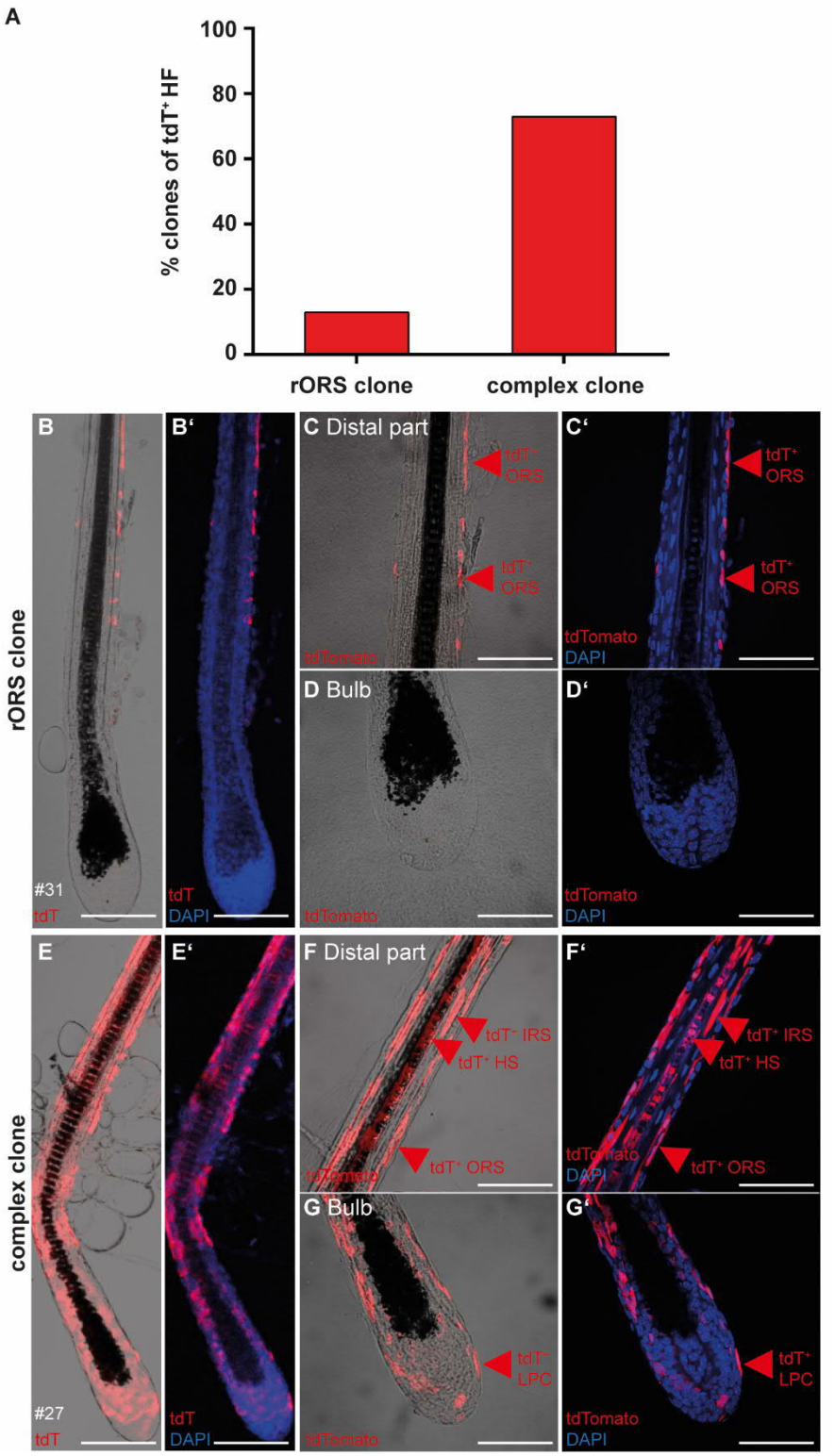

Figure 34. The progeny of *CD4Cre*-targeted cells grows as rORS and complex clones in anagen hair follicles of murine dorsal skin.

(A-G') Percentage share of clone type (rORS or complex) **(A)** and representative images **(B-G')** of isolated hair follicle of anagen *CD4Cre R26-tdT* dorsal skin (43 weeks old). Naïve tdTomato is shown (red). Nuclei were visualised with DAPI (blue). Red arrowheads: tdT^+ cells. Scale bars: 50 µm in **B, B', E, E'**; 33 µm in **C, C', D, D', F, F', G, G'**. Abbreviations: HS: hair shaft, IRS: inner root sheath, LPC: lower proximal cup, ORS: outer root sheath. For details regarding the mice see Table 17.

Beyond that, also the contribution of the progeny of *CD4Cre*-targeted cells to the different HF lineages was analysed in more detail. Therefore, the number of iHF that contained tdT^+ cells in the outer layer, internal structures (IRS, HS), LPC, DS, surrounding DP and DP was determined (Figure 35). Among the 30 analysed tdT^+ iHF, tdT^+ cells were found in 26 of 30 iHF (86%) in the outer layer, in 22 of 30 iHF (73%) in internal structures, in 12 of 30 iHF (40%) in the LPC, in two of 30 iHF (7%) in the DS and in two of 30 iHF (7%) tdT^+ cells surround the DP but never were found in the DP itself (Figure 35 A). These results demonstrate that the progeny of *CD4Cre*-targeted cells contribute to all epidermal lineages of the anagen HF.

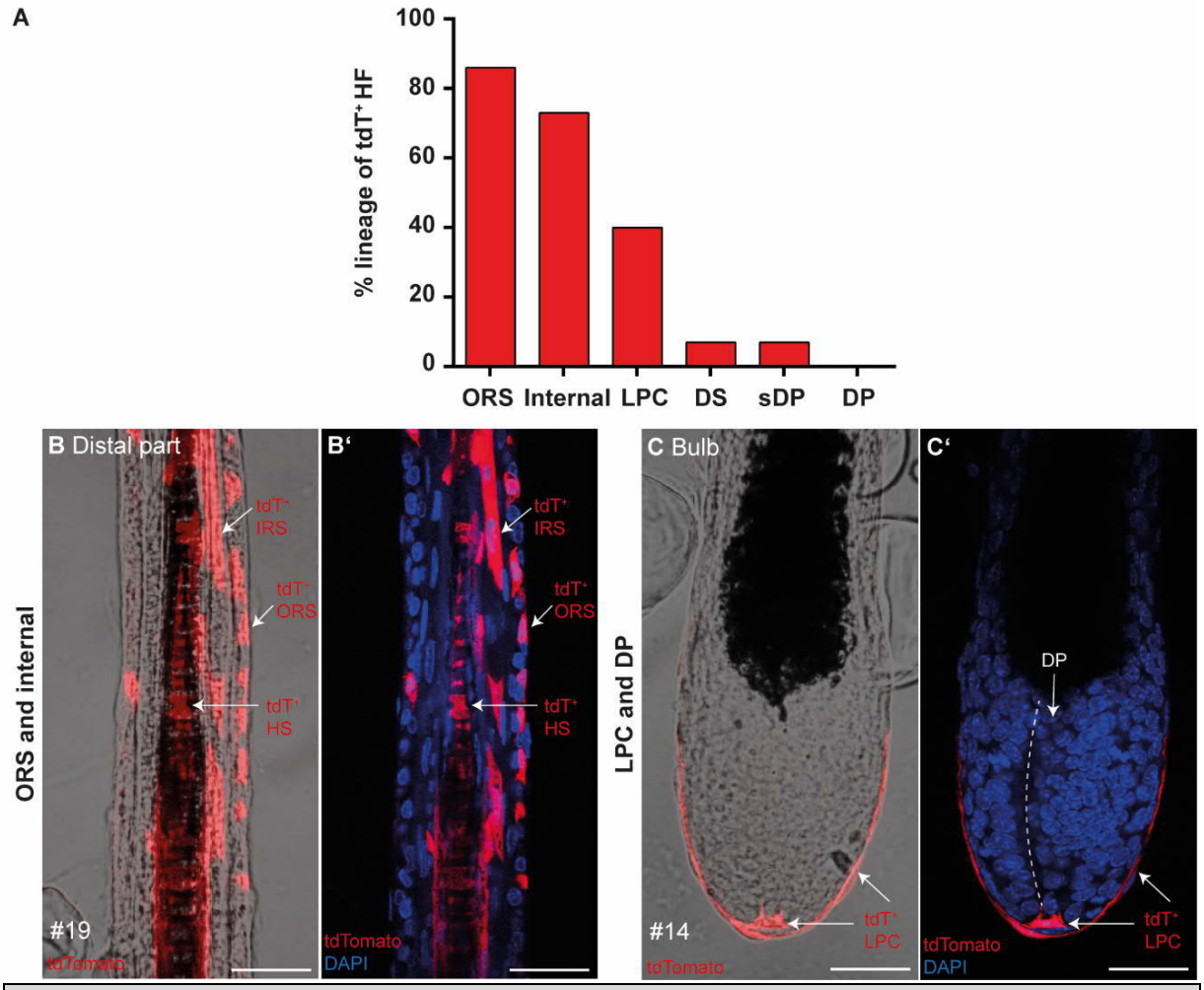

Figure 35. The progeny of *CD4Cre*-targeted cells grows in all epidermal hair follicle lineages in anagen hair follicles of murine dorsal skin.

(A-G') Percentage share of lineage contribution **(A)** and representative images **(B-C')** of isolated hair follicle of anagen *CD4Cre R26-tdT* dorsal skin (43 weeks old). Naïve tdTomato is shown (red). Nuclei were visualised with DAPI (blue). White arrows: tdT^+ cells. Scale bars: 16.5 µm in **B, B', C, C'**. Abbreviations: DP: dermal papilla, DS: dermal sheath, HS: hair shaft, IRS: inner root sheath, LPC: lower proximal cup, ORS: outer root sheath, sDP: surrounding DP. For details regarding the mice see Table 17.

Since tdT$^+$ cells were found in the different HF layers (ORS, IRS, HS, LPC) and grow as complex clones the existence of Cp layer cells that descend from *CD4Cre*-expressing cells can be hypothesized. Cells of the Cp layer show a flattened morphology and express K75, in contrast to basal ORS cells that have a cuboid morphology and express K14 and K5 [249]. Antibody stainings against the ORS marker K5 and the Cp layer marker K75 confirmed the outer localisation of K5$^+$ cuboid cells and the inner localisation of K75$^+$ elongated cells (Figure 36 A, A'). Next, further tdT$^+$ iHF were isolated and antibody stainings against the Cp layer marker K75 or the ORS marker K5 were performed. These approaches indeed confirmed that in tdT$^+$ rORS clones tdT$^+$ cells are restricted to the basal ORS but are absent from the K75$^+$ Cp layer (Figure 36 B, B'). Contrary to this, in tdT$^+$ complex clones tdT$^+$ cells exist in the K5$^+$ basal ORS (Figure 36 C, C') and in the K75$^+$ Cp layer (Figure 36 D, D').

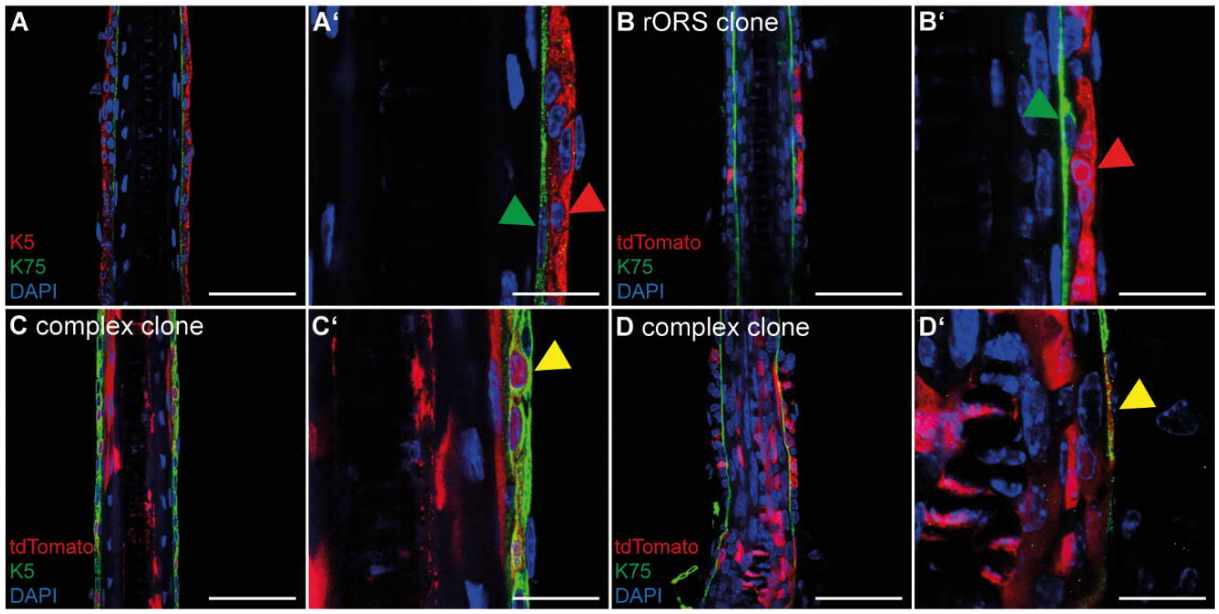

Figure 36. The progeny of *CD4Cre*-targeted cells grows in the companion layer of complex clones in anagen hair follicles of murine dorsal skin.

(A-D') Representative images of antibody stainings against the outer root sheath marker K5 **(A, A', C, C')** and the companion layer marker K75 **(A-B', D, D')** of isolated hair follicles of anagen *CD4Cre R26-tdT* dorsal skin. Naïve tdTomato is shown (red). Nuclei were visualised with DAPI (blue). Red arrowheads: K5$^+$ cell **(A')** or tdT$^+$ cell **(B')**, green arrowheads: K75$^+$ cells, yellow arrowheads: double positive cells. Scale bars: 33 µm in **A, B, C, D**; 10 µm in **A', B', C', D'**. For details regarding the mice and antibody staining, see Table 17 and Table 13, respectively.

5.2.5 Wound-induced activation of epidermal stem cell-like cells that descent from *CD4Cre*-targeted cells

After injury, SC of the IFE and the HF participate in the re-epithelisation of the wound side. In doing so, HF SC are able to leave their own niche and give rise to epidermal cells of the IFE (see chapter 1.2.5). Hence, it was investigated whether the progeny of *CD4Cre*-targeted IFE cells and/or HF SC also contributes to wound healing.

In general, for the analysis of wound healing processes in mice a distinction is made between longitudinal cuts (incisional wounding) and the removal of larger areas of skin (excisional wounding). Excisional wound healing produces new IFE, which better corresponds to the process of wound healing in humans [250] in comparison to incisional wounds that are less suited for the analysis of re-epithelisation due to the limited volume of wound healing activity [61]. However, the wound induced hair anagen re-entry/growth (WIH-A) that occurs in tissue adjacent to wound sites can be examined in both: excisional and incisional wounds [251]. In line with the known role of macrophages in SC activation during HF cycling and after hair plucking injury [252-254] epidermal wounding leads to the recruitment and activation of macrophages that in turn initiate WIH-A by activating bulge SC via tumour necrosis factor (TNF) signalling [255, 256].

As already described, the progeny of *CD4Cre*-targeted cells persists as HF bulge cells in resting HF, but becomes activated during anagen initiation and differentiates into all HF layers (Figure 31, Figure 32, Figure 34, Figure 35). Thus, next it was analysed whether the progeny of *CD4Cre*-targeted cells also contribute to WIH-A (Figure 37 A). In unwounded dorsal skin of 11-week-old *CD4Cre R26-tdT* mice, only few anagen HF that contain tdT^+ cells were detected (Figure 37 B-B''). In contrast, 18 days after wounding the healed dorsal skin of age-matched *CD4Cre R26-tdT* mice possesses many WIH-A HF that contain tdT^+ cells (Figure 37 C-C''). This finding showed that the progeny of *CD4Cre*-targeted cells plays a significant role during WIH-A.

In order to investigate whether descendants of *CD4Cre*-expressing cells can also participate in the re-epithelisation of incisional wounds a longer time period (35 days) between wounding and sample preparation was chosen to achieve a complete re-epithelisation of the wounded area (Figure 38 A). Indeed, the re-epithelised IFE as well as IFE and HF of wound-near regions contain RFP^+K5^+ cells of the IFE and HF (Figure 38 B-E'') and RFP^+K5^{neg} cells which most probably represent suprabasal IFE cells due to their morphology (Figure 38 B, C, E, E'). These results unravelled that the progeny of *CD4Cre*-targeted IFE cells and/or HF SC also contribute to the marginal re-epithelisation of incisional wounds.

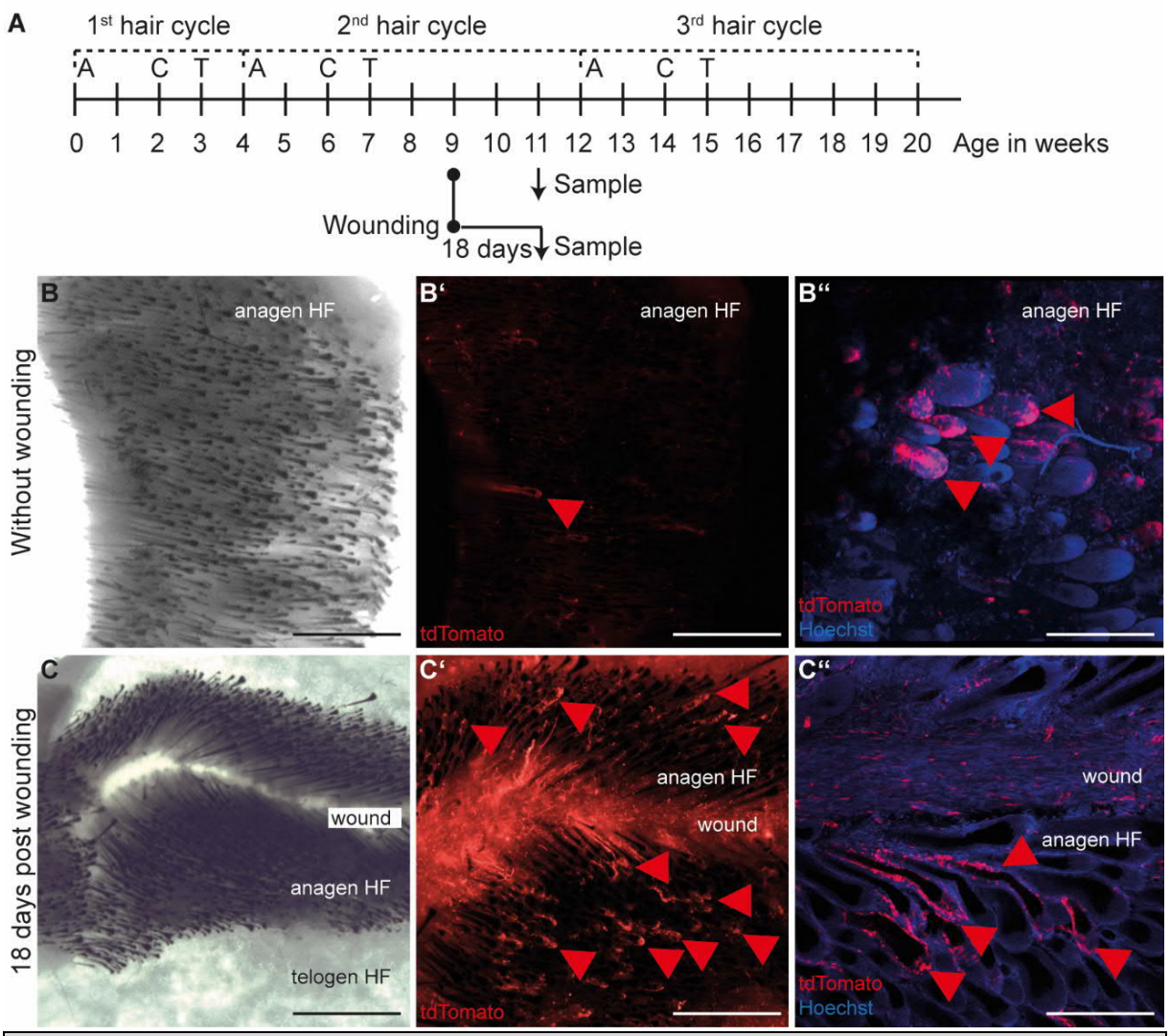

Figure 37. Wound-induced enrichment of the progeny of *CD4Cre*-targeted cells in wound-near hair follicles.

(A) Schematic overview of the experimental setups for incisional wounded and unwounded control *CD4Cre R26-tdT* dorsal skin. **(B-C'')** Representative images of whole mount preparations of unwounded **(B-B'')** and wounded **(C-C'')** *CD4Cre R26-tdT* dorsal skin. Transmitted light images **(B, C)** and red fluorescence channel **(B', C')** showing anagen hair follicles (HF) **(B, B')** and wound induced telogen-to-anagen transition of wound-surrounding HF **(C, C')** with naïve tdTomato (red) in **B'-B'', C'-C''**. Nuclei were visualised with Hoechst (blue). Red arrowheads: tdT^+ cells. Scale bars: 2.5 mm in **B, C**; 1 mm in **B', C'**; 200 µm in **B'', C''**. Abbreviations: A: anagen, C: catagen, T: telogen. For details regarding the mice see Table 17.

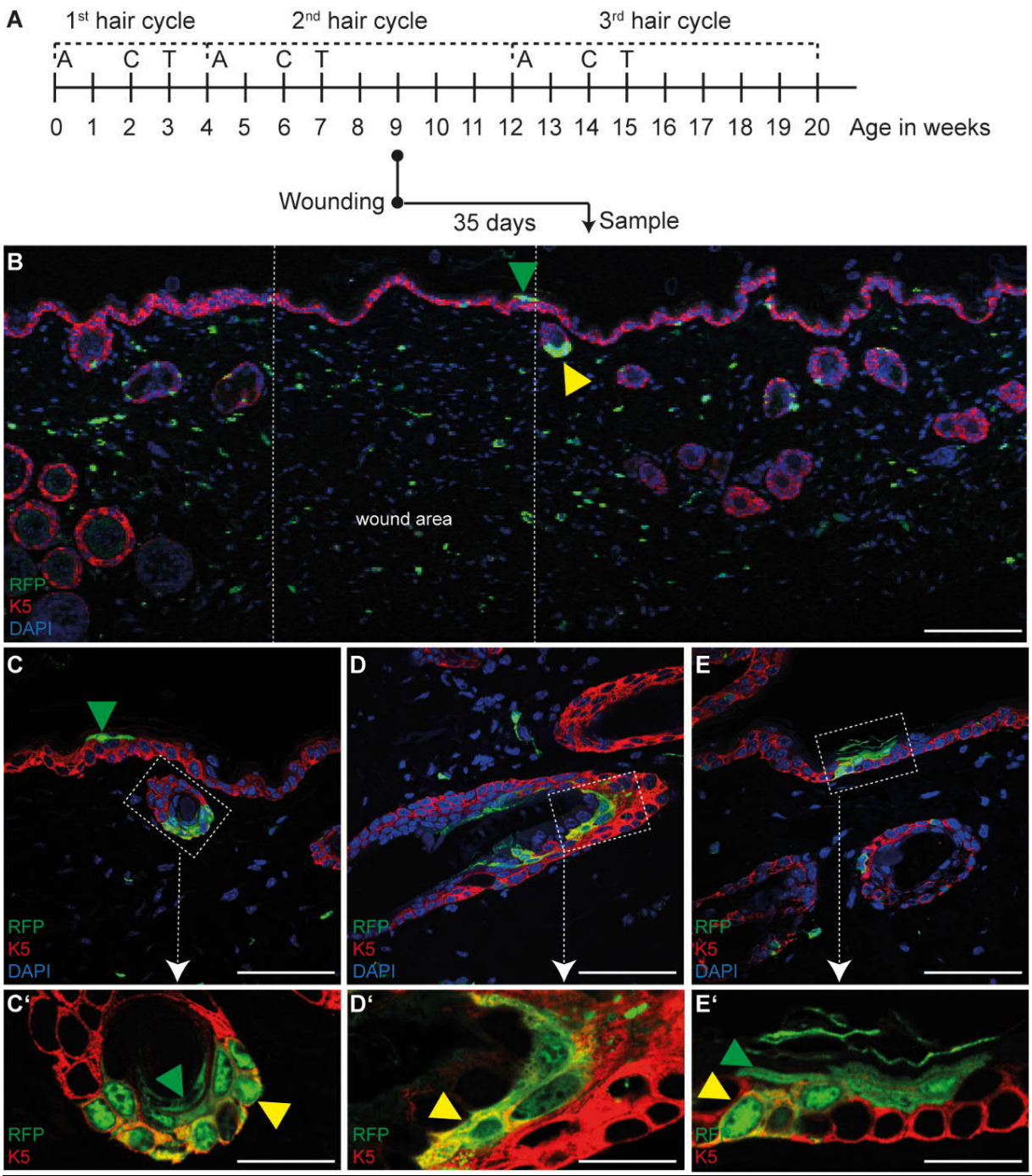

Figure 38. Contribution to the wound-induced re-epithelisation of the interfollicular epidermis of the progeny of *CD4Cre*-targeted cells.

(A) Schematic overview of the experimental setup for incisional wounded *CD4Cre R26-tdT* dorsal skin. **(B-E')** Representative images of antibody stainings against the outer root sheath and basal interfollicular epidermis marker K5 and RFP for visualisation of tdT expression on paraffin sections of wounded *CD4Cre R26-tdT* dorsal skin. Green arrowheads: RFP positive cells; yellow arrowheads: double positive cells. Scale bars: 67 µm in **B**; 33 µm in **C, D, E**; 10 µm in **C', D', E'**. Abbreviations: A: anagen, C: catagen, T: telogen. For details regarding the mice and antibody staining, see Table 17 and Table 13, respectively.

5.2.6 The quantity of epidermal stem cell-like cells that descent from *CD4Cre*-targeted cells increases with age

The progeny of *CD4Cre*-targeted cells comprises SC of the HF bulge and the uHF as well as basal cells of the IFE. However and as stated already this observation is noteworthy because all of these populations have high tumourigenic potential in case of a homozygous *Ptch* mutation [197, 200, 202], but *Ptch*$^{fl/fl}$ *CD4Cre* mice do not spontaneously develop BCC [193, 199]. Possible explanations might be that the progeny of *CD4Cre*-targeted cells either represents a too low number of cells or persists a too short time period in murine skin to induce tumour formation.

To determine the quantity and the persisting time of keratinocytes that descent from *CD4Cre*-trageted cells in the murine epidermis, the number of tdT-expressing epidermal cells of different aged *CD4Cre R26-tdT* mice was determined. The microscopic analysis of skin from young (7, 11 weeks old), adult (16-27 weeks old) and old (55 weeks old) mice (Figure 39 A) revealed that dorsal and tail skin of aged mice showed high numbers of tdT$^+$ HF and tdT$^+$ epidermal patches compared to younger mice (Figure 39 B1-D4). In more detail, the dorsal anagen skin in the 3rd hair cycle phase consists of only isolated tdT$^+$ HF, whereas in the 4th hair cycle phase several tdT$^+$ HF and in the 5th and 9th hair cycle phase high numbers of tdT$^+$ HF were observed (Figure 39 B1-B4). Similarly, the dorsal telogen skin in the 2nd hair cycle phase does not contain tdT$^+$ HF, but in the 4th hair cycle phase isolated tdT$^+$ HF and in the 5th hair cycle phase many tdT$^+$ HF were detectable (Figure 39 C1-C4). Unfortunately, the epidermal sheet of the 9th hair cycle phase contains only a few HF, from which however several are tdT$^+$ (Figure 39 C4).

Likewise, in tail skin of young mice the number of tdT$^+$ epidermal patches in tail skin was low, but increases continuous during adulthood and reached high numbers in 22 and 55-week-old mice (Figure 39 D1-D4, E1). Remarkably, not only the number of tdT$^+$ epidermal patches in tail skin increases, but also the mean area of the tdT$^+$ epidermal patches enlarges from ~93 µm^2 and ~97 µm^2 in 7 and 11-week-old mice to ~224 µm^2, ~283 µm^2 and ~413 µm^2 in 18, 22 and 55-week-old mice, respectively (Figure 39 D1-D4, E2). The tdT$^+$ epidermal patches with an increased area occur in 22 and 55-week-old mice, but are absent or rare in 7, 11 and 18-week-old mice (Figure 39 D1-D4, Appendix C). Nevertheless, numerous small tdT$^+$ epidermal patches also occur in 22 and 55-week-old mice (more when compared with 7, 11 and 18-week-old mice, see Figure 39 D1-D4, Appendix C), which corresponds to the increased colony number in aged mice (Figure 39 E1). Similarly, in tail skin sections of adult 22-week-old mice small tdT$^+$ clones with one to few tdT$^+$ basal cells were observed (Figure 39 E3), whereas in aged 88-week-old mice additionally huge tdT$^+$ clones with many tdT$^+$ basal cells were found (Figure 39 E4).

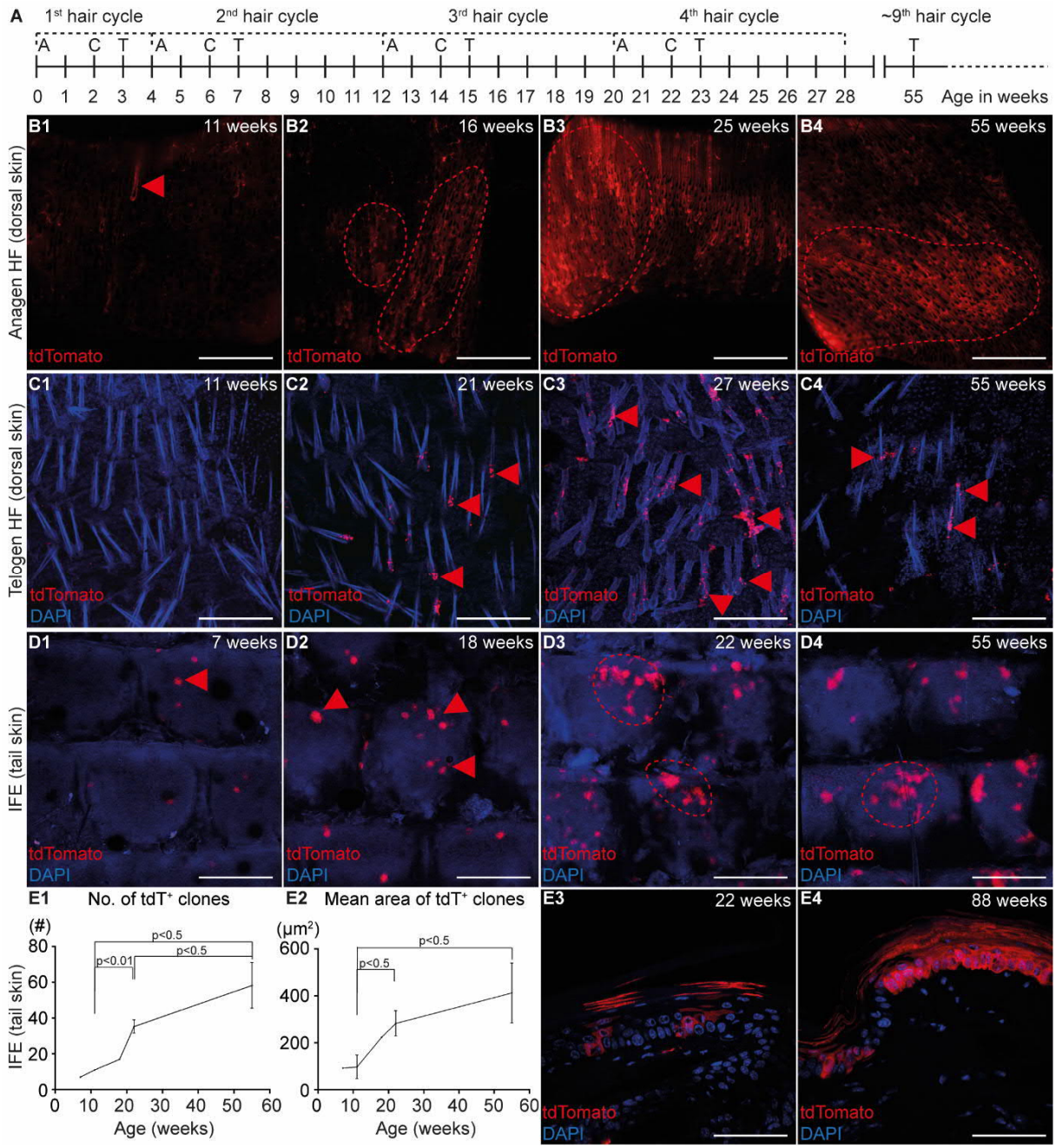

Figure 39. The quantity of the progeny of *CD4Cre*-targeted cells in hair follicles and the interfollicular epidermis increases during ageing.

(A) Schematic representation of the murine hair cycle phases in relation to the mouse age. **(B1-C4)** Dermal view **(B1-B4)** on epidermal whole mount preparations with anagen hair follicles (HF) and **(C1-C4)** on epidermal sheets with telogen HF of dorsal skin isolated from *CD4Cre R26-tdT* mice. **(D1-D4)** Top views on epidermal sheets isolated from tail skin of *CD4Cre R26-tdT* mice. **(E1-E2)** Quantification of single tdT$^+$ clones **(E1)** and mean area of single tdT$^+$ clones **(E2)** on epidermal sheets isolated from tail skin of *CD4Cre R26-tdT* mice (for details regarding the measurement see chapter 4.3.6). **(E3-E4)** Representative images of cryotome sections isolated from tail skin of 22-week old **(E3)** and 88-week-old **(E4)** *CD4Cre R26-tdT* mice. Naïve tdTomato signal was visualised in red. Nuclei in C1-D4, E3, E4 were visualised with DAPI stainng (blue). Red arrowheads: tdT$^+$ HF/epidermal patches; red, dotted circles: lots of tdT$^+$ HF/epidermal patches. Scale bars: 1 mm in **B1-B4**; 200 µm in **C1-C4, D1-D4**. Abbreviations: A: anagen, C: catagen, T: telogen. For details regarding the mice see Table 17.

Flow cytometric quantification of tdT$^+$ cells in epidermal isolates from the dorsal telogen skin of young (5, 9 weeks old; 2nd hair cycle), adult (21, 22 weeks old; 4th hair cycle) and old (55,

59 weeks old; approx. 9th hair cycle) *CD4Cre R26-tdT* mice (Figure 40 A) substantiate the findings of the microscopic examination (Figure 40).

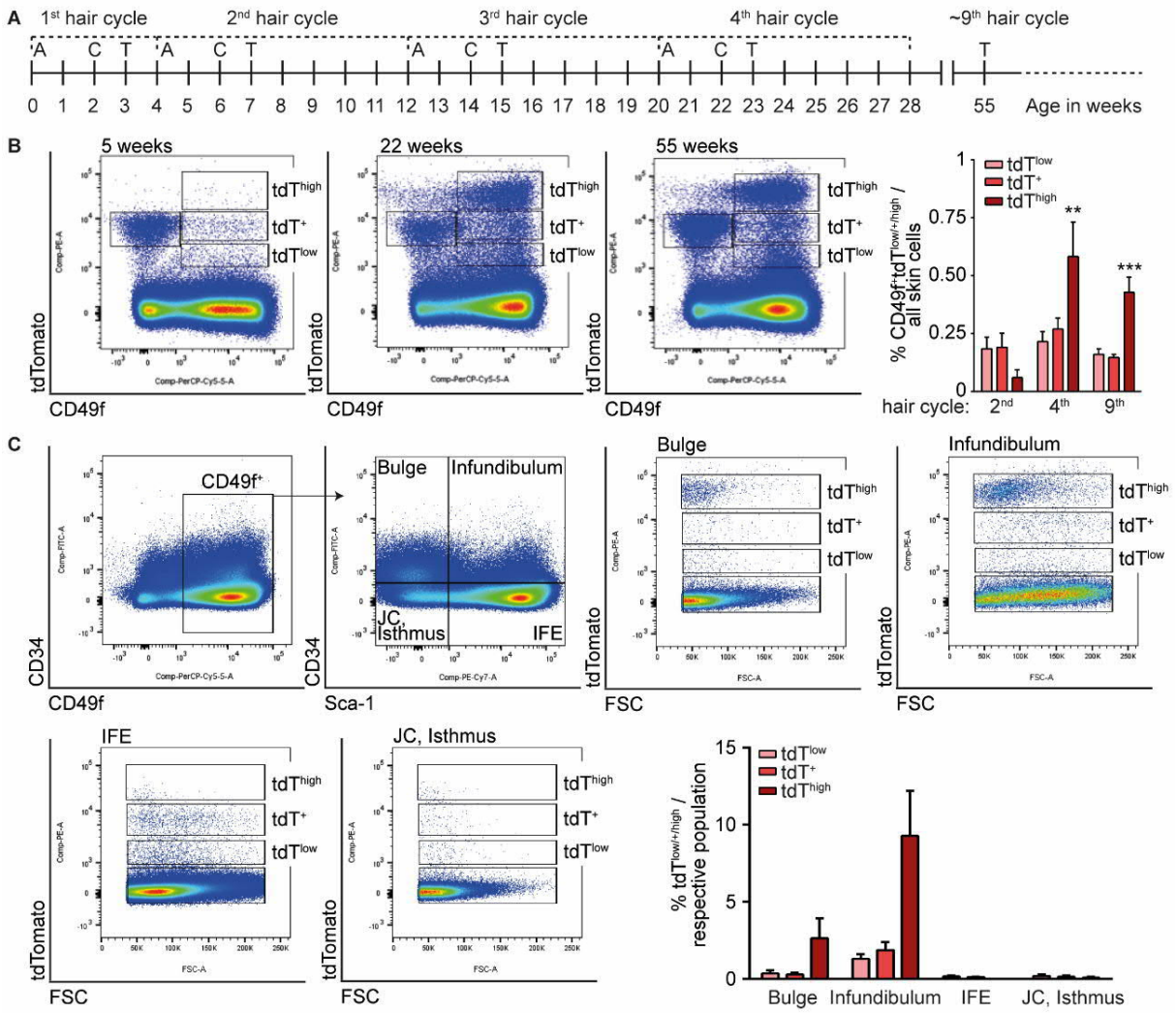

Figure 40. The quantity of bulge and infundibulum cells that descent from *CD4Cre*-targeted cells increases during ageing.

(A) Schematic representation of the murine hair cycle phases in relation to the mouse age. **(B)** Flow cytometric analyses of 2,500,000 cells from *CD4Cre R26-tdT* dorsal skin (5, 22 and 55 weeks old). tdT/CD49f plots for visualisation of CD49f and tdT expression on living skin cells (not shown). Three different CD49f$^+$tdT-expressing populations were distinguishable (tdT^{low}, tdT$^+$, tdT^{high}). Right panel: Quantification of CD49f$^+$tdT^{low}/tdT$^+$/tdT^{high} cells during the 2nd, 4th and 9th hair cycle phase, respectively. Significance was tested by the Holm-Sidak method (* $P < 0.05$, ** $P < 0.01$, *** $P < 0.001$). **(C)** Flow cytometric analyses of 2,500,000 cells from *CD4Cre R26-tdT* dorsal skin (55 weeks old). Upper left panels: CD34/CD49f plot for gating CD49f$^+$ cells and CD34/Sca-1 plot to distinguish bulge (CD34$^+$Sca-1^{neg}), infundibulum (CD34$^+$Sca-1$^+$), IFE (CD34^{neg}Sca-1$^+$) and JC, isthmus (CD34^{neg}Sca-1^{neg}) cells. tdT/FSC plot for bulge, infundibulum, IFE and JC, isthmus cells for visualisation of the three tdT-expressing populations (tdT^{low}, tdT$^+$, tdT^{high}). Lower right panel: Quantification of tdT^{low}/tdT$^+$/tdT^{high} cells in bulge, infundibulum, IFE and JC, isthmus cell populations. Abbreviations: A: anagen, C: catagen, IFE: interfollicular epidermis, JC: junctional zone, T: telogen. For details regarding the mice see Table 17.

In detail, the quantification of CD49f-expressing tdT^{low}, tdT$^+$ and tdT^{high} cells of the different aged mice (Figure 40 B) revealed that regardless of the age of the mice or the number of the hair cycle phase the cell number of the tdT^{low} and the tdT$^+$ population do not change (each approx. 0.2% of all skin cells) (Figure 40 B). However, previous analyses of dorsal skin isolates

showed that the tdT$^+$ fraction mainly consists of immune cells (Figure 24) and although the tdT^{low} population comprises predominantly non-haematopoietic (Figure 24) IFE (CD49f$^+$CD34^{neg}Sca-1$^+$) cells, it contains only few HF-associated (bulge, uHF) cells (Figure 25). In contrast to the tdT^{low} and tdT$^+$ cells, the quantity of tdT^{high} cells increases significantly from ~0.05% in the 2nd hair cycle phase to ~0.5% in the 4th and 9th hair cycle phase (Figure 40 B). In light of the result that the tdT^{high} population consists mainly of non-haematopoietic (Figure 24), bulge (CD49f$^+$CD34$^+$Sca-1^{neg}) and infundibulum (CD49f$^+$CD34$^+$Sca-1$^+$) cells (Figure 25) these data indicate that with increasing mouse age an increasing number of bulge and infundibulum cells represent descendants from *CD4Cre*-expressing cells. In fact, flow cytometric discrimination of HF bulge (CD49f$^+$CD34$^+$Sca-1^{neg}), infundibulum (CD49f$^+$CD34$^+$Sca-1$^+$), IFE (CD49f$^+$CD34^{neg}Sca-1$^+$) and uHF (CD49f$^+$CD34^{neg}Sca-1^{neg}) cells in the 9th hair cycle phase revealed that the numbers of tdT^{high} bulge (~2.6%) and tdT^{high} infundibulum cells (~9.3%) were much higher compared to the respective tdT^{low} (approx. 0.4% and 1.3%) and tdT$^+$ counterparts (approx. 0.3% and 1.9%) as well as to the tdT-expressing IFE, JC and isthmus cells (< 0.5%) (Figure 40 C). Although the overall proportion of the CD49f$^+$ tdT-expressing cells in the epidermis is small (~0.7%), these data demonstrate that a non-negligible proportion of bulge (~2.6%) and infundibulum (~9.3%) cells descent from *CD4Cre*-targeted cells in aged mice.

5.2.7 Rare keratinocytes of the murine anagen skin express CD4

The knowledge about the identity of CD4$^+$ cells, which may represent the origin of all epidermal cell types as well as of BCC, may help on the one hand to use these cells for clinical applications (e.g. skin recovery) and on the other hand to refine the understanding of BCC development and thus the establishment of targeted therapies against BCC. So far, the results described in this work suggest that either cells of the basal layer of the IFE including the infundibulum and/or HF SC compartment express CD4 under certain circumstances or that CD4$^+$ stromal cells (BM-derived MSC or skin-resident fibroblasts, see chapter 5.1) can (trans-) differentiate into epidermal cells. Noteworthy, the first possibility indeed is highly probable since in the murine skin CD4$^+$ cells exist that possess the CD49f$^+$CD34$^+$Sca-1$^+$ infundibulum expression profile described in this work [193]. To verify the existence of CD4$^+$ CD49f$^+$CD34$^+$Sca-1$^+$ epidermal cells and to extend the analysis to different hair cycle phases, the CD4 expression of epidermal isolates from dorsal anagen or telogen skin of wild type and *CD4* KO mice were analysed for their CD4, CD49f, CD34 and Sca-1 surface expression by flow cytometric analyses (see chapter 5.2.1). However, initially the *Cd4* deficiency of *CD4* KO mice (for details regarding the mouse strain see chapter 3.10.2.5) was verified by analysing the CD4 and CD8 expression of *CD4* KO thymocytes by flow cytometry. As expected and in

contrast to wild type control mice (Figure 41 A) *CD4* KO thymi neither contain $CD4^+CD8^+$ nor $CD4^+$ T-lymphocytes (Figure 41 B, C).

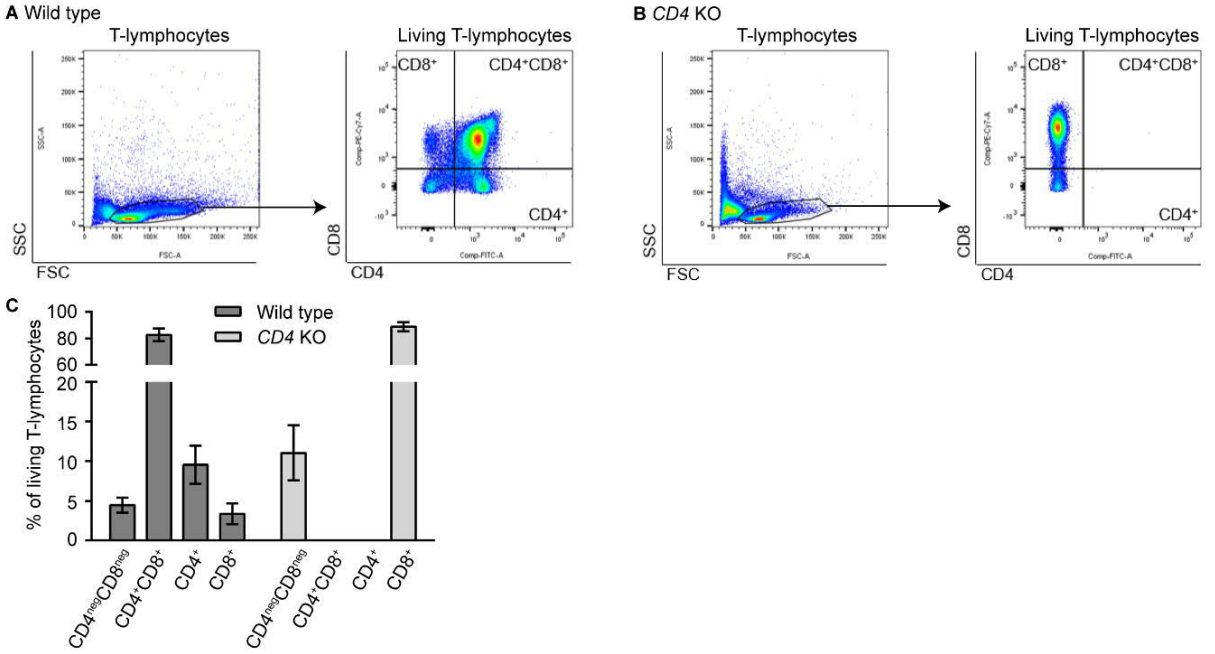

Figure 41. Flow cytometric verification of the *Cd4* deficiency in T-lymphocytes of *CD4* knockout mice.

(A-B) Flow cytometric analyses of 100,000 cells from thymi of wild type **(A)** and *CD4* knockout (KO) **(B)** mice. Left panels: SSC/FSC plots for gating living cells. Right panel: CD4/CD8 plot for visualisation of CD4 and CD8 expression of living T-lymphocytes. **(C)** Quantification of the T-lymphocyte populations: double negative ($CD4^{neg}CD8^{neg}$), double positive ($CD4^+CD8^+$) and single positive ($CD4^+$ and $CD8^+$) cells of thymi of wild type and *CD4* KO mice. For details regarding the mice see Table 17.

Next, the existence and the age- and hair cycle phase-dependent occurrence of $CD4^+$ epidermal cells were investigated. For this purpose, the CD4, CD49f, CD34 and Sca-1 expression profile of epidermal isolates from the dorsal **anagen** skin of 5-week-old (2^{nd} hair cycle phase) and 14-week-old (3^{rd} hair cycle phase) wild type mice and from dorsal **telogen** skin of 3-week-old (1^{st} hair cycle phase), 11-week-old (2^{nd} hair cycle phase), 18-week-old (3^{rd} hair cycle phase), 30-week-old (5^{th} hair cycle phase) and 56-week-old (9^{th} hair cycle phase) wild type mice were determined by flow cytometry (Figure 42 A). Epidermal isolates from the dorsal **anagen** skin of 5-week-old (2^{nd} hair cycle phase) *CD4* KO mice and from dorsal **telogen** skin of 31-week-old (5^{th} hair cycle phase) *CD4* KO mice served as controls. Then, bulge ($CD49f^+CD34^+Sca\text{-}1^{neg}$), IFE ($CD49f^+CD34^{neg}Sca\text{-}1^+$), infundibulum ($CD49f^+CD34^+Sca\text{-}1^+$) and uHF JC/isthmus cells ($CD49f^+CD34^{neg}Sca\text{-}1^{neg}$) were gated (Figure 42 B) [78, 228] (this work, Figure 25 and chapter 5.2.2). This analysis revealed that the cellular compositions of the epidermal isolates from wild type and *CD4* KO mice are similar and reflect described literature values [228]. Thus, the $CD49f^+$ population of wild type and *CD4* KO mice consist of ~75 and 77% IFE, ~17 and 17% JC/isthmus, ~4 and 4% bulge and ~3 and 1% $CD49f^+CD34^+Sca\text{-}1^+$ infundibulum cells in anagen and telogen phase, respectively (Figure 42 C). Next, the putative CD4 surface expression of the respective wild type and *CD4* KO epidermal populations were

analysed via CD4 expression histogram plots (Figure 42 D-G). Background clean-up for each measurement was performed by calculating the number of $CD4^+$ cells of wild type epidermal isolates in comparison to that of *CD4* KO mice (set to 0) (Figure 42 H-K).

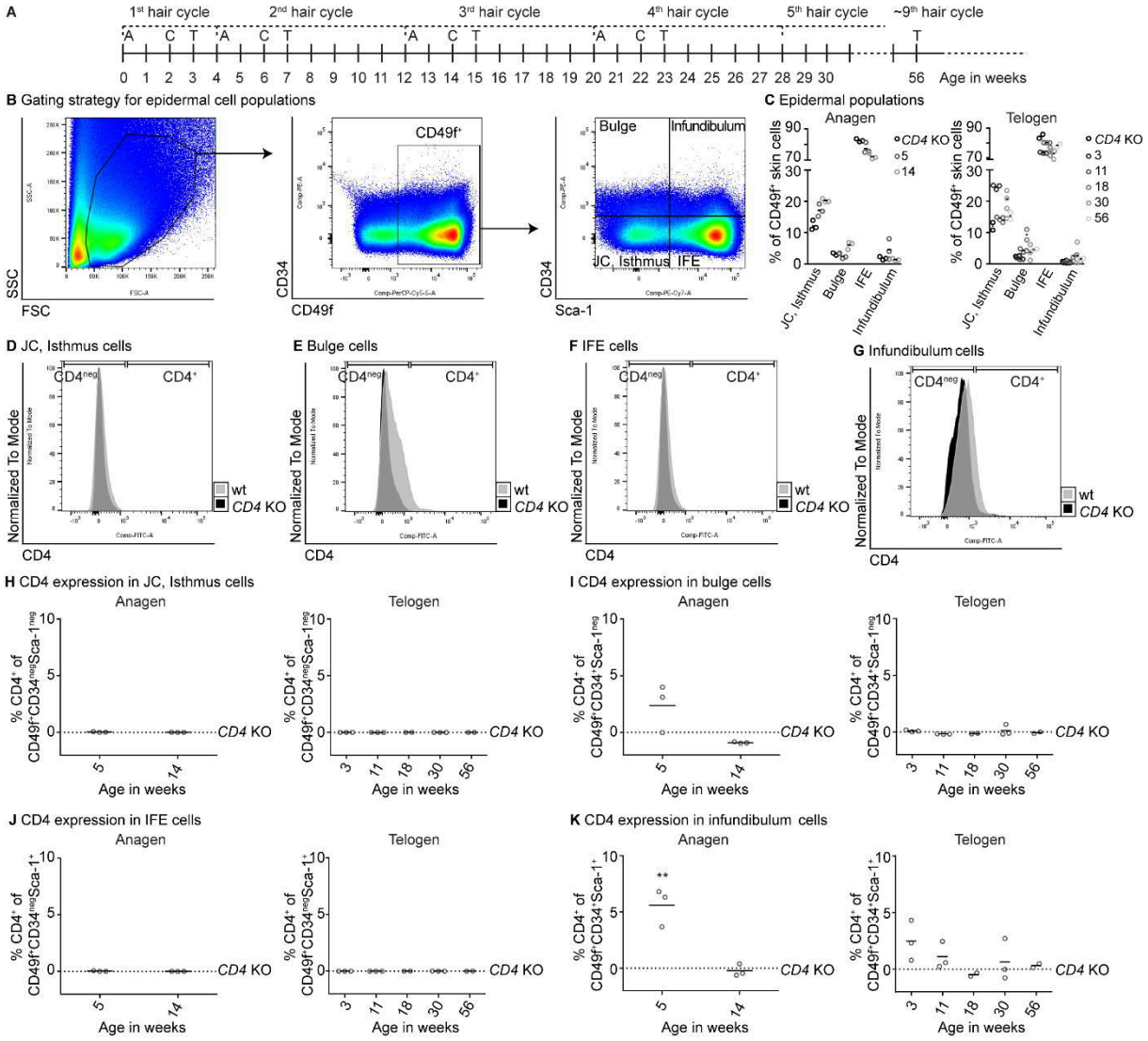

Figure 42. Infundibulum cells of anagen hair follicles express CD4 exclusively in 5-week-old mice.

(A) Schematic representation of the murine hair cycle phases in relation to the mouse age. **(B-K)** Flow cytometric analyses of 2,500,000 cells from wild type and *CD4* knockout (KO) dorsal skin. **(B)** Left panel: SSC/FSC plot for gating living skin cells. Middle panels: CD34/CD49f plot for visualisation of CD49f expression on the gated living skin cells and CD34/Sca-1 plot to distinguish $CD34^{neg}Sca\text{-}1^{neg}$ (JC, Isthmus), $CD34^{+}Sca\text{-}1^{neg}$ (bulge), $CD34^{neg}Sca\text{-}1^{+}$ (IFE) and $CD34^{+}Sca\text{-}1^{+}$ (infundibulum) cells. **(C)** Quantification of epidermal populations in anagen and telogen wild type and *CD4* KO dorsal skin. **(D-G)** Histogram for visualisation of CD4 expression of JC, Isthmus **(D)**, bulge **(E)**, IFE **(F)** and infundibulum **(G)** cells from wild type and *CD4* KO dorsal skin (5 weeks old). **(H-K)** Quantification of $CD4^+$ cells of JC, Isthmus **(H)**, bulge **(I)**, IFE **(J)** and infundibulum **(K)** cells in anagen and telogen dorsal skin. The background fluorescence signal for CD4 that was detected in *CD4* KO mice was subtracted from the values for the wild type mice. Significance was tested by the Holm-Sidak method (** $P < 0.01$). Abbreviations: A: anagen, C: catagen, JC: junctional zone, IFE: interfollicular epidermis, T: telogen, wt: wild type. For details regarding the mice see Table 17.

The analysis showed that independent of the hair cycle phase neither JC/isthmus (Figure 42 D, H) nor IFE populations (Figure 42 F, J) of wild type mice contain $CD4^+$ cells. In contrast,

CD4$^+$ bulge (Figure 42 E, I) and CD4$^+$ infundibulum cells (Figure 42 G, K) were detected in two of three biological replicates or in all three replicates of anagen epidermal isolates from 5-week-old wild type mice, respectively. However, only the expression level of CD4$^+$ infundibulum cells reached significance (Figure 42 K). Bulge and infundibulum cells of anagen skin from 14-week-old wild type mice and bulge cells of telogen wild type skin never contain CD4$^+$ cells (Figure 42 E, G, I, K), whereas in epidermal isolates from telogen skin of very young mice (3 and 11 weeks old) a moderate increase of CD4$^+$ cells in the infundibulum population was observed (Figure 42 K).

To exclude a haematopoietic identity of the CD4$^+$ cells of anagen HF, epidermal isolates from anagen dorsal skin of a 5-week-old wild type mouse were stained against the general immune cell marker CD45 and analysed by flow cytometry. This approach revealed that the CD4^{neg} population contains ~3.6% CD45$^+$ immune cells (Figure 43). Besides, also a minor fraction of CD4$^+$ cells express CD45 (~9.3%) (Figure 43). However, in the anagen dorsal skin of 5-week-old wild type mice ~0.05% CD4$^+$CD45$^+$ haematopoietic and ~0.4% non-haematopoietic CD4$^+$CD45^{neg} epidermal cells exist.

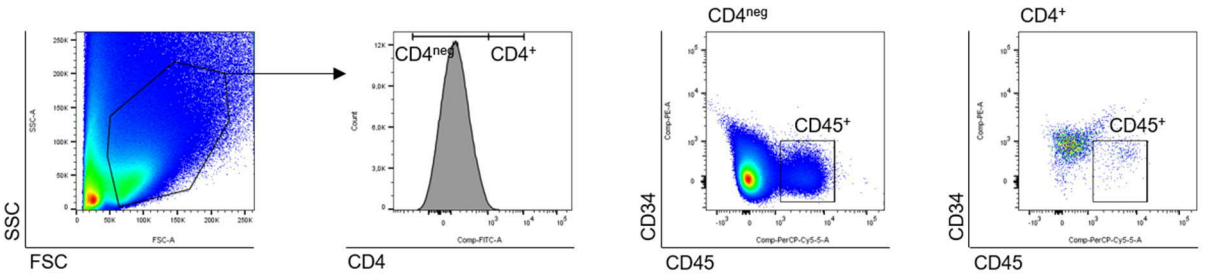

Figure 43. The major fraction of CD4$^+$ cells in anagen dorsal skin represents non-haematopoietic cells.

Flow cytometric analysis of 2,500,000 cells from anagen wild type dorsal skin (5 weeks old). Left panel: SSC/FSC plot for gating living skin cells; middle left panel: histogram for visualisation of CD4 expression of living skin cells; right panels: CD45/CD34 plots to visualise CD45 expression in CD4^{neg} and CD4$^+$ cells.

Beyond that, the CD4 expression of uHF JC/isthmus, bulge, IFE and infundibulum cells was investigated by a second approach. For this purpose, immunofluorescent stainings of cytospun uHF JC/isthmus (CD49f$^+$CD34^{neg}Sca-1^{neg}), bulge (CD49f$^+$CD34$^+$Sca-1^{neg}), IFE (CD49f$^+$CD34^{neg}Sca-1$^+$) and infundibulum (CD49f$^+$CD34$^+$Sca-1$^+$) FACS-isolated cells from anagen dorsal skin of 5-week-old wild type mice were performed (for FACS-based isolation see chapter 4.5.1). Cells of JC/isthmus, bulge or IFE populations of the same skin isolates did not stain positive for CD4 expression although a slight, incomplete (not enclosing the entire cell) signal was visible for some IFE cells (Figure 44 A). Contrary to this, several cells of the CD49f$^+$CD34$^+$Sca-1$^+$ infundibulum population show a complete (enclosing the entire cell) CD4 antibody staining (Figure 44 A). Moreover, the CD49f$^+$CD34$^+$Sca-1$^+$ infundibulum population contains CD4$^+$K5$^+$ basal keratinocytes and CD4^{neg}K5$^+$ basal keratinocytes as well as small amounts of CD4$^+$K5^{neg} epidermal cells that might be suprabasal keratinocytes or

haematopoietic cells (Figure 44 B). Control stainings of infundibulum cells isolated from anagen dorsal skin of 5-week-old *CD4* KO mice (Figure 44 B) never showed CD4 expression.

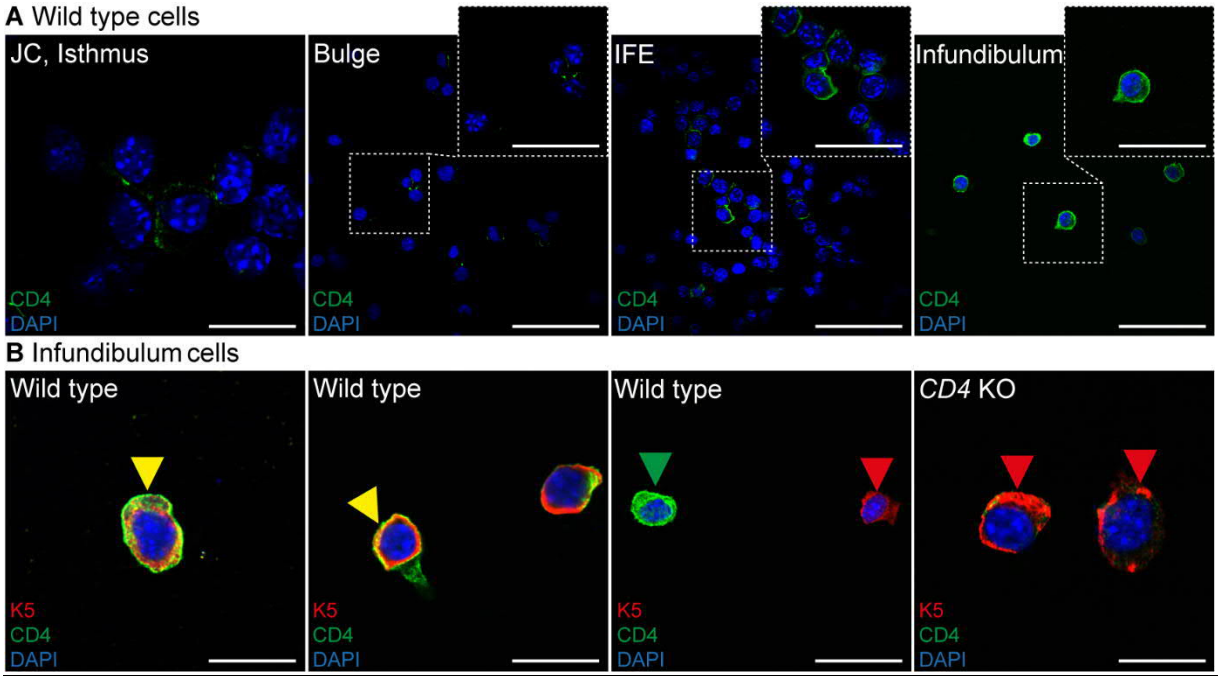

Figure 44. Infundibulum cells of anagen hair follicles express CD4 and K5.

(A) Representative images of antibody stainings against CD4 on cytospun CD49f$^+$CD34^{neg}Sca-1^{neg} (JC, Isthmus), CD49f$^+$CD34$^+$Sca-1^{neg} (bulge), CD49f$^+$CD34^{neg}Sca-1$^+$ (IFE) and CD49f$^+$CD34$^+$Sca-1$^+$ (infundibulum) FACS-isolated cells (see chapter 4.5.1) of anagen wild type dorsal skin (5 weeks old). **(B)** Representative images of antibody stainings against the basal keratinocyte marker K5 and CD4 on cytospun infundibulum FACS-isolated cells (see chapter 4.5.1) of anagen wild type and *CD4* knockout (KO) dorsal skin (5 weeks old). Nuclei were visualised with DAPI in **A, B**. Red arrowheads: K5$^+$ cells; green arrowhead: CD4$^+$ cell; yellow arrowheads: double positive cells. Scale bars: 33 µm in **A** (Bulge, IFE, infundibulum); 20 µm in **A** (close-ups); 10 µm in **A** (JC, Isthmus), **B**. For details regarding the mice and antibody staining, see Table 17 and Table 13, respectively.

5.2.8 CD4$^+$ keratinocytes of the anagen dorsal skin grow in the infundibulum

So far, the results of this work strongly hint toward the assumption that K5$^+$ infundibulum cells of the anagen HF can express the CD4 protein and thus represent *CD4Cre*-expressing ancestors of tdT$^+$ keratinocytes in *CD4Cre R26-tdT* skin and of BCC of *Ptch$^{fl/fl}$ CD4Cre* mice. To finally unravel the cellular identity of CD4$^+$ CD49f$^+$CD34$^+$Sca-1$^+$ K5$^+$ cells, a scRNA-Seq analysis of epidermal isolates from 5-week-old wild type mice was performed (see chapter 4.7.6). Since clustering of different populations is an initial and essential step in scRNA-Seq data evaluation the knowledge about the isolated compartments is crucial. However, so far it was not determined whether all cells of late anagen HF compartments (e.g. uHF, bulge, lower HF and bulb) are efficiently isolated by using the thermolysin method (see chapter 4.4.1.1). Thus, H&E stainings of paraffin sections of untreated anagen dorsal skin and of anagen dorsal skin after thermolysin treatment were compared (Figure 45 A, B). This revealed that the thermolysin method for isolation of dorsal epidermal cells completely removes the IFE and uHF of anagen HF, whereas lower HF compartments remain in the dermis (Figure 45 A, B). Indeed,

immunofluorescent stainings against the basal IFE and HF ORS marker K5 and the bulge cell marker K15 confirmed the absence of $K5^+$ IFE and uHF cells after thermolysin treatment (Figure 45 C-D') but also showed that the dermis of thermolysin-treated skin still contains $K5^+K15^+$ cells of the HF, which most likely represent bulge cells (Figure 45 D, D'). Moreover, stainings against the HF ORS marker K17 and the HF IRS marker TCHH clearly demonstrated that ORS and IRS cells of the lower HF remain in the skin after thermolysin treatment (Figure 45 E-F'). Thus, the thermolysin method is suitable for isolation of IFE, uHF and partially bulge cells from anagen dorsal skin, whereas HF cells of the lower HF and bulb are not efficiently prepared with this technique.

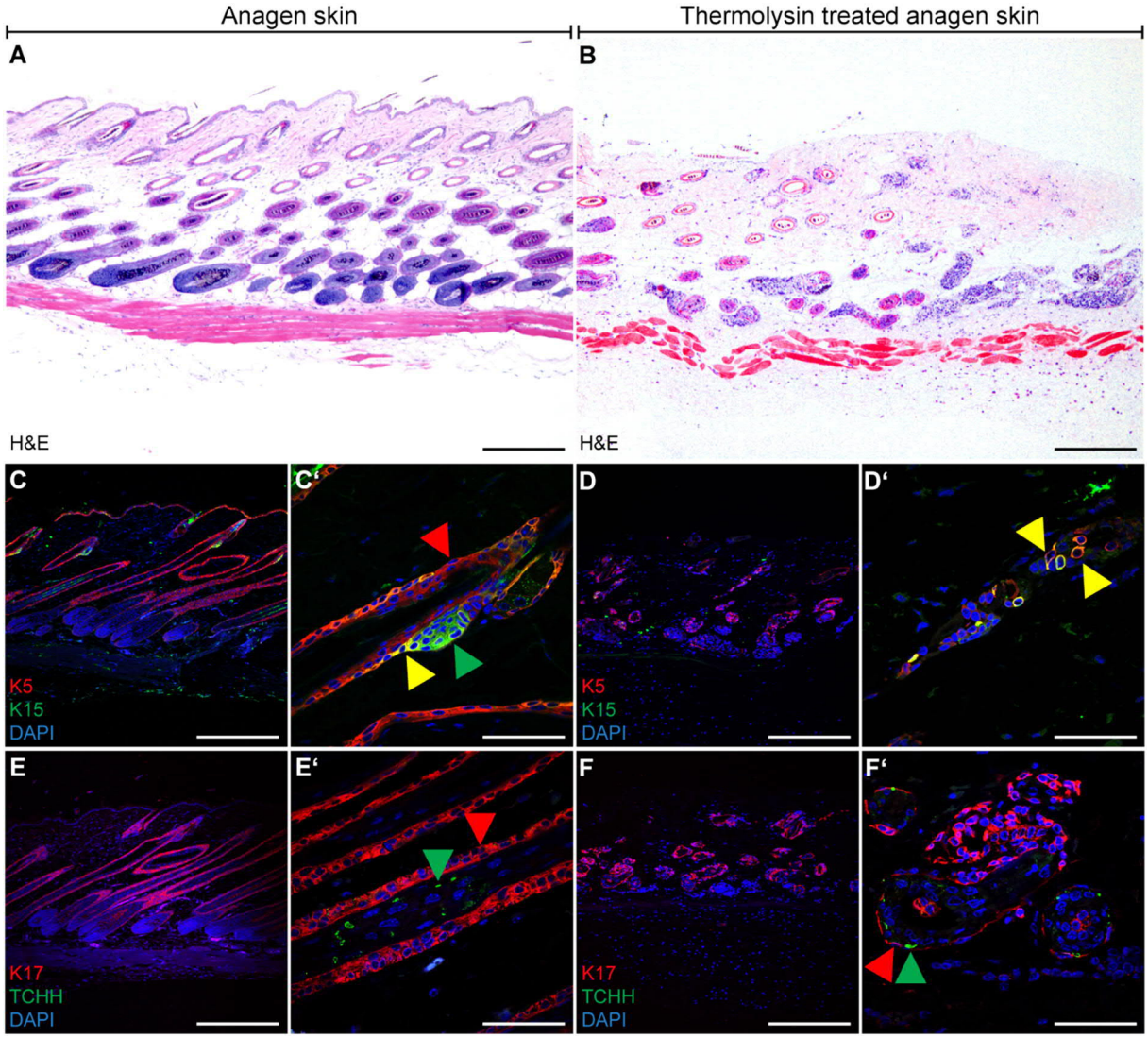

Figure 45. Thermolysin method for isolation of epidermal cells from anagen skin results in the isolation of mainly cells of the interfollicular epidermis and the upper hair follicle.

(A-F') Representative images of haematoxylin and eosin (H&E) staining **(A, B)** and antibody stainings against the outer root sheath (ORS) and basal interfollicular epidermis marker K5 **(C-D')**, the HF bulge marker K15 **(C-D')**, the ORS marker K17 **(E-F')** and the inner root sheath marker TCHH **(E-F')** on paraffin sections of anagen and thermolysin treated anagen wild type dorsal skin (5 weeks old). Nuclei were visualised with DAPI. Red arrowheads: $K5^+$ **(C')** or $K17^+$ **(E', F')** cells; green arrowheads: $K15^+$ **(C')** or $TCHH^+$ **(E', F')** cells; yellow arrowheads: double positive cells. Scale bars: 250 µm in **A, B**; 200 µm in **C, D, E, F**; 33 µm in **C', D', E', F'**. For details regarding the mice and antibody staining, see Table 17 and Table 13, respectively.

Indeed, this result was also reflected by the data obtained from the scRNA-Seq of epidermal isolates from anagen dorsal skin since clustering based on key markers revealed that mainly IFE, uHF and bulge cells were sequenced (Table 25). Seven different epidermal, non-haematopoietic populations were distinguishable: basal cycling IFE cells, basal Bhlhe40^{+} IFE cells, basal IFE cells, suprabasal IFE cells, uHF suprabasal cells, HF ORS basal cells and HF bulge cells [11] (Table 25). Thereby, most of the sequenced cells (60%) represent basal and suprabasal IFE cells those major proportion belongs to the basal IFE cell population (~43%) and only a minor proportion of the cells (4%) were identified as HF-associated (e.g. uHF, ORS and bulge) (Table 25). Additionally, the haematopoietic cell populations: T-lymphocytes, macrophages and Langerhans cells as well as dermal fibroblasts and vascular cells and epidermal melanocytes were determined (Table 25).

Table 25. List of epidermal and non-epidermal populations with their key markers that were identified in single-cell transcriptome sequencing of epidermal isolates from dorsal anagen skin of wild type mice.

The key markers of the different populations and the number of cells and the percentage share of the respective population are given. References for the respective key markers are given in the last column.

Population name	Marker	# of cells	%	References
IFE basal cycling	*Ccnb1*$^{+}$ *Cdk1*$^{+}$	727	5	[76]
IFE basal Bhlhe40+	*Bhlhe40*$^{+}$*Thbs1*$^{+}$*Avpi1*^{high}*K16*$^{+}$	728	5	[11]
IFE basal	*K14*^{high}*Ly6a*$^{+}$*Ptprc*^{neg}*Vim*^{neg}	5735	43	/
IFE suprabasal	*K10*^{high}*Kdap*$^{+}$*K79*^{neg}*Cst6*^{low}	1204	9	[11]
uHF suprabasal	*K79*$^{+}$*Cst6*^{high}	216	2	[11]
HF ORS basal	*Il11ra1*$^{+}$*Sfrp1*$^{+}$	138	1	[76]
HF bulge	*Postn*$^{+}$*PDGFR*α^{neg}*Vim*^{neg} *CD34*$^{+}$*PDGFR*α^{neg}*Vim*^{neg}	120	1	/
Fibroblasts	*Lum*$^{+}$ *PDGFR*α^{+} *Vim*$^{+}$*Ptprc*^{neg}	93	1	/
Vascular cells	*Cldn5*$^{+}$ *Fabp4*$^{+}$	108	1	[76]
Melanocytes	*Dct*$^{+}$	151	1	[76]
T-lymphocytes	*Cd3*ε^{+}	645	5	/
Macrophages	*C1qa*$^{+}$ *Ccl6*$^{+}$	97	1	[76]
Langerhans Cells	*Cd207*$^{+}$ *H2-M2*$^{+}$	62	< 1	[76]

An uniform manifold approximation and projection plot was used to visualise the global structure and distances of the cellular populations since this method tends to preserve the continuity of cell states and thus is appropriate to analyse and distinguish differentiation stages [257]. In this plot the basal IFE cell populations cluster at the top, suprabasal IFE and uHF

cells in the middle and basal HF ORS and HF bulge cells at the bottom (Figure 46 A). The haematopoietic, dermal and melanocyte populations cluster separately according to their transcriptional profile (Figure 46 A). Moreover, a clustered heatmap for visualisation of the global gene expression of all clustered populations confirmed the generally different expression profiles of the epidermal non-haematopoietic populations and the haematopoietic, dermal and melanocyte populations (Figure 46 B). Besides, it also revealed similarities within the groups, for instance HF bulge and basal HF ORS cells cluster together confirming their similar gene expression pattern (Figure 46 B). Remarkably, *Cd4* expression was only detected in the clusters of T-lymphocytes and Langerhans cells as well as in the epidermal population 'IFE basal cycling' (Figure 46 C), which can be differentiated from other epidermal populations by its high expression of proliferation marker (e.g. *Mki67*, *Budding uninhibited by benzimidazoles 1)*, Cdc proteins (e.g. *Cdc20*, *Cdc25c*, *Cdca8*) and Ccn proteins (e.g. *Ccna2*, *Ccnb1*, *Ccnb2*) (Figure 46 D).

These results excellently substantiate the findings from the flow cytometry (Figure 42) and antibody-stained cytospins (Figure 44) that hint towards the existence of $CD4^+$ basal ($K5^+$) infundibulum ($CD49f^+CD34^+Sca\text{-}1^+$) cells in the dorsal anagen skin. However, to proof the existence and localisation of 'basal cycling IFE' cells in dorsal anagen skin immunofluorescent stainings against the proliferation marker MKI67 and the basal IFE and HF ORS marker K5 were conducted (Figure 47 A-D). This approach showed that apart from individual $K5^+MKI67^+$ cells in the basal layer of the IFE (Figure 47 B) also a large number of $K5^+MKI67^+$ cells are located in the infundibulum of anagen HF (Figure 47 C). Beyond that, also the bulb of the lower anagen HF consists of high numbers of proliferative active matrix cells (Figure 47 D) which however do not express K5 (Figure 47 D) and which are only rarely isolated by the thermolysin method (Figure 45). Thus, most probably the infundibulum, but not the matrix cell compartment, represents the morphological niche of 'basal cycling IFE' cells.

Remarkably, $CD49f^+CD34^+Sca\text{-}1^+$ epidermal cells possess an infundibulum expression profile, are $K5^+$ and can express CD4. 'Basal cycling IFE' cells also can express *Cd4*, are characterised by their expression of K5 and proliferation markers, like MKI67, and are most properly located in the infundibulum[3]. Thus, it can be assumed that $CD49f^+CD34^+Sca\text{-}1^+$ and 'basal cycling IFE' cells are identical and grow as infundibulum cells. However, at the first glance the expression of the bulge marker CD34 does not support this conclusion. However, the fact that infundibulum cells also can express the HF bulge marker *Postn* [11] hints towards the possibility that they also express other bulge marker like CD34/*Cd34*.

[3] Although single $CD4^+tdT^+$ cells and numerous tdT^+ cells that grew together were found in the infundibulum of dorsal skin from *CD4Cre R26-tdT* mice, there is so far no clear evidence for the existence of non-haematopoietic, epidermal $CD4^+$ cells in the infundibulum by immunofluorescence stainings of skin sections.

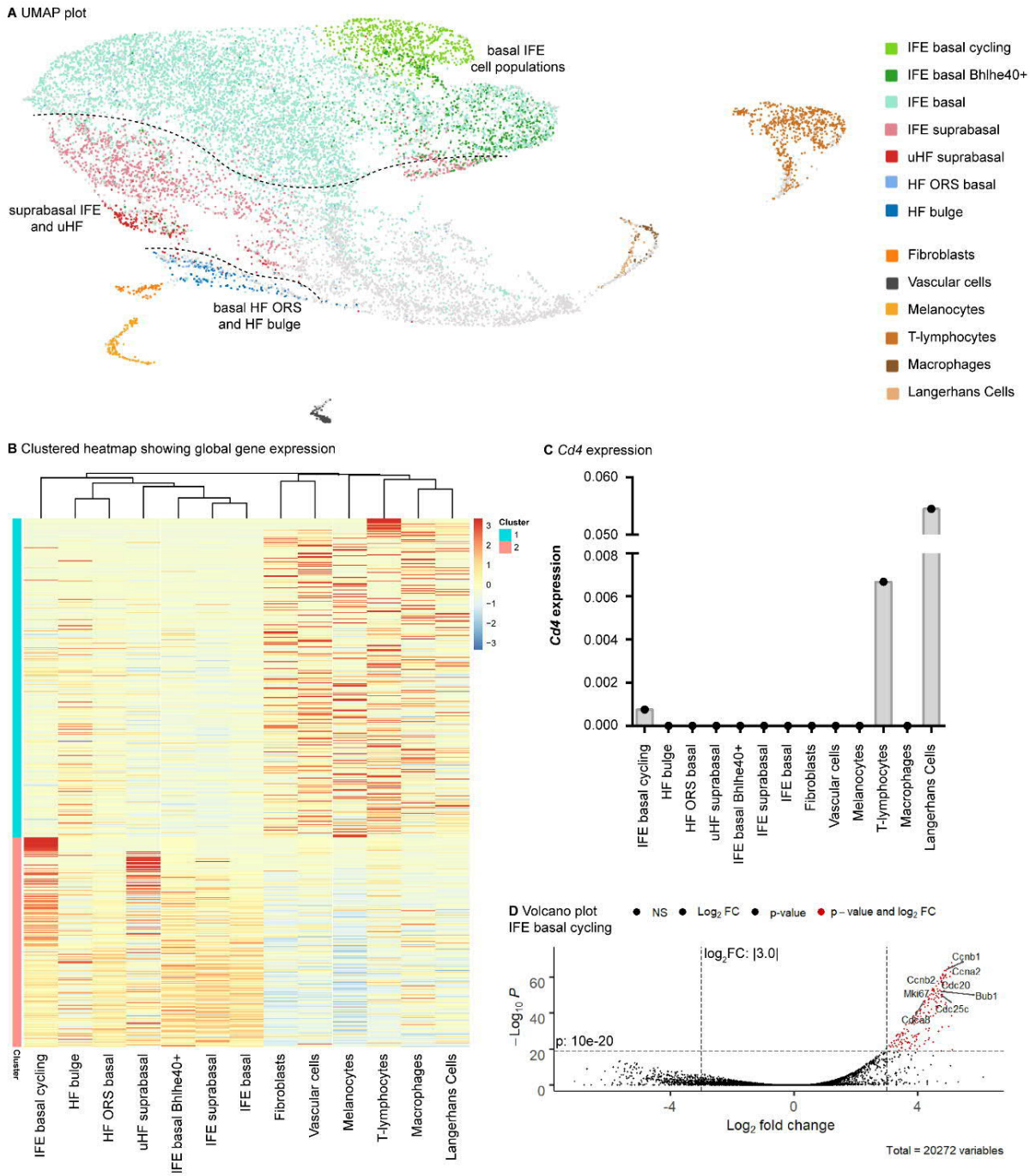

Figure 46. Single-cell transcriptome sequencing analysis of epidermal isolates from wild type mice identifies CD4⁺ basal cycling interfollicular epidermis cells.

(A-D) Transcriptome-based differential gene expression analysis of 13,397 sequenced cells of anagen wild type dorsal skin (5 weeks old). Populations were determined according to key markers shown in Table 25. Visualisation of differential gene expression with Uniform Manifold Approximation and Projection (UMAP) plot **(A)**, clustered heatmap **(B)**, quantification of *Cd4* gene expression **(C)** and volcano plot **(D)** of up-regulated genes in the interfollicular epidermis (IFE) basal cycling cell population in comparison to all other populations. Significant (p-value below 10^{-20}) up-regulated (log_2 fold change above 3) genes are marked in red. Dotted lines in **A**: differential clustering of basal IFE populations (top), suprabasal IFE populations (middle) and hair follicle (HF)-associated populations (bottom). Abbreviations: Bub1: Budding uninhibited by benzimidazoles 1, Ccn: Cyclin, Cdc: Cell division cycle, Mki67: marker of proliferation Ki-67, ORS: outer root sheath, uHF: upper HF. For details regarding the mice see Table 17.

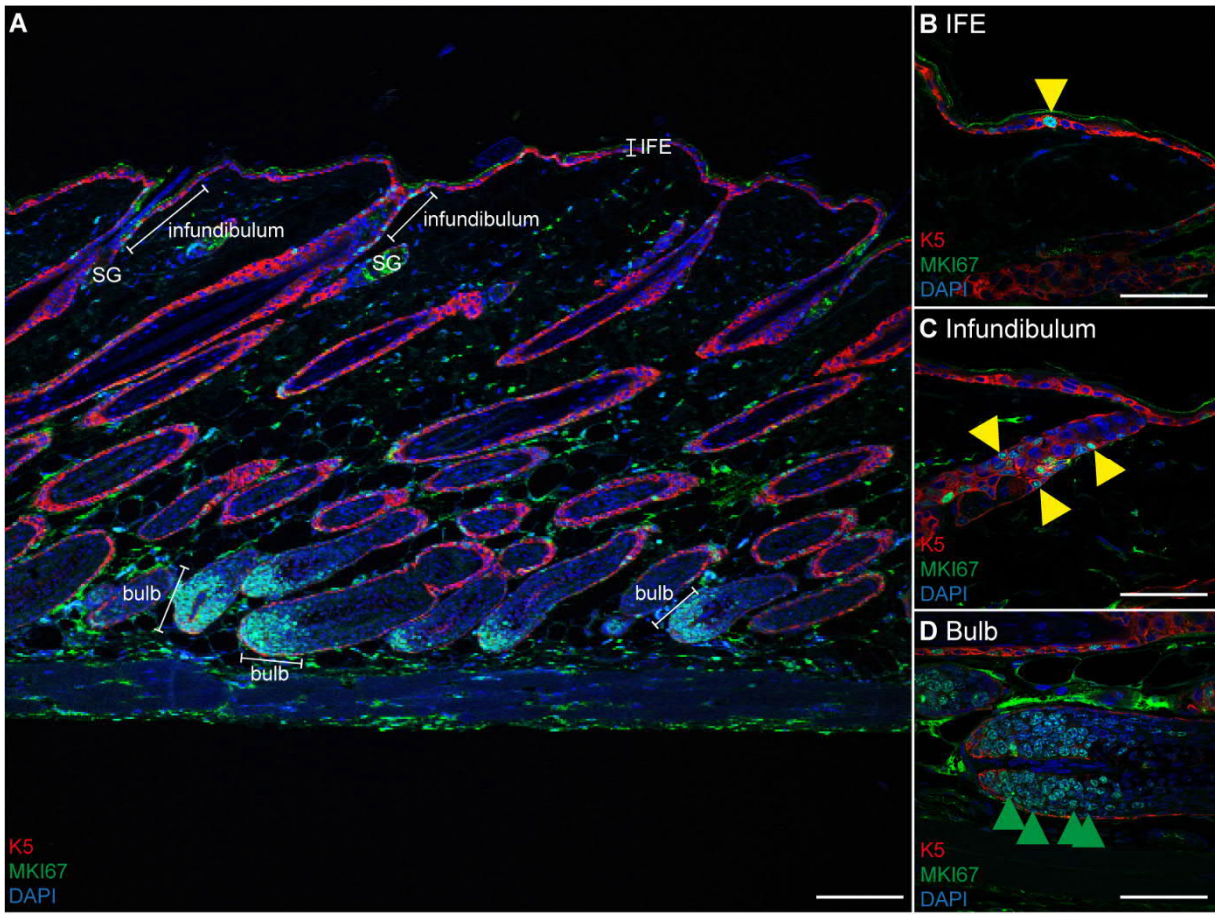

Figure 47. Proliferative active cells in the interfollicular epidermis, infundibulum and hair follicle bulb in anagen dorsal skin.

(A-D) Representative images of antibody stainings against the outer root sheath and basal interfollicular epidermis (IFE) marker K5 and the proliferation marker MKI67 on paraffin sections of anagen wild type dorsal skin (5 weeks old). Nuclei were visualised with DAPI. Yellow arrowheads: $K5^+MKI67^+$ cells; green arrowheads: $MKI67^+$ cells. Scale bars: 67 µm in **A**; 33 µm in **B, C, D**. For details regarding the mice and antibody staining, see Table 17 and Table 13, respectively.

5.2.9 *CD4Cre*-transgene expression in lineage ambiguous epidermal cells *in vitro*

Since the progeny of *CD4Cre*-targeted cells grows in the IFE and in HF, whereas non-haematopoietic $CD4^+$ ancestors were so far only found in the infundibulum they might give rise to cells of both compartments, which would be extraordinary with respect to the findings on HF SC that do not contribute to the IFE under homeostatic conditions [69, 74] and, *vice versa*, this has not been shown previously for IFE cells. In order to proof the assumption that $CD4^+$ ancestors (most likely infundibulum cells) can differentiate into both: IFE and HF-associated cells, *in vitro* studies with dorsal skin isolates from *CD4Cre R26-tdT* mice shall help to trace those cells and to determine the cellular identity of their offspring cells. However, it was initially tested whether basal IFE and/or HF bulge cells itself express the *CD4Cre* transgene during *in vitro* cultivation. Thus, it was analysed first whether epidermal cells of the dorsal skin from *CD4Cre R26-tdT* mice express the *CD4Cre* transgene *in vitro*. For this

purpose, epidermal isolates from a 19-week-old mouse were grown on collagen I-coated dishes in feeder-free culture medium (Table 10) and analysed for tdT expression and additionally their basal epidermal identity was analysed by K5 antibody staining. The rationale behind this was that the skin of young mice (< 20 weeks old) contains only low numbers of tdT^+ cells (Figure 39) and thus the probability to isolate and seed tdT^+ epidermal cells is very low. Indeed, until 26 days after seeding no tdT^+ cell was observed. However, first tdT^+ cells were detected 27 days after seeding (Figure 48 A-A2') demonstrating that these cells possess *CD4Cre* activity under *in vitro* culture conditions. However, in total only 0.15-0.8% of all basal keratinocytes (determined by morphology after 41 days culture or by K5 expression after 55 days culture) express tdT after 41 or 55 days (Figure 48 B-C') indicating that *CD4Cre* transgene expression is a relatively rare event in *in vitro* cultured epidermal cells. Since tdT^+ cells also express K5 (Figure 48 C-C') these cells represent basal keratinocytes.

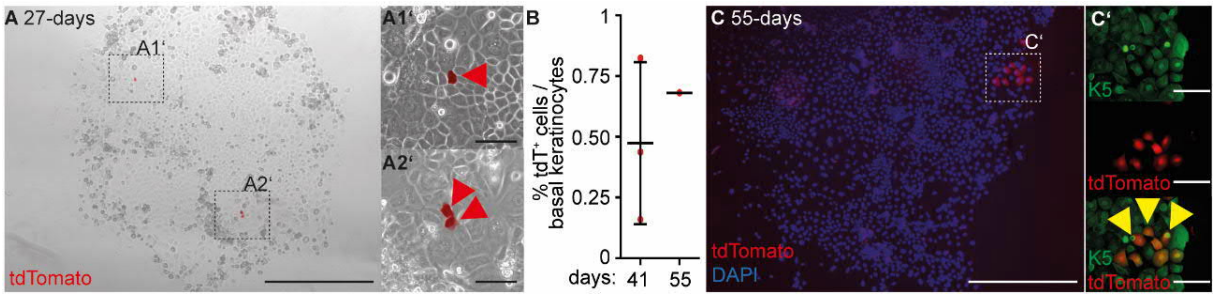

Figure 48. Basal keratinocytes can express the *CD4Cre*-transgene under *in vitro* culture conditions.

(A-C') Representative images of skin-derived cells of *CD4Cre R26-tdT* dorsal skin (19 weeks old) cultured for 27 days **(A-A2')**, 41 days **(B)** or 55 days **(B-C')** in passage 0 on collagen I-coated dishes in feeder-free culture medium (Table 10). **(B)** Quantification of the tdT^+ cells 41 and 55 days after seeding. **(C-C')** Representative images of antibody staining against the outer root sheath and basal interfollicular epidermis marker K5. Naïve tdTomato signal was visualised (red, A-A2', C-C'). Nuclei were visualised with DAPI (blue, C). Red arrowheads: tdT^+ cells; yellow arrowheads: tdT^+K5^+ cells. Scale bars: 500 µm in **A, C**; 200 µm in **A1', A2''**; 100 µm in **C'**. For details regarding the mice and antibody staining, see Table 17 and Table 13, respectively.

Next, it was analysed whether basal IFE and/or HF bulge cells can express the *CD4Cre* transgene under *in vitro* culture conditions. For this purpose, basal IFE ($CD49f^+CD34^{neg}Sca\text{-}1^+$) and HF bulge ($CD49f^+CD34^+Sca\text{-}1^{neg}$) cells of 26-week-old mice were isolated by FACS (see chapter 4.5.1) and grown on collagen I-coated dishes in feeder-free culture medium (Table 10) (Figure 49). 17 days after seeding tdT^{neg} keratinocyte colonies were grown (Figure 49 A, B). Interestingly, 21 days after seeding tdT^+ cells were firstly detected in the bulge cell culture (Figure 49 C), whereas cultured IFE cells never showed a tdT expression until 21 days after seeding (data not shown; due to the soon differentiation of cultured IFE cells it was not possible to culture them for a longer time period).

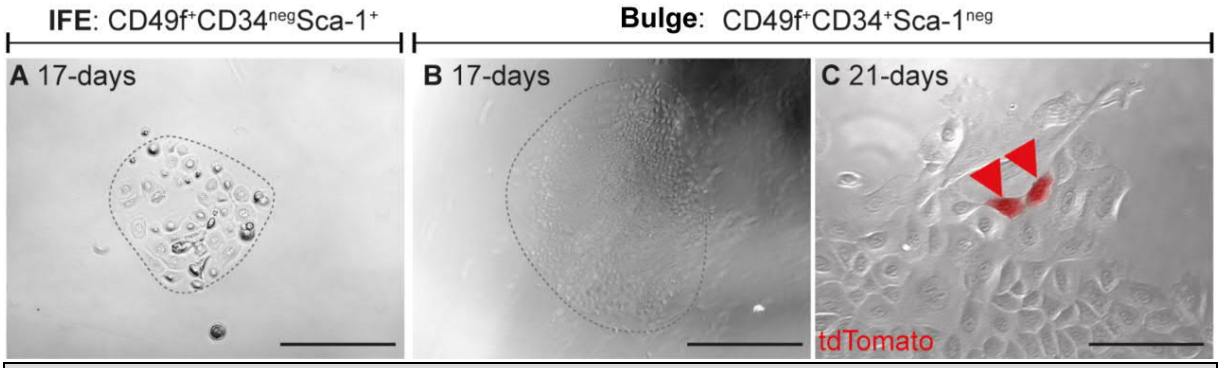

Figure 49. *CD4Cre*-mediated recombination in bulge but not in interfollicular epidermis cells under *in vitro* culture conditions.

(A-C) Representative images of FACS-isolated (for FACS-based isolation see chapter 4.5.1) IFE ($CD49f^+CD34^{neg}Sca\text{-}1^+$) **(A)** and bulge ($CD49f^+CD34^+Sca\text{-}1^{neg}$) **(B-C)** cells of *CD4Cre R26-tdT* dorsal skin (26 weeks old) cultured for 17 days **(A, B)** or 21 days **(C)** in passage 0 on collagen I coated dishes in feeder-free culture medium (Table 10). Naïve tdTomato was visualised (red, C). Red arrowheads: tdT^+ cells. Scale bars: 500 µm in **B**; 200 µm in **A**; 100 µm in **C**. For details regarding the mice see Table 17.

These data suggest that bulge cells (or their offspring) can express the *CD4Cre* transgene under *in vitro* culture conditions and thus most properly express CD4, whereas basal cells of the IFE most likely are not the origin of a *CD4Cre*-mediated recombination. However, the identity as bulge cells has not been proven during *in vitro* culture, hence the cellular identity might have changed during the cultivation (e.g. into infundibulum cells that were suggested to express *Cd4*/CD4). Indeed, similar to wounding, *in vitro* culturing of HF SC leads to downregulation of quiescent SC TF (e.g. *Nfatc1*, *Lhx2*), with the exception of *Sox9*, which is expressed at slightly lower levels *in vitro*, yet ablation of *Sox9* in adult HF SC leads to a decrease in CFE *in vitro* [258]. Antibody stainings of *in vitro* cultured dorsal skin isolates from wild type mice 6 days after seeding, revealed an expression of the HF bulge marker Sox9 and CD34 in all cells (Figure 50 A, B), but also of the basal IFE and infundibulum marker Sca-1 in some isolated cells (Figure 50 C). Co-staining against the HF ORS marker K17 and the basal IFE and infundibulum marker Sca-1 confirmed that some of the $K17^+$ cells also express Sca-1 (Figure 50 D). However, this supports the hypothesis of 'lineage infidelity' in which HF SC adopt a molecular profile that is partly HF and partly epidermal after wounding and/or culturing [80, 258]. Noteworthy, basal cells of the infundibulum show *in vivo* in addition to the IFE signature also expression of low levels of uHF markers, bulge marker and pan-HF marker [11], therefore *in vitro* cultured skin isolates may reflect in parts infundibulum cells. Moreover, both *in vitro* cultured skin isolates and infundibulum cells show expression of the *CD4Cre* transgene and *Cd4*/CD4, respectively.

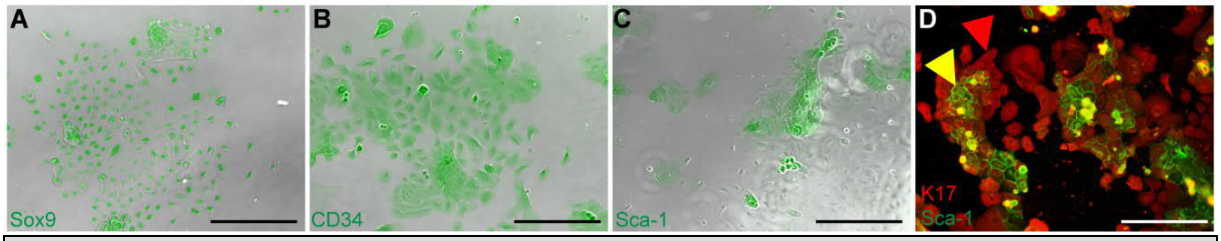

Figure 50. Cultivation of dorsal skin isolates leads to growth of lineage ambiguous epidermal cells.

(A-D) Representative images of antibody stainings against the hair follicle (HF) bulge marker Sox9 **(A)** and CD34 **(B)**, the basal interfollicular epidermis (IFE) marker Sca-1 **(C-D)** and the HF outer root sheath (ORS) marker K17 **(D)** of epidermal isolates of wild type dorsal skin (18 weeks old) cultured for 6 days in passage 0 on collagen IV coated dishes in feeder-free culture medium (Table 10). Red arrowhead: $K17^+$ cell, yellow arrowhead: double positive cell. Scale bars: 200 µm in **A-D**. For details regarding the mice and antibody staining, see Table 17 and Table 13, respectively.

Nevertheless, the *in vitro* behaviour of infundibulum cells was investigated next. For this purpose, infundibulum cells that derive from *CD4Cre*-targeted cells (tdT^+ $CD49f^+CD34^+Sca\text{-}1^+$) of 47-week-old mice were isolated by FACS (see chapter 4.5.1) and seeded on mitomycin C-inactivated NIH3T3 feeder cells in mKera medium (Table 10). 21 days after seeding tdT^+ keratinocyte colonies were stained for the bulge TF Sox9. Indeed, tdT^+ cells expressed Sox9 (Figure 51). Interestingly, although infundibulum cells belong to the IFE, they survive and grew nicely for 21 days after seeding, whereas basal IFE cells ($CD49f^+CD34^{neg}Sca\text{-}1^+$) differentiate soon (see above). However, since *in vitro* cultivation of epidermal cells changes their expression profile, it is difficult to conclude whether in fact HF bulge cells express the *CD4Cre* transgene (Figure 49 C) and/or infundibulum cells can give rise to $Sox9^+$ bulge cells (Figure 51) in the skin.

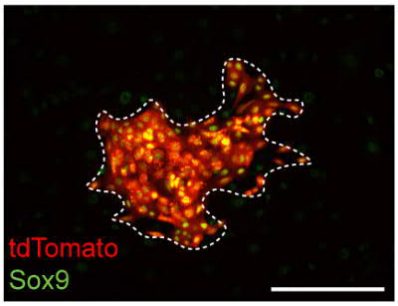

Figure 51. Cultivation of infundibulum cells that derive from *CD4Cre*-targeted cells express the hair follicle bulge transcription factor Sox9.

Representative image of antibody staining against the hair follicle (HF) bulge marker Sox9 of FACS-isolated (for FACS-based isolation see chapter 4.5.1) infundibulum cells that derive from cells with *CD4Cre* activity (tdT^+ $CD49f^+CD34^+Sca\text{-}1^+$) of *CD4Cre R26-tdT* dorsal skin (47 weeks old) cultured for 21 days in passage 0 on mitomycin C-inactivated NIH3T3 feeder cells in mKera medium (Table 10). Naïve tdTomato was visualised (red). White dotted line circles the keratinocyte colony. Scale bar: 200 µm. For details regarding the mice and antibody staining, see Table 17 and Table 13, respectively.

5.2.10 Summary and conclusion

This chapter focused on the cellular identity and the appearance of the progeny of *CD4Cre*-targeted cells and their $CD4^+$ ancestor in the epidermis of the murine skin. Such analyses are of special interest as previous findings have shown that *Ptch* deficiency in the progeny of *CD4Cre*-targeted cells can lead to BCC formation upon additional treatment with DMBA/TPA [193]. Thus, unravelling the cellular identity of the progeny of *CD4Cre*-targeted cells and their ancestor may help to better understand the circumstances that lead to BCC development. In this context the analyses described in this chapter showed that the epidermal progeny of *CD4Cre*-targeted cells comprises not only haematopoietic cells, but also basal and suprabasal keratinocytes of the IFE and HF. Noteworthy, the so far undescribed $CD49f^+CD34^+Sca\text{-}1^+$ basal epidermal cell population has been identified as epidermal cells of the infundibulum. During hair cycle progression, the progeny of *CD4Cre*-targeted cells persists as HF SC in resting HF, becomes activated during anagen initiation, proliferates and subsequently differentiates into suprabasal cells of the HF and thus contributes to HF growth. Beyond that, in growing HF the progeny of *CD4Cre*-targeted cells grows as complex clones, contributing to all HF lineages. In the IFE, the progeny of *CD4Cre*-targeted cells grows as basal cells that give rise to the differentiated upper layers of the IFE. Remarkably, the progeny of *CD4Cre*-targeted cells multiplies with increasing mouse age and upon epidermal wound healing. Thus, these data suggest that telogen-to-anagen transitions (endogenous or WIH-A) might play an important role in the multiplication of HF that contain progenies of *CD4Cre*-expressing cells. Interestingly, the findings described in this chapter also indicate that the $CD4^+$ ancestor of the tdT^+ cells of the IFE and HF may be infundibulum cells. This is highly remarkable since together with the lineage-tracing data it indicates that cells of the infundibulum can give rise to IFE and HF cells as well as to IFE-associated BCC which has not been described before [199].

5.3 CD4 expression in human epidermal stem cells

In human skin also $CD4^+$ SC-like cells, which might present the equivalent to the murine non-haematopoietic $CD4^+$ SC-like cells, were identified [247, 248]. An haematopoietic identity of these skin-resident human $CD4^+$ cells has been already excluded since they do not express the T-lymphocyte marker CD3 [259], the monocyte/macrophage marker CD14 [260] or the dendritic cell/Langerhans cell marker CD1a [261], respectively [247, 248]. Instead skin-resident human $CD4^+$ cells express the keratinocyte marker CD49f [94] as well as the epidermal SC markers CD29 [91] and K15 [92] indicating their epidermal SC identity [248]. This conclusion is further supported by the absence of CD71 expression [247, 248], as a negative marker for SC [262]. Interestingly, human $CD4^+$ $CD49f^+CD29^+K15^+$ cells neither express the ORS marker CD34 nor the bulge marker CD200 [83] suggesting that these cells, similarly to their murine counterparts, possess an IFE identity [247, 248]. Indeed double immunofluorescent stainings verified the existence of $CD4^+$ $K15^+/CD29^+/Sox2^+$ cells in the basal layer of human breast skin samples [247, 248]. Furthermore, a localisation within the epidermal rete ridges can by supposed for human $CD4^+$ epidermal cells because of their expression of K15 [92] and Sox2 [93].

5.3.1 Rare epidermal stem cell-like cells of the human skin express CD4

The studies on murine skin showed that the epidermis of young mice contains higher numbers of $CD4^+$ epidermal cells compared to older mice. To investigate whether the occurrence of $CD4^+$ epidermal cells in human skin also depends on donors age the expression profile of skin epidermal isolates from two 22 to 24-year-old women and from three 56 to 58-year-old women were compared via flow cytometry (Figure 52).

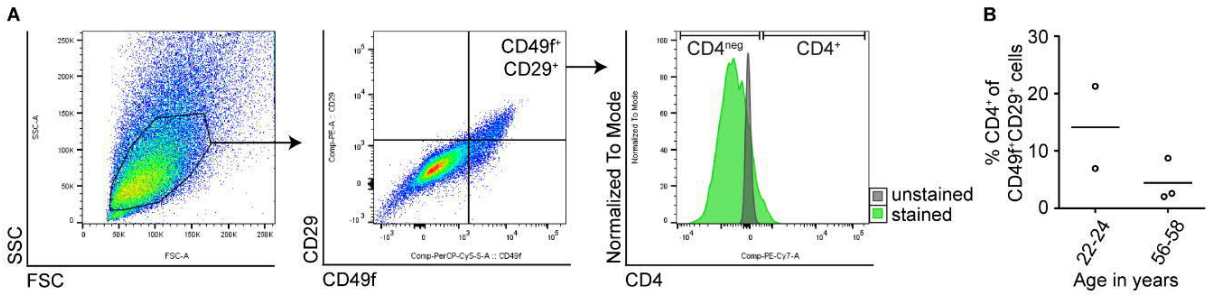

Figure 52. Human epidermal $CD49f^+CD29^+$ stem cells express CD4.

(A-D) Flow cytometric analyses of 60,000 **(A)** or 43,000-60,000 **(B)** cells from human skin. **(A)** Left panel: SSC/FSC plot for gating living skin cells. Middle panel: CD29/CD49f plot for visualisation of $CD49f^+CD29^+$ cells of the gated living skin cells. Right panel: Histogram for visualisation of CD4 expression of unstained living cells (grey) and stained $CD49f^+CD29^+$ living cells (green). **(B)** Quantification of $CD4^+$ $CD49f^+CD29^+$ epidermal cells in human skin (22-24 and 56-58 years old). For details regarding the human skin samples see Table 18.

This approach revealed that the portion of $CD4^+$ $CD49f^+CD29^+$ epidermal SC was slightly higher in the skin of 22 to 24-year-old women (~7-21%) compared to those of 56 to 58-year-old women (~2-9%) (Figure 52 B). This indicates that similar to the murine skin CD4 expression of epidermal SC-like cells is more frequent in skin of younger individuals.

5.3.2 *In vitro* analysis of human $CD4^+$ epidermal cells

5.3.2.1 Establishment of optimal culture conditions for human keratinocytes

5.3.2.1.1 Growth behaviour of human keratinocytes cultured on feeder cells with variations of classical keratinocyte medium

Before starting detailed *in vitro* culture analyses, the culture conditions for human keratinocytes were optimized. The basis for doing so was an already established technique [246, 248], which comprises the following conditions: culture of the keratinocytes on a feeder cell layer (e.g. mitomycin C inactivated MEF) [208, 209], in medium containing insulin, isoproterenol and hydrocortisone (for medium composition see Table 26 medium '1') and adding of EGF 3-4 days after seeding. Thereby the supplementation of medium '1' with the latter mentioned chemicals/factors (e.g. insulin, isoproterenol, hydrocortisone, EGF) should improve the proliferation and growth of keratinocyte colonies [209, 263]. However, initial analysis of the growth behaviour of FACS-isolated $CD4^+$ $CD49f^+CD29^+$ and $CD4^{neg}$ $CD49f^+CD29^+$ epidermal cells under these conditions revealed that the keratinocyte colonies were composed of small, round cells in the centre, from which larger plate-like, flattened cells grew into the clone periphery [223, 248]. This colony morphology reflects those of keratinocyte colonies growing as a mixture of proliferating (small, round cells in the centre) and terminal differentiating cells (large, flattened cells in the periphery) [264, 265]. Nevertheless, the colony number and growth were suboptimal since only a few, small colonies grew [223, 248].

Thus, different variations of medium '1' that have been previously described for optimal keratinocyte culture were compared to classical medium '1' to determine the most effective keratinocyte culture conditions (Table 26).

First, the supplementation of adenine, which has been described to improve the colony forming ability of keratinocytes [266, 267] was tested (Table 26 medium '2').

Secondly, the Ca^{2+} concentration of the media was varied (Table 26 medium '3'). The rational for this was, that high extracellular Ca^{2+} concentrations (up to 1.2 mM) lowers the proliferation rate and induces differentiation of attached keratinocytes [268-271]. Thus, primary keratinocytes that are cultured under low Ca^{2+} conditions (0.05-0.1 mM) proliferate rapidly, do not stratify and grow in a monolayer, but terminally differentiate upon culture with Ca^{2+} concentration above 1.2 mM [270]. To reduce the high Ca^{2+} concentrations (1.44 mM) that result from supplementation with 10% FCS (e.g. in classical keratinocyte culture medium, like

'medium 199') [270, 272], media that are supplemented with lower amounts of FCS that was treated with Chelex 100 resin are commonly used [273]. Thus, keratinocyte media (e.g. 'medium 199') supplemented with chelexed FCS and Ca^{2+} concentrations below 0.1 mM are optimal for *in vitro* culture of undifferentiated human keratinocytes [270, 274].

Earlier studies also used keratinocyte growth media without supplementation of antibiotics/antimycotics (e.g. pen/strep) [117, 264, 275] and with high FCS amounts (e.g. 20%) [264, 276]. Thus, third also media without supplementation of pen/strep (Table 26 medium '4') and with supplementation of 20% FCS were tested (Table 26 medium '5').

Forth and finally, the growth behaviour of primary human keratinocytes in media supplemented with isoproterenol and cholera toxin were compared (Table 26 medium '3' and '6'), since these chemicals are described to increase the cyclic adenosine monophosphate (cAMP) level and thus leading to increased proliferation of epidermal keratinocyte colonies [276].

To test the different media (see Table 26), 180,000 keratinocytes and 400,000 MEF feeder cells were seeded and cultured for 14 days in the respective medium. To determine the degree of differentiation of the clones, the cells were afterwards fixed and stained with rhodamine B and nile blue A (clonal growth assay) [228]. Nile blue A stains all basic substances in blue (e.g. cell nuclei, elastic fibrils), while rhodamine B visualises all epithelial cells in red-violet (e.g. differentiated keratinocytes, keratinized epidermal cells). In line with the previous observation of Wiebke Maurer, the culture of human keratinocytes in medium '1' results in the formation of typical keratinocyte colonies, but only a moderate number of colonies grew (Figure 53) [223, 248]. Similarly, human keratinocytes cultured in medium '2' and '4' grew as typical keratinocyte colonies and in similar quantities to cells cultured in medium '1' (Figure 53). Thus, neither supplementation of adenine (medium '2') nor absence of pen/strep (medium '4') leads to a substantive increase of the colony growth rates of human keratinocytes. In contrast, a considerable increased colony number and growth was observed for human keratinocytes grown in medium '3' supplemented with chelexed FCS compared to medium '1' (Figure 53). This demonstrates that the Ca^{2+} concentration is indeed a critical aspect in keratinocyte cultivation most properly because low Ca^{2+} concentrations are known to prevent keratinocyte differentiation and improve the SC properties and/or proliferative capacities of the epidermal cells [268-271]. No keratinocyte colonies grew in medium '5' and '6' demonstrating that keratinocytes are sensitive to excessive FCS concentrations (medium '5') and prefer isoproterenol in comparison to cholera toxin (medium'6') (data not shown). In summary, human keratinocytes grew best in medium '3', which differ from basic medium '1' by supplementation of 5% chelexed FCS and adenine. Although adenine supplementation seems to have only a minor effect on keratinocyte proliferation (medium '2'), low Ca^{2+} concentrations are important for maintaining the SC-like and/or proliferative abilities of human keratinocytes *in vitro*. Thus,

for all subsequent *in vitro* culture experiments of human keratinocytes on feeder cells medium '3' was used (termed from now on: hkera medium, Table 10).

Table 26. Composition and characteristics of media tested for *in vitro* culture of human keratinocytes and summary of the growth of human keratinocyte colonies after culture in the respective medium.

Primary human keratinocytes were cultured on mitomycin C-inactivated mouse embryonic fibroblast feeder cells. Distinctive composition of the media '2'-'6' in comparison to the basic medium '1' are written in bold letters and summarized in column three 'Characteristics compared to medium '1''. The observed colony growth of the keratinocytes is given in the last column 'Colony growth'.

Medium #	Composition	Characteristics compared to medium '1'	Colony growth
'1'	DMEM-F12-Ham medium (3:1) 5% FCS 1% pen/strep 5 µg/ml Insulin 0,4 µg/ml Hydrocortisone 1 µM Isoproterenol	Basic medium	Colony number > 20
'2'	DMEM-F12-Ham medium (3:1) 5% FCS 1% pen/strep 5 µg/ml Insulin 0,4 µg/ml Hydrocortisone 1 µM Isoproterenol **1,8*10^{-4} M Adenine**	Supplementation with: Adenine	Colony number > 20
'3'	DMEM-F12-Ham medium (3:1) **5% FCS (chelex-treated)** 1% pen/strep 5 µg/ml Insulin 0,4 µg/ml Hydrocortisone 1 µM Isoproterenol **1,8*10^{-4} M Adenine**	Supplementation with: 5% Ca^{2+}-free FCS Adenine	Colony number > 50
'4'	DMEM-F12-Ham medium (3:1) **5% FCS (chelex-treated)** 5 µg/ml Insulin 0,4 µg/ml Hydrocortisone 1 µM Isoproterenol **1,8*10^{-4} M Adenine**	Supplementation with: 5% Ca^{2+}-free FCS Adenine Omission of: pen/step	Colony number > 10
'5'	DMEM-F12-Ham medium (3:1) **20% FCS (chelex-treated)** 0,4 µg/ml Hydrocortisone 1 µM Isoproterenol **1,8*10^{-4} M Adenine**	Supplementation with: 5% Ca^{2+}-free FCS Adenine Omission of: pen/step Insulin	No colony growth
'6'	DMEM-F12-Ham medium (3:1) **5% FCS (chelex-treated)** 1% pen/strep 5 µg/ml Insulin 0,4 µg/ml Hydrocortisone **1*10^{-10} M Cholera toxin** **1,8*10^{-4} M Adenine**	Supplementation with: 5% Ca^{2+}-free FCS Adenine Cholera toxin Omission of: Isoproterenol	No colony growth

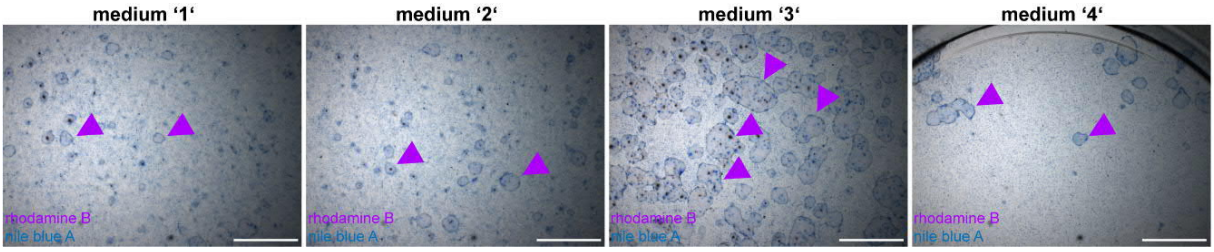

Figure 53. Rhodamine B/nile blue A-based analysis of different media for *in vitro* cultivation of human keratinocytes.

Representative images of 180,000 human epidermal cells cultured for 14 days on mitomycin C-inactivated mouse embryonic fibroblasts in medium '1', '2', '3' and '4' (Table 26), respectively, fixed and stained with rhodamine B (violet) and nile blue A (blue). Medium '1': basic keratinocyte medium [208, 209]; medium '2': supplementation of adenine; medium '3': supplementation of adenine and 5% chelexed FCS; medium '4': supplementation of adenine, 5% chelexed FCS, without penicillin and streptomycin. Violet arrowheads: rhodamine B^+ colonies. Scale bars: 200 µm. For details regarding the human skin samples see Table 18.

5.3.2.1.2 Growth behaviour of human keratinocytes under feeder- and serum-free conditions

In contrast to early reports in which human keratinocytes mostly were *in vitro* cultured on non-proliferating murine feeder cells [264] in FCS-supplemented medium, in clinical settings the use of feeder cells and animal-derived components like FCS potentially expose patients to zoonotic pathogens and immunogenic agents. Thus, the usage of serum-free media [277-280] and hDF instead of murine feeder cells or complete feeder-free systems have been developed for human keratinocyte culture in the last years. Thereby feeder-free systems are based on coating of culture plates with proteins that are associated with basement membranes, such as fibronectin and collagens. To establish the culture of human keratinocytes under feeder- and serum-free conditions besides the classical method (see above) FACS-isolated $CD4^{neg}$ $CD49f^+CD29^+$ epidermal cells (for FACS-based isolation see chapter 4.5.2) were seeded on collagen I-coated plates and cultured in feeder-free culture medium (Table 10) (Figure 54). 14 days after seeding first microscopic visible colonies were grown (Figure 54). The cells show the regular 'cobblestone' pattern (Figure 54) that is described for basal epidermal cells [270].
In comparison to the human epidermal cells that were grown on feeder cells, the culture on collagen I-coated plates in serum-free medium leads to a more homogenous, uniform-cell morphology (compare Figure 53 and Figure 54). This approach demonstrates, that human $CD49f^+CD29^+$ epidermal SC indeed can be cultured under feeder- and serum-free conditions, albeit with lower efficiencies compared to the culture on feeder cells.

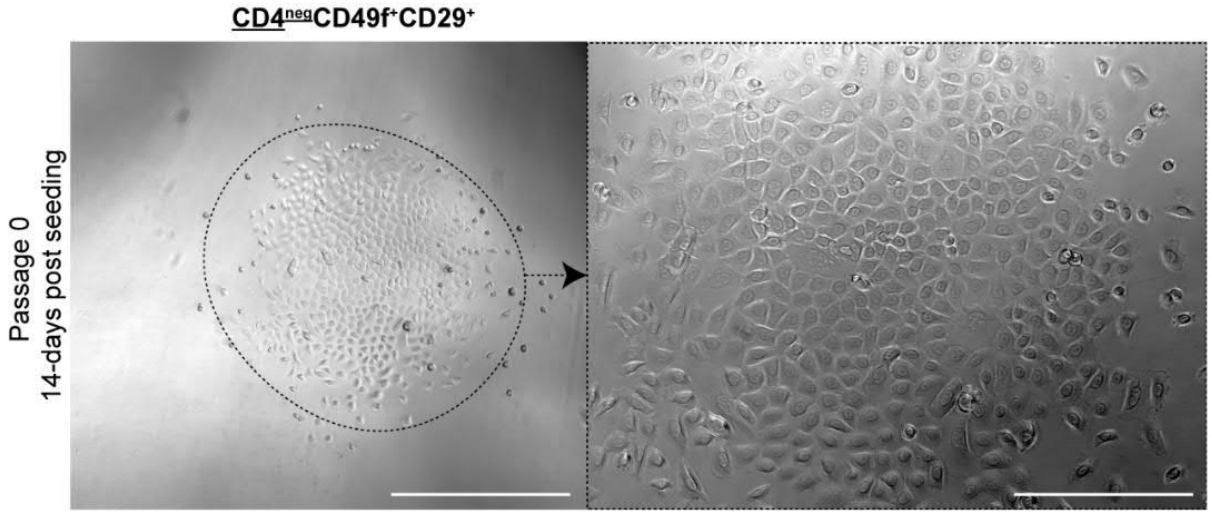

Figure 54. Feeder- and serum-free culture of human keratinocytes.

Representative images of FACS-isolated $CD4^{neg}CD49f^{+}CD29^{+}$ human epidermal cells (for FACS-based isolation see chapter 4.5.2) cultured for 14 days in passage 0 on collagen I coated dishes in feeder-free culture medium (Table 10). Scale bars: 500 µm in **A**; 200 µm in **B**. For details regarding the human skin samples see Table 18.

Together these data show that feeder- and serum-free culture of human keratinocytes is possible but less efficient compared to the classical culture method on feeder cells and with serum-supplementation. Moreover, according to several reports the usage of feeder cells is the 'gold standard' of human keratinocytes culture [264, 281, 282]. Thus, in subsequent analyses human keratinocytes were cultured in hkera medium (Table 10) on mitomycin C-inactivated hDF since these showed more robust growth capacities compared to MEF.

5.3.3 Human epidermal $CD4^{+}$ cells show stem-cell characteristics and high colony forming efficiency *in vitro*

For evaluating the colony forming abilities of human epidermal $CD4^{+}$ SC-like cells the growth capacities of clones derived from single cells [117] of FACS-isolated $CD4^{+}$ $CD49f^{+}CD29^{+}$ in comparison to $CD4^{neg}$ $CD49f^{+}CD29^{+}$ cells were analysed. According to Barrandon and Green, three different classes of clones were defined: holoclones, meroclones and paraclones (for key characteristics and marker expression see Table 27) [117]. In brief, holoclones form large rapidly growing colonies, whereas paraclones form only small, terminal colonies [117]. Holoclones consist of a basal layer of small cells that is covered by upper terminally differentiated cells [117]. As a result, holoclones are assumed to derive from SC and paraclones from late stage TAC. Meroclones form growing as well as terminal colonies [117] and are discussed to give rise to both SC and terminally differentiating cells. A more recent study that focused on a prostate cancer cell line, identified lower sphere forming efficiency (SC assay) of meroclones when compared to holoclones, indicating that meroclones contain less self-renewing SC [283]. However, several studies only compare holoclones and paraclones.

Similar to human *in vitro* cultured epidermal cells also epidermal cells from neonatal mice grow as holoclones, meroclones or paraclones [284].

Table 27. Characteristic features and marker expression of holoclones, meroclones and paraclones derived from human primary keratinocytes [117].

	Holoclone	Meroclone	Paraclone
Characteristic features			
Area size	10-30 mm^2	< holoclone	< 5 mm^2
Perimeter	Nearly circular	Wrinkled	Irregular
Number of cells	2-5 x 10^4	-	-
Cell morphology	Basal layer of small cells, covered with upper differentiating flattened cells	Heterogeneous	Large and flattened
Marker expression			
Involucrin	Small cells: Inv^{neg}	-	Inv^+
Trp63 [285]	$Trp63^+$	$Trp63^{low}$	$Trp63^{neg}$

First, the *in vitro* growth of FACS-isolated human $CD4^+$ $CD49f^+CD29^+$ epidermal SC-like cells was compared to that of $CD4^{neg}$ counterparts. Six days after seeding, the first small colonies consisting of several dozen cells were visible in both $CD4^+$ $CD49f^+CD29^+$ and $CD4^{neg}$ $CD49f^+CD29^+$ cultures (Figure 55 A, B). The cells were small and had a roundish or rather cobblestone morphology corresponding to those of basal keratinocytes, which is a characteristic of holoclones (Table 27). Already 11 days after seeding, huge colonies with an almost circular perimeter (feature of holoclones, see Table 27) were grown, almost touching the surface of the neighbouring colonies (Figure 55 C, D). Thus, the cells were passaged 12 days after seeding, cultured for additional 2 days and then fixed for anti-Trp63 antibody staining (Figure 55 E, F') since Trp63 expression can be used to distinguish holoclones ($Trp63^+$), meroclones ($Trp63^{low}$) and paraclones ($Trp63^{neg}$) [285] (Table 27). This approach revealed that almost all keratinocytes of the colonies that have been grown from $CD4^+$ $CD49f^+CD29^+$ and $CD4^{neg}$ $CD49f^+CD29^+$ cells express Trp63 (Figure 55 E, F'), demonstrating that $CD4^+$ $CD49f^+CD29^+$ epidermal SC-like cells form holoclones und thus indeed possess SC-like characteristics.

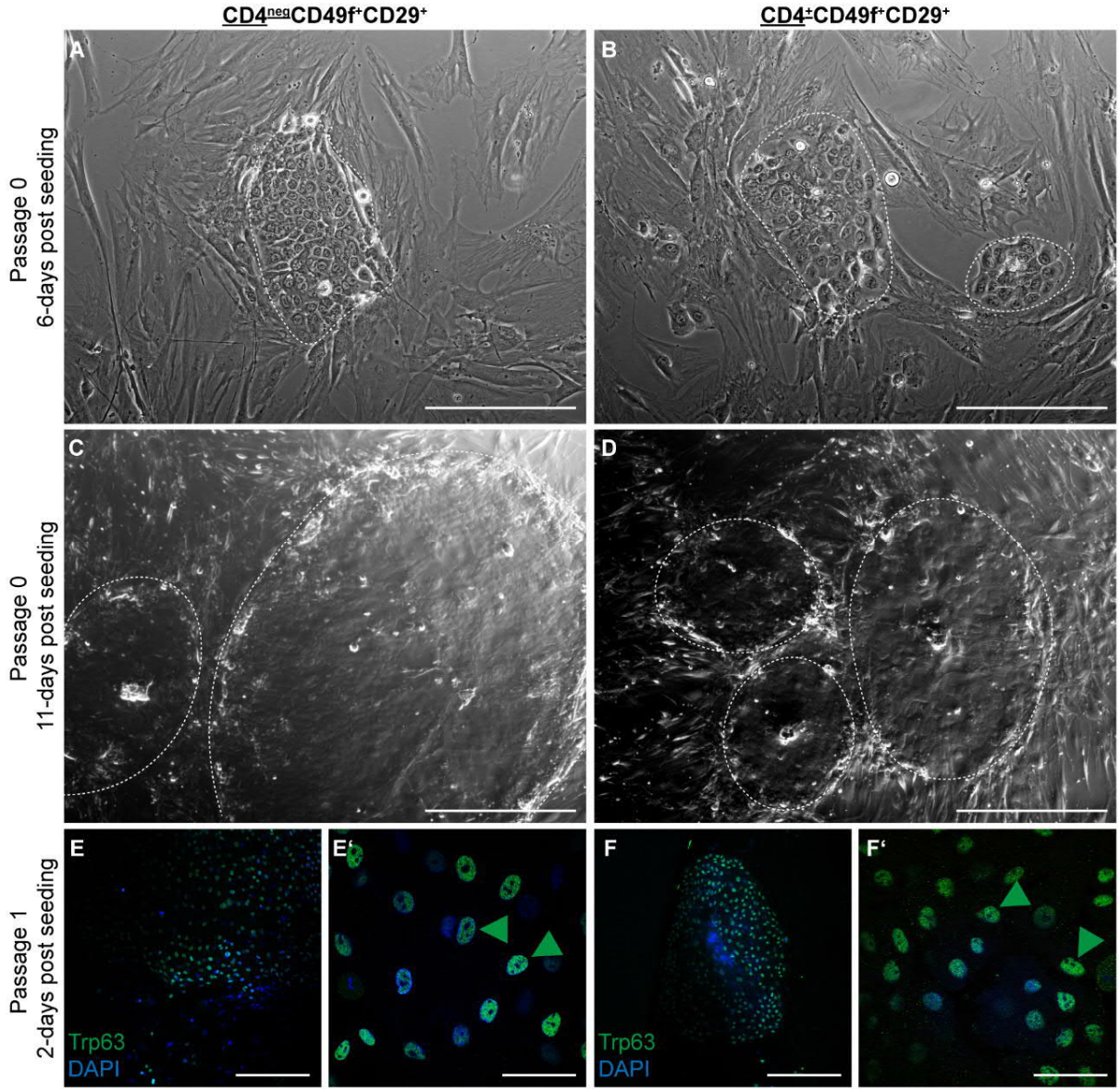

Figure 55. CD49f$^+$CD29$^+$ human epidermal cells grow as holoclones independent of their CD4 expression.

(A-F') Representative images of FACS-isolated CD4^{neg} CD49f$^+$CD29$^+$ and CD4$^+$ CD49f$^+$CD29$^+$ human epidermal cells (for FACS-based isolation see chapter 4.5.2) cultured for 11 days without passaging **(C, D)** or for 2 days in passage one (14 days after initial seeding) **(E-F')** on human dermal fibroblasts in hkera medium (Table 10). **(E-F')** Antibody staining against the epidermal basal cell marker Trp63. Nuclei were visualised with DAPI (blue, **E-F'**). Green arrowheads: Trp63$^+$ cells. Scale bars: 500 µm in **C, D**; 200 µm in **A, B, E, F**; 33 µm in **E', F'**. For details regarding the human skin samples see Table 18 and for antibody staining see Table 13.

Next, the CFE of FACS-isolated CD4$^+$ CD49f$^+$CD29$^+$ epidermal SC-like cells was compared to that of CD4^{neg} counterparts. For this purpose, 1,500 FACS-isolated cells of the respective population were seeded on 500,000 mitomycin C-inactivated hDF in Ø10 cm dishes and cultured for 22 days without passaging. To additionally analyse the capacity to form secondary colonies, in a second approach 60,000 FACS-isolated cells of the respective population were seeded on 100,000 mitomycin C-inactivated hDF in Ø10 cm dishes, cultured until passage two for a total of 42 days (14 days in passage 0, 17 days in passage one and 11 days in passage two). To subsequently visualise primary and secondary keratinocyte colonies, the cells were

fixed, stained with rhodamine B and nile blue A (Figure 56) and the numbers of primary and secondary colonies as well as the numbers of colonies with a diameter of more than 5 mm were determined.

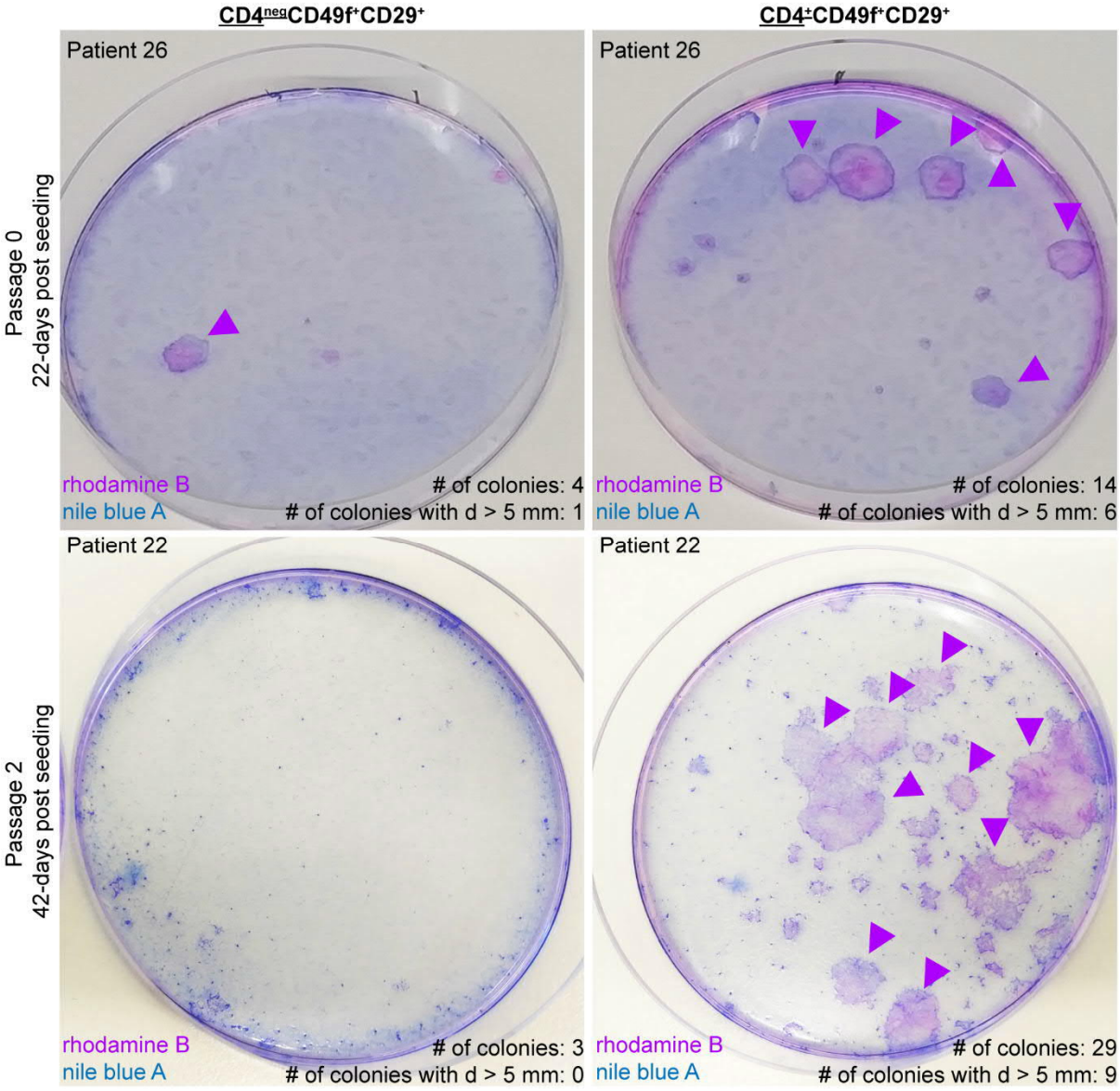

Figure 56. Enormous clonal growth capacity of *in vitro* cultured epidermal CD4$^+$ CD49f$^+$CD29+ stem cell-like cells.

Representative images of 1,500 (top) or 60,000 (bottom) FACS-isolated CD4^{neg} CD49f$^+$CD29$^+$ and CD4$^+$ CD49f$^+$CD29$^+$ human epidermal cells (for FACS-based isolation see chapter 4.5.2) cultured for 22 days in passage 0 (top) or 42 days in passage two (bottom) on inactivated human dermal fibroblasts in hkera medium (Table 10). Bottom: Keratinocytes were cultured for 14 days in passage 0 (split 1:3), additional 17 days in passage one (split 1:3) and further 11 days in passage two. Colonies were stained with rhodamine B (violet) and nile blue A (blue). Violet arrowheads: rhodamine B$^+$ colonies with a diameter (d) above 5 mm. For details regarding the human skin samples see Table 18.

This approach revealed that the number of primary colonies that were formed from epidermal CD4$^+$ CD49f$^+$CD29$^+$ SC-like cells was higher (14 primary colonies, six of them with a diameter > 5 mm or rather an area of more than 19.5 mm^2) compared to that of CD4^{neg} counterparts

(four primary colonies, one of them > 5 mm/19.5 mm^2) (Figure 56). Similarly, the number of secondary colonies grown from epidermal $CD4^+$ $CD49f^+CD29^+$ SC-like cells were enormous higher (29 secondary colonies, nine of them > 5 mm/19.5 mm^2) than those of $CD4^{neg}$ counterparts (three colonies) (Figure 56). Only holoclones (but neither meroclones nor paraclones) are capable of extensive proliferation and self-renewal, thus a characteristic feature of holoclones is the formation of huge colonies with an area size of 10-30 mm^2 (Table 27). Therefore, the growth of primary and secondary colonies with an area above 19.5 mm^2 (Figure 56), supports the hypothesis that $CD4^+$ $CD49f^+CD29^+$ cells have a SC-like character since they grow as holoclones *in vitro*. Besides, these findings impressively show that epidermal $CD4^+$ $CD49f^+CD29^+$ SC-like cell possess a high CFE *in vitro*, which is even higher than those of the 'classical' human epidermal $CD4^{neg}$ $CD49f^+CD29^+$ SC-like cells.

5.3.4 Summary and conclusion

This chapter describes the refinement of the *in vitro* culture of human keratinocytes. The newly established culture method was then used to analyse the assumed SC characteristics and the primary and secondary CFE of human epidermal $CD4^+$ $CD49f^+CD29^+$ SC-like cells. The results of these approaches demonstrate that $CD4^+$ $CD49f^+CD29^+$ cells like their $CD4^{neg}$ counterparts grow as $Trp63^+$ holoclones. However, in contrast to $CD4^{neg}$ $CD49f^+CD29^+$ cells human epidermal $CD4^+$ $CD49f^+CD29^+$ SC-like cells possess a high CFE substantiating the proposed SC-like character of these cells. Moreover, the high proliferation rate of human epidermal $CD4^+$ $CD49f^+CD29^+$ SC-like cells compared with their $CD4^{neg}$ counterparts, unravelled similarities to the murine $CD4^+$ epidermal SC-like cells ($CD4^+$ $CD49f^+CD34^+Sca\text{-}1^+$), which are proposed to be proliferative active cells of the infundibulum. Accordingly, the human epidermal $CD4^+$ $CD49f^+CD29^+$ SC-like cells, similar to the murine equivalent, seem to persist in the IFE basal layer (in the rete ridges).

6 Discussion

BCC represent the most common type of human skin cancer [134]. They mainly form due to HH signalling activating mutations, especially *PTCH* mutations or loss of heterozygosity are commonly found in sporadic BCC [137, 138]. Thus, the HH receptor and HH signalling repressor PTCH is thought to act as a 'gate keeper' for BCC development [201]. Based on this, it is not surprising that genetically engineered mouse models with biallelic *Ptch* mutations in SC of the HF or in basal cells of the IFE spontaneously develop BCC [197, 200]. Recently, our group described the existence of a $CD4^+$ $CD49f^+CD34^+Sca\text{-}1^+$ non-haematopoietic skin-resident cell population, which also can give rise to BCC upon biallelic *Ptch* mutation and additional DMBA/TPA treatment [193]. However, the cellular identity of these cells was unclear, but of high interest because the knowledge about a potential unknown tumour progenitor has critical impact on the understanding of skin cancer development. Thus, the main goal of this thesis was to identify and characterise this non-haematopoietic $CD4^+$ cell population. For this purpose, not only SC of epidermal lineages (e.g. HF SC, basal cells of the IFE) but also BM-derived MSC were considered as putative BCC progenitors since the latter ones possess the capacity to differentiate into epidermal keratinocytes [96-101].

The results gained by *in vitro* and *in vivo* lineage tracing, CD4 protein detection and scRNA-Seq analysis revealed that (1) BM-derived MSC, dermal fibroblasts and epidermal cells of the infundibulum can express CD4, (2) BM-derived MSC, dermal fibroblasts as well as keratinocytes of all layers of the IFE and the HF represent descendants of *CD4Cre*-expressing cells, (3) $CD4^+$ epidermal cells of the infundibulum most likely are the origin of $Ptch^{fl/fl}$ *CD4Cre* BCC and of the descendants in the IFE and/or HF and (4) $CD4^+$ non-haematopoietic cells of the human skin possess SC-like characteristics as their murine counterparts.

6.1 BM- and skin-resident *CD4Cre*-targeted cells and their progenies as basal cell carcinoma precursors

BM-derived MSC can express *CD4* transcripts [162], are phenotypically indistinguishable from fibroblasts [114] and possess the potential to differentiate into multiple skin cell types like epidermal keratinocytes and HF cells [96-100] or SG cells [102]. Thus, in this thesis BM-derived MSC and/or fibroblasts were analysed as putative progenitors of $Ptch^{fl/fl}$ *CD4Cre* BCC. Indeed, the analyses revealed that a subpopulation of murine BM-derived Lin^{neg} $CD90^+CD44^+CD29^+$ MSC-like cells derive from cells with CD4 promoter activity (Figure 16). Moreover, spindle/fibroblast-like shaped, plastic-adherent murine BM-derived Lin^{neg} cells derive from *CD4Cre*-targeted cells (Figure 17) and thus most likely represent the tdT^+ $CD90^+CD44^+CD29^+$ MSC population determined by flow cytometry (Figure 16). In line with the fact that BM-derived MSC and fibroblasts can develop to various cell types including

myofibroblasts in response to stress (e.g. after injuries [104], reviewed in [59] or upon *in vitro* cultivation [231]) also α-SMA$^+$ myofibroblasts were identified as descendants of cells with CD4 promoter activity (Figure 17). Moreover, the progeny of *CD4Cre*-targeted BM-derived cells grows as discrete colonies initiated by single cells (CFU) (Figure 21), which is typical for BM-derived MSC culture [108], and express the CD4 surface protein (Figure 21). Similarly, also dermal fibroblasts of either spindle-shaped or flattened-shaped morphology, the latter ones might represent myofibroblasts, descend from cells with *CD4Cre* activity (Figure 18) or even show *CD4Cre* activity (Figure 20) *in vitro*. Finally, the existence of CD4$^+$ PDGFRα$^+$/α-SMA$^+$ fibroblasts in the murine dermis and their fibroblast descendants that persist in the dermis were demonstrated (Figure 23). These data show that BM-derived MSC and dermal fibroblasts of adult mice can express CD4 and that their offspring grow in the murine BM and dermis. However, the progeny of *CD4Cre*-targeted cells were also found in the epidermis (Figure 23). Together with the fact that differentiation of BM-derived MSC into epidermal keratinocytes has been described [96-101] CD4$^+$ stromal cells (e.g. CD4$^+$ BM-derived Lin^{neg} MSC and/or CD4$^+$ dermal fibroblasts and/or their descendants) may represent putative BCC precursors in the *Ptch$^{fl/fl}$ CD4Cre$^{+/-}$* mice. Remarkably, murine CD4$^+$ BM-derived MSC co-express the pluripotency marker Oct-3/4 (Figure 21), whose overexpression together with Sox2, Nanog and Lin-28 is known to artificially reprogram somatic cells into induced pluripotent SC [286] that subsequently can be differentiated into various cell types including keratinocytes [287, 288]. However, this thesis does not experimentally prove whether CD4$^+$ BM-derived MSC or CD4$^+$ dermal fibroblasts indeed represent the origin of epidermal keratinocytes and/or *Ptch$^{fl/fl}$ CD4Cre* BCC although such scenario may be conceivable due to the capacity of BM-derived MSC to differentiate into epidermal cells [96-101]. To proof this hypothesis *in vitro* differentiation and *in vivo* transplantation experiments of CD4$^+$ BM-derived MSC and/or CD4$^+$ dermal fibroblasts have to be performed. For example, *in vitro* differentiation protocols used for keratinocyte differention from human MSC [289], might be also applicable for studying the proposed differentiation potential of murine FACS-isolated CD4$^+$ BM-derived MSC and CD4$^+$ dermal fibroblasts. However, *in vitro* culture changes the cell shape, behaviour and differentiation capacities of SC. Thus, cultivation of MSC leads to cell flattening, which influences cell fate and reduces the proliferation rate [290, 291] most likely because standard *in vitro* culture conditions do not mimic the physiological three-dimensional (3D) microenvironment, especially complex SC niches (e.g. spatial interactions, gradients of nutrients, ECM components) can hardly be offered (reviewed in [292]). Alternatively, 3D culture methods like MSC spheroids could be analysed since these have been shown to improve the differentiation potential of MSC [293]. Similarly, transplantation allows the investigation of the differentiation capacity of SC because, depending on the location to which the cells are transplanted, they receive appropriate signals

from the niche/microenvironment and show their differentiation potential. In particular, transplantation of MSC results in differentiation into various cell lineages dependent on the characteristics of the surrounding *in vivo* microenvironment. Thus, tissue-specific transplantation of MSC results in their differentiation to bone, haematopoiesis supportive stroma and/or marrow adipocytes when transplanted into the BM [294] or they differentiate to keratinocytes of the epidermis, HF and SG when transplanted into the skin [99]. Therefore, the potential of $CD4^+$ BM-derived MSC or $CD4^+$ dermal fibroblasts to differentiate into epidermal cells could be evaluated by intradermal transplantation of fluorescent-labelled (e.g. GFP^+ cells isolated from transgenic mice[4] [295]) $CD4^+$ BM-derived MSC or $CD4^+$ dermal fibroblasts together with neonatal epidermal keratinocytes and neonatal dermal fibroblasts into the skin of immunocompromised nude mice (*Foxn1^{nu}*) similarly to Zheng *et al.* [296]. The capacity of $CD4^+$ BM-derived MSC or $CD4^+$ dermal fibroblasts to differentiate into keratinocytes would then be demonstrated by the *de novo* formation of fluorescent-labelled HF and IFE at the injection side. However, as mentioned above both *in vitro* culture and grafting are known to change the behaviour and differentiation capacities of SC. Thus, it would be more interesting to unravel the role of $CD4^+$ BM-derived MSC and/or $CD4^+$ dermal fibroblasts in epidermal maintenance during homeostasis and/or wound healing to clarify whether stromal cells can indeed represent BCC precursors under physiological conditions. Up to date and due to the lack of specific markers, MSC could only be tracked by transplantation experiments. However, the contribution of transplanted BM-derived MSC to the murine epidermis occurs only with a very low frequency (< 0.0003% [105] or 0.14% [96]). Moreover, the proportion of transplanted MSC in wound-near regions is small and strongly decreases over time [109] and often persist as single cells in the wound site of the epidermis [96]. These observations may be the results of a displacement of transplanted MSC and their offspring by the endogenous MSC pool of the recipient which in turn would hamper the analysis of the actual long-term involvement of MSC in wound healing and regeneration by transplantation experiments. Nevertheless, intra-BM transplantation appears to be sufficient for effective tracking of BM-derived MSC, as implantation of MSC in bones results in detectable differentiation into pericytes, myofibroblasts, BM stromal cells, osteocytes in bone, bone-lining osteoblasts and endothelial cells, whereas after intravenous transplantation nearly no MSC or their descendants were detectable [238]. Moreover, if mice that already received BM-derived MSC transplantation obtained skin grafts[5] higher numbers of MSC descendants that cluster in the epidermis, express K5 and maintain in the epidermis and HF were found in comparison to mice that were injured [101]. Since descendants of the transplanted MSC persists up to 5 months in the skin, their switch to an epidermal SC or progenitor identity is highly likely due to the fast turnover rate of epidermal

[4] *C57BL/6-Tg(CAG-EGFP)1Osb/J* mice with an EGFP cDNA under the control of a chicken beta-actin promoter have widespread EGFP fluorescence.

[5] This means that full-thickness skin from a donor is transplanted onto the back of the recipient

tissue [101]. Thus, a combination of intra-BM transplantation (to achieve an integration of the transplanted MSC into the haematopoietic BM niche, [238]) and skin grafting (that leads to a recruitment of BM-derived MSC to the skin and (trans) differentiation into keratinocytes, [101]) might represent the best experimental setup to detect the putative contribution of $CD4^+$ BM-derived MSC to skin regeneration.

However, lineage-tracing studies for specifically tracking MSC and their progeny cells in various tissues including the skin would eliminate the need for extensive transplantation experiments and would prevent competition between endogenous and transplanted MSC. Moreover, the analysis of progeny cells for instance in the epidermis of young and old mice would shed light on a putative contribution of BM-derived MSC to epidermal homeostasis, whereas wounding experiments might unravel the role of BM-derived MSC during healing processes and re-epithelisation of skin wounds. Besides, lineage-tracing studies combined with HH signalling activation in BM-derived MSC could be used to investigate whether those are actually BCC precursors. Unfortunately, to date no exclusive marker for BM-derived MSC is known, although all stromal cells (e.g. BM-derived MSC, dermal fibroblasts, lung fibroblasts) express PDGFRα and thus *PdgfrαCreER^{T2}* [297, 298] or *PdgfrαGFPCreER^{T2}* [299] deleter mouse strains could be used to trace stromal cells and their progeny. In case of differentiation of PDGFRα^+ stromal cells (e.g. BM-derived MSC) into epidermal keratinocytes, progeny cells that express a reporter gene would be detectable in the IFE and/or HF. Finally, *Ptch$^{fl/fl}$ PdgfrαCreER^{T2}* or *Ptch$^{fl/fl}$ PdgfrαGFPCreER^{T2}* strains could be used to unravel whether stromal cells are putative progenitors of BCC upon *Ptch* depletion. Nevertheless, activation of HH signalling in fibroblasts induces their differentiation into myofibroblasts and furthermore fibrosis [300]; hence *Ptch* depletion may effect the differentiation of stromal cells to keratinocytes. Indeed, homozygous *Ptch* inactivation in dermal stromal cells (*Col1a2CreER* deleter) results in increased stromal cell density and formation of highly condensed dermal cell clusters adjacent to the infundibulum and underneath the IFE [50]. However, *Ptch$^{fl/fl}$ Col1a2Cre^{ER}* mice do not spontaneously develop BCC properly because of the low differentiation rate of stromal cells to keratinocytes or because similar to *Ptch$^{fl/fl}$ CD4Cre* mice an additional trigger like DMBA/TPA treatment may be necessary for BCC initiation from these cells (see discussion about DMBA/TPA treatment in chapter 6.1.2).

However, independent of the cellular identity of the $CD4^+$ ancestor, progeny of *CD4Cre*-targeted cells were also identified in the epidermis (Figure 23). Since different epidermal populations including basal IFE cells and HF SC are known to give rise to BCC upon homozygous *Ptch* depletion, next the cellular identity of the epidermal progeny of *CD4Cre*-targeted cells as putative BCC precursors in *Ptch$^{fl/fl}$ CD4Cre$^{+/-}$* mice was analysed. Initial flow cytometric analysis indicated that these cells comprise the common BCC precursor cell types: $CD34^+$ outer bulge cells, $Sca\text{-}1^+$ basal IFE cells and uHF cells (Figure 25) [197, 200].

Moreover, transcriptome-based differential gene expression analysis (Figure 26, Figure 27) and immunofluorescence stainings (Figure 30, Figure 31) verified that the epidermal progeny of *CD4Cre*-targeted cells indeed grows as known BCC precursor cell types (e.g. HF SC of the bulge, sHG, uHF and as basal cells of the IFE). Unexpectedly, a so far undescribed cell population that also contains the progeny of *CD4Cre*-targeted cells and that expresses CD49f, CD34 and Sca-1 was detected (Figure 25). Due to its expression of IFE and HF marker genes this population was characterised as basal cells of the infundibulum (Figure 26, Figure 27) [11]. Beyond that, the *in vivo* growth behaviour of the epidermal progeny of *CD4Cre*-targeted cells verified their transit-amplifying character of basal IFE cells and their SC properties of HF SC, respectively. This is the case since the progeny of *CD4Cre*-targeted cells clonally grows as basal and suprabasal cells in all layers of the IFE in dorsal and tail skin (Figure 30) as well as in all HF layers (Figure 31, Figure 32). During hair cycle progression, the progeny of *CD4Cre*-targeted cells persists as $CD34^+$ bulge SC in resting HF (Figure 31), becomes activated during anagen initiation, proliferates and subsequently differentiates into suprabasal cells of the HF and thus contributes to HF growth (Figure 32). Moreover, the progeny of *CD4Cre*-targeted cells grows as complex clones, contributing to all HF lineages and as rORS clones maintaining the ORS lineage in growing HF (Figure 34). However, this raises the question whether the progeny of *CD4Cre*-targeted cells has SC-like properties in growing HF. Remarkably, *in vivo* clonal analysis through labelling of single HF cells lead to the assumption that only in telogen and during anagen initiation multipotent HF SC exist that during anagen progression form the germinative layer (located in the bulb) and the ORS precursors [301]. The ORS precursors only give rise to ORS cells of the distal part of the HF, whereas the germinative layer cells are precursors of the Cp layer, the IRS and the HS [249, 301]. During early anagen, the multipotent HF SC have been replaced by the ORS restricted precursors and oligopotent internal precursors of the bulb, which can give rise to the different internal lineages (Cp layer, IRS and HS) [301]. Subsequently, during mid anagen the oligopotent precursors become layer-restricted internal precursors that only give rise to one certain HF lineage (e.g. HS cuticle or HS medulla) [302]. Together, the transition from telogen to anagen involves the separation of the ORS from the internal structures and no multipotent precursor that contributes to both: the ORS and to the internal structures is detectable during anagen (only during telogen and telogen-to-anagen transition) [301]. Accordingly, if single cells are labelled during the initial stages of hair growth (telogen/anagen initiation, early anagen, mid anagen) and observed during the following late anagen when all distinct HF structures are recognizable, different patterns of progeny cells within the different HF structures can be identified. Thus, the labelling of single cells during telogen can result in the presence of progeny cells in the ORS and in internal lineages (complex clones) if multipotent HF SC were labelled or alternatively the progeny cells are restricted to the ORS (rORS clones) when ORS

precursors are marked [249]. In contrast, labelling of single cells during early anagen results in the detection of a third clone type with progeny cells restricted to the different internal lineages since oligopotent internal precursors can be marked, too [301]. Contrarily, labelling of single cells during mid anagen leads to the occurrence of descendants in only one structure: ORS, IRS, HS cuticle/cortex or HS medulla, because layer-restricted precursors are labelled [302]. Intriguingly, in late anagen HF the progeny of *CD4Cre*-targeted cells grows mainly (73%) as complex clones, contributing to all HF lineages, whereas only a minor fraction (13%) grows as rORS clones, but progeny cells were never restricted to one or several internal lineages (Figure 34, Figure 35). This finding leads to the assumption that *CD4Cre* activity occurs in multipotent HF SC and in ORS precursors during telogen/anagen initiation and thus to labelling of these precursors in resting/activated HF and their descendants in the growing HF. Conversely, neither the oligopotent nor the unipotent internal precursors of the bulb seem to express the *CD4Cre* transgene, because then descendants restricted to the internal layers or to one certain internal layer, respectively, should have been detected. Together, it can be assumed that *CD4Cre*-targeted cells and/or their descendants have a multipotent character as HF SC during telogen/anagen initiation. Similarly also other HF SC were described to contribute to all HF lineages, including $CD34^+/K15^+$ SC of the central bulge, $Lgr5^+$ SC of the lower bulge and sHG and $Gli1^+$ SC of the upper and lower bulge and the sHG [65-67]. Moreover, labelling of single $Gli1^+$ bulge/sHG SC during telogen demonstrated their multipotency because during late anagen clones with progeny cells in at least two lineages were detectable [66]. Strikingly, the progeny of *CD4Cre*-targeted cells grows as single cells distant from each other, in a patchy pattern (Figure 34-Figure 36). Remarkably, this can be explained by the polyclonal origin of the HF lineages, each formed by several SC. Moreover, this patchy pattern of descendants from labelled SC is also observed if single HF SC are labelled randomly [302].

Moreover, in growing HF the progeny of *CD4Cre*-targeted cells is not restricted to a certain hair type since it grows in all hair types (zigzag, awl/auchene, guard; Figure 29). The hair type is determined by cells of the DP and the number of DP cells specifies the hair type so changes in the DP cell number induce the formation of another hair type [303]. Accordingly, the SC of a particular HF can give rise to different hair types in successive hair cycles, excluding the assumption that HF are distinct depending on the hair type they produce [303]. The only exception are HF that produce guard hairs, which continue to make guard hairs and normally do not produce other hair types [303].

Thus, this thesis shows that the epidermal progeny of *CD4Cre*-targeted cells grows on the one hand as stromal cells of the murine BM and skin and on the other hand as keratinocytes of the HF bulge, of the uHF of resting HF and of basal cells of the IFE. Nevertheless, although more detailed future studies are needed to proof stromal cells as BCC precursors the identity of

epidermal progeny of *CD4Cre*-targeted cells as potential BCC precursors is highly probable. This is the case since all epidermal populations that can descent from $CD4^+$ non-haematopoietic cells (e.g. basal cells of the IFE and/or HF SC [bulge, sHG, uHF]) also can give rise to BCC in case of a homozygous *Ptch* mutation [197, 200]. Confusingly $Ptch^{fl/fl}$ *CD4Cre* mice do not spontaneously develop BCC [193] indicating a decisive difference between BCC development and/or precursors in $Ptch^{fl/fl}$ *CD4Cre* mice compared to other BCC mouse models. However, the data of this thesis clearly demonstrate that known BCC precursor cell types can possess *CD4Cre* activity itself ($K5^+$ basal and/or ORS cells [Figure 48]) and that they can descent from *CD4Cre*-expressing cells (e.g. $K5^+$ basal IFE cells [Figure 30], $CD34^+$ bulge cells [Figure 31]). Thus, it seems to be implausible why *Ptch* deficiency in the progeny of *CD4Cre*-targeted cells does *per se* not lead to BCC formation [193]. Possible explanations might be a restricted temporal occurrence or limited growth capacities of the epidermal progeny of *CD4Cre*-targeted cells in the IFE and/or HF.

6.1.1 The epidermal progeny of *CD4Cre*-targeted cells grow as long-living skin stem cells

Basal IFE cells and HF SC descent from *CD4Cre*-expressing cells in adult murine skin. Nevertheless, during development no descendants of *CD4Cre*-targeted cells were detectable in the epidermis (Figure 15) and during puberty (~6 to 10 weeks old) only individual HF or IFE areas descend from *CD4Cre*-targeted cells (Figure 39), which indicates that the progeny of cells with *CD4Cre* activity mainly persist in adults. As a result, $CD4^+$ and/or their progeny SC might be dispensable for skin development but might be more relevant for maintenance of adult skin. Moreover, descendants of *CD4Cre*-expressing cells are still detectable in senescent skin of old mice (~18 to 24 months old) and persist as huge clones in the IFE (Figure 39). Thereby the age-related enlargement of epidermal areas comprising of descendants from *CD4Cre*-expressing cells (Figure 39), matches the concept of population asymmetry (stochastic model) for IFE homeostasis, which assumes that the continual loss of SC clones is compensated by the expansion of neighbouring clones [38]. On the contrary, the concept of invariant asymmetry (hierarchical model) implies the presence of permanent clones that are self-sustaining and do not change in their size. However, the population asymmetry model suggests that progenitor cells (most probably of the basal layer) can divide either symmetrically or asymmetrically leading to different sizes of the respective clones and thus to a different number of basal cells that derive from one ancestor [38]. According to this model, in *CD4Cre R26-tdT* skin clones with one to few but also with numerous basal cells that descent from *CD4Cre*-expressing cells were observed (Figure 39), indicating their ancestry from one common SC that divides either asymmetrically (leading to one progeny basal cell) or symmetrically (leading to numerous progeny basal cells) (see chapter 1.2.2, Figure 2).

However, it is still under debate whether stochastical replacement or selective elimination of unfit cells through cell competition drives the expansion of single clones while other clones get lost [304-308]. A recent study of Liu and colleagues supports the hypothesis that cell competition between basal SC drives the expansion of single clones while neighbouring clones get lost since they observed that COL17A1^{high} SC, which divide symmetrically, have a higher clonogenic potential and eliminate adjacent stressed, asymmetrically dividing clones that express low levels of COL17A1 [118]. In light of these results, the data gained in this thesis suggest that the progeny of *CD4Cre*-expressing cells possess a survival benefit and outcompete adjacent unfit clones since the size of epidermal tdT$^+$ patches increases with age in *CD4Cre R26-tdT* mice (Figure 39).

Together, the data of this thesis show that a subpopulation of epidermal progeny of *CD4Cre*-targeted cells grows as HF SC and SC-like cells of the IFE, persist and actually expand in aged murine skin. These conclusions are supported by the findings that the progeny of *CD4Cre*-targeted cells possess the quiescent SC-like behaviour of LRC in mice [223, 246-248] and that also human skin contains CD4$^+$ epidermal SC-like cells [247, 248] that show high CFE (Figure 56) as a typical SC characteristic of human bulge SC [86] and human IFE SC [91]. Thus, temporal restrictions or limited growth capacities of the *CD4Cre*-targeted cells or their offspring in adult mice have to be excluded as reasons for the absence of spontaneous BCC development in *Ptch$^{fl/fl}$ CD4Cre* mice. However, the latter observation might be explained by the small quantity of simultaneous *CD4Cre*-mediated recombination events leading to a very low number of *Ptch*-mutant cells that remain below a critical tumour-inducing cell number.

6.1.2 *Patched*-mutant descendants of *CD4Cre*-expressing basal cell carcinoma precursors do not spread like their wild type *Patched* counterparts

To determine the number of the epidermal progeny of *CD4Cre*-targeted cells that persist as basal IFE cells and HF cells and thus to specify the number of putative BCC precursors, flow cytometric quantification of epidermal isolates from dorsal telogen skin was performed. Although the overall proportion of the basal CD49f$^+$ offspring of *CD4Cre*-expressing cells is small (~0.7%), a non-negligible proportion of bulge (~2.6%) and infundibulum (~9.3%) cells descent from *CD4Cre*-targeted cells in adult mice (Figure 40). Remarkably, although descendants of *CD4Cre*-targeted cells are easily detectable in aged *CD4Cre R26-tdT* dorsal skin (> 22 weeks old), *Ptch* deficient keratinocytes are only hardly detectable in age-matched *Ptch$^{fl/fl}$ CD4Cre* dorsal skin [199]. Nevertheless, an immune cell-mediated suppression/depletion of *Ptch*-mutant keratinocytes has been already excluded since *Ptch$^{fl/fl}$ CD4Cre$^{+/-}$* mice do not show alterations in T cell function (e.g. of cytotoxic T cells) [191, 192] and *Ptch$^{fl/fl}$ CD4Cre$^{+/-}$* mice grafted with wild type *Ptch* BM do not display higher numbers of *Ptch*-mutant keratinocytes compared to *Ptch$^{fl/fl}$ CD4Cre$^{+/-}$* mice [193, 199]. However,

supposedly, cell competition might play a role in the suppression of *Ptch*-mutant keratinocytes in *Ptch*$^{fl/fl}$ *CD4Cre* mice [199]. This kind of process is involved in tissue homeostasis because it guarantees the selection and exclusion of harmful cells by elimination (reviewed in [309]). It also seems to contribute to the differential survival of mutant cells in the human epidermis [310]. Cell competition plays on the one hand a role during tissue maintenance like in the epidermis where less fit *Col17a1*-deficient epidermal basal cells are eliminated when surrounded by a sufficient number of COL17A1^{+} cells [118], but on the other hand also guarantees cancer prevention since for example a defect cell competition of BM-derived T-lymphocyte progenitors and thymus-resident T-lymphocyte progenitors causes T-lymphocyte acute lymphoblastic leukaemia-like phenotype [311]. In mammals, cell competition can lead to different fates for outcompeted cells including (1) apoptosis [312-314], (2) senescence [315] and/or (3) apical extrusions/epithelial defence against cancer (EDAC) [316, 317]. During the process called EDAC normal cells sense and actively eliminate neighbouring transformed/mutated cells via cytoskeletal proteins (filamin and vimentin) (reviewed in [309]). One major prerequisite for this is that the genetically altered cells are surrounded by wild type cells [318] which is most likely the case for *Ptch*-mutant keratinocytes in *Ptch*$^{fl/fl}$ *CD4Cre*$^{+/-}$ mice. Furthermore, since also other organs contain small numbers of non-haematopoietic progenies of *CD4Cre*-targeted cells (Figure 13 and Figure 14), from which some can give rise to tumours upon Ras signalling activation (e.g. lung cancer, cartilage tumours, Table 3) [171, 174-177], but not upon *Ptch* depletion [193], isolated *Ptch*-mutant cells may be suppressed in other organs, too. On cellular level, this hypothesis would imply that a *Ptch* mutation results in 'unfit' cells that are eliminated by surrounding wild type cells independently of the tissue, whereas mutations in the Ras signalling pathway induce super-competition, in which a clone of transformed cells outcompetes wild type neighbours leading to tumour formation. Moreover, it should be noticed that global *Ptch*/*PTCH* mutation and thus active HH signalling (e.g. in Gorlin syndrome patients or heterozygous *Ptch* KO mice) induces tumours (e.g. lung cancer [182]) as well as skeletal defects [319] and thus the low number of *Ptch*-mutant descendants in *Ptch*$^{fl/fl}$ *CD4Cre*$^{+/-}$ mice remains under a critical tumour-inducing cell number, although *Ptch* depletion is associated with formation of those tumours/defects.

Remarkably, treatment of *R26-LacZ Ptch*$^{fl/fl}$ *CD4Cre*$^{+/-}$ skin with DMBA/TPA increases the probability to detect LacZ^{+} *Ptch* mutant epidermal cell clusters in individual HF and IFE and also induces BCC development [193, 199]. These observations indicate that the chemicals either confer a survival benefit of the rare *Ptch*-mutant keratinocytes in *Ptch*$^{fl/fl}$ *CD4Cre*$^{+/-}$ skin (due to an accumulation of further oncogenic mutations) or prevent processes like apoptosis, senescence or apical extrusions/EDAC, which avoids the elimination of *Ptch* deficient cells. In the two-stage skin carcinogenesis DMBA/TPA protocol, 'initiation' occurs following a single

dose of a carcinogen (the polycyclic aromatic hydrocarbon DMBA) and 'promotion' by the repeated application of a tumour promoting agent (the phorbol ester TPA) (reviewed in [320]). The carcinogen DMBA mostly induces activating mutations in codon 61 of the *Hras* gene that is found in over 90% of DMBA/TPA-induced papilloma and carcinoma [195, 196]. Nevertheless, aberrant Ras signalling apparently does not play a role in DMBA/TPA-induced *Ptch*$^{fl/fl}$ *CD4Cre* BCC, because these tumours do not harbour the *Hras* G61L mutation [193]. TPA treatment reduces the number of quiescent LRC in HF and induces cell division of basal IFE, SG and HF cells [222]. However, the TPA-induced increased proliferation rate does not induce an augmented occurrence of descendants from *CD4Cre*-targeted cells [246, 248]. DMBA/TPA treatment also mediates the disruption of physiological apoptotic responses and downregulates *Tp53* expression [321]. Therefore, these chemicals might have abrogated apoptotic processes in *Ptch*$^{fl/fl}$ *CD4Cre*$^{+/-}$ skin, which normally would erase isolated *Ptch*-mutant cells. Consequently, DMBA/TPA-treatment enables detection of *Ptch* mutant epidermal cell clusters in individual HF and IFE of *R26-LacZ Ptch*$^{fl/fl}$ *CD4Cre*$^{+/-}$ skin [199]. Subsequently, *Ptch* mutant epidermal cells can multiply, accumulate additional mutations and are predisposed to BCC development. Fitting to this assumption, cyclopamine (HH antagonist) administration that is accompanied by Fas upregulation, which augments apoptosis, reduces the formation of UV light-induced BCC in heterozygous *Ptch* KO mice by ~66% [322], indicating apoptosis as an important process to prevent BCC formation.

Since wounding/wound healing is also a process associated with tumour 'promotion' (reviewed in [320]) and can initiate or accelerate the initiation frequency and growth of BCC-like lesions [197, 198], the tumour-promoting effect of wounds on *Ptch*$^{fl/fl}$ *CD4Cre* skin was investigated but did not result in BCC formation [193]. This result is even more remarkable since the results of this thesis show that the wild type *Ptch* progeny of *CD4Cre*-targeted cells comprises SC of the HF bulge and the uHF as well as basal cells of the IFE, which are known to contribute to wound healing [66, 69, 74, 79]. Moreover, the wild type *Ptch* progeny of *CD4Cre*-targeted cells multiply upon epidermal wound healing (Figure 37), indicating that an increased proliferation and/or *de novo CD4Cre*-mediated recombination in epidermal keratinocytes is not sufficient for inducing BCC development in *Ptch*$^{fl/fl}$ *CD4Cre* mice. However, TPA treatment was shown to cause the release of pro-proliferative and chemotactic factors including TNFα [323] and thus initiates bulge SC activation but without any sign of apoptosis [222]. Contrary to this, wounding is accompanied by apoptosis and secretion of the apoptosis signal-regulating kinase 1 protein that leads to recruitment and activation of macrophages that in turn initiate WIH-A by activating bulge SC via TNFα signalling [255, 256]. The wound-induced apoptosis might result in elimination of *Ptch* deficient 'unfit' epidermal cells by surrounding wild type cells, whereas the prevention of apoptosis by DMBA/TPA might lead to the survival of *Ptch*-mutant cells.

Histologically, homozygous *Ptch* mutation in HF SC populations (sHG, bulge or uHF) leads to the formation of BCC-like lesions that are associated with the compartment of their *Ptch* mutated ancestor (bulge or uHF isthmus) [197, 200], whereas *Ptch* depletion in all basal IFE and HF ORS cells induces spontaneous BCC development that originate from IFE and HF structures [197, 203]. Intriguingly, BCC of DMBA/TPA-treated *Ptch*$^{fl/fl}$ *CD4Cre* skin exclusively occur at the IFE in HF-near regions but never grow as tumours of the HF bulge [199] (Figure 7). Since TPA treatment induces sHG cells to migrate from the HF into the IFE [197], the chemical treatment may preferably induce BCC development from IFE cells. Moreover, a similar effect is known for wounding because *Ptch*-mutant Lgr5^{+} sHG/lower bulge SC develop HF-associated BCC in unwounded skin, but multiple IFE- and infundibulum-associated BCC in wounded skin [197]. Nevertheless, BCC of DMBA/TPA-treated heterozygous *Ptch* KO mice arise from HF and IFE structures [199], suggesting that the origin of DMBA/TPA-induced BCC is not determined by the chemical treatment but, rather, by the compartment of the genetically targeted cell type. Accordingly, in this work basal IFE cells of the infundibulum have been identified as CD4^{+} ancestors of *CD4Cre*-targeted epidermal keratinocytes and therefore might be the origin of *Ptch*$^{fl/fl}$ *CD4Cre* BCC. Indeed, infundibulum-associated neoplasms have been identified as manifestations of human BCC and are connected to the epidermis [324].

6.1.3 Concluding remarks on basal cell carcinoma development and treatment in light of the new data

The results of this thesis show that the progeny of *CD4Cre*-targeted cells grows as known BCC precursors such as K5^{+} basal infundibulum cells (~9.3%) and CD34^{+} bulge cells (~2.6%) in adult murine skin. Intriguingly, homozygous *Ptch* deletion, and thus HH signalling activation, in *CD4Cre*-targeted cells (e.g. infundibulum cells) lead to their eradication under physiological conditions [199] (Figure 57 A). Supposedly, a cell competition mechanism that is an important safety tool to prevent cancer formation by eradicating single-mutated cells is implicated in this process. Nevertheless, the inhibition of such safety mechanisms, e.g. by inhibiting apoptosis via DMBA/TPA treatment, allows single-mutated cells to accumulate further mutations and eventually induce tumour formation (Figure 57 B). Considering the histological occurrence of the *Ptch*$^{fl/fl}$ *CD4Cre* BCC [199] and the data demonstrating that the CD4-expressing ancestors most likely are infundibulum cells the BCC precursors can be mapped as basal cells of the infundibulum.

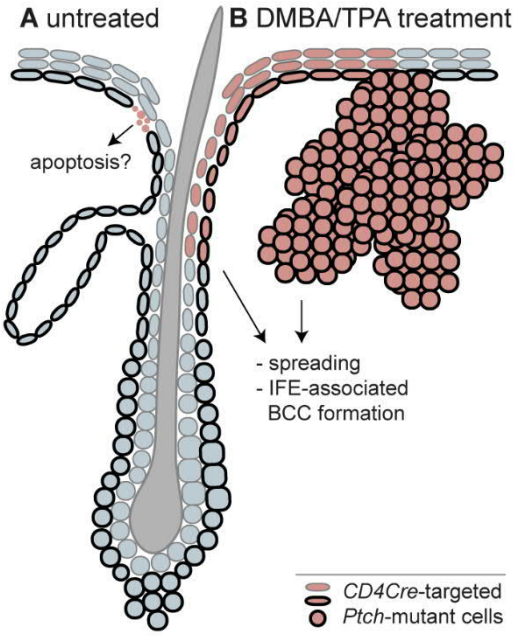

Figure 57. Schematic representation of *Ptch*$^{fl/fl}$ *CD4Cre*$^{+/-}$ dorsal skin.

(A) The initial *CD4Cre* activity occurs most probably in basal cells of the infundibulum. However, *Patched* (*Ptch*) mutant cells are almost undetectable, since they may be recognized by neighbouring cells and eradicated e.g. by apoptosis. **(B)** Upon 7,12-dimethylbenz[a]anthracene/12-O-tetradecanoylphorbol-13-acetate-treated (DMBA/TPA) treatment the progeny of *CD4Cre*-targeted *Ptch*-mutant cells persists, proliferates and repopulates the interfollicular epidermis (IFE) and hair follicles. Moreover, probably due to the accumulation of further mutation(s), basal cell carcinoma (BCC) that are associated to the IFE arise [193, 199].

One major statement from revealing the precursor of *Ptch*$^{fl/fl}$ *CD4Cre* BCC is that the homozygous *Ptch* mutation in isolated basal IFE cells and HF SC is not sufficient for BCC development (this work, [193, 199]). This conclusion is highly relevant with regard to the current BCC therapy based on HH signalling inhibitors since these treatments do not target secondly accumulated mutations although several lines of evidence hint towards remaining, therapy-resistant BCC cells that switch their expression signature. Thus, it was shown that treatment of *Ptch/Tp53*-mutant BCC with the HH signalling inhibitor vismodegib results in a cell identity switch from a HF bulge to a uHF/IFE signature of the residual BCC cells [325]. In humans, inhibition of HH signalling for treatment of BCC can lead to the development of BCC-adjacent cutaneous SCC [326-328], which show decreased HH but increased Ras/MAPK signalling [329]. However, the genetic differences of pre-treatment BCC and post-treatment cutaneous SCC are only minor (3%) [329]. Thus, mutations associated with cutaneous SCC development (e.g. in effectors of the Hippo-YAP pathway and in MYCN) [330-333] have also been identified in BCC [334]. Actually, in a study including 293 human BCC samples, apart from mutations in the HH pathway genes *PTCH* (73%), *SMO* (20%) and *SUFU* (8%) and the tumour suppressor *TP53* (61%), 85% of BCC also possess additional mutations in cancer-related genes, such as in *LATS1* (8%), a component of the Hippo-YAP pathway, *MYCN* (30%) or Ras family members (2%) [335]. All together, these facts suggest, that an effective BCC therapy should include the targeting of secondly accumulated mutations, which however

would require the knowledge about all mutations of the respective tumour. Alternatively, it would be also conceivable to include the pharmacologically restoration of apoptotic signalling pathways in anti-BCC therapies since BCC often possess mutations associated with misregulating apoptosis, such as mutations in *TP53* [336], in *MYCN* [337] or in components of the Hippo-YAP pathway [338]. However, the data of this thesis clearly demonstrate that BCC models such as *Ptch*$^{fl/fl}$ *CD4Cre* mice will not only allow to investigate BCC-initiating events beyond HH signalling activation, but also to develop new treatment options against BCC.

6.2 The putative role of CD4-expressing stem cell-like cells in the skin

Apart from the discovery of the cellular origin of *Ptch*$^{fl/fl}$ *CD4Cre* BCC, this thesis also questions the role of non-haematopoietic CD4$^+$ SC-like cells in murine and human skin and, consequently, the function of the CD4 protein on different non-haematopoietic SC-like cells (e.g. epidermal SC, BM-derived MSC and fibroblasts). If one wants to understand the role of CD4-expressing non-haematopoietic SC-like cells in the skin, it is also relevant to know when these cells appear or rather start to express *Cd4*/CD4. As already mentioned, *CD4Cre* activity in *CD4Cre R26-tdT* mice and thus *Cd4*/CD4 expression mainly occurs in adult skin. This can be assumed since during development and in the skin of young mice no or only isolated descendants of *CD4Cre*-targeted cells were detectable, respectively, whereas in aged murine skin numerous HF and huge clones in the IFE descent from *CD4Cre*-targeted cells. Since the IFE clones that descent from *CD4Cre*-targeted cells expand during skin ageing, proliferation of the progeny of *CD4Cre*-expressing cells that leads to growing clone size of the epidermal tdT$^+$ patches can be assumed. Besides, also the progeny of *CD4Cre*-targeted cells that persists as HF SC of the bulge are activated and start to proliferate during telogen-to-anagen transitions, probably induced through TNFα signalling activation by macrophages that is known to provoke anagen initiation during homeostatic hair cycling, after hair pluck injury and WIH-A [252-256]. However, the proliferation of progenies of *CD4Cre*-expressing cells cannot explain the repopulation of adjacent HF or distant epidermal patches with tdT$^+$ cells (Figure 39). Thus, additionally to proliferation of already existing progeny of *CD4Cre*-expressing cells also *de novo* recombination at the *R26-tdT* locus in epidermal cells due to *CD4Cre* activity has to be assumed. Indeed, the occurrence of CD4$^+$ infundibulum cells in anagen skin in comparison to the few CD4$^+$ infundibulum cells during telogen (Figure 42) suggests *CD4Cre* expression and thus *de novo* recombination in adult *CD4Cre R26-tdT* mice during specific hair cycle phases. Since the number of tdT$^+$ HF multiply upon epidermal wound healing (Figure 37) and with cumulative hair cycle phases (Figure 39 and Figure 40), telogen-to-anagen transitions (either endogenous or WIH-A) seem to play an important role in the occurrence of descendants of

CD4Cre-expressing cells in individual HF (e.g. by inducing CD4 promoter activity and/or *CD4Cre* expression). Interestingly, HF that contain descendants of *CD4Cre*-targeted cells cluster together (Figure 39), suggesting that a local event (e.g. an injury, inflammation, infection or micro traumata) is the cause for *Cd4*/*CD4Cre* expression in HF SC or the recruitment of the progeny of *CD4Cre*-targeted cells to HF (e.g. from other HF, the adjacent IFE or BM-derived MSC). It should be considered that in adult mice (> 2nd hair cycle phase) telogen-to-anagen transitions can hardly be predicted and when they occur it results in patches of hair growth (that become smaller during ageing) and thus can be assumed as a local event, too [339, 340]. Indeed, analysis of hair cycling revealed a collective, population-level regenerative/growth behaviour for HF [340]. Accordingly, neighbouring HF communicate with each other during telogen-to-anagen transitions and exchange growth-inducing signals [341]. Thus, future studies should investigate the proposed *Cd4*/*CD4Cre* expression in epidermal keratinocytes and the potential recruitment of the progeny of *CD4Cre*-targeted cells to HF in response to treatment with molecules that are produced in the skin during telogen-to-anagen transitions and/or after injuries. Several growth factors and cytokines participate in wound healing and induce proliferation and/or migration of keratinocytes, but the major contributors are: EGF, FGF-2, TGF-β, PDGF, VEGF, IL-1, IL-6 and TNFα (reviewed in [342]). Interestingly, several of those molecules are also associated with telogen-to-anagen transitions and/or induce proliferation of epidermal SC. As already mentioned, TNFα signalling activation by macrophages is sufficient to induce telogen-to-anagen transitions [255]. Besides, IL-1 secretion from keratinocytes indirectly (through γδT-cells) stimulates epidermal SC proliferation [343]. Remarkably, IL-1, but not TNFα, induces expression of *Cd4* transcripts in microglia [344]. However, FGF-1, FGF-2, FGF-10 [345] and PDGF [346] induce anagen entry and thus hair growth. Similarly, VEGF leads to increased proliferation of HF ORS cells [347]. On the contrary, *Il-6* expression is dispensable for anagen entry and HF growth [255], whereas EGF and TGF-β promote the transition to catagen [47]. Thus, it is likely that TNFα, IL-1, members of the FGF family, PDGF or VEGF might induce *Cd4*/CD4 expression in epidermal keratinocytes. Therefore, it should be analysed whether the mentioned signalling molecules can induce *Cd4*/CD4 expression (e.g. via qRT-PCR and/or Western blot) and/or migration of basal keratinocytes (e.g. primary keratinocytes cultured under growth conditions for basal epidermal cells) after incubation with the respective molecules. Moreover, if primary epidermal cells isolated from *CD4Cre R26-tdT* mice are used, the induced *Cd4*/*CD4Cre* expression can be easily recognized through the *de novo* recombination at the *R26-tdT* locus and thus tdT protein expression. Finally, candidate molecules could also be applied (topical or intradermal injections) on the skin of *CD4Cre R26-tdT* mice and a putative increased occurrence of the progeny of *CD4Cre*-targeted cells (tdT^{+}) in the epidermis can be analysed. However, independent of the stimulus that induces CD4 expression in non-haematopoietic SC-like cells

of the skin knowledge about the identity and behaviour of those cells might help to unravel their putative role in skin maintenance.

6.2.1 CD4-expressing epidermal cells of the infundibulum

The results of this thesis show that the $CD4^+$ ancestor of the IFE and HF descendants most probably are infundibulum cells (see chapter 5.2.7 and 5.2.8) which also represents the origin of IFE-associated BCC in *Ptch*$^{fl/fl}$ *CD4Cre* skin [199]. The infundibulum that connects the IFE and HF is assumed as a subpopulation of IFE cells, although infundibulum cells express low levels of HF marker genes [11]. In accordance to its morphological continuity to the IFE, the infundibulum represents only a weak barrier to the external milieu but also has a specialized immune system and defence (e.g. it contains MHC class I^+ antigen-presenting ORS keratinocytes, MHC class II^+ Langerhans cells, numerous T-lymphocytes and various antimicrobial peptides, reviewed in [348]). Transcriptionally the expression pattern of keratinocytes of the infundibulum has been described as a basal IFE signature together with low levels of uHF, bulge and pan-HF markers (e.g. *Krt79, Postn* and *Sostdc1*, respectively) [11]. In fact, the expression profile of $CD49f^+CD34^+Sca\text{-}1^+$ epidermal cells that also comprise progeny of *CD4Cre*-targeted cells matches the signature of infundibulum cells (Figure 26). However, although putative protein markers to distinguish the infundibulum from other epidermal keratinocytes have been suggested (e.g. Sprr1, K17, cystatin 6, Sca-1 and K79), these proteins are also expressed by other populations of the HF or IFE (reviewed in [348]). Noteworthy, $MKI67^+$ proliferative active cells were identified in the infundibulum of anagen HF (Figure 47) and telogen HF [65, 69] and supportive to that also *Mki67* expression was detected in $CD49f^+CD34^+Sca\text{-}1^+$ infundibulum cells of telogen skin (see chapter 5.2.2), indicating that infundibulum cells proliferate independently of the hair phase. Moreover, infundibulum cells proliferate faster than cells of the IFE [349] suggesting a unique proliferative behaviour for them. Actually, cultivation of basal infundibulum cells confirmed their special proliferative behaviour since they survived longer when compared to basal IFE cells, although they are thought to belong to the IFE compartment as they express basal IFE marker proteins (e.g. Sca-1, K14) (see chapter 5.2.9). Nevertheless, due to the lack of specific infundibulum markers, little is known about these cells including their capacities during homeostasis or regeneration. Remarkably, long-term clonal analysis revealed that uHF cells (*Lrig1CreER*^{T2} deleter) maintain the uHF and SG as well as the infundibulum, but contribute to neither the HF nor the IFE, which are assumed to be maintained by distinct SC populations [69]. These data indicate that the upward movement of uHF SC replenishes the infundibulum. However, *Cd4*/CD4 expression was only detectable in infundibulum cells (see chapter 5.2.7 and 5.2.8) but their descendants appear in the IFE and in HF indicating that a subpopulation of infundibulum cells, supposedly with CD4/*CD4Cre* expression, can give rise to cells of both

compartments. At least cultured infundibulum cells expressed Sox9 (Figure 51), a HF SC marker of the bulge region, indicating a putative switch of their lineage identity from IFE to HF-like cells. Since infundibulum cells express marker of the IFE (e.g. *Ly6a*/Sca-1, *K14*/K14) and of the HF (e.g. *Sostdc1*, *Aqp3* and *Fst*) [11], a contribution of CD4/*CD4Cre*-expressing infundibulum cells to both compartments are indeed conceivable. Accordingly, tracing of the descendants of $K14^+$ uHF cells (*K14CreER* deleter) showed that occasionally progeny cells extended not only into the infundibulum but also into the IFE [30]. Furthermore, treatment with an IFE proliferative stimulus lead to an expansion of uHF progeny cells into the infundibulum and IFE [30]. Although a contribution of uHF cells to the IFE during homeostasis depends on the considered study [30, 69], pulse labelling of infundibulum cells (with two different nucleotides based on the distinct cell cycle length of infundibulum cells) demonstrated an emigration of infundibulum cells into the IFE [349]. Moreover, the restricted *Cd4*/CD4 expression in infundibulum cells but the occurrence of their descendants in the IFE further hints towards the involvement of infundibulum cells (that derive from the uHF) to the maintenance of the IFE. Remarkably, for other epidermal SC populations a high degree of plasticity has been reported since in skin reconstitution assays and similarly during wound healing, HF SC (of the bulge, sHG, uHF) show their potential to give rise to all epidermal lineages of the HF, SG and IFE (see chapter 1.2.5). In this process, HF SC can enter a transient state of ‘lineage infidelity’ characterised by a mixed HF/IFE molecular profile in response to injury or culture [80, 258] and that is similar to that of infundibulum cells. For instance, single-cell transcriptome studies of cells from murine wounded skin showed that $Lgr5^+$ sHG cells gradually lose their sHG/bulge identity and instead upregulate an interfollicular identity while migrating through the uHF to the IFE [81]. Accordingly, superficial burn wounds (second-degree) and small deep wounds (third-degree) that destroy the IFE but leave adjacent HF intact can heal spontaneously by migration of HF cells, whereas large deep burn wounds in which also closed-by HF are destroyed cannot re-epithelise [350], emphasizing the important role of HF SC in IFE regeneration. Nevertheless, although $CD34^+$/$K15^+$ bulge SC are indispensable for HF and HS formation, as death of $K15^+$ bulge cells leads to hair loss and destroyed HF, but the epidermis survives, indicating that HF SC of the bulge are not required for IFE maintenance [74]. However, another example of the HF SC plasticity is that depletion of $Lgr5^+$ sHG cells that prevents hair growth, is rescued by $CD34^+$ bulge SC [351]. Thereby $CD34^+$ bulge SC start *Lgr5* expression most likely in response to altered niche signals and restore the lower bulge and sHG [351]. This most properly is explained by the idea that sHG SC derive from bulge SC during hair cycling [44, 45]. Nevertheless, not only depletion (via laser ablation) of the sHG but also of the putative ancestor bulge leads to the complete recovery of the lost cell population [352]. Remarkably, after laser ablation of the bulge not only sHG cells proliferate and contribute to the ‘new’ bulge, but also infundibulum cells restore the

bulge region [352]. Intriguingly, the infundibulum-derived 'new' bulge cells subsequently change to LRC (characteristic of bulge cells; although infundibulum cells are normally proliferative active, see above) and participate in the subsequent hair growth [352]. These findings elegantly show that loss of epidermal cells due to injury can induce not only HF SC (of the bulge, sHG, uHF), but also IFE-associated cells of the infundibulum to contribute to another epidermal niche and to switch their lineage identity. Moreover, these data highlight the high degree of plasticity of skin SC and lead to the assumption that niche factors are responsible for shaping the respective SC identity. The importance of niche factors that govern continued self-renewal or differentiation is also described for other SC populations, such as ESC, which retain their pluripotency when injected into the embryonic inner cell mass but are also capable to differentiate into cells of all three germ layers (reviewed in [353]). Furthermore, niches for multipotent SC have been identified in various adult tissues, for instance the HSC niche in the BM, the intestinal crypt niche and the subventricular zone as a neural SC niche of the brain (reviewed in [354]). Anyway, further studies are needed to unravel whether $CD4^+$ infundibulum cells are capable to give rise to keratinocytes of the IFE and/or the HF compartments (e.g. bulge, sHG, uHF), therefore skin reconstitution assays should be performed. A suitable assay for this purpose is intradermal grafting of fluorescent-labelled (e.g. GFP^+ cells isolated from transgenic mice, see chapter 6.1) FACS-isolated $CD4^+$ $CD49f^+CD34^+Sca\text{-}1^+$ infundibulum cells together with neonatal epidermal keratinocytes and neonatal dermal fibroblasts into the skin of immunocompromised nude mice (*Foxn1*^{nu}) [296]. The capacity of $CD4^+$ infundibulum cells to differentiate into keratinocytes of the IFE and/or HF would then be observable by the *de novo* formation of fluorescent-labelled HF and IFE at the injection side. Besides, excisional wounding in lineage-tracing mice allows for determination of a contribution of tracked cells to newly formed IFE after re-epithelisation and secondly to wound-induced HF neogenesis. For this approach, the inducible lineage tracing mouse *CD4CreER*^{T2} *R26-tdT* could be used after confirmation of a successful recombination in infundibulum cells (but not in bulge, uHF, basal IFE cells). Therefore, tamoxifen application in 5-week-old mice might be appropriate due to the assumed *Cd4* expression in infundibulum cells at this age (Figure 46). However, the differentiation capacity of FACS-isolated ($CD4^+$) $CD49f^+CD34^+Sca\text{-}1^+$ infundibulum cells can also be tested *in vitro* by increasing the Ca^{2+} concentration of the medium (above 0.1 mM Ca^{2+} for 2 days) and a subsequent antibody staining against epidermal differentiation marker of the suprabasal cell layers (e.g. K1, K10). However, this kind of experiment only hints towards the capacity of cells to differentiate into IFE layer cells and thus to potentially contribute to epidermal stratification, whereas HF reconstruction *in vitro* is still challenging due to the complex interaction between mesenchymal DP fibroblasts and HF SC (and so far only successful when using embryonic skin cells) (reviewed in [355]). Therefore, *in vivo* skin reconstitution assays are more promising.

Nevertheless, alternatively, it may be that the putative contribution of $CD4^+$ BM-derived MSC to the IFE and/or HF or hitherto unknown $CD4^+$ SC/keratinocytes exist in the murine skin that might explain the discrepancy between the epidermal $CD4^+$ infundibulum cells and the progeny of *CD4Cre*-targeted cells in the IFE and HF. Indeed, some of the data shown in this work suggest a possible existence of $CD4^+$ HF bulge cells (Figure 42, Figure 49), although other experiments did not support this hypothesis (Figure 44, Figure 46).

6.2.2 The putative function of the CD4 receptor on non-haematopoietic stem cell-like cells

Remarkably, the fact that none of the non-haematopoietic $CD4^+$ cell types (e.g. epidermal SC, BM-derived MSC and fibroblasts) express the T-lymphocyte receptor CD3 suggests a TCR/CD3-independent function of the CD4 protein in these cells. Interestingly, TCR/CD3-independent CD4 signalling is also described in T-lymphocytes in which a dimerisation of CD4 molecules or the ligation of CD4 and MHCII molecules increases intracellular Ca^{2+} levels and decreases intracellular cAMP levels via inhibition of the adenylate cyclase and induction of the phosphodiesterases type 1 and 4 [159]. In addition, CD4-MHCII ligation in TCR/$CD3^{neg}$ monocytes induces their differentiation to macrophages [157]. Moreover, the CD4 ligand IL-16 (or lymphocyte chemoattractant factor) has been shown to also induce Ca^{2+} flux and migration of inactivated T-lymphocytes and monocytes [356, 357]. Actually, numerous skin cell types express IL-16 and keratinocytes of the IFE and the uHF can express MHCII molecules in response to microbiota [358]. Thus, similarly to T-lymphocytes or monocytes a TCR/CD3-independent activation of CD4 signalling that regulates Ca^{2+} flux is also conceivable for $CD4^+$ epidermal keratinocytes.

In fact, Ca^{2+} levels regulate keratinocyte differentiation. In healthy human and murine skin, the Ca^{2+} levels are low in the basal layer, which keeps keratinocytes proliferating. However, in the more differentiated, less proliferative granular layer the Ca^{2+} level increases to a maximum and drops to a minimum in the *stratum corneum* [359, 360]. Similarly, in primary keratinocyte culture low Ca^{2+} concentrations (0.05-0.1 mM) mediate rapid proliferation and prevent stratification, whereas higher Ca^{2+} concentrations (up to 1.2 mM) inhibit cell proliferation and induce terminal differentiation [270]. Actual known mechanisms underlying the Ca^{2+}-induced differentiation of keratinocytes include desmosome formation (for mechanical strength and to provide a signalling complex) [361, 362] and activation of calcium-responsive promoters as of the *activator protein 1* gene those protein is suggested to activate marker genes of keratinocyte differentiation like *Involucrin* and *K1* [363-365].

Interestingly, the β2 adrenoreceptor (ADRB2) has been recently identified in yeast-two hybrid screens as a novel putative CD4-interaction partner [366, 367]. In fact, this transmembrane receptor is also expressed on keratinocytes and its activation by norepinephrine and/or

epinephrine has been shown to induce increased intracellular Ca^{2+} concentrations [368] and expression of the differentiation markers K1 and K10 *in vitro* [369]. Thus, Schallreuter and colleagues suggested that epinephrine, produced by basal layer keratinocytes activate ADRB2 signalling in upper epidermal layers to increase their intracellular Ca^{2+} level and thus induce keratinocyte differentiation [370]. Besides, norepinephrine/ADRB2 signalling is also involved in stress-induced hair greying due to depletion of melanocyte SC [131]. These reports indicate that ADRB2 activation on epidermal SC causes their differentiation and subsequent loss.
In fact, the comparative transcriptome and scRNAseq analyses conducted within this thesis verified the *Adrb2* expression in different epidermal populations in murine anagen and telogen dorsal skin (Appendix D). Thus, *Adrb2* is highly expressed in basal keratinocytes of the IFE and in infundibulum cells, but lowly in HF bulge cells (Appendix D). Additionally, basal cycling IFE cells, which represent the *Cd4*-expressing population (Figure 46), also express *Adrb2* transcripts (Appendix D). *Adrb2* expression is also described for $nestin^+$ MSC and its overexpression is associated with unilateral anterior crossbite-induced condylar subchondral bone loss and cartilage degradation, whereas *Adrb2* deletion attenuates this phenotype [371]. All together, these data indicate that *Cd4*/CD4 and *Ardb2*/ADRB2 are co-expressed in the same epidermal and/or stromal cell type(s) and potentially (as indicated by the yeast-two hybrid assay) interact. In conclusion, a TCR/CD3-independent activation of CD4 signalling (e.g. via MHCII ligation or epinephrine activation of the putative interacting partner ADRB2) that regulates Ca^{2+} flux and subsequently induces differentiation is conceivable for $CD4^+$ epidermal keratinocytes.

6.2.3 Concluding remarks on the putative function of CD4-expressing stem cell-like cells of the skin and their putative relevance to medical applications

Based on the facts discussed in this chapter a hypothesis for the role of the CD4 protein in non-haematopoietic SC-like cells (e.g. epidermal SC and/or BM-derived MSC) was formulated. Within this hypothesis, a local event such as an injury leads to a spatial restricted anagen entry that induces proliferation (and migration). Subsequently, the proliferative active epidermal cells (e.g. infundibulum cells) express CD4 to achieve susceptibility to extracellular signalling molecules (e.g. MHCII ligation or epinephrine activation of the putative interacting partner ADRB2) (Figure 58 A). Activation of CD4 signalling then induces differentiation (e.g. via Ca^{2+} flux) (Figure 58 B). Dependent on the niche signals, differentiation of multipotent HF SC (that might derive from infundibulum cells) into keratinocytes of different HF lineages to guarantee HF growth and/or of basal cells into suprabasal layer keratinocytes for IFE maintenance or even re-epithelisation after tissue damage occurs. However, future studies are needed to

evaluate this hypothesis, for example by MHCII incubation of $CD4^+$ non-haematopoietic cells and following analyses of Ca^{2+} flux, proliferation rate and expression of differentiation marker.

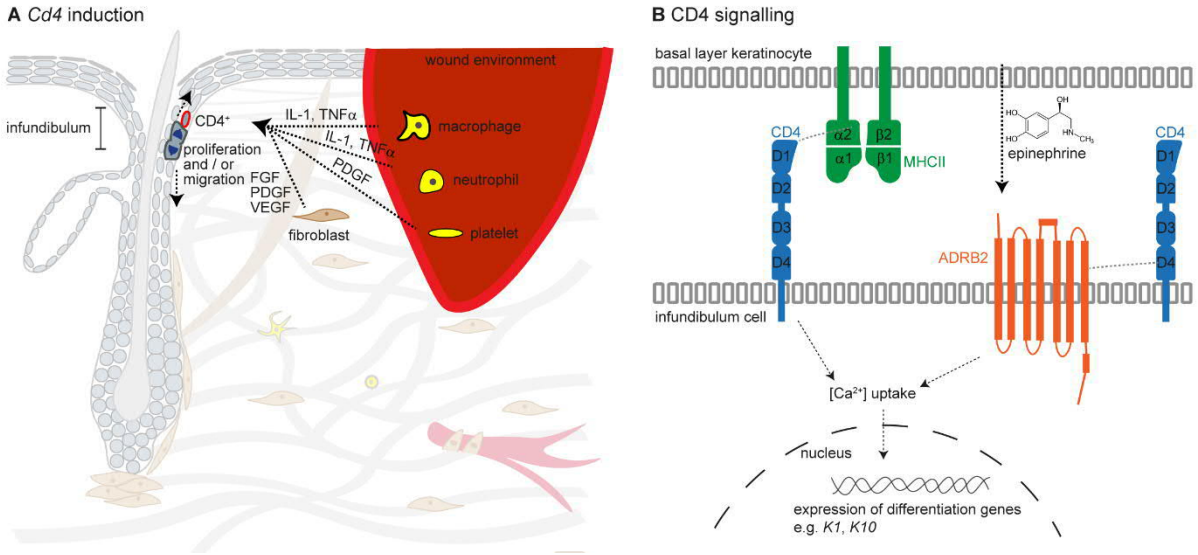

Figure 58. Schematic presentation of proposed models for induction of *Cd4* expression and CD4 signalling in epidermal keratinocytes.

(A) Schematic presentation of wounded skin in telogen phase and wound-induced secretion of growth factors (FGF, PDGF, VEGF) and cytokines (IL-1, TNFα) that are produced by various infiltrating immune cells (e.g. macrophages, neutrophils), platelets and fibroblasts and that participate in wound healing and induce proliferation and/or migration of keratinocytes (reviewed in [342]) and putatively also *Cd4* expression. *Cd4* expression is most probably induced in basal cells of the infundibulum that after proliferation might migrate and contribute to the interfollicular epidermal and/or the hair follicle. **(B)** Schematic presentation of proposed concepts for CD4 signalling in epidermal keratinocytes resulting in their differentiation. Thus, either MHCII ligation or activation of the β2 adrenoreceptor (ADRB2), a putative CD4 interacting partner, might induce calcium (Ca^{2+}) influx, leading to transcriptional changes and keratinocyte differentiation. Abbreviations: FGF: fibroblast growth factor, IL: interleukin, PDGF: platelet derived growth factor, TNFα: tumour necrosis factor alpha, VEGF: vascular endothelial growth factor.

Remarkably, the hypothesized 'lineage infidelity' of ($CD4^+$) infundibulum cells is of high interest due to (1) their proliferative activity, which could allow for tremendous *in vitro* expansion and (2) their proposed plasticity as precursors of IFE and HF lineages, which could allow for differentiation into various epidermal cell types and thus improve skin tissue reconstruction. A comprehensive knowledge about the plasticity of epidermal SC, their possibilities and limitations, and factors that govern their renewal and differentiation is important for clinical applications, such as for the reconstitution of burns, chronic wounds or ulcers. Most commonly, for epithelial reconstitution, skin grafting from unaffected skin is conducted, but the expansion of epidermal SC *in vitro* would reduce the required area of unaffected skin from which to harvest the keratinocytes for culture. Furthermore, as already mentioned, the treatment of genetic skin diseases such as junctional epidermolysis bullosa by transplantation of *in vitro* expanded, genetically modified epidermal SC has been successful and was permitted through long-lived SC [116]. Besides, skin diseases such as psoriasis are associated with uncontrolled proliferation and dysfunctional differentiation of epidermal keratinocytes (caused by a

continuous inflammation), so understanding the physiological control of epidermal SC proliferation and differentiation may also help to develop treatment options that limit uncontrolled hyper proliferation.

Last but not least, the CD4 protein represents the main entry side for HIV infection of host T-lymphocytes [144, 145]. The virus achieves the entrance to the cells through binding of its envelope protein glycoprotein 120 to the D1 domain of the CD4 receptor [148]. Subsequently, a conformational change allows HIV to bind to the co-receptors CC motive chemokine receptor type 5 (CCR5) or CXC motive chemokine receptor type 4 (CXCR4) of the host cell. The structural change in viral protein glycoprotein 41, finally allows the fusion of the viral membrane with the host cell membrane. In light of the role of the CD4 protein in HIV infection, the discovery of non-haematopoietic $CD4^+$ cell populations raises the question whether those are also susceptible to HIV. Nevertheless, CD4 receptor density plays a crucial role in the efficiency of HIV infectivity, as cells with low CD4 expression require high levels of co-receptor for efficient viral infection [372]. However, lung fibroblasts of HIV-patients are also HIV-infected [164] and embryonic [165] and foetal lung fibroblasts [160] as well as human BM-derived MSC [162] are susceptible to HIV infection. Moreover, the human $CD4^+$ keratinocytes of the skin express the chemokine receptor CXCR4, but not CCR5 [247, 248] and thus may represent a previously unknown reservoir for HIV. However, further studies are needed to evaluate whether this comes true. Such experiments should include the *in vitro* expansion of human $CD4^+$ $CD49f^+CD29^+$ epidermal SC-like cells (using the established optimal culture conditions, see chapter 5.3.2.1) followed by HIV infection and replication studies.

7 Appendix

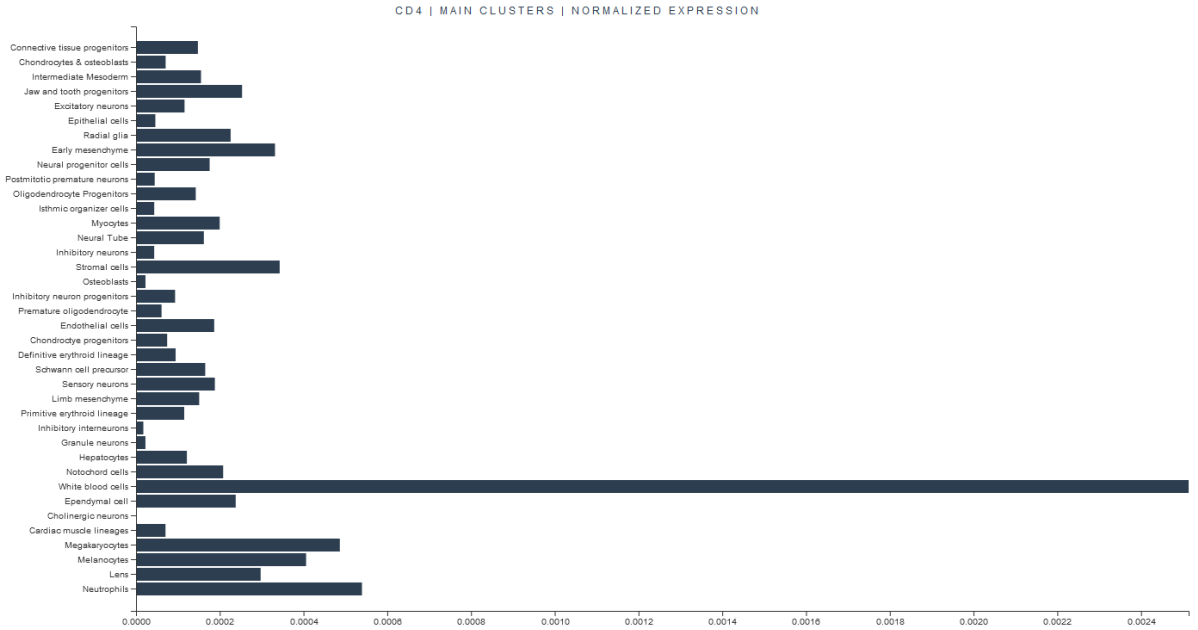

Appendix A. *Cd4* RNA expression in murine embryonic cells derived from 61 embryos staged between embryonic day 9.5 and 13.5.

Data were obtained from single-cell transcriptome analysis of ~2 x 10^6 cells and are available at the 'mouse organogenesis cell atlas' (https://oncoscape.v3.sttrcancer.org/atlas.gs.washington.edu.mouse.rna/genes).

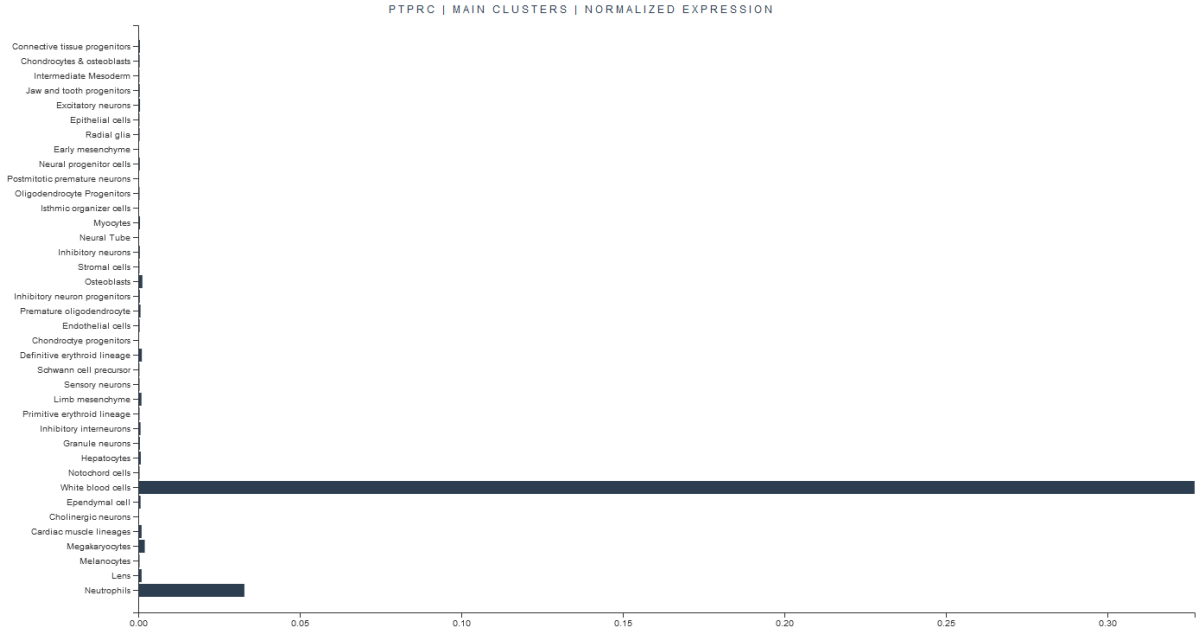

Appendix B. *Ptprc* RNA expression in murine embryonic cells derived from 61 embryos staged between embryonic day 9.5 and 13.5.

Data were obtained from single-cell transcriptome analysis of ~2 x 10^6 cells and are available at the 'mouse organogenesis cell atlas' (https://oncoscape.v3.sttrcancer.org/atlas.gs.washington.edu.mouse.rna/genes). *Ptprc* encodes the leucocyte marker CD45.

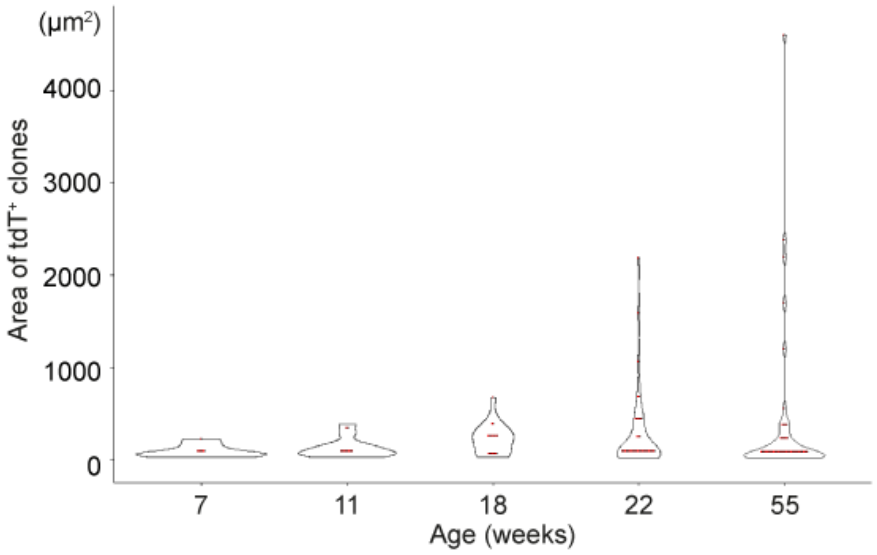

Appendix C. Violin plot representing the area of single tdT-expressing epidermal patches in murine tail skin.

Violin plot that shows the probability density of the data as well as it includes the measured data (red dots) of the tdT⁺ epidermal patches on an epidermal sheet area of ~480,000 µm². Samples were isolated from tail skin of *CD4Cre R26-tdT* mice (for information regarding the measurement see chapter 4.3.6, for details regarding the mice see Figure 39/Table 17).

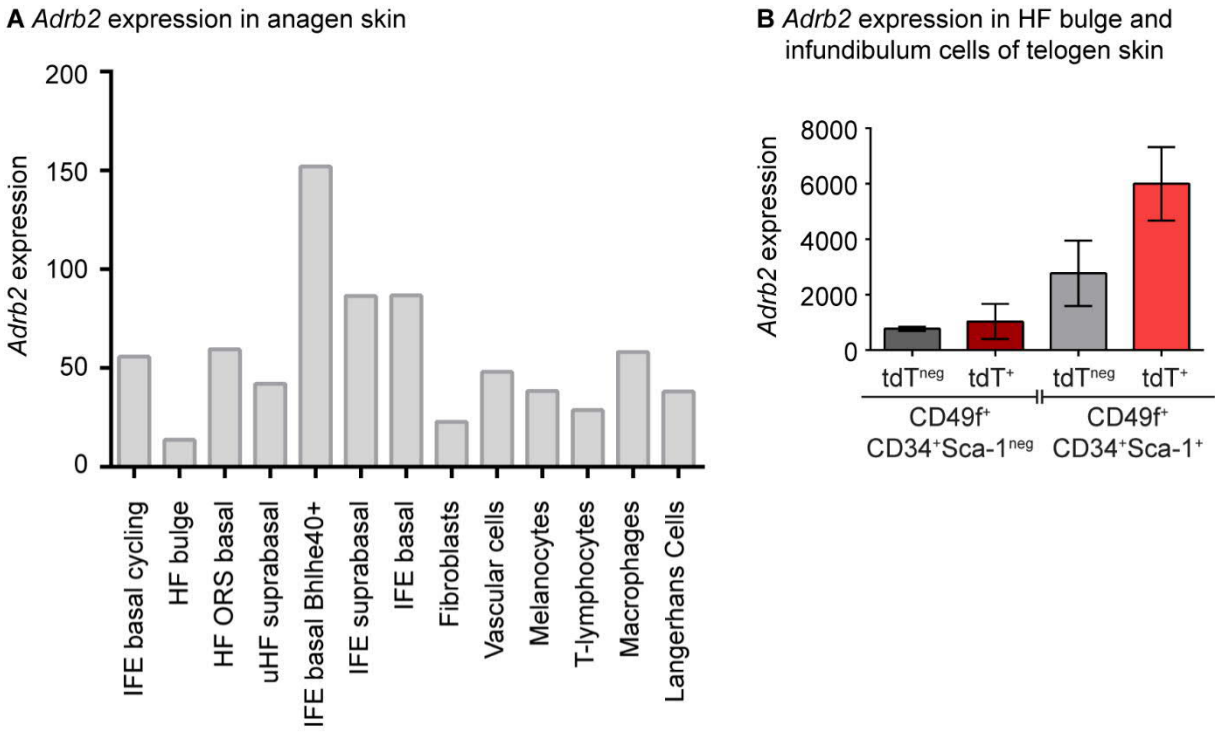

Appendix D. *Adrb2* RNA expression in murine anagen and telogen skin.

Data were obtained from single-cell transcriptome **(A)** or whole transcriptome **(B)** sequencing analyses of epidermal isolates from anagen wild type dorsal skin **(A)** or telogen *CD4Cre R26-tdT* dorsal skin **(B)**. **(B)** FACS-based sorting of the cellular populations: tdT⁺ and tdT^{neg} CD49f⁺CD34⁺Sca-1^{neg} (= HF bulge population) as well as tdT⁺ and tdT^{neg} CD49f⁺CD34⁺Sca-1⁺ (= infundibulum population) was performed as described in chapter 4.5.1. For details regarding the sequencing, see chapter 4.7.5 and 4.7.6.

8 References

1. Garrod, D. and M. Chidgey, *Desmosome structure, composition and function.* Biochim Biophys Acta, 2008. **1778**(3): p. 572-87.
2. Alberts, B.J., A.; Lewis, J.; Raff, M.; Roberts, K.; Walter, P., *Hemidesmosomen*, in *Molecular Biology of the Cell*, G. Science, Editor 2002, Garland Science: New York.
3. Tortora, G.J.D., B., *The Integumentary System*, in *Principles of anatomy and physiology*, I. John Wiley & Sons, Editor 2014, John Wiley & Sons, Inc.: USA.
4. Blanpain, C. and E. Fuchs, *Epidermal stem cells of the skin.* Annu Rev Cell Dev Biol, 2006. **22**: p. 339-73.
5. Lavker, R.M. and T.T. Sun, *Heterogeneity in epidermal basal keratinocytes: morphological and functional correlations.* Science, 1982. **215**(4537): p. 1239-41.
6. Briggaman, R.A. and C.E. Wheeler, Jr., *The epidermal-dermal junction.* J Invest Dermatol, 1975. **65**(1): p. 71-84.
7. Braverman, I.M., *The cutaneous microcirculation.* J Investig Dermatol Symp Proc, 2000. **5**(1): p. 3-9.
8. Potten, C.S., *Epidermal cell production rates.* J Invest Dermatol, 1975. **65**(6): p. 488-500.
9. Gomez, C., et al., *The interfollicular epidermis of adult mouse tail comprises two distinct cell lineages that are differentially regulated by Wnt, Edaradd, and Lrig1.* Stem Cell Reports, 2013. **1**(1): p. 19-27.
10. Rognoni, E. and F.M. Watt, *Skin Cell Heterogeneity in Development, Wound Healing, and Cancer.* Trends Cell Biol, 2018. **28**(9): p. 709-722.
11. Joost, S., et al., *Single-Cell Transcriptomics Reveals that Differentiation and Spatial Signatures Shape Epidermal and Hair Follicle Heterogeneity.* Cell Syst, 2016. **3**(3): p. 221-237 e9.
12. Fuchs, E., *Scratching the surface of skin development.* Nature, 2007. **445**(7130): p. 834-42.
13. Schneider, M.R., R. Schmidt-Ullrich, and R. Paus, *The hair follicle as a dynamic miniorgan.* Curr Biol, 2009. **19**(3): p. R132-42.
14. Slominski, A., et al., *Hair follicle pigmentation.* J Invest Dermatol, 2005. **124**(1): p. 13-21.
15. Schlake, T., *FGF signals specifically regulate the structure of hair shaft medulla via IGF-binding protein 5.* Development, 2005. **132**(13): p. 2981-90.
16. Duverger, O. and M.I. Morasso, *Epidermal patterning and induction of different hair types during mouse embryonic development.* Birth Defects Res C Embryo Today, 2009. **87**(3): p. 263-72.
17. Lechner, S.G. and G.R. Lewin, *Hairy sensation.* Physiology (Bethesda), 2013. **28**(3): p. 142-50.
18. Driskell, R.R., et al., *Sox2-positive dermal papilla cells specify hair follicle type in mammalian epidermis.* Development, 2009. **136**(16): p. 2815-23.
19. Brown, A.G. and A. Iggo, *A quantitative study of cutaneous receptors and afferent fibres in the cat and rabbit.* J Physiol, 1967. **193**(3): p. 707-33.
20. Zotterman, Y., *Touch, pain and tickling: an electro-physiological investigation on cutaneous sensory nerves.* J Physiol, 1939. **95**(1): p. 1-28.
21. Buffoli, B., et al., *The human hair: from anatomy to physiology.* Int J Dermatol, 2014. **53**(3): p. 331-41.
22. Driskell, R.R., et al., *Distinct fibroblast lineages determine dermal architecture in skin development and repair.* Nature, 2013. **504**(7479): p. 277-281.
23. Yang, C.C. and G. Cotsarelis, *Review of hair follicle dermal cells.* J Dermatol Sci, 2010. **57**(1): p. 2-11.
24. Forni, M.F., M. Trombetta-Lima, and M.C. Sogayar, *Stem cells in embryonic skin development.* Biol Res, 2012. **45**(3): p. 215-22.
25. Lechler, T. and E. Fuchs, *Asymmetric cell divisions promote stratification and differentiation of mammalian skin.* Nature, 2005. **437**(7056): p. 275-80.

26. Niemann, C. and V. Horsley, *Development and homeostasis of the sebaceous gland.* Semin Cell Dev Biol, 2012. **23**(8): p. 928-36.
27. Schmidt-Ullrich, R. and R. Paus, *Molecular principles of hair follicle induction and morphogenesis.* Bioessays, 2005. **27**(3): p. 247-61.
28. Snippert, H.J., et al., *Lgr6 marks stem cells in the hair follicle that generate all cell lineages of the skin.* Science, 2010. **327**(5971): p. 1385-9.
29. Nowak, J.A., et al., *Hair follicle stem cells are specified and function in early skin morphogenesis.* Cell Stem Cell, 2008. **3**(1): p. 33-43.
30. Jensen, K.B., et al., *Lrig1 expression defines a distinct multipotent stem cell population in mammalian epidermis.* Cell Stem Cell, 2009. **4**(5): p. 427-39.
31. Gonzales, K.A.U. and E. Fuchs, *Skin and Its Regenerative Powers: An Alliance between Stem Cells and Their Niche.* Dev Cell, 2017. **43**(4): p. 387-401.
32. Blanpain, C. and E. Fuchs, *Epidermal homeostasis: a balancing act of stem cells in the skin.* Nat Rev Mol Cell Biol, 2009. **10**(3): p. 207-17.
33. Simons, B.D. and H. Clevers, *Strategies for homeostatic stem cell self-renewal in adult tissues.* Cell, 2011. **145**(6): p. 851-62.
34. Watt, F.M. and B.L. Hogan, *Out of Eden: stem cells and their niches.* Science, 2000. **287**(5457): p. 1427-30.
35. Amoyel, M., B.D. Simons, and E.A. Bach, *Neutral competition of stem cells is skewed by proliferative changes downstream of Hh and Hpo.* EMBO J, 2014. **33**(20): p. 2295-313.
36. Potten, C.S., R. Saffhill, and H.I. Maibach, *Measurement of the transit time for cells through the epidermis and stratum corneum of the mouse and guinea-pig.* Cell Tissue Kinet, 1987. **20**(5): p. 461-72.
37. Sada, A., et al., *Defining the cellular lineage hierarchy in the interfollicular epidermis of adult skin.* Nat Cell Biol, 2016. **18**(6): p. 619-31.
38. Clayton, E., et al., *A single type of progenitor cell maintains normal epidermis.* Nature, 2007. **446**(7132): p. 185-9.
39. Jones, K.B. and O.D. Klein, *Oral epithelial stem cells in tissue maintenance and disease: the first steps in a long journey.* Int J Oral Sci, 2013. **5**(3): p. 121-9.
40. Sun, T.T., G. Cotsarelis, and R.M. Lavker, *Hair follicular stem cells: the bulge-activation hypothesis.* J Invest Dermatol, 1991. **96**(5): p. 77S-78S.
41. Muller-Rover, S., et al., *A comprehensive guide for the accurate classification of murine hair follicles in distinct hair cycle stages.* J Invest Dermatol, 2001. **117**(1): p. 3-15.
42. Stenn, K.S. and R. Paus, *Controls of hair follicle cycling.* Physiol Rev, 2001. **81**(1): p. 449-494.
43. Plikus, M.V., et al., *Cyclic dermal BMP signalling regulates stem cell activation during hair regeneration.* Nature, 2008. **451**(7176): p. 340-4.
44. Greco, V., et al., *A two-step mechanism for stem cell activation during hair regeneration.* Cell Stem Cell, 2009. **4**(2): p. 155-69.
45. Zhang, Y.V., et al., *Distinct self-renewal and differentiation phases in the niche of infrequently dividing hair follicle stem cells.* Cell Stem Cell, 2009. **5**(3): p. 267-78.
46. Rompolas, P., et al., *Live imaging of stem cell and progeny behaviour in physiological hair-follicle regeneration.* Nature, 2012. **487**(7408): p. 496-9.
47. Alonso, L. and E. Fuchs, *The hair cycle.* J Cell Sci, 2006. **119**(Pt 3): p. 391-3.
48. St-Jacques, B., et al., *Sonic hedgehog signaling is essential for hair development.* Curr Biol, 1998. **8**(19): p. 1058-68.
49. Chiang, C., et al., *Essential role for Sonic hedgehog during hair follicle morphogenesis.* Dev Biol, 1999. **205**(1): p. 1-9.
50. Sun, X., et al., *Coordinated hedgehog signaling induces new hair follicles in adult skin.* Elife, 2020. **9**.
51. Paus, R. and G. Cotsarelis, *The biology of hair follicles.* N Engl J Med, 1999. **341**(7): p. 491-7.
52. Paus, R. and K. Foitzik, *In search of the "hair cycle clock": a guided tour.* Differentiation, 2004. **72**(9-10): p. 489-511.

53. Quigley, D.A., et al., *Gene Expression Architecture of Mouse Dorsal and Tail Skin Reveals Functional Differences in Inflammation and Cancer.* Cell Rep, 2016. **16**(4): p. 1153-1165.
54. Argyris, T.S., *Growth induced by damage.* Adv Morphog, 1968. **7**: p. 1-43.
55. Sun, B.K., Z. Siprashvili, and P.A. Khavari, *Advances in skin grafting and treatment of cutaneous wounds.* Science, 2014. **346**(6212): p. 941-5.
56. Werner, S. and R. Grose, *Regulation of wound healing by growth factors and cytokines.* Physiol Rev, 2003. **83**(3): p. 835-70.
57. Aragona, M., et al., *Defining stem cell dynamics and migration during wound healing in mouse skin epidermis.* Nat Commun, 2017. **8**: p. 14684.
58. Park, S., et al., *Tissue-scale coordination of cellular behaviour promotes epidermal wound repair in live mice.* Nat Cell Biol, 2017. **19**(2): p. 155-163.
59. Hinz, B., et al., *The myofibroblast: one function, multiple origins.* Am J Pathol, 2007. **170**(6): p. 1807-16.
60. Gurtner, G.C., et al., *Wound repair and regeneration.* Nature, 2008. **453**(7193): p. 314-21.
61. Masson-Meyers, D.S., et al., *Experimental models and methods for cutaneous wound healing assessment.* Int J Exp Pathol, 2020. **101**(1-2): p. 21-37.
62. Dekoninck, S. and C. Blanpain, *Stem cell dynamics, migration and plasticity during wound healing.* Nat Cell Biol, 2019. **21**(1): p. 18-24.
63. Sun, Z.Y., et al., *A very rare complication: new hair growth around healing wounds.* J Int Med Res, 2009. **37**(2): p. 583-6.
64. Wong, T.W., M. Hughes, and S.H. Wang, *Never too old to regenerate? Wound induced hair follicle neogenesis after secondary intention healing in a geriatric patient.* J Tissue Viability, 2018. **27**(2): p. 114-116.
65. Jaks, V., et al., *Lgr5 marks cycling, yet long-lived, hair follicle stem cells.* Nat Genet, 2008. **40**(11): p. 1291-9.
66. Brownell, I., et al., *Nerve-derived sonic hedgehog defines a niche for hair follicle stem cells capable of becoming epidermal stem cells.* Cell Stem Cell, 2011. **8**(5): p. 552-65.
67. Tumbar, T., et al., *Defining the epithelial stem cell niche in skin.* Science, 2004. **303**(5656): p. 359-63.
68. Blanpain, C., et al., *Self-renewal, multipotency, and the existence of two cell populations within an epithelial stem cell niche.* Cell, 2004. **118**(5): p. 635-48.
69. Page, M.E., et al., *The epidermis comprises autonomous compartments maintained by distinct stem cell populations.* Cell Stem Cell, 2013. **13**(4): p. 471-82.
70. Horsley, V., et al., *Blimp1 defines a progenitor population that governs cellular input to the sebaceous gland.* Cell, 2006. **126**(3): p. 597-609.
71. Suzuki, Y., et al., *Targeted disruption of LIG-1 gene results in psoriasiform epidermal hyperplasia.* FEBS Lett, 2002. **521**(1-3): p. 67-71.
72. Jensen, K.B. and F.M. Watt, *Single-cell expression profiling of human epidermal stem and transit-amplifying cells: Lrig1 is a regulator of stem cell quiescence.* Proc Natl Acad Sci U S A, 2006. **103**(32): p. 11958-63.
73. Jiang, L., et al., *Lgr6 is dispensable for epidermal cell proliferation and wound repair.* Exp Dermatol, 2017. **26**(2): p. 105-107.
74. Ito, M., et al., *Stem cells in the hair follicle bulge contribute to wound repair but not to homeostasis of the epidermis.* Nat Med, 2005. **11**(12): p. 1351-4.
75. Liao, X.H. and H. Nguyen, *Epidermal expression of Lgr6 is dependent on nerve endings and Schwann cells.* Exp Dermatol, 2014. **23**(3): p. 195-8.
76. Joost, S., et al., *The Molecular Anatomy of Mouse Skin during Hair Growth and Rest.* Cell Stem Cell, 2020. **26**(3): p. 441-457 e7.
77. Triel, C., et al., *Side population cells in human and mouse epidermis lack stem cell characteristics.* Exp Cell Res, 2004. **295**(1): p. 79-90.
78. Jensen, U.B., et al., *A distinct population of clonogenic and multipotent murine follicular keratinocytes residing in the upper isthmus.* J Cell Sci, 2008. **121**(Pt 5): p. 609-17.

79. Mascre, G., et al., *Distinct contribution of stem and progenitor cells to epidermal maintenance.* Nature, 2012. **489**(7415): p. 257-62.
80. Ge, Y., et al., *Stem Cell Lineage Infidelity Drives Wound Repair and Cancer.* Cell, 2017. **169**(4): p. 636-650 e14.
81. Joost, S., et al., *Single-Cell Transcriptomics of Traced Epidermal and Hair Follicle Stem Cells Reveals Rapid Adaptations during Wound Healing.* Cell Rep, 2018. **25**(3): p. 585-597 e7.
82. Inoue, K., et al., *Differential expression of stem-cell-associated markers in human hair follicle epithelial cells.* Lab Invest, 2009. **89**(8): p. 844-56.
83. Welle, M.M. and D.J. Wiener, *The Hair Follicle: A Comparative Review of Canine Hair Follicle Anatomy and Physiology.* Toxicol Pathol, 2016. **44**(4): p. 564-74.
84. Kretzschmar, K. and F.M. Watt, *Markers of epidermal stem cell subpopulations in adult mammalian skin.* Cold Spring Harb Perspect Med, 2014. **4**(10).
85. Purba, T.S., et al., *Mapping the expression of epithelial hair follicle stem cell-related transcription factors LHX2 and SOX9 in the human hair follicle.* Exp Dermatol, 2015. **24**(6): p. 462-7.
86. Ohyama, M., et al., *Characterization and isolation of stem cell-enriched human hair follicle bulge cells.* J Clin Invest, 2006. **116**(1): p. 249-60.
87. Jones, P.H., S. Harper, and F.M. Watt, *Stem cell patterning and fate in human epidermis.* Cell, 1995. **80**(1): p. 83-93.
88. Adams, J.C. and F.M. Watt, *Fibronectin inhibits the terminal differentiation of human keratinocytes.* Nature, 1989. **340**(6231): p. 307-9.
89. Adams, J.C. and F.M. Watt, *Changes in keratinocyte adhesion during terminal differentiation: reduction in fibronectin binding precedes alpha 5 beta 1 integrin loss from the cell surface.* Cell, 1990. **63**(2): p. 425-35.
90. Jensen, U.B., S. Lowell, and F.M. Watt, *The spatial relationship between stem cells and their progeny in the basal layer of human epidermis: a new view based on whole-mount labelling and lineage analysis.* Development, 1999. **126**(11): p. 2409-18.
91. Jones, P.H. and F.M. Watt, *Separation of human epidermal stem cells from transit amplifying cells on the basis of differences in integrin function and expression.* Cell, 1993. **73**(4): p. 713-24.
92. Webb, A., A. Li, and P. Kaur, *Location and phenotype of human adult keratinocyte stem cells of the skin.* Differentiation, 2004. **72**(8): p. 387-95.
93. Laga, A.C., et al., *Expression of the embryonic stem cell transcription factor SOX2 in human skin: relevance to melanocyte and merkel cell biology.* Am J Pathol, 2010. **176**(2): p. 903-13.
94. Li, A., P.J. Simmons, and P. Kaur, *Identification and isolation of candidate human keratinocyte stem cells based on cell surface phenotype.* Proc Natl Acad Sci U S A, 1998. **95**(7): p. 3902-7.
95. Schluter, H., et al., *Functional characterization of quiescent keratinocyte stem cells and their progeny reveals a hierarchical organization in human skin epidermis.* Stem Cells, 2011. **29**(8): p. 1256-68.
96. Sasaki, M., et al., *Mesenchymal stem cells are recruited into wounded skin and contribute to wound repair by transdifferentiation into multiple skin cell type.* J Immunol, 2008. **180**(4): p. 2581-7.
97. Wu, Y., et al., *Mesenchymal stem cells enhance wound healing through differentiation and angiogenesis.* Stem Cells, 2007. **25**(10): p. 2648-59.
98. Deng, W., et al., *Engrafted bone marrow-derived flk-(1+) mesenchymal stem cells regenerate skin tissue.* Tissue Eng, 2005. **11**(1-2): p. 110-9.
99. Kataoka, K., et al., *Participation of adult mouse bone marrow cells in reconstitution of skin.* Am J Pathol, 2003. **163**(4): p. 1227-31.
100. Brittan, M., et al., *Bone marrow cells engraft within the epidermis and proliferate in vivo with no evidence of cell fusion.* J Pathol, 2005. **205**(1): p. 1-13.
101. Tamai, K., et al., *PDGFRalpha-positive cells in bone marrow are mobilized by high mobility group box 1 (HMGB1) to regenerate injured epithelia.* Proc Natl Acad Sci U S A, 2011. **108**(16): p. 6609-14.

102. Li, H., et al., *Adult bone-marrow-derived mesenchymal stem cells contribute to wound healing of skin appendages.* Cell Tissue Res, 2006. **326**(3): p. 725-36.
103. Rustad, K.C., et al., *Enhancement of mesenchymal stem cell angiogenic capacity and stemness by a biomimetic hydrogel scaffold.* Biomaterials, 2012. **33**(1): p. 80-90.
104. Mishra, P.J. and D. Banerjee, *Keratinocyte Induced Differentiation of Mesenchymal Stem Cells into Dermal Myofibroblasts: A Role in Effective Wound Healing.* Int J Transl Sci, 2016. **2016**(1): p. 5-32.
105. Fan, Q., et al., *Bone marrow-derived keratinocytes are not detected in normal skin and only rarely detected in wounded skin in two different murine models.* Exp Hematol, 2006. **34**(5): p. 672-9.
106. Friedenstein, A.J., et al., *Heterotopic of bone marrow. Analysis of precursor cells for osteogenic and hematopoietic tissues.* Transplantation, 1968. **6**(2): p. 230-47.
107. Friedenstein, A.J., R.K. Chailakhyan, and U.V. Gerasimov, *Bone marrow osteogenic stem cells: in vitro cultivation and transplantation in diffusion chambers.* Cell Tissue Kinet, 1987. **20**(3): p. 263-72.
108. Friedenstein, A.J., R.K. Chailakhjan, and K.S. Lalykina, *The development of fibroblast colonies in monolayer cultures of guinea-pig bone marrow and spleen cells.* Cell Tissue Kinet, 1970. **3**(4): p. 393-403.
109. Bianco, P., P.G. Robey, and P.J. Simmons, *Mesenchymal stem cells: revisiting history, concepts, and assays.* Cell Stem Cell, 2008. **2**(4): p. 313-9.
110. Richardson, G.D., et al., *Cultured cells from the adult human hair follicle dermis can be directed toward adipogenic and osteogenic differentiation.* J Invest Dermatol, 2005. **124**(5): p. 1090-1.
111. Beltrami, A.P., et al., *Multipotent cells can be generated in vitro from several adult human organs (heart, liver, and bone marrow).* Blood, 2007. **110**(9): p. 3438-46.
112. Jiang, Y., et al., *Multipotent progenitor cells can be isolated from postnatal murine bone marrow, muscle, and brain.* Exp Hematol, 2002. **30**(8): p. 896-904.
113. Chang, Y., H. Li, and Z. Guo, *Mesenchymal stem cell-like properties in fibroblasts.* Cell Physiol Biochem, 2014. **34**(3): p. 703-14.
114. Denu, R.A., et al., *Fibroblasts and Mesenchymal Stromal/Stem Cells Are Phenotypically Indistinguishable.* Acta Haematol, 2016. **136**(2): p. 85-97.
115. Dominici, M., et al., *Minimal criteria for defining multipotent mesenchymal stromal cells. The International Society for Cellular Therapy position statement.* Cytotherapy, 2006. **8**(4): p. 315-7.
116. Hirsch, T., et al., *Regeneration of the entire human epidermis using transgenic stem cells.* Nature, 2017. **551**(7680): p. 327-332.
117. Barrandon, Y. and H. Green, *Three clonal types of keratinocyte with different capacities for multiplication.* Proc Natl Acad Sci U S A, 1987. **84**(8): p. 2302-6.
118. Liu, N., et al., *Stem cell competition orchestrates skin homeostasis and ageing.* Nature, 2019. **568**(7752): p. 344-350.
119. Kurban, R.S. and J. Bhawan, *Histologic changes in skin associated with aging.* J Dermatol Surg Oncol, 1990. **16**(10): p. 908-14.
120. Gosain, A. and L.A. DiPietro, *Aging and wound healing.* World J Surg, 2004. **28**(3): p. 321-6.
121. Kohl, E., et al., *Skin ageing.* J Eur Acad Dermatol Venereol, 2011. **25**(8): p. 873-84.
122. Bonta, M., L. Daina, and G. Mutiu, *The process of ageing reflected by histological changes in the skin.* Rom J Morphol Embryol, 2013. **54**(3 Suppl): p. 797-804.
123. Mine, S., et al., *Aging alters functionally human dermal papillary fibroblasts but not reticular fibroblasts: a new view of skin morphogenesis and aging.* PLoS One, 2008. **3**(12): p. e4066.
124. Zhang, S. and E. Duan, *Fighting against Skin Aging: The Way from Bench to Bedside.* Cell Transplant, 2018. **27**(5): p. 729-738.
125. Makrantonaki, E. and C.C. Zouboulis, *William J. Cunliffe Scientific Awards. Characteristics and pathomechanisms of endogenously aged skin.* Dermatology, 2007. **214**(4): p. 352-60.

126. Moragas, A., C. Castells, and M. Sans, *Mathematical morphologic analysis of aging-related epidermal changes.* Anal Quant Cytol Histol, 1993. **15**(2): p. 75-82.
127. Watanabe, M., et al., *Type XVII collagen coordinates proliferation in the interfollicular epidermis.* Elife, 2017. **6**.
128. Langton, A.K., et al., *The impact of intrinsic ageing on the protein composition of the dermal-epidermal junction.* Mech Ageing Dev, 2016. **156**: p. 14-6.
129. Nishimura, E.K., S.R. Granter, and D.E. Fisher, *Mechanisms of hair graying: incomplete melanocyte stem cell maintenance in the niche.* Science, 2005. **307**(5710): p. 720-4.
130. Nishimura, E.K., *Melanocyte stem cells: a melanocyte reservoir in hair follicles for hair and skin pigmentation.* Pigment Cell Melanoma Res, 2011. **24**(3): p. 401-10.
131. Zhang, B., et al., *Hyperactivation of sympathetic nerves drives depletion of melanocyte stem cells.* Nature, 2020. **577**(7792): p. 676-681.
132. Kligman, L.H., *Photoaging. Manifestations, prevention, and treatment.* Clin Geriatr Med, 1989. **5**(1): p. 235-51.
133. Liu-Smith, F., J. Jia, and Y. Zheng, *UV-Induced Molecular Signaling Differences in Melanoma and Non-melanoma Skin Cancer.* Adv Exp Med Biol, 2017. **996**: p. 27-40.
134. Gandhi, S.A. and J. Kampp, *Skin Cancer Epidemiology, Detection, and Management.* Med Clin North Am, 2015. **99**(6): p. 1323-35.
135. Robinson, J.K. and M. Dahiya, *Basal cell carcinoma with pulmonary and lymph node metastasis causing death.* Arch Dermatol, 2003. **139**(5): p. 643-8.
136. Hahn, H., et al., *Mutations of the human homolog of Drosophila patched in the nevoid basal cell carcinoma syndrome.* Cell, 1996. **85**(6): p. 841-51.
137. Taipale, J. and P.A. Beachy, *The Hedgehog and Wnt signalling pathways in cancer.* Nature, 2001. **411**(6835): p. 349-54.
138. Gailani, M.R. and A.E. Bale, *Developmental genes and cancer: role of patched in basal cell carcinoma of the skin.* J Natl Cancer Inst, 1997. **89**(15): p. 1103-9.
139. Epstein, E.H., *Basal cell carcinomas: attack of the hedgehog.* Nat Rev Cancer, 2008. **8**(10): p. 743-54.
140. Reifenberger, J., et al., *Somatic mutations in the PTCH, SMOH, SUFUH and TP53 genes in sporadic basal cell carcinomas.* Br J Dermatol, 2005. **152**(1): p. 43-51.
141. Yang, S.H., et al., *Pathological responses to oncogenic Hedgehog signaling in skin are dependent on canonical Wnt/beta3-catenin signaling.* Nat Genet, 2008. **40**(9): p. 1130-5.
142. El-Bahrawy, M., et al., *Expression of beta-catenin in basal cell carcinoma.* Br J Dermatol, 2003. **148**(5): p. 964-70.
143. Eberl, M., et al., *Hedgehog-EGFR cooperation response genes determine the oncogenic phenotype of basal cell carcinoma and tumour-initiating pancreatic cancer cells.* EMBO Mol Med, 2012. **4**(3): p. 218-33.
144. Maddon, P.J., et al., *The T4 gene encodes the AIDS virus receptor and is expressed in the immune system and the brain.* Cell, 1986. **47**(3): p. 333-48.
145. McDougal, J.S., et al., *Binding of HTLV-III/LAV to T4+ T cells by a complex of the 110K viral protein and the T4 molecule.* Science, 1986. **231**(4736): p. 382-5.
146. Maddon, P.J., et al., *Structure and expression of the human and mouse T4 genes.* Proc Natl Acad Sci U S A, 1987. **84**(24): p. 9155-9.
147. Doyle, C. and J.L. Strominger, *Interaction between CD4 and class II MHC molecules mediates cell adhesion.* Nature, 1987. **330**(6145): p. 256-9.
148. Esser, U., et al., *Molecular function of the CD4 D1 domain in coreceptor-mediated entry by HIV type 1.* AIDS Res Hum Retroviruses, 2000. **16**(17): p. 1845-54.
149. Vignali, D.A. and K.M. Vignali, *Profound enhancement of T cell activation mediated by the interaction between the TCR and the D3 domain of CD4.* J Immunol, 1999. **162**(3): p. 1431-9.
150. Liu, Y., et al., *Identification of a CD4 domain required for interleukin-16 binding and lymphocyte activation.* J Biol Chem, 1999. **274**(33): p. 23387-95.
151. Wu, H., P.D. Kwong, and W.A. Hendrickson, *Dimeric association and segmental variability in the structure of human CD4.* Nature, 1997. **387**(6632): p. 527-30.

152. Claeys, E.V., K., *The CD4 Receptor: An Indispensable Protein in T Cell Activation and A Promising Target for Immunosuppression.* Archives of Microbiology & Immunology, 2019. **3**(3): p. 133-150.
153. Janeway, C.J.T., P.; Walport, M.; et al. , *Antigen recognition by T cells*, in *Immunobiology: The Immune System in Health and Disease*2001, Garland Science: New York.
154. Wyatt, R. and J. Sodroski, *The HIV-1 envelope glycoproteins: fusogens, antigens, and immunogens.* Science, 1998. **280**(5371): p. 1884-8.
155. Lynch, G.W., et al., *Marked differences in the structures and protein associations of lymphocyte and monocyte CD4: resolution of a novel CD4 isoform.* Immunol Cell Biol, 2006. **84**(2): p. 154-65.
156. Pelchen-Matthews, A., et al., *Lack of p56lck expression correlates with CD4 endocytosis in primary lymphoid and myeloid cells.* Eur J Immunol, 1998. **28**(11): p. 3639-47.
157. Zhen, A., et al., *CD4 ligation on human blood monocytes triggers macrophage differentiation and enhances HIV infection.* J Virol, 2014. **88**(17): p. 9934-46.
158. Lisco, A., et al., *Lost in translation: Lack of CD4 expression due to a novel genetic defect.* J Infect Dis, 2021.
159. Zhou, W. and R. Konig, *T cell receptor-independent CD4 signalling: CD4-MHC class II interactions regulate intracellular calcium and cyclic AMP.* Cell Signal, 2003. **15**(8): p. 751-62.
160. Ikeuchi, K., et al., *Infection of nonlymphoid cells by human immunodeficiency virus type 1 or type 2.* J Virol, 1990. **64**(9): p. 4226-31.
161. Derdak, S., et al., *CD4 expression in lung fibroblasts.* Lancet, 1991. **337**(8737): p. 374.
162. Scadden, D.T., et al., *Human immunodeficiency virus infection of human bone marrow stromal fibroblasts.* Blood, 1990. **76**(2): p. 317-22.
163. Gibellini, D., et al., *HIV-1 and recombinant gp120 affect the survival and differentiation of human vessel wall-derived mesenchymal stem cells.* Retrovirology, 2011. **8**: p. 40.
164. Plata, F., et al., *HIV-1 infection of lung alveolar fibroblasts and macrophages in humans.* AIDS Res Hum Retroviruses, 1990. **6**(8): p. 979-86.
165. Mellert, W., et al., *Infection of human fibroblasts and osteoblast-like cells with HIV-1.* AIDS, 1990. **4**(6): p. 527-35.
166. Clapham, *Human Immunodeficiency Virus Infection of Non-haematopoietic Cells. The Role of CD4-Independent Entry.* Reviews in Medical Virology, 1991. **I**: p. 51-58.
167. Clapham, P.R., et al., *Soluble CD4 blocks the infectivity of diverse strains of HIV and SIV for T cells and monocytes but not for brain and muscle cells.* Nature, 1989. **337**(6205): p. 368-70.
168. Weber, J., et al., *Infection of brain cells by diverse human immunodeficiency virus isolates: role of CD4 as receptor.* J Gen Virol, 1989. **70 (Pt 10)**: p. 2653-60.
169. Cao, Y.Z., et al., *CD4-independent, productive human immunodeficiency virus type 1 infection of hepatoma cell lines in vitro.* J Virol, 1990. **64**(6): p. 2553-9.
170. Cohen, M., et al., *Lung Single-Cell Signaling Interaction Map Reveals Basophil Role in Macrophage Imprinting.* Cell, 2018. **175**(4): p. 1031-1044 e18.
171. Chen, P., et al., *Efficient CD4Cre-Mediated Conditional KRas Expression in Alveolar Macrophages and Alveolar Epithelial Cells Causes Fatal Hyperproliferative Pneumonitis.* J Immunol, 2019. **203**(5): p. 1208-1217.
172. Cao, J., et al., *The single-cell transcriptional landscape of mammalian organogenesis.* Nature, 2019. **566**(7745): p. 496-502.
173. Thunemann, M., et al., *Cre/lox-assisted non-invasive in vivo tracking of specific cell populations by positron emission tomography.* Nat Commun, 2017. **8**(1): p. 444.
174. Miah, S.M.S., et al., *Ptpn11 Deletion in CD4(+) Cells Does Not Affect T Cell Development and Functions but Causes Cartilage Tumors in a T Cell-Independent Manner.* Front Immunol, 2017. **8**: p. 1326.

175. Wehenkel, M., et al., *Extracellular Signal-Regulated Kinase Signaling in CD4-Expressing Cells Inhibits Osteochondromas.* Front Immunol, 2017. **8**: p. 482.
176. Guittard, G., et al., *Unexpected Cartilage Phenotype in CD4-Cre-Conditional SOS-Deficient Mice.* Front Immunol, 2017. **8**: p. 343.
177. Guittard, G., et al., *Absence of both Sos-1 and Sos-2 in peripheral CD4(+) T cells leads to PI3K pathway activation and defects in migration.* Eur J Immunol, 2015. **45**(8): p. 2389-95.
178. Rohatgi, R. and M.P. Scott, *Patching the gaps in Hedgehog signalling.* Nat Cell Biol, 2007. **9**(9): p. 1005-9.
179. Skoda, A.M., et al., *The role of the Hedgehog signaling pathway in cancer: A comprehensive review.* Bosn J Basic Med Sci, 2018. **18**(1): p. 8-20.
180. Roberts, W.M., et al., *Amplification of the gli gene in childhood sarcomas.* Cancer Res, 1989. **49**(19): p. 5407-13.
181. Berman, D.M., et al., *Widespread requirement for Hedgehog ligand stimulation in growth of digestive tract tumours.* Nature, 2003. **425**(6960): p. 846-51.
182. Watkins, D.N., et al., *Hedgehog signalling within airway epithelial progenitors and in small-cell lung cancer.* Nature, 2003. **422**(6929): p. 313-7.
183. Goodrich, L.V., et al., *Altered neural cell fates and medulloblastoma in mouse patched mutants.* Science, 1997. **277**(5329): p. 1109-13.
184. Hahn, H., et al., *Rhabdomyosarcomas and radiation hypersensitivity in a mouse model of Gorlin syndrome.* Nat Med, 1998. **4**(5): p. 619-22.
185. Mancuso, M., et al., *Basal cell carcinoma and its development: insights from radiation-induced tumors in Ptch1-deficient mice.* Cancer Res, 2004. **64**(3): p. 934-41.
186. Uhmann, A., et al., *The Hedgehog receptor Patched controls lymphoid lineage commitment.* Blood, 2007. **110**(6): p. 1814-23.
187. Outram, S.V., et al., *Hedgehog signaling regulates differentiation from double-negative to double-positive thymocyte.* Immunity, 2000. **13**(2): p. 187-97.
188. Shah, D.K., et al., *Reduced thymocyte development in sonic hedgehog knockout embryos.* J Immunol, 2004. **172**(4): p. 2296-306.
189. Bhardwaj, G., et al., *Sonic hedgehog induces the proliferation of primitive human hematopoietic cells via BMP regulation.* Nat Immunol, 2001. **2**(2): p. 172-80.
190. Lowrey, J.A., et al., *Sonic hedgehog promotes cell cycle progression in activated peripheral CD4(+) T lymphocytes.* J Immunol, 2002. **169**(4): p. 1869-75.
191. Uhmann, A., et al., *T cell development critically depends on prethymic stromal patched expression.* J Immunol, 2011. **186**(6): p. 3383-91.
192. Michel, K.D., et al., *The hedgehog receptor patched1 in T cells is dispensable for adaptive immunity in mice.* PLoS One, 2013. **8**(4): p. e61034.
193. Uhmann, A., et al., *DMBA/TPA treatment is necessary for BCC formation from patched deficient epidermal cells in Ptch(flox/flox)CD4Cre(+/-) mice.* J Invest Dermatol, 2014. **134**(10): p. 2620-2629.
194. Indra, A.K., et al., *Malignant transformation of DMBA/TPA-induced papillomas and nevi in the skin of mice selectively lacking retinoid-X-receptor alpha in epidermal keratinocytes.* J Invest Dermatol, 2007. **127**(5): p. 1250-60.
195. Quintanilla, M., et al., *Carcinogen-specific mutation and amplification of Ha-ras during mouse skin carcinogenesis.* Nature, 1986. **322**(6074): p. 78-80.
196. Kemp, C.J., F. Fee, and A. Balmain, *Allelotype analysis of mouse skin tumors using polymorphic microsatellites: sequential genetic alterations on chromosomes 6, 7, and 11.* Cancer Res, 1993. **53**(24): p. 6022-7.
197. Kasper, M., et al., *Wounding enhances epidermal tumorigenesis by recruiting hair follicle keratinocytes.* Proc Natl Acad Sci U S A, 2011. **108**(10): p. 4099-104.
198. Wong, S.Y. and J.F. Reiter, *Wounding mobilizes hair follicle stem cells to form tumors.* Proc Natl Acad Sci U S A, 2011. **108**(10): p. 4093-8.
199. Brandes, N., et al., *Spreading of Isolated Ptch Mutant Basal Cell Carcinoma Precursors Is Physiologically Suppressed and Counteracts Tumor Formation in Mice.* Int J Mol Sci, 2020. **21**(23).

200. Peterson, S.C., et al., *Basal cell carcinoma preferentially arises from stem cells within hair follicle and mechanosensory niches.* Cell Stem Cell, 2015. **16**(4): p. 400-12.
201. Adolphe, C., et al., *Patched1 functions as a gatekeeper by promoting cell cycle progression.* Cancer Res, 2006. **66**(4): p. 2081-8.
202. Adolphe, C., et al., *Patched 1 and patched 2 redundancy has a key role in regulating epidermal differentiation.* J Invest Dermatol, 2014. **134**(7): p. 1981-1990.
203. Nitzki, F., et al., *Patched knockout mouse models of Basal cell carcinoma.* J Skin Cancer, 2012. **2012**: p. 907543.
204. Love, M.I., W. Huber, and S. Anders, *Moderated estimation of fold change and dispersion for RNA-seq data with DESeq2.* Genome Biol, 2014. **15**(12): p. 550.
205. Liao, Y., G.K. Smyth, and W. Shi, *featureCounts: an efficient general purpose program for assigning sequence reads to genomic features.* Bioinformatics, 2014. **30**(7): p. 923-30.
206. Schneider, C.A., W.S. Rasband, and K.W. Eliceiri, *NIH Image to ImageJ: 25 years of image analysis.* Nat Methods, 2012. **9**(7): p. 671-5.
207. Dobin, A., et al., *STAR: ultrafast universal RNA-seq aligner.* Bioinformatics, 2013. **29**(1): p. 15-21.
208. Ponec, M., J.A. Kempenaar, and E.R. De Kloet, *Corticoids and cultured human epidermal keratinocytes: specific intracellular binding and clinical efficacy.* J Invest Dermatol, 1981. **76**(3): p. 211-4.
209. Gibbs, S., C. Backendorf, and M. Ponec, *Regulation of keratinocyte proliferation and differentiation by all-trans-retinoic acid, 9-cis-retinoic acid and 1,25-dihydroxy vitamin D3.* Arch Dermatol Res, 1996. **288**(12): p. 729-38.
210. Nowak, J.A. and E. Fuchs, *Isolation and culture of epithelial stem cells.* Methods Mol Biol, 2009. **482**: p. 215-32.
211. Lee, P.P., et al., *A critical role for Dnmt1 and DNA methylation in T cell development, function, and survival.* Immunity, 2001. **15**(5): p. 763-74.
212. Aghajani, K., et al., *Generation of CD4CreER(T(2)) transgenic mice to study development of peripheral CD4-T-cells.* Genesis, 2012. **50**(12): p. 908-13.
213. Rahemtulla, A., et al., *Normal development and function of CD8+ cells but markedly decreased helper cell activity in mice lacking CD4.* Nature, 1991. **353**(6340): p. 180-4.
214. Madisen, L., et al., *A robust and high-throughput Cre reporting and characterization system for the whole mouse brain.* Nat Neurosci, 2010. **13**(1): p. 133-40.
215. Sauer, B., *Inducible gene targeting in mice using the Cre/lox system.* Methods, 1998. **14**(4): p. 381-92.
216. Sauer, B. and N. Henderson, *Site-specific DNA recombination in mammalian cells by the Cre recombinase of bacteriophage P1.* Proc Natl Acad Sci U S A, 1988. **85**(14): p. 5166-70.
217. Kretzschmar, K. and F.M. Watt, *Lineage tracing.* Cell, 2012. **148**(1-2): p. 33-45.
218. Feil, R., et al., *Ligand-activated site-specific recombination in mice.* Proc Natl Acad Sci U S A, 1996. **93**(20): p. 10887-90.
219. Sawada, S., et al., *A lineage-specific transcriptional silencer regulates CD4 gene expression during T lymphocyte development.* Cell, 1994. **77**(6): p. 917-29.
220. Westendorf, K., et al., *Chromosomal localisation of the CD4cre transgene in B6.Cg-Tg(Cd4-cre)1Cwi mice.* J Immunol Methods, 2016. **436**: p. 54-7.
221. Sequeira, I., et al., *Microdissection and visualization of individual hair follicles for lineage tracing studies.* Methods Mol Biol, 2014. **1195**: p. 247-58.
222. Braun, K.M., et al., *Manipulation of stem cell proliferation and lineage commitment: visualisation of label-retaining cells in wholemounts of mouse epidermis.* Development, 2003. **130**(21): p. 5241-55.
223. Maurer, W., *Histologische und zelluläre Charakterisierung CD4-positiver Zellen der murinen und humanen Haut*, in *Fakultät für Biologie und Psychologie*2017, Georg-August-Universität Göttingen: Göttingen.
224. Donnenberg, V.S., et al., *Flow cytometric detection of most proteins in the cell surface proteome is unaffected by trypsin treatment.* Cytometry A, 2018. **93**(8): p. 803-810.

225. Walzer, C., M. Benathan, and E. Frenk, *Thermolysin treatment: a new method for dermo-epidermal separation.* J Invest Dermatol, 1989. **92**(1): p. 78-81.
226. Gragnani, A., C.S. Sobral, and L.M. Ferreira, *Thermolysin in human cultured keratinocyte isolation.* Braz J Biol, 2007. **67**(1): p. 105-9.
227. Walmsley, G.G., et al., *Murine Dermal Fibroblast Isolation by FACS.* J Vis Exp, 2016(107).
228. Jensen, K.B., R.R. Driskell, and F.M. Watt, *Assaying proliferation and differentiation capacity of stem cells using disaggregated adult mouse epidermis.* Nat Protoc, 2010. **5**(5): p. 898-911.
229. Penit, C. and F. Vasseur, *Cell proliferation and differentiation in the fetal and early postnatal mouse thymus.* J Immunol, 1989. **142**(10): p. 3369-77.
230. Xiao, S.Y., Y. Li, and W.F. Chen, *Kinetics of thymocyte developmental process in fetal and neonatal mice.* Cell Res, 2003. **13**(4): p. 265-73.
231. Peled, A., et al., *Expression of alpha-smooth muscle actin in murine bone marrow stromal cells.* Blood, 1991. **78**(2): p. 304-9.
232. Goetz, B., et al., *A novel CBL-Bflox/flox mouse model allows tissue-selective fully conditional CBL/CBL-B double-knockout: CD4-Cre mediated CBL/CBL-B deletion occurs in both T-cells and hematopoietic stem cells.* Oncotarget, 2016. **7**(32): p. 51107-51123.
233. Zeitrag, J., et al., *Gene dose matters: Considerations for the use of inducible CD4-CreER(T2) mouse lines.* Eur J Immunol, 2020. **50**(4): p. 603-605.
234. Zeineddine, D., et al., *The Oct4 protein: more than a magic stemness marker.* Am J Stem Cells, 2014. **3**(2): p. 74-82.
235. Scholer, H.R., et al., *A family of octamer-specific proteins present during mouse embryogenesis: evidence for germline-specific expression of an Oct factor.* EMBO J, 1989. **8**(9): p. 2543-50.
236. Riekstina, U., et al., *Embryonic stem cell marker expression pattern in human mesenchymal stem cells derived from bone marrow, adipose tissue, heart and dermis.* Stem Cell Rev Rep, 2009. **5**(4): p. 378-86.
237. Rolf, H.J., et al., *Intercellular transport of Oct4 in mammalian cells: a basic principle to expand a stem cell niche?* PLoS One, 2012. **7**(2): p. e32287.
238. Muguruma, Y., et al., *Reconstitution of the functional human hematopoietic microenvironment derived from human mesenchymal stem cells in the murine bone marrow compartment.* Blood, 2006. **107**(5): p. 1878-87.
239. Trempus, C.S., et al., *Enrichment for living murine keratinocytes from the hair follicle bulge with the cell surface marker CD34.* J Invest Dermatol, 2003. **120**(4): p. 501-11.
240. Ghazizadeh, S. and L.B. Taichman, *Multiple classes of stem cells in cutaneous epithelium: a lineage analysis of adult mouse skin.* EMBO J, 2001. **20**(6): p. 1215-22.
241. Watt, F.M., *Role of integrins in regulating epidermal adhesion, growth and differentiation.* EMBO J, 2002. **21**(15): p. 3919-26.
242. Horsley, V., et al., *NFATc1 balances quiescence and proliferation of skin stem cells.* Cell, 2008. **132**(2): p. 299-310.
243. Lay, K., T. Kume, and E. Fuchs, *FOXC1 maintains the hair follicle stem cell niche and governs stem cell quiescence to preserve long-term tissue-regenerating potential.* Proc Natl Acad Sci U S A, 2016. **113**(11): p. E1506-15.
244. Rhee, H., L. Polak, and E. Fuchs, *Lhx2 maintains stem cell character in hair follicles.* Science, 2006. **312**(5782): p. 1946-9.
245. Vidal, V.P., et al., *Sox9 is essential for outer root sheath differentiation and the formation of the hair stem cell compartment.* Curr Biol, 2005. **15**(15): p. 1340-51.
246. Müllen, A., *Charakterisierung von CD4 exprimierenden Zellen der murinen und humanen Epidermis*, in *Fakultät für Biologie und Psychologie*2016, Georg-August-Universität Göttingen: Göttingen.
247. Scheile, H., *CD4+ epidermale Zellen: Nachweis und Charakterisierung in humaner und muriner Epidermis*, in *Medizinische Fakultät*2020, Georg-August-Universität Göttingen: Göttingen.
248. Uhmann, A., unpublished data, University Medical Center Göttingen.

249. Sequeira, I. and J.F. Nicolas, *Redefining the structure of the hair follicle by 3D clonal analysis.* Development, 2012. **139**(20): p. 3741-51.
250. Chen, L., et al., *The murine excisional wound model: Contraction revisited.* Wound Repair Regen, 2015. **23**(6): p. 874-7.
251. Argyris, T.S., *The effect of wounds on adjacent growing or resting hair follicles in mice.* AMA Arch Pathol, 1956. **61**(1): p. 31-6.
252. Castellana, D., R. Paus, and M. Perez-Moreno, *Macrophages contribute to the cyclic activation of adult hair follicle stem cells.* PLoS Biol, 2014. **12**(12): p. e1002002.
253. Paus, R., et al., *Generation and cyclic remodeling of the hair follicle immune system in mice.* J Invest Dermatol, 1998. **111**(1): p. 7-18.
254. Chen, C.C., et al., *Organ-level quorum sensing directs regeneration in hair stem cell populations.* Cell, 2015. **161**(2): p. 277-90.
255. Wang, X., et al., *Macrophages induce AKT/beta-catenin-dependent Lgr5(+) stem cell activation and hair follicle regeneration through TNF.* Nat Commun, 2017. **8**: p. 14091.
256. Osaka, N., et al., *ASK1-dependent recruitment and activation of macrophages induce hair growth in skin wounds.* J Cell Biol, 2007. **176**(7): p. 903-9.
257. Becht, E., et al., *Dimensionality reduction for visualizing single-cell data using UMAP.* Nat Biotechnol, 2018.
258. Adam, R.C., et al., *Pioneer factors govern super-enhancer dynamics in stem cell plasticity and lineage choice.* Nature, 2015. **521**(7552): p. 366-70.
259. Samstag, Y., F. Emmrich, and T. Staehelin, *Activation of human T lymphocytes: differential effects of CD3- and CD8-mediated signals.* Proc Natl Acad Sci U S A, 1988. **85**(24): p. 9689-93.
260. Jersmann, H.P., *Time to abandon dogma: CD14 is expressed by non-myeloid lineage cells.* Immunol Cell Biol, 2005. **83**(5): p. 462-7.
261. Mizumoto, N. and A. Takashima, *CD1a and langerin: acting as more than Langerhans cell markers.* J Clin Invest, 2004. **113**(5): p. 658-60.
262. Tani, H., R.J. Morris, and P. Kaur, *Enrichment for murine keratinocyte stem cells based on cell surface phenotype.* Proc Natl Acad Sci U S A, 2000. **97**(20): p. 10960-5.
263. O'Keefe, E., T. Battin, and R. Payne, Jr., *Epidermal growth factor receptor in human epidermal cells: direct demonstration in cultured cells.* J Invest Dermatol, 1982. **78**(6): p. 482-7.
264. Rheinwald, J.G. and H. Green, *Serial cultivation of strains of human epidermal keratinocytes: the formation of keratinizing colonies from single cells.* Cell, 1975. **6**(3): p. 331-43.
265. Sun, T.T. and H. Green, *Differentiation of the epidermal keratinocyte in cell culture: formation of the cornified envelope.* Cell, 1976. **9**(4 Pt 1): p. 511-21.
266. Allen-Hoffmann, B.L. and J.G. Rheinwald, *Polycyclic aromatic hydrocarbon mutagenesis of human epidermal keratinocytes in culture.* Proc Natl Acad Sci U S A, 1984. **81**(24): p. 7802-6.
267. Flaxman, B.A. and R.A. Harper, *In vitro analysis of the control of keratinocyte proliferation in human epidermis by physiologic and pharmacologic agents.* J Invest Dermatol, 1975. **65**(1): p. 52-9.
268. Missero, C., et al., *The absence of p21Cip1/WAF1 alters keratinocyte growth and differentiation and promotes ras-tumor progression.* Genes Dev, 1996. **10**(23): p. 3065-75.
269. Bikle, D.D., et al., *Changes in calcium responsiveness and handling during keratinocyte differentiation. Potential role of the calcium receptor.* J Clin Invest, 1996. **97**(4): p. 1085-93.
270. Hennings, H., et al., *Calcium regulation of growth and differentiation of mouse epidermal cells in culture.* Cell, 1980. **19**(1): p. 245-54.
271. Pillai, S. and D.D. Bikle, *Role of intracellular-free calcium in the cornified envelope formation of keratinocytes: differences in the mode of action of extracellular calcium and 1,25 dihydroxyvitamin D3.* J Cell Physiol, 1991. **146**(1): p. 94-100.

272. Cali, J.P., G.N. Bowers, Jr., and D.S. Young, *A referee method for the determination of total calcium in serum.* Clin Chem, 1973. **19**(10): p. 1208-13.
273. Brennan, J.K., et al., *Improved methods for reducing calcium and magnesium concentrations in tissue culture medium: application to studies of lymphoblast proliferation in vitro.* In Vitro, 1975. **11**(6): p. 354-60.
274. Micallef, L., et al., *Effects of extracellular calcium on the growth-differentiation switch in immortalized keratinocyte HaCaT cells compared with normal human keratinocytes.* Exp Dermatol, 2009. **18**(2): p. 143-51.
275. Simon, M. and H. Green, *Enzymatic cross-linking of involucrin and other proteins by keratinocyte particulates in vitro.* Cell, 1985. **40**(3): p. 677-83.
276. Green, H., *Cyclic AMP in relation to proliferation of the epidermal cell: a new view.* Cell, 1978. **15**(3): p. 801-11.
277. Shi, G., et al., *Expression and functional role of Sox9 in human epidermal keratinocytes.* PLoS One, 2013. **8**(1): p. e54355.
278. Noel-Hudson, M.S., et al., *Human epidermis reconstructed on synthetic membrane: influence of experimental conditions on terminal differentiation.* In Vitro Cell Dev Biol Anim, 1995. **31**(7): p. 508-15.
279. Font, J., et al., *A new three-dimensional culture of human keratinocytes: optimization of differentiation.* Cell Biol Toxicol, 1994. **10**(5-6): p. 353-9.
280. Yang, E.K., et al., *Tissue engineered artificial skin composed of dermis and epidermis.* Artif Organs, 2000. **24**(1): p. 7-17.
281. Higham, M.C., et al., *Development of a stable chemically defined surface for the culture of human keratinocytes under serum-free conditions for clinical use.* Tissue Eng, 2003. **9**(5): p. 919-30.
282. Hynds, R.E., P. Bonfanti, and S.M. Janes, *Regenerating human epithelia with cultured stem cells: feeder cells, organoids and beyond.* EMBO Mol Med, 2018. **10**(2): p. 139-150.
283. Beaver, C.M., A. Ahmed, and J.R. Masters, *Clonogenicity: holoclones and meroclones contain stem cells.* PLoS One, 2014. **9**(2): p. e89834.
284. Vollmers, A., et al., *Two- and three-dimensional culture of keratinocyte stem and precursor cells derived from primary murine epidermal cultures.* Stem Cell Rev Rep, 2012. **8**(2): p. 402-13.
285. Pellegrini, G., et al., *p63 identifies keratinocyte stem cells.* Proc Natl Acad Sci U S A, 2001. **98**(6): p. 3156-61.
286. Takahashi, K. and S. Yamanaka, *Induction of pluripotent stem cells from mouse embryonic and adult fibroblast cultures by defined factors.* Cell, 2006. **126**(4): p. 663-76.
287. Bilousova, G., J. Chen, and D.R. Roop, *Differentiation of mouse induced pluripotent stem cells into a multipotent keratinocyte lineage.* J Invest Dermatol, 2011. **131**(4): p. 857-64.
288. Kogut, I., D.R. Roop, and G. Bilousova, *Differentiation of human induced pluripotent stem cells into a keratinocyte lineage.* Methods Mol Biol, 2014. **1195**: p. 1-12.
289. Dos Santos, J.F., et al., *Mesenchymal stem cells differentiate into keratinocytes and express epidermal kallikreins: Towards an in vitro model of human epidermis.* J Cell Biochem, 2019. **120**(8): p. 13141-13155.
290. Bara, J.J., et al., *Concise review: Bone marrow-derived mesenchymal stem cells change phenotype following in vitro culture: implications for basic research and the clinic.* Stem Cells, 2014. **32**(7): p. 1713-23.
291. Bruder, S.P., N. Jaiswal, and S.E. Haynesworth, *Growth kinetics, self-renewal, and the osteogenic potential of purified human mesenchymal stem cells during extensive subcultivation and following cryopreservation.* J Cell Biochem, 1997. **64**(2): p. 278-94.
292. McKee, C. and G.R. Chaudhry, *Advances and challenges in stem cell culture.* Colloids Surf B Biointerfaces, 2017. **159**: p. 62-77.
293. Erickson, G.R., et al., *Chondrogenic potential of adipose tissue-derived stromal cells in vitro and in vivo.* Biochem Biophys Res Commun, 2002. **290**(2): p. 763-9.

294. Robey, P.G., et al., *Bone marrow stromal cell assays: in vitro and in vivo.* Methods Mol Biol, 2014. **1130**: p. 279-293.
295. Okabe, M., et al., *'Green mice' as a source of ubiquitous green cells.* FEBS Lett, 1997. **407**(3): p. 313-9.
296. Zheng, Y., et al., *Organogenesis from dissociated cells: generation of mature cycling hair follicles from skin-derived cells.* J Invest Dermatol, 2005. **124**(5): p. 867-76.
297. Rivers, L.E., et al., *PDGFRA/NG2 glia generate myelinating oligodendrocytes and piriform projection neurons in adult mice.* Nat Neurosci, 2008. **11**(12): p. 1392-401.
298. O'Rourke, M., et al., *Evaluating Tissue-Specific Recombination in a Pdgfralpha-CreERT2 Transgenic Mouse Line.* PLoS One, 2016. **11**(9): p. e0162858.
299. Miwa, H. and T. Era, *Generation and characterization of PDGFRalpha-GFPCreERT2 knock-In mouse line.* Genesis, 2015. **53**(5): p. 329-36.
300. Horn, A., et al., *Hedgehog signaling controls fibroblast activation and tissue fibrosis in systemic sclerosis.* Arthritis Rheum, 2012. **64**(8): p. 2724-33.
301. Legue, E., I. Sequeira, and J.F. Nicolas, *Hair follicle renewal: authentic morphogenesis that depends on a complex progression of stem cell lineages.* Development, 2010. **137**(4): p. 569-77.
302. Legue, E. and J.F. Nicolas, *Hair follicle renewal: organization of stem cells in the matrix and the role of stereotyped lineages and behaviors.* Development, 2005. **132**(18): p. 4143-54.
303. Chi, W., E. Wu, and B.A. Morgan, *Dermal papilla cell number specifies hair size, shape and cycling and its reduction causes follicular decline.* Development, 2013. **140**(8): p. 1676-83.
304. Morata, G. and P. Ripoll, *Minutes: mutants of drosophila autonomously affecting cell division rate.* Dev Biol, 1975. **42**(2): p. 211-21.
305. Vincent, J.P., A.G. Fletcher, and L.A. Baena-Lopez, *Mechanisms and mechanics of cell competition in epithelia.* Nat Rev Mol Cell Biol, 2013. **14**(9): p. 581-91.
306. Merino, M.M., R. Levayer, and E. Moreno, *Survival of the Fittest: Essential Roles of Cell Competition in Development, Aging, and Cancer.* Trends Cell Biol, 2016. **26**(10): p. 776-788.
307. Claveria, C. and M. Torres, *Cell Competition: Mechanisms and Physiological Roles.* Annu Rev Cell Dev Biol, 2016. **32**: p. 411-439.
308. Maruyama, T. and Y. Fujita, *Cell competition in mammals - novel homeostatic machinery for embryonic development and cancer prevention.* Curr Opin Cell Biol, 2017. **48**: p. 106-112.
309. Kajita, M. and Y. Fujita, *EDAC: Epithelial defence against cancer-cell competition between normal and transformed epithelial cells in mammals.* J Biochem, 2015. **158**(1): p. 15-23.
310. Lynch, M.D., et al., *Spatial constraints govern competition of mutant clones in human epidermis.* Nat Commun, 2017. **8**(1): p. 1119.
311. Martins, V.C., et al., *Cell competition is a tumour suppressor mechanism in the thymus.* Nature, 2014. **509**(7501): p. 465-70.
312. Sancho, M., et al., *Competitive interactions eliminate unfit embryonic stem cells at the onset of differentiation.* Dev Cell, 2013. **26**(1): p. 19-30.
313. Claveria, C., et al., *Myc-driven endogenous cell competition in the early mammalian embryo.* Nature, 2013. **500**(7460): p. 39-44.
314. Villa Del Campo, C., et al., *Cell competition promotes phenotypically silent cardiomyocyte replacement in the mammalian heart.* Cell Rep, 2014. **8**(6): p. 1741-1751.
315. Bondar, T. and R. Medzhitov, *p53-mediated hematopoietic stem and progenitor cell competition.* Cell Stem Cell, 2010. **6**(4): p. 309-22.
316. Hogan, C., et al., *Characterization of the interface between normal and transformed epithelial cells.* Nat Cell Biol, 2009. **11**(4): p. 460-7.
317. Ohoka, A., et al., *EPLIN is a crucial regulator for extrusion of RasV12-transformed cells.* J Cell Sci, 2015. **128**(4): p. 781-9.

318. Tanimura, N. and Y. Fujita, *Epithelial defense against cancer (EDAC).* Semin Cancer Biol, 2020. **63**: p. 44-48.
319. Gorlin, R.J., *Nevoid basal cell carcinoma syndrome.* Dermatol Clin, 1995. **13**(1): p. 113-25.
320. Abel, E.L., et al., *Multi-stage chemical carcinogenesis in mouse skin: fundamentals and applications.* Nat Protoc, 2009. **4**(9): p. 1350-62.
321. Kong, Y.H. and S.P. Xu, *Salidroside prevents skin carcinogenesis induced by DMBA/TPA in a mouse model through suppression of inflammation and promotion of apoptosis.* Oncol Rep, 2018. **39**(6): p. 2513-2526.
322. Athar, M., et al., *Inhibition of smoothened signaling prevents ultraviolet B-induced basal cell carcinomas through regulation of Fas expression and apoptosis.* Cancer Res, 2004. **64**(20): p. 7545-52.
323. Cataisson, C., et al., *Protein kinase C alpha-mediated chemotaxis of neutrophils requires NF-kappa B activity but is independent of TNF alpha signaling in mouse skin in vivo.* J Immunol, 2005. **174**(3): p. 1686-92.
324. Weyers, W., S. Horster, and C. Diaz-Cascajo, *Tumor of follicular infundibulum is Basal cell carcinoma.* Am J Dermatopathol, 2009. **31**(7): p. 634-41.
325. Biehs, B., et al., *A cell identity switch allows residual BCC to survive Hedgehog pathway inhibition.* Nature, 2018. **562**(7727): p. 429-433.
326. Zhu, G.A., U. Sundram, and A.L. Chang, *Two different scenarios of squamous cell carcinoma within advanced Basal cell carcinomas: cases illustrating the importance of serial biopsy during vismodegib usage.* JAMA Dermatol, 2014. **150**(9): p. 970-3.
327. Orouji, A., et al., *Multiple highly and moderately differentiated squamous cell carcinomas of the skin during vismodegib treatment of inoperable basal cell carcinoma.* Br J Dermatol, 2014. **171**(2): p. 431-3.
328. Aasi, S., et al., *New onset of keratoacanthomas after vismodegib treatment for locally advanced basal cell carcinomas: a report of 2 cases.* JAMA Dermatol, 2013. **149**(2): p. 242-3.
329. Zhao, X., et al., *RAS/MAPK Activation Drives Resistance to Smo Inhibition, Metastasis, and Tumor Evolution in Shh Pathway-Dependent Tumors.* Cancer Res, 2015. **75**(17): p. 3623-35.
330. Wang, N.J., et al., *Loss-of-function mutations in Notch receptors in cutaneous and lung squamous cell carcinoma.* Proc Natl Acad Sci U S A, 2011. **108**(43): p. 17761-6.
331. Pickering, C.R., et al., *Mutational landscape of aggressive cutaneous squamous cell carcinoma.* Clin Cancer Res, 2014. **20**(24): p. 6582-92.
332. Dong, X., et al., *YAP/TAZ: a promising target for squamous cell carcinoma treatment.* Cancer Manag Res, 2019. **11**: p. 6245-6252.
333. Kato, H., et al., *Loss of protein phosphatase 6 in mouse keratinocytes increases susceptibility to ultraviolet-B-induced carcinogenesis.* Cancer Lett, 2015. **365**(2): p. 223-8.
334. Pellegrini, C., et al., *Understanding the Molecular Genetics of Basal Cell Carcinoma.* Int J Mol Sci, 2017. **18**(11).
335. Bonilla, X., et al., *Genomic analysis identifies new drivers and progression pathways in skin basal cell carcinoma.* Nat Genet, 2016. **48**(4): p. 398-406.
336. Aubrey, B.J., A. Strasser, and G.L. Kelly, *Tumor-Suppressor Functions of the TP53 Pathway.* Cold Spring Harb Perspect Med, 2016. **6**(5).
337. Welcker, M., et al., *The Fbw7 tumor suppressor regulates glycogen synthase kinase 3 phosphorylation-dependent c-Myc protein degradation.* Proc Natl Acad Sci U S A, 2004. **101**(24): p. 9085-90.
338. Zhao, B., Q.Y. Lei, and K.L. Guan, *The Hippo-YAP pathway: new connections between regulation of organ size and cancer.* Curr Opin Cell Biol, 2008. **20**(6): p. 638-46.
339. Plikus, M.V., *New activators and inhibitors in the hair cycle clock: targeting stem cells' state of competence.* J Invest Dermatol, 2012. **132**(5): p. 1321-4.
340. Chen, C.C., et al., *Regenerative hair waves in aging mice and extra-follicular modulators follistatin, dkk1, and sfrp4.* J Invest Dermatol, 2014. **134**(8): p. 2086-2096.

341. Plikus, M.V., et al., *Self-organizing and stochastic behaviors during the regeneration of hair stem cells.* Science, 2011. **332**(6029): p. 586-9.
342. Barrientos, S., et al., *Growth factors and cytokines in wound healing.* Wound Repair Regen, 2008. **16**(5): p. 585-601.
343. Lee, P., et al., *Stimulation of hair follicle stem cell proliferation through an IL-1 dependent activation of gammadeltaT-cells.* Elife, 2017. **6**.
344. Yu, N., et al., *IL-1-alpha and TNF-alpha differentially regulate CD4 and Mac-1 expression in mouse microglia.* Neuroimmunomodulation, 1998. **5**(1-2): p. 42-52.
345. Lin, W.H., et al., *Fibroblast growth factors stimulate hair growth through beta-catenin and Shh expression in C57BL/6 mice.* Biomed Res Int, 2015. **2015**: p. 730139.
346. Festa, E., et al., *Adipocyte lineage cells contribute to the skin stem cell niche to drive hair cycling.* Cell, 2011. **146**(5): p. 761-71.
347. Yano, K., L.F. Brown, and M. Detmar, *Control of hair growth and follicle size by VEGF-mediated angiogenesis.* J Clin Invest, 2001. **107**(4): p. 409-17.
348. Schneider, M.R. and R. Paus, *Deciphering the functions of the hair follicle infundibulum in skin physiology and disease.* Cell Tissue Res, 2014. **358**(3): p. 697-704.
349. Taylor, G., et al., *Involvement of follicular stem cells in forming not only the follicle but also the epidermis.* Cell, 2000. **102**(4): p. 451-61.
350. Green, H., *Cultured cells for the treatment of disease.* Sci Am, 1991. **265**(5): p. 96-102.
351. Hoeck, J.D., et al., *Stem cell plasticity enables hair regeneration following Lgr5(+) cell loss.* Nat Cell Biol, 2017. **19**(6): p. 666-676.
352. Rompolas, P., K.R. Mesa, and V. Greco, *Spatial organization within a niche as a determinant of stem-cell fate.* Nature, 2013. **502**(7472): p. 513-8.
353. Fuchs, E., T. Tumbar, and G. Guasch, *Socializing with the neighbors: stem cells and their niche.* Cell, 2004. **116**(6): p. 769-78.
354. Gattazzo, F., A. Urciuolo, and P. Bonaldo, *Extracellular matrix: a dynamic microenvironment for stem cell niche.* Biochim Biophys Acta, 2014. **1840**(8): p. 2506-19.
355. Castro, A.R. and E. Logarinho, *Tissue engineering strategies for human hair follicle regeneration: How far from a hairy goal?* Stem Cells Transl Med, 2020. **9**(3): p. 342-350.
356. Cruikshank, W.W., et al., *Lymphocyte chemoattractant factor induces CD4-dependent intracytoplasmic signaling in lymphocytes.* J Immunol, 1991. **146**(9): p. 2928-34.
357. Cruikshank, W.W., et al., *Lymphokine activation of T4+ T lymphocytes and monocytes.* J Immunol, 1987. **138**(11): p. 3817-23.
358. Tamoutounour, S., et al., *Keratinocyte-intrinsic MHCII expression controls microbiota-induced Th1 cell responses.* Proc Natl Acad Sci U S A, 2019. **116**(47): p. 23643-23652.
359. Menon, G.K. and P.M. Elias, *Ultrastructural localization of calcium in psoriatic and normal human epidermis.* Arch Dermatol, 1991. **127**(1): p. 57-63.
360. Menon, G.K., et al., *Localization of calcium in murine epidermis following disruption and repair of the permeability barrier.* Cell Tissue Res, 1992. **270**(3): p. 503-12.
361. Niessen, C.M., *Tight junctions/adherens junctions: basic structure and function.* J Invest Dermatol, 2007. **127**(11): p. 2525-32.
362. Hennings, H. and K.A. Holbrook, *Calcium regulation of cell-cell contact and differentiation of epidermal cells in culture. An ultrastructural study.* Exp Cell Res, 1983. **143**(1): p. 127-42.
363. Ng, D.C., et al., *Regulation of involucrin gene expression by calcium in normal human keratinocytes.* Front Biosci, 1996. **1**: p. a16-24.
364. Huff, C.A., S.H. Yuspa, and D. Rosenthal, *Identification of control elements 3' to the human keratin 1 gene that regulate cell type and differentiation-specific expression.* J Biol Chem, 1993. **268**(1): p. 377-84.

365. Rothnagel, J.A., et al., *Identification of a calcium-inducible, epidermal-specific regulatory element in the 3'-flanking region of the human keratin 1 gene.* J Invest Dermatol, 1993. **101**(4): p. 506-13.
366. Luck, K., et al., *A reference map of the human binary protein interactome.* Nature, 2020. **580**(7803): p. 402-408.
367. Kittanakom, S., et al., *CHIP-MYTH: a novel interactive proteomics method for the assessment of agonist-dependent interactions of the human beta(2)-adrenergic receptor.* Biochem Biophys Res Commun, 2014. **445**(4): p. 746-56.
368. Koizumi, H., et al., *Beta-adrenergic stimulation induces intracellular Ca++ increase in human epidermal keratinocytes.* J Invest Dermatol, 1991. **96**(2): p. 234-7.
369. Mammone, T., et al., *The induction of terminal differentiation markers by the cAMP pathway in human HaCaT keratinocytes.* Skin Pharmacol Appl Skin Physiol, 1998. **11**(3): p. 152-60.
370. Schallreuter, K.U., et al., *Catecholamines in human keratinocyte differentiation.* J Invest Dermatol, 1995. **104**(6): p. 953-7.
371. Sun, J.L., et al., *Conditional deletion of Adrb2 in mesenchymal stem cells attenuates osteoarthritis-like defects in temporomandibular joint.* Bone, 2020. **133**: p. 115229.
372. Platt, E.J., et al., *Effects of CCR5 and CD4 cell surface concentrations on infections by macrophagetropic isolates of human immunodeficiency virus type 1.* J Virol, 1998. **72**(4): p. 2855-64.

9 Acknowledgements

First of all, I have to admit that writing this thesis would not have been possible without the support of several people:

I am especially grateful to my supervisor, **Anja Uhmann**, for giving me the opportunity to write my doctoral thesis. I would also like to thank you for sharing your 'favorite project' with me and for working on it together for the past three years. Even after your friendly instruction to the laboratory work and the methods established especially by you, also you have always accompanied me in the past years, both with technical and content-related problems, and through the helpful brainstorming meetings I never had the feeling of being alone with this 'risky' project. Since I benefitted significantly from your research experience and expertise, I am grateful that with your help I have come to such interesting findings that finally resulted in a scientific publication. Thank you, for always answering my questions and encouraging me, for always taking time for me – to sum up: for your excellent supervision!

Thank you, **Heidi Hahn**, for the opportunity to work in your group. I would like to further thank you for the discussions about my experimental progress and my results and for your valuable advices. Besides, I am grateful for your support during the manuscript writing process.

My gratitude is extended to **Rüdiger Behr** and **Sigrid Hoyer-Fender** for your guidance during my doctoral time and the helpful discussions and critical advice regarding my work. I am grateful to **Michael Schön**, who kindly agreed to be my second reviewer at short notice. My thanks are extended to **Peter Burfeind** and **Nico Posnien** for being members on my examination board.

Additionally, I would like to thank past and present members of our group for their support, kind instructions in the laboratory and constructive scientific discussions. Particularly noteworthy are the technicians, **Anke Frommhold** and **Ina Heß**, who made the extent of the mouse experiments possible at all. Furthermore, I would like to thank **Slavica Hristomanova Mitkovska** as it was a great pleasure to work with you on the CD4 project and I enjoyed our scientific discussions and your friendliness. Besides, even though you have only recently joined our group, **Nada Ragab**, you have already become an important support to me and I want to thank you for your mental support during my last year of doctoral studies and your helpful advice.

I would also like to thank my parents, who made my studies and doctorate possible and always supported me. The countless discussions about fascinating scientific and especially biological phenomena such as the plasticity and regenerative potential of stem cells on the one hand, and on the other hand the not yet understood loss of these properties leading to ageing, were probably decisive for my decision to become a scientist and to do this doctoral thesis. However, without the support of my family and my partner, I would not have been able to do this time-consuming and sometimes exhausting work. The view from the outside (from non-biologists) often helped me to keep an overview and to ask the relevant questions. Thank you to my family and partner, who have always been there for me, listening and encouraging me.